

NASA CR-175,477

NASA-CR-175477  
19850012140

# A Reproduced Copy

OF

NASA CR-175,477

---

Reproduced for NASA

*by the*

**NASA** Scientific and Technical Information Facility

LIBRARY COPY

AUG 19 1985

LANGLEY RESEARCH CENTER  
LIBRARY, NASA  
HAMPTON, VIRGINIA

# Middle Atmosphere Program

(NASA-CR-175477) MIDDLE ATMOSPHERE PROGRAM.  
HANDBOOK FOR EAF, VOLUME 1C (International  
Council of Scientific Unions) 229 p  
HC A11/MP A01; also available from SCOSTEE

N65-20450  
TRBU  
N65-20491  
Unclas  
CSCI 04A G3/42 10262

N85-20450 #

M I D D L E  
A T M O S P H E R E  
P R O G R A M

HANDBOOK FOR MAP

Volume 10

Papers presented at the International Symposium on  
Ground-Based Studies of the Middle Atmosphere  
May 9-13, 1983, Schwerin, German Democratic Republic

Edited by

J. Taubenhein

May 1984

Published for the ICSU Scientific Committee on Solar-  
Terrestrial Physics (SCOSTEP) with financial assistance  
from the National Aeronautics and Space Administration  
Contract NASW 3805

Copies available from SCOSTEP Secretariat, University of  
Illinois, 1406 W. Green Street, Urbana, Illinois 61801

## FOREWORD

The International Symposium on Ground-Based Studies of the Middle Atmosphere was held at Schwerin, German Democratic Republic, from May 10 to 13, 1983. It was organized by the Academy of Sciences of the German Democratic Republic, and hosted by its Central Institute of Solar-Terrestrial Physics (Heinrich Hertz Institute) under the direction of Prof. Dr. W. Mundt.

The aim of this symposium was to point out the valuable contribution which ground-based investigations, with their particular capabilities for long-term continuous monitoring of atmospheric processes and parameter variations on various time scales, can render to the scope of the Middle Atmosphere Program. We believe that the symposium has well served its function to provide a useful forum for the exchange of ideas, results, and experiences, and to aid the mutual stimulation between 'meteorological' and 'aeronomical' approaches to the problems of the middle atmosphere.

We wish to thank the GDR National Committee on Geodesy and Geophysics and the international organizations that co-sponsor the symposium: The Scientific Committee on Solar-Terrestrial Physics (SCOSTEP), the International Association of Geomagnetism and Aeronomy (IAGA), and the Committee on Space Research (COSPAR).

The volume contains the extended abstracts of almost all of the 16 invited and 28 contributed papers presented at Schwerin. We would like to thank the IAP Publications Committee with its chairman, Prof. C. F. Sechrist, Jr., for providing the possibility to publish this report as a volume of the Handbook for IAP. The assistance of Belva Edwards, Penny Roth, and Edward Lovekamp in the production of this volume is gratefully acknowledged.

J. Taubenheim  
Chairman, Program Committee and Editor

PRECEDING PAGE BLANK NOT FILMED

CONTENTS

FOREWORD. . . . . iii

CONTENTS. . . . . v

A. Diagnostic of the Middle Atmosphere from D-Region Properties

Neutral atmosphere properties determining D-region electron densities.  
J. Taubenheim (invited paper) . . . . . 1

Variation of derived mesospheric nitric oxide in relation to wind and  
temperature in winter, M. Friedrich and K. M. Torkar (invited paper). . . 6

Middle atmosphere temperature and dynamics as revealed from D-region  
observations, A. D. Danilov (invited paper) . . . . . 16

Synopsis of mid-latitude radio wave absorption in Europe. K. M. Torkar  
and M. Friedrich. . . . . 24

Ionospheric absorption on 1539 kHz in relation to solar ionizing  
radiation, J. Boska . . . . . 31

Indirect phase height measurements in Central and Eastern Europe for  
monitoring D region plasma. G. v. Cossart and S. V. Pakhomov. . . . . 34

Measurements of partial reflections at 3.18 MHz using the CW radar  
technique, J. Priese and W. Singer. . . . . 39

Abnormal circulation changes in the winter stratosphere, detected  
through variations of D region ionospheric absorption, E. A.  
de la Morena. . . . . 45

B. Winter Anomaly

Winter anomaly of the lower ionosphere and its possible causes.  
Z. Ts. Rapoport (invited paper) . . . . . 52

Autumn and winter anomalies in ionospheric absorption as measured by  
riometers. H. Ranta . . . . . 60

Winter anomaly 1982/83 in comparison with earlier winters (1960/82),  
J. Lastovicka . . . . . 62

A model of the influence of neutral air dynamics on the seasonal  
variation in the low ionosphere. G. Nestorov, P. Velinov, and  
T. Pancheva . . . . . 66

Explanation of the normal winter anomaly from the seasonal variation of  
short-wave absorption, P. J. Velinov, N. V. Smirnova, and  
V. A. Vlaskov . . . . . 70

RECORDING PAGE BLANK NOT FILLED

C. Seasonal Variations, Transitions and Disturbances

- Seasonal characteristics of mesospheric plasma and their transitions,  
E. A. Lauter (invited paper). . . . . 75
- Midwinter disturbances in the middle atmosphere, K. Labitzke  
(invited paper) . . . . . 79
- Spring changeover of the middle atmosphere circulation compared with  
rocket and wind data up to 80 km. G. Entzian, D. A. Tarasenko, and  
E. A. Lauter. . . . . 86
- Large-scale winter-time disturbances in meteor winds over Central and  
Eastern Europe, K. M. Greisiger, Yu. I. Portnyagin, and I. A. Lysenko . 91
- VHF-radar observations in the stratosphere and mesosphere during a  
stratospheric warming, R. Ruster, P. Czechowsky, G. Schmidt, and  
K. Labitzke . . . . . 96
- Changes in the ozone content over Central Europe during reversals of  
stratospheric circulation in late winter, G. Entzian, and K. H.  
Grasnick. . . . . 97

D. Dynamics and Theoretical Models

- Some aspects of general circulation and tides in the middle atmosphere,  
A. I. Ivanovskiy (invited paper) . . . . . 101
- Aspects of planetary wave transports in the middle atmosphere,  
G. Schmitz (invited paper). . . . . 110
- Coupling between the thermosphere and the stratosphere: The role of  
nitric oxide, G. Brasseur . . . . . 116
- Atmospheric-profile imprint in fireball ablation coefficients,  
Z. Cepelcha, and P. Pecina. . . . . 122

E. Winds and Waves, and their Tracking by Ground-Based Methods

- Meteor wind results from Atlanta, U.S.A., and Ramey, Puerto Rico,  
R. G. Roper (invited paper) . . . . . 127
- Basic features of global circulation in the mesopause - lower thermo-  
sphere region, Yu. I. Portnyagin (invited paper). . . . . 134
- Winds and waves (4 min - 11 yrs) in the upper middle atmosphere (60-  
110 km) at Saskatoon, Canada (52°N, 107°W): H.F. radar (2.2 MHz)  
soundings 1973-1983. A. H. Hanson, C. E. Meek, and J. B. Gregory  
(invited paper) . . . . . 143
- The dynamics of ionospheric D-region over East Siberia, E. S.  
Kazimirovsky (invited paper). . . . . 152

Measurement of the vertical gradient of the semidiurnal tidal wind phase in winter at the 95 km level. R. Schindler and D. Kurschner . . .	.160
Medium frequency radar observations in the middle atmosphere, P. Czechowsky, G. Schmidt, and H. Kopka . . . . .	.165
Stratwam effects in the ionospheric D region wind field, G. V. Vergasova . . . . .	.166
<b>F. Lower Thermosphere Phenomena</b>	
Orographic disturbances of upper atmosphere emissions, N. N. Shefov and N. N. Pertsev (invited paper) . . . . .	.171
Twilight intensity variation of the infrared hydroxyl airglow. R. P. Lowe, K. L. Gilbert, and R. J. Niciejewski. . . . .	.176
Investigation of aeronomic processes on the basis of ionospheric sporadic E, P. Bencze . . . . .	.179
Space and time variations and turbopause dynamical structure, O. G. Ovezgeldiyev, L. P. Korsunova, and Yu. Karadzhayev. . . . .	.183
<b>G. Solar-Terrestrial Influences upon the Middle Atmosphere</b>	
The high-latitude D-region during electron precipitation events, J. K. Hargreaves, P. N. Collis, and A. Korth (invited paper). . . . .	.188
High-energy particle effects in the D-region during and after geomagnetic storms, E. A. Lauter and C. U. Wagner (invited paper) . . .	.192
Solar flare and IMF sector structure effects in the lower ionosphere, J. Lastovicka (invited paper) . . . . .	.193
Dependence of the high latitude middle atmosphere ionization on structures in interplanetary space, J. Bremer and E. A. Lauter. . . . .	.200
Solar-terrestrial influences on the D-region as shown by the level of atmospheric radio noise, G. Satori and B. Schuning . . . . .	.205
Latitudinal dependence of the energy input by high-energy electrons into the mesosphere, C. U. Wagner, B. Nikutowski, and H. Ranta. . . . .	.211
Ozone measurements in the mesosphere during a solar proton event, W. Lippert and D. Felske. . . . .	.213
Geomagnetic disturbances caused by internal atmospheric dynamics, G. Sonnemann. . . . .	.216

N85

20451

UNCLAS

N 85-20451 7

NEUTRAL ATMOSPHERE PROPERTIES DETERMINING D-REGION ELECTRON DENSITIES

J. Taubenheim

Academy of Sciences of the GDR  
 Central Institute of Solar-Terrestrial Physics  
 (Heinrich Hertz Institute)  
 DDR-1199 Berlin-Adlershof, GDR

A rather large number of papers of this symposium is devoted to the ionospheric D region, which is situated near the upper boundary of the middle atmosphere. This has a historical root, as it was the phenomenon of D region 'winter anomaly', first discovered by Sir Edward Appleton more than forty years ago, which gave the first impulse to look for seasonal meteorological peculiarities of the middle atmosphere. Up to now, however, the number of various manifestations of meteorological control of the D region ionization (see, e.g., TAUBENHEIM (1983)), as well as the arsenal of experimental techniques, including very efficient ground-based ones, for its measurement have steadily grown. This is a permanent challenge both for aeronomers and for meteorologists to test their insight into middle atmosphere processes with the physical interpretation and evaluation of the phenomena of the D layer.

For investigating the meteorological control of D region ionization, the height region between 75 and 85 km is particularly appropriate. At these altitudes, ion production is almost exclusively due to photoionization of the minor atmospheric constituent nitric oxide (NO) by quasi-monochromatic solar Lyman-alpha (L $\alpha$ ) radiation, so that the equilibrium formula for the electron density, N, in this case takes the simple form

$$N^2 = \alpha_{\text{eff}}^{-1} \sigma_1 n_{\text{NO}} I_{\text{L}\alpha}^0 \exp(-\tau), \quad (1)$$

where  $\alpha_{\text{eff}}$  is the effective recombination coefficient,  $\sigma_1$  and  $n_{\text{NO}}$  are the ionization cross section and number density of nitric oxide, respectively,  $I_{\text{L}\alpha}^0$  is the extraterrestrial L $\alpha$  photo flux, and  $\tau$  is the optical depth for L $\alpha$  at the altitude in question.

Absorption of L $\alpha$  in the Earth's atmosphere is virtually exerted by molecular oxygen only, which is a major constituent. Therefore, in the homosphere its optical depth is proportional to the neutral air pressure, P,

$$\tau = p \sec \chi, \quad (2)$$

where  $\chi$  is the zenith angle of the incident solar radiation. On the other hand, the effective recombination coefficient is determined by the relative composition of positive from molecular ( $\text{NO}^+$ ,  $\text{O}_2^+$ , represented below by the subscript mi) and cluster ions (like  $\text{NO}^+\cdot\text{H}_2\text{O}$ ,  $\text{H}^+(\text{H}_2\text{O})_n$ , etc., represented by the subscript ci), the recombination coefficients of which being remarkably different in magnitude,

$$\alpha_{\text{eff}} = \sum [(N_{\text{mi}}/N)\alpha_{\text{mi}} + (N_{\text{ci}}/N)\alpha_{\text{ci}}] \quad (3)$$

where the sum has to be extended over all species of positive ions. Since the rate of conversion of molecular ions into cluster ions strongly depends on temperature, the resulting ion composition will vary with temperature and, consequently,  $\alpha_{\text{eff}}$  (after eq. (3)) and N (after eq. (1)) will be sensibly modulated by neutral air temperature variations (DANILOV and SIMONOV, 1982; DANILOV and TAUBENHEIM, 1983). The molecular-to-cluster ion conversion rate varies with  $T^{-n}$ , where the value of n depends on the details of the ion-chemical reaction scheme adopted by the respective authors. BREMER et al.

(1981) claim a value  $n = 7.2$ , which leads to a temperature dependence of the ion percentage distribution and of  $\alpha_{eff}$  as shown in Figure 1 (for mid-latitudes at 80 km height).

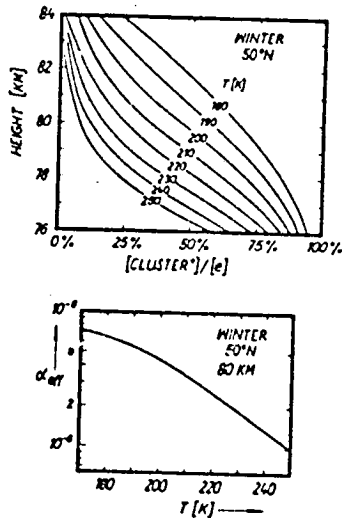


Figure 1. Upper part: Ratio (per cent) of clustered ions to total electron density near 80 km in mid-latitude winter, for different temperatures. - Lower part: Temperature dependence of effective recombination coefficient,  $\alpha_{eff}$ , derived from the curves shown above.

Finally, according to eq. (1), the electron density depends on the nitric oxide concentration. At this altitude level,  $n_{NO}$  is mainly controlled by downward transport of neutral NO (or N) from the thermosphere, partly by eddy diffusion but probably even more efficiently by a bulk transport with the vertical component of the wind circulation, since the photochemical lifetime of neutral NO molecules at medium and high latitudes is of the order of one day or more.

The only 'non-meteorological' factor in eq. (1) is the L $\alpha$  irradiation, which can be either taken from direct satellite measurements (e.g., HINTEREGGER (1981)), or parameterized as a function of solar activity parameters (e.g., VIDAL-MADJAR (1977), BOSSY and NICOLET (1981), LEAN and SKUMANICH (1983)). It turns out, however, that at least in the mid-latitude winter variability of D region electron densities, the L $\alpha$  control is by far overshadowed by the meteorological influences (TAUBENHEIM, 1983).

In subsequent papers of the symposium (COSSART and PAKHOMOV, 1983; LAUTER, 1983) a ground-based measuring technique of low-frequency radio reflection (phase) heights will be presented which is capable for a day-by-day monitoring of the altitude at which a pre-selected fixed value of electron density,  $N_r$ , is attained. This technique is in use since many years continuously at Kuehlungsborn. An example given in Figure 2 shows how well these l.f. reflection heights follow the variations of the height of the 0.01 mbar isobaric surface, thus indicating a dominant pressure control through the optical depth of the L $\alpha$  radiation. Further, from these measurements we can easily derive a daily characteristic,  $f = \ln \sec X_{80}$  (specified in more detail in LAUTER et al. (1984)), which describes the day-to-day variations of the state of ionization at 80 km height. Its deviations,  $\Delta f$ , from a certain reference state (to be chosen from the observed data time series), can be interpreted in terms of the corresponding deviations of pressure,  $\alpha_{eff}$ , and NO density at the 80 km level: from eqs. (1) and (2) follows

$$\Delta f = -\Delta \ln p + \Delta \ln \ln \left\{ \sigma_1 I_{L\alpha}^0 / N_r^2 \right\} (n_{NO} / \alpha_{eff}) \quad (4)$$

In this formula, the dominant role of pressure variations is obvious, however modified to a lesser degree by a  $n_{NO}$  (i.e., circulation) and an  $\alpha_{eff}$  (i.e., temperature) control.

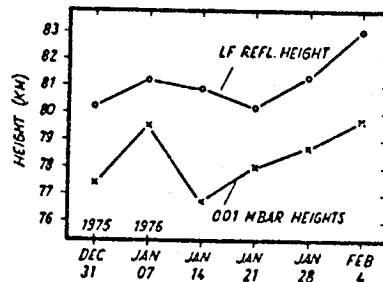


Figure 2. Heights of the 0.01 mbar surface at a grid-point 60°N, 10°E taken from LABITZKE et al. (1978), compared with LF radio wave reflection heights observed at Kuehlungsborn, in winter 1975/76.

Figures 3 and 4 illustrate the analysis of meteorological control in individual winter data series of this type. The variations of a 'relative electron density index' at 80 km, defined by  $1 + 0.8 \times \Delta f$ , are presented for the late winter periods of 1980/81 (Figure 3) and 1981/82 (Figure 4). The step curves show the march of the 5-day (pentade) mean values of the observed data of Kuehlungsborn, where in both cases the second pentade of December was adopted as the reference level ( $\Delta f = 0$ ). The dashed curve gives the long-term average (25 years) of these observed data. They are characterized by the midwinter ionization at 80 km being generally higher than in spring (and summer), thus representing the well-known 'average winter anomaly' of the D region. From both diagrams it can be noted (as well as from other years, not shown here) that major stratospheric warmings lead to a sudden decrease ('breakdown') of winter-anomalous electron densities near 80 km (LAUTER and ENTZIAN, 1982). Further, Figure 3 shows evidence that the extremely cold stratospheric temperatures in December 1980/January 1981 (cf. LABITZKE and GORETZKI, 1982) were associated with an exceptional enhancement of D region ionization (LAUTER and ENTZIAN, 1982).

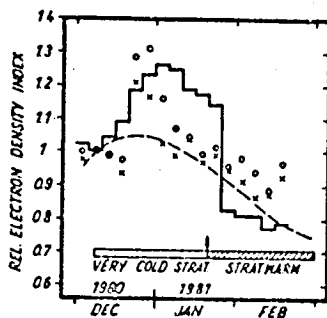


Figure 3. Electron density variations near 80 km in winter 1980/81, derived from ground-based radio observations (curves), and from model calculations (crosses, circles) as described in the text.

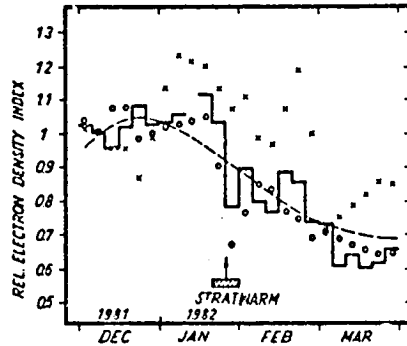


Figure 4. Same as Figure 3 but for winter 1981/82.

An approach to the interpretation of these ground-based radio data is represented by the crosses and open circles in Figures 3 and 4, which are values calculated by means of eq. (4), making use of rocket data of pressure and temperature measured near 80 km altitude over Volgograd (published in CAO BULLETIN), at a latitude comparable to those of the radio paths observed at Kuchlungsborn. The crosses are the first-order approximation by taking into account the pressure variation only (first right-hand term of eq. (4)), the open circles are the second-order approximation computed with both the pressure variation and the temperature-induced  $\alpha_{\text{eff}}$  variation (as in Figure 1).

The agreement of the crosses and circles with the step curves in Figures 3 and 4 is only partly satisfactory. Obviously, the general seasonal variation between December and March can be well understood in terms of the pressure and temperature variations. Also, the sudden increase of ionization in the second half of December 1980, as well as the 'breakdown' with the stratwarm event in late January 1982 are clearly explainable by the combined effect of pressure and temperature near 80 km. The duration of the ionization excess in January 1981, and its sudden breakdown in the last pentade of January, however, are not well reproduced by the Volgograd rocket data of pressure and temperature. This may partly be due to the fact that Volgograd is not near enough to the Kuehlungsborn observation paths to expect a good point-to-point correlation. On the other hand, however, there is no doubt that sudden changes of neutral NO content, for which no data are available, will also sensibly influence the D region ionization through the second term of equation (4). A plausible scenario (TAUBENHEIM, 1983) predicts that variations of pressure, temperature, and NO advection near 80 km are jointly controlled by the circumpolar vortex of the strato-mesospheric circulation system in that way, that with intensification of cyclonic vortex motion the mesospheric pressure is enhanced lowered, temperature enhanced, and downward NO transport is strengthened, which altogether act 'cooperatively' in enhancing the D region electron density (cf. eq. (4)), and vice versa.

Therefore we may conclude that D region electron density variations, which can be readily monitored by ground-based techniques, can provide an efficient diagnostic tool for the detection of perturbations of the circulation state of the middle atmosphere.

The author is indebted to Prof. E. A. Lauter and to Dr. G. v. Cossart for providing the results of phase-height measurements at Kuchlungsborn.

## REFERENCES

- CAO Bulletin: Bulletin of Atmospheric Rocket Sounding Results, issued by the Central Aerological Observatory, Hydrometeorological Service, Moscow, USSR.
- Bossy, L. and M. Nicolet (1981), Planet. Space Sci., 27, 907.
- Bremer, J., K. Evers and J. Taubenheim (1981), Gerlands Beitr. Geophys., Leipzig, 90, 295.
- v. Cossart G. and S. V. Pakhomov (1983), This volume.
- Danilov, A. D. and A. G. Simonov (1982), J. Atmos. Terr. Phys., 44, 567.
- Danilov, A. D. and J. Taubenheim (1983), Space Sci. Rev., 34, 413.
- Hinteregger, J. E. (1981), Adv. Space Sci., 1, 39.
- Labitzke, K., K. Petzoldt and J. Knittel (1978), Paper presented at the Solar-Terr. Physics Symposium, Innsbruck.
- Labitzke, K. and B. Goretzki (1982), Handbook for MAP, vol. 5.
- Lauter, E. A. (1983), This volume.
- Lauter, E. A. and G. Entzian (1982), Phys. Solariterr., Potsdam, 18, 83.
- Lauter, E. A., J. Taubenheim and G. v. Cossart (1984), J. Atmos. Terr. Phys., (to be published).
- Lean, J. L. and A. Skumanich (1983), J. Geophys. Res., 88, 5751.
- Taubenheim, J. (1983), Space Sci. Rev., 34, 397.
- Vidal-Madjar, A. (1977), in The Solar Output and Its Variations, (ed. by O. R. White), Colorado Assoc. Univ. Press, Boulder, CO. P. 213.

N85  
20452

UNCLAS

D2  
N85-20452

VARIATION OF DERIVED MESOSPHERIC NITRIC OXIDE IN RELATION  
TO WIND AND TEMPERATURE IN WINTER

H. Friedrich

Department of Communications and Wave Propagation  
Technical University Graz  
Inffeldgasse 12, A-8010 Graz, Austria

K. M. Torkar

Space Research Institute of the Austrian Academy of Sciences  
c/o Technical University Graz  
Austria

As a good approximation changes of the NO-density are solely responsible for changes of the non-auroral D-region. Under the assumption that other ion production processes are either known or negligible, one can hence derive (NO) from electron densities using a suitable effective electron loss rate. In the Winter Anomaly Campaign 1975/76 nineteen rocket payloads carried electron density measurements on fifteen days. On two of these days (NO) was measured in-situ by photometers. For these days one can establish the production not due to Lyman- $\alpha$  and NO. This rest production can then be applied to all (NO) derivations based on electron density measurements.

In addition, in this campaign winds and temperatures were measured from the ground to approximately the base of the thermosphere. The derived field of NO densities between December 1975 and February 1976 from 70 to 100 km is compared to corresponding fields of winds (zonal and meridional), temperatures, pressure and Richardson numbers. The derivation of the latter is dependent on a number of assumptions and should stimulate discussion rather than being a result per-se.

INTRODUCTION

D-region electron densities are almost exclusively the reason for radio wave absorption. In order to explain the large excursions of absorption in winter ('winter anomaly'), the following cause-and-effect scheme may help to identify or reject various causes (Figure 1).

Absorption at the frequencies and altitudes in question ( $>1$  MHz, 70 to 100 km) is proportional to electron density and collision frequency  $\nu_M$  (because  $f \gg \nu_M$ ). The collision frequency is -- according to laboratory measurements -- to a very good approximation proportional to neutral pressure. The latter is fairly well known from empirical models (better than  $\pm 10\%$ ) and the proportionality factor varies only slightly with temperature ( $\pm 5\%$  between 200 and 300 K, AGGARWAL and SETTY, 1980). Hence variations of the collision frequency can only contribute to the regular, seasonal behaviour of absorption, but not to the day-to-day variations by factors of two or more.

It is therefore the electron density  $N_e$  which must undergo large variations. For steady state (appr. at noon)  $N_e$  is balanced by the square root of the ion-pair production  $q$  divided by the effective electrons loss rate  $\psi$ . The latter is an inverse function of temperature; however, even the large variations observed in winter ('warmings') can -- according to model calculations -- only account for changes of  $\psi$  by as much as perhaps  $\pm 50\%$ . The concentration of atomic oxygen has great influence on the nature of the positive ions (molecular or cluster) which have widely different recombination rates; O also drastically alters the relative distribution between electrons and negative

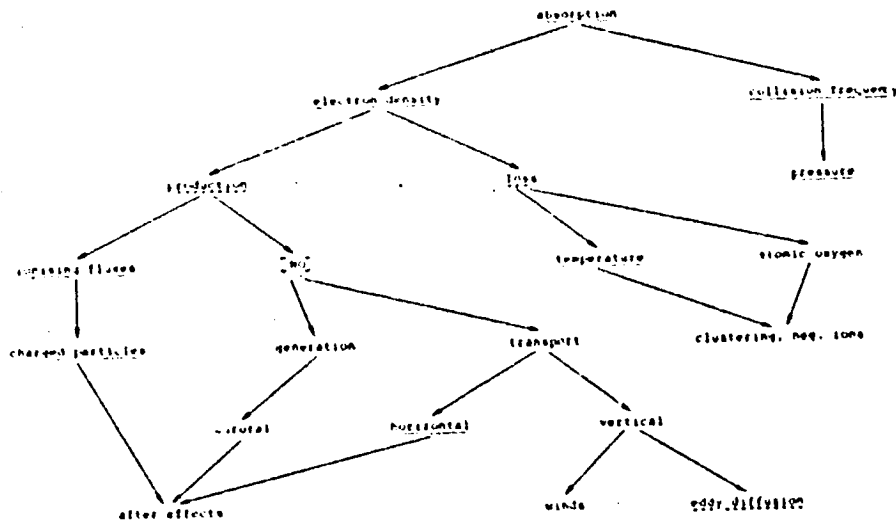


Figure 1. Simplified cause-and-effect scheme for variations of ionospheric radio wave absorption. Parameters measured in the Winter Anomaly Campaign 1975/76 are underlined by full, derived quantities by broken lines.

ions. Nonetheless, the concentration of O has its main influence at heights below 80 km which contribute only little (ca. 30%) to the total radio wave absorption. Furthermore, the variation of [O] is, even according to different models and measurements, reasonably predictable (within a factor of 2, cf. e.g. THOMAS and BOWMAN, 1972; DICKINSON et al., 1980; SOLOMON et al., 1982).

The ion-pair production rate  $q$  is a function of the relevant fluxes and the overhead absorbing air column. The latter is -- similar to the collision frequencies -- rather well known from pressure models of the lower thermosphere, and certainly does not change sufficiently to explain the observed effects in  $N_2$ . Also the main daytime ionising fluxes vary, even over a sunspot cycle, only by much less than a factor of two for Lyman- $\alpha$ , of five for Lyman-B and of ten for the less important medium X-rays. The often proposed fluxes of charged particles may contribute to  $q$  at geomagnetically higher latitudes in North America (cf. the argumentation by MAHLUM, 1967), but can safely be ruled out in Europe (THRANE et al., 1979). Trapped particles, however, constitute a possible mechanism for the observed after-effects of geomagnetic disturbances (cf. MARGREAVES, 1973; TORKAR et al., 1980).

In the daytime D-region the dominant process is the ionisation of nitric oxide (NO) by the strong and fairly constant solar Lyman- $\alpha$  line. Hence variations of the ion production must be due to variations of the concentration of NO. Nitric oxide in the D-region (mesosphere to lower thermosphere) originates -- according to model computations -- in the E-region due to a variety of processes including ionisation by solar X-rays or charged particles. It is subsequently transported downwards by eddy diffusion or vertical winds and destroyed by photo-dissociation during transport. Hence, [NO] is the E-region is larger during solar maximum (or PCA), whereas its concentration in the D-region follows the production not directly, because of the likewise increased photo-dissociation at times of high solar activity.

The main candidates for winter anomalous absorption are therefore local variations of [NO] by either horizontal winds (transport from areas of higher concentrations, such as the polar regions), or a variation of the vertical transport efficiency, i.e. the eddy diffusion coefficient. In the following the emphasis is therefore on derived [NO] as a function of temperature and horizontal wind.

#### DERIVATION OF NITRIC OXIDE

The Winter Anomaly Campaign 1975/76, conducted at the Spanish rocket range "El Arenosillo", was aimed at identifying the causes of enhanced radio wave absorption in winter. More than eleven institutes participated with various measurements aboard rockets, balloons and satellites, as well as ground based. For a description of the campaign and its original aims and the launch strategy see OFFERMANN (1977a) and (1979). Parameters of the schematic in Figure 1 which were measured or derived are underscored by full and broken lines, respectively.

On two days of that campaign ("salvo days") [NO] was measured by a dedicated instrument, a  $\gamma$ -band photometer, between 50 and 110 km (BERAN and BANGERT, 1979). However, on another twelve days between December 17, 1975, and February 8, 1976, electron densities were measured (FRIEDRICH et al., 1979).

Figure 2 shows the time and altitude coverage of the measurements of electron densities and neutral temperatures.

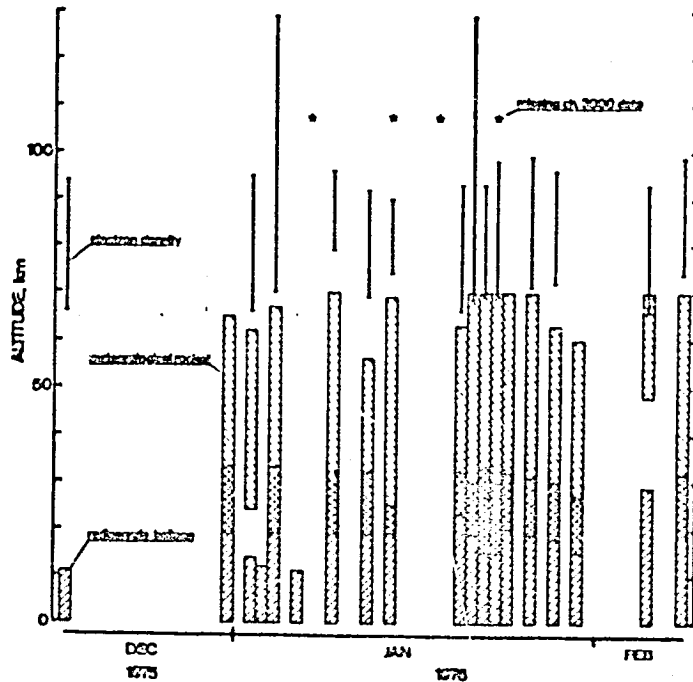


Figure 2. Height coverage of the electron density and temperature measurements during the Winter Anomaly Campaign. Days of missing radiance data of the satellite Nimbus-6 are also indicated.

TAUBENHEIM (1977) demonstrated a method of deducing [NO] from electron densities  $N_e$ . For steady state the following relations hold:

$$q = \nu N_e^2 \quad (\nu = \text{effective electron loss rate})$$

$$q = [\text{NO}] \cdot \sigma_{\text{Ly-}\alpha} + q_{\text{rest}} \quad (\sigma = \text{ionisation cross section, } \phi_{\text{Ly-}\alpha} = \text{local Lyman-}\alpha \text{ flux, } q_{\text{rest}} = \text{ion pair production not due to Lyman-}\alpha \text{ and NO})$$

Hence the NO-density is:

$$[\text{NO}] = \frac{N_e^2 \nu - q_{\text{rest}}}{\sigma_{\text{Ly-}\alpha}}$$

Apart from the measured electron densities  $N_e$ , the quantities  $\nu$ ,  $q_{\text{rest}}$  and the local Lyman- $\alpha$  flux have to be known.

The electron loss rate  $\nu$  could in principle be computed using an ion-chemical model (e.g. TORRAR and FRIEDRICH, 1983); here, however, an empirical mean derived from many daytime rocket flights is used, i.e. when both  $q$  and  $N_e$  were available. Figure 3 shows these empirical loss rates as a function of neutral density. The broken lines indicate the regions of the standard deviation (on a logarithmic scale).

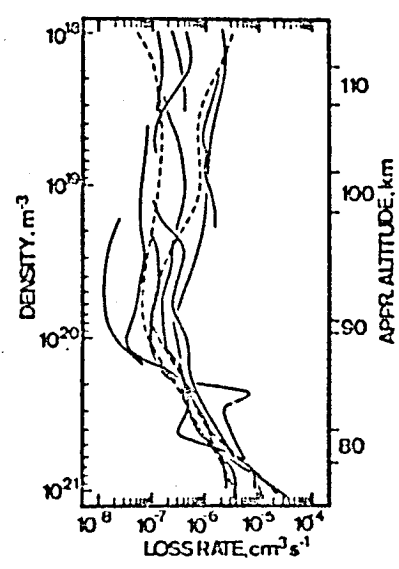


Figure 3. Collection of electron loss rates vs. neutral number density from daytime rocket flights. Dashed lines indicate the range of the standard deviation.

The ion production  $q_{\text{rest}}$  is mainly due to solar X-rays at higher altitudes (>80 km) and galactic cosmic rays below 70 km. On the two days when [NO] was measured one can deduce the rest production directly. For other days this  $q$

is applied with a suitable correction for the slightly different solar zenith angles.

The absorption of solar Lyman- $\alpha$  is computed using standard atmospheric models (COLE and KANTOR, 1978 and MSIS i.e., HEDIN et al., 1979). One can thus derive [NO] not only on the two salvo days, but for a total of fourteen days in the period of the Winter Anomaly Campaign.

Every day the signal strength of a transmitter at Aranjuez on 2.83 MHz was measured. Two receiver sites were in operation: one at the rocket range "El Arenosillo" and the other at Ealerma. The paths' mid-points were some 250 km from the rocket trajectories. The absorption was available as  $L_0$  (extrapolated subsolar value at  $\chi = 0^\circ$ ) and the exponent  $n$  of the empirical relation  $L = L_0 (\cos \chi)^n$ . In the further treatment the two absorption data sets which proved to be very similar were averaged, i.e.  $L_{0m} = \sqrt{L_{01} L_{02}}$  and  $n_m = (n_1 + n_2)/2$ .

The derivation of a statistical relationship between [NO] and A3 absorption requires reasonable parameterization of the NO-density. In a first order approximation  $[NO] \sim N_e^2 \sim L^2$  if changes of the ray geometry and production rates other than by Lyman- $\alpha$  are neglected. An altitude profile of [NO] which is not too far from current model calculations may consist of a region with constant mixing ratio below approx. the mesopause and of an exponential increase above that height. The latter assumption is only valid well below the known maximum of NO in the lower thermosphere.

[NO] on a particular day was approximated by

$$\frac{[NO]}{\rho} = a_1 + a_2 \exp(a_3 h)$$

$\rho$  total atmospheric density

where the coefficients  $a_i$  are at the same time functions of a normalised absorption  $L_{75}$  for a zenith angle of  $75^\circ$  which is about the mean throughout the electron density measurements and the exponent  $n_m$  in the form:

$$a_1 = b_{11} + b_{12} L_{75}^2 + b_{13} n_m$$

with

$$L_{75} = L(t) \left( \frac{\cos 75^\circ}{\cos \chi(t)} \right)^{n_m}$$

$L_{75}$  is thus the absorption measured at the time of the rocket flights, corrected for the solar zenith angle dependence which has been derived on that particular day.

In a multiple regression analysis the nine parameters  $b_{ij}$  are found which determine [NO] as a function of height,  $L_{75}$ , and  $n_m$ . One can now, although solely based on statistics, compute NO-profiles for every day from absorption data. Figure 4 shows the variation of [NO] thus derived between 70 and 100 km and Dec. 17, 1975, and Feb. 8, 1976. The profiles are not unique, are, however, plausible and possible. The latter was tested by inserting the [NO] into an ion-chemical scheme (TORKAR and FRIEDRICH, 1983) to compute electron densities for various solar zenith angles. The diurnal variation of simulated absorption agreed reasonably well with the one actually measured ( $L_0$ ,  $n$ ) on the particular days.

#### RELATION TO OTHER, RELEVANT MEASUREMENTS

A scenario such as shown in Figure 1 had been anticipated long before the

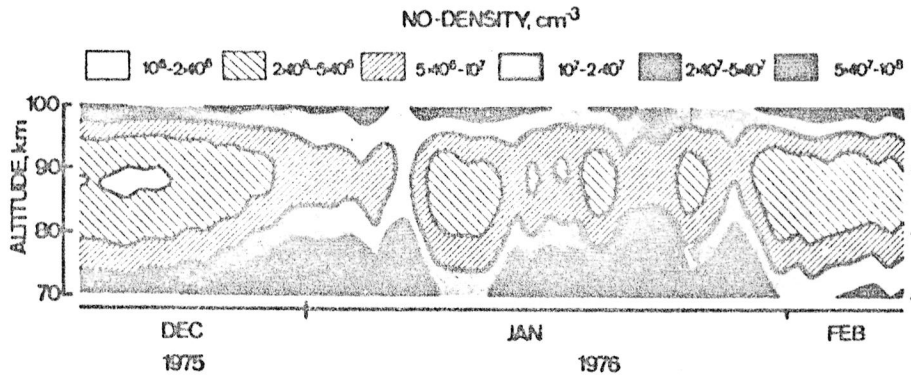


Figure 4. Variation of (NO) deduced from absorption measurements during the Winter Anomaly Campaign.

Winter Anomaly Campaign (e.g. ZIMMERMAN and NARCISI, 1970). The choice of the instruments for the campaign was therefore either to be able to rule out certain explanations of enhanced absorption, such as charged particles, changes in the Lyman- $\alpha$  and X-ray fluxes, or to support certain concepts such as enhanced [NO] and its transport (wind measurements). Of relevance to the concept that NO-transport is the dominant cause for winter anomaly, are the measurements of winds, temperature and pressure.

From the balloon and rocket-borne temperature measurements (cf. Figure 2) one can -- with a little interpolation -- establish a temperature field up to 70 km. In addition, there are radiance data available from the PMR (= Pressure Modulator Radiometer) aboard the satellite Nimbus-6. The weighting function peaks somewhere just below 80 km and has a width of about 20 km. Temperatures above 70 km were deduced by inserting the temperatures below that height (from the rocket and balloon data) into the weighting function; the temperatures from an atmospheric model (COLF and KANTOR, 1978) were modified until agreement between the radiances modelled and observed by the satellite instrument was achieved. The departures from the reference were forced to return at greater height (>90 km) since the radiance data are no longer relevant for these heights. The resulting temperature field is depicted in Figure 5 from the ground to 110 km. With the temperatures of that figure and the ground pressure, altitudes of constant pressure were established using the hydrostatic equation. Figure 6 shows these levels, crosses indicate the corresponding altitudes of the 10 pa values on World Meteorological Days as derived by LABITZKE et al. (1979). Figure 7 shows the zonal and meridional winds which were measured between 1500 and 1800 LT by the same rockets as indicated in Figure 2 (after REES et al., 1979).

Many authors have sought connections between radio wave absorption and temperature (BOSSALASCO and ELENA, 1963; OFFERMANN, 1977b) or with winds (e.g. DIEMINGER et al., 1974). None of these attempts was particularly convincing, not even if a multiple correlation was applied (REES et al., 1979). Similarly, the present data show no striking connection to derived [NO] (absorption), except perhaps increased NO-densities following the temperatures around 80 km with a delay of a few days. One could similarly try to associate winter anomaly to southward winds (early Jan, 1976), although after the time of winter anomalous absorption (February) winds are also directed southward. The relation to the zonal winds is even less conclusive.

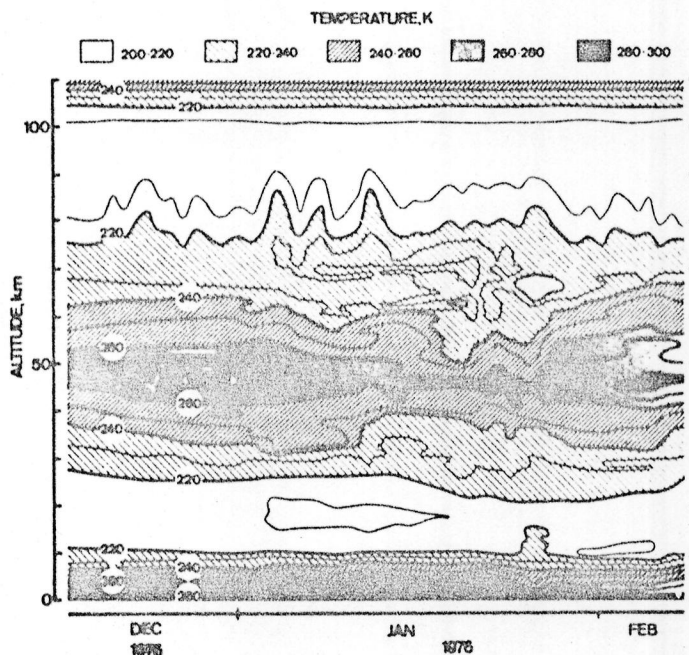


Figure 5. Temperatures during the Winter Anomaly Campaign.

From the observations, but also from theoretical considerations, it appears unrealistic to expect a correlation to the wind velocities, their directions, or temperatures, i.e. NO transport from the dark polar region and the temperature control of the electron loss rate contribute only negligibly to the observed variations of absorption. Neither the ionising fluxes, nor the electron loss rates showed significant variations, hence the winter anomaly observed in that campaign must have been of the truly meteorological type ("NO-anomaly"). Since there was no evidence for horizontal transport, downward eddy transport is expected to have been the main cause of the absorption anomaly.

A measure of turbulence, which in turn gives rise to eddy transport, is the Richardson number.

$$R_i = \frac{g}{T} \frac{(dT/dh) + \Gamma}{(dv_z/dh)^2 + (dv_m/dh)^2}$$

g acceleration due to gravity  
T temperature  
 $\Gamma$  adiabatic lapse rate ( $9.8 \text{ K km}^{-1}$ )  
h height  
 $v_z$  zonal wind component  
 $v_m$  meridional wind component

$R_i$  below 0.25 initiate turbulence, whereas below 1 maintains it. In Figure 8 areas are indicated where  $R_i$  is below 1 and 20. These values do not indicate turbulent regions, but suggest that turbulence is likely to have occurred at

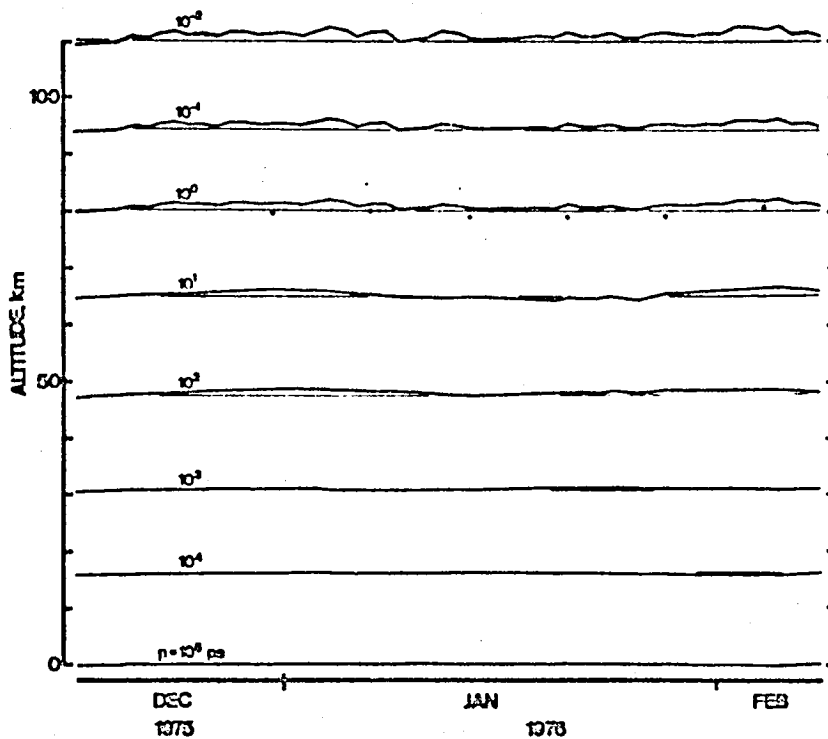


Figure 6. Heights of constant pressures built up from the temperatures in Figure 5. Crosses mark the corresponding heights from the analysis by LABITZKE et al. (1979). Straight lines represent the reference atmosphere.

other times of the day (outside 1500 to 1800 LT). Unfortunately, again no clear-cut relation can be seen, but one has to bear in mind that the wind data are restricted to 95 km, whereas transport from above that height is probably more relevant for the D-region NO-densities.

#### CONCLUSIONS

The daily derivation of NO-densities as demonstrated here is an indirect method, however, backed by two direct measurements and tested by simulating the diurnal variation of absorption. No unique connection to temperature, wind or Richardson number could be found, but perhaps sophisticated atmospheric theories can explain the occurrence of large NO-densities from this unique set of ionospheric/atmospheric data.

#### ACKNOWLEDGEMENTS

The radiance data of the satellite Nimbus 6 were generously made available by Dr. C. D. Rodgers of the University of Oxford. The Austrian participation in the Winter Anomaly Campaign was covered by Grant 2671 of the Austrian Research Council.

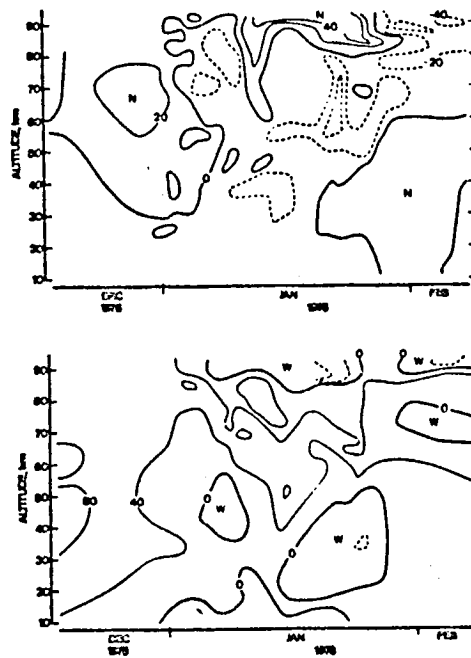


Figure 7. Zonal and meridional wind field (in  $\text{m s}^{-1}$ ) after REES et al. (1979). N = northwards, W = westward.

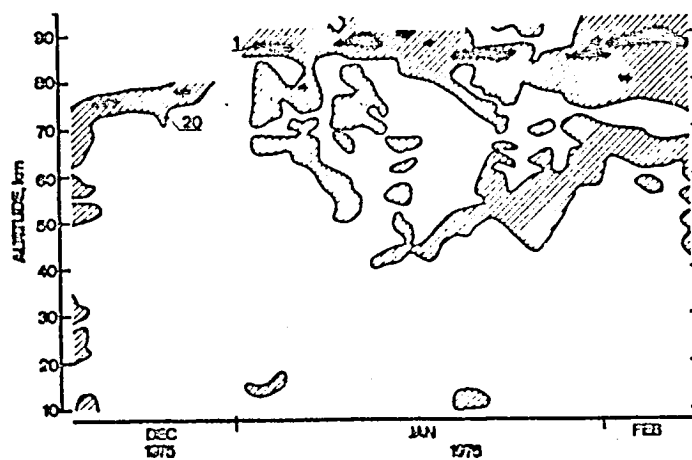


Figure 8. Height and time variation of Richardson numbers below 1 and 20 deduced from the data in Figures 5 and 7.

## REFERENCES

- Aggarwal, K. M. and C. S. G. Setty (1980), *Indian J. Radio Space Sci.*, 9, 105.
- Beran, D. and W. Bangert (1979), *J. Atmos. Terr. Phys.*, 41, 1091.
- Bossalasco, M. and A. Elena (1963), *Compt. Rend.*, 256, 4491.
- Cole, A. E. and A. J. Kantor (1978), *Air Force Reference Atmospheres*, AFGL-TR-78-0051.
- Dickinson, P. H. G., W. C. Bain, L. Thomas, E. R. Williams, D. K. Jenkins and N. D. Twiddy (1980), *Proc. R. Soc. London*, 369, 279.
- Dieminger, W., G. Rose and H. U. Widdel (1974), *Naturwissenschaften*, 61, 225.
- Friedrich, M., K. M. Torkar, K. Spenner, G. Rose and H. U. Widdel (1979), *J. Atmos. Terr. Phys.*, 41, 1121.
- Hargreaves, J. K. (1973), *J. Atmos. Terr. Phys.*, 35, 291.
- Hedin, A. E., C. A. Reber, N. W. Spencer, H. C. Brinton and D. C. Kayser (1979), *J. Geophys. Res.*, 84, 1.
- Labitzke, K., K. Petzold and H. Schwentek (1979), *J. Atmos. Terr. Phys.*, 41, 1149.
- Maehlum, B. (1967), *J. Geophys. Res.*, 72, 2287.
- Offermann, D. (1977a), *Geophysics*, 44, 1.
- Offermann, D. (1977b), in *Dynamical and Chemical Coupling Between Neutral and Ionized Atmosphere*, B. Grandal and J. A. Holtet (eds.), D. Reidel Publ. Co., pp. 235-252.
- Offermann, D. (1979), *J. Atmos. Terr. Phys.*, 41, 1047.
- Rees, D., A. F. D. Scott, J. M. Cisneros, J. M. Satrustegui, H. Widdel and G. Rose (1979), *J. Atmos. Terr. Phys.*, 41, 1063.
- Solomon, S., P. J. Crutzen and R. G. Roble (1982), *J. Geophys. Res.*, 87, 7206.
- Taubenheim, J. (1977), *Space Res.*, XVII, 271.
- Thomas, L. and M. R. Bowman (1972), *J. Atmos. Terr. Phys.*, 34, 1843.
- Thrane, E. V., B. Grandal, O. Hagen, F. Ugletveit, W. Bangert, D. Beran, M. Friedrich, A. Loidl, H. Schwentek and K. M. Torkar (1979), *J. Atmos. Terr. Phys.*, 41, 1097.
- Torkar, K. M., M. Friedrich and P. Stauning (1980), *J. Atmos. Terr. Phys.*, 42, 183.
- Torkar, K. M. and M. Friedrich (1983), *J. Atmos. Terr. Phys.*, 45, 369.
- Zimmerman, S. P. and R. S. Narcisi (1970), *J. Atmos. Terr. Phys.*, 32, 1305.

N85

20453

UNCLAS

D3  
16

N 85 - 20453

MIDDLE ATMOSPHERE TEMPERATURE AND DYNAMICS AS REVEALED  
FROM D-REGION OBSERVATIONS

A. D. Danilov

Institute of Applied Geophysics  
Glebovskaya 20-b  
Moscow 107258, USSR

The concept of so-called meteorological control of the ionospheric D-region is presently undergoing development (see, e.g., TAUBENHEIM, 1983; DANILOV and TAUBENHEIM, 1983). According to this concept the electron concentration in this region is governed not only by solar and geomagnetic parameters ( $W$ ,  $X$ ,  $A_p$ , etc.) but strongly depends on the temperature and dynamical regime of the mesosphere and stratosphere. The aim of this paper is to consider how the above connection between D-region and meteorological parameters can be used to obtain some information about middle atmosphere temperature and dynamics. For this purpose it is worthwhile summarizing briefly the essential points of the meteorological control concept.

The best illustration of the meteorological control presents the well-known phenomenon of Winter Anomaly in radio wave absorption (WA). There are two components of the WA. Average absorption,  $L$ , in the SW-band in winter is higher than that in summer ("normal" WA component). On some winter days ("anomalous" days of WA)  $L$  is much higher than on previous and following days. Since the increase of  $L$  is due to the enhancement of electron concentration,  $[e]$ , at altitudes 75-85 km (FRIEDRICH et al., 1979; OFFERMANN, 1979), WA provides a good example of  $[e]$  variations in the D region, which are not directly connected with any changes in solar zenith angle  $X$ , solar or geomagnetic activity.

Using a data bank of rocket  $[e]$  measurements, compiled by DANILOV and LEDOMSKAYA (1983a), it was pointed out by DANILOV et al. (1982), that there is one more difference in  $[e]$  behavior in the upper D region between summer and winter. If we look to the electron concentration at fixed altitude in summer there is nearly no day-to-day scattering of the data and the variation with  $X$  is well pronounced. In winter, however, even for undisturbed days (non-anomalous days) there is strong day-to-day scattering of  $[e]$ . This is illustrated in Figure 1, where rocket data for 80 km height taken from the above-mentioned data bank, only for quiet geomagnetic conditions ( $K_p < 4$ ) and middle geomagnetic latitudes, are presented.

To explain the effects of the meteorological control mentioned above one should examine possible mechanisms of neutral atmosphere influence on the electron concentration. The principal approach to the problem is rather simple. The electron concentration in the upper D region is governed by the photochemical equilibrium equation.

$$q = [e]^2 \alpha_{\text{eff}} \quad (1)$$

where  $q$  is the ionization rate and  $\alpha_{\text{eff}}$  the effective recombination coefficient. Thus changes in  $[e]$  can be due to variations of either  $q$ , or  $\alpha_{\text{eff}}$  or both. To reveal the mechanisms of meteorological control it is necessary to look for the dependence of  $q$  and  $\alpha_{\text{eff}}$  on the meteorological situation in the strato-mesosphere.

It is widely known (MITRA and ROWZ, 1972; MITRA, 1974; DANILOV, 1975) that the effective recombination coefficient depends on the positive ion composition:

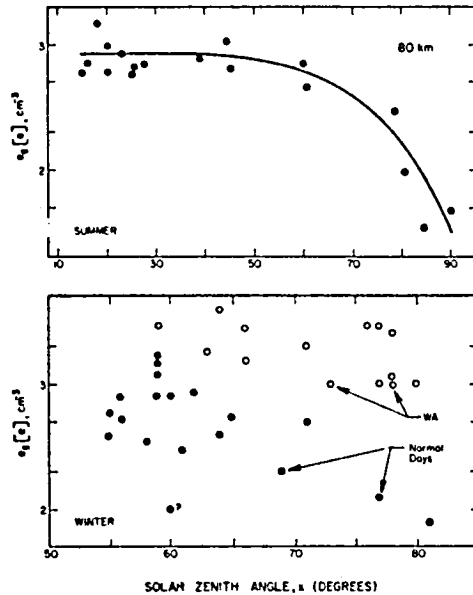


Figure 1. Electron concentration versus solar zenith angle  $\lambda$  at 80 km (DANILOV et al., 1982) for quiet conditions ( $K_p < 4$ ) and middle geomagnetic latitudes ( $\Lambda = 30-52^\circ$ ).

$$\alpha_{\text{eff}} = \frac{\alpha^*(\text{NO}^+, \text{O}_2^+) + f^+ \alpha^*(\text{clust}^+)}{1 + f^+} \quad (2)$$

$f^+$  being an ion composition parameter,  $f^+ = [\text{clust}^+]/[\text{NO}^+ + \text{O}_2^+]$ , and  $\alpha^*(\text{NO}^+, \text{O}_2^+)$ ,  $\alpha^*(\text{clust}^+)$  the dissociative recombination coefficients for normal and clustered positive ions, respectively. Though the constants  $\alpha^*$  themselves depend on neutral temperature as  $T^{-n}$ , with  $n = 0.5$  to 1, the major effect on the meteorological control through  $\alpha_{\text{eff}}$  is due to  $f^+$  variations.

It was shown by DANILOV and SIMONOV (1981, 1982), that  $f^+$  has a well pronounced seasonal variation: at fixed altitude  $f^+$  is higher in summer than in winter, and that this change of  $f^+$  accounts for a variation of the effective recombination coefficient, the latter being under quiet conditions in summer 1.5 to 2 times higher than in winter. This seasonal effect in  $\alpha_{\text{eff}}$  explains the existence of the normal component of the WA (average [e] in quiet conditions being about a factor of 1.5 higher in winter than in summer).

The reason of  $f^+$  seasonal variation is in the strong temperature dependence of the formation rate of clustered ions (DANILOV and TAUBENHEIM, 1983; SMIRNOVA et al., 1983). Reactions, leading to cluster ions, first of all the reaction



have an inverse temperature dependence, whereas most of the reverse reactions destroying clusters have a direct dependence on temperature. As a result, the net effectiveness of cluster formation from  $\text{NO}^+$  ions  $B(\text{NO}^+)$  has a strong inverse temperature dependence. Figure 2 from SMIRNOVA et al. (1983) shows the life time,  $\tau(\text{NO}^+) = 1/B(\text{NO}^+)$ , as a function of temperature according to ARNOLD and KRANKOWSKY's (1980) ion composition data and to calculations based on REID'S (1977) theoretical scheme. One can see, that the experimental and the theoretical data fit each other and lead to a very strong temperature dependence of the type of  $B(\text{NO}^+) \propto T^{-14}$ .

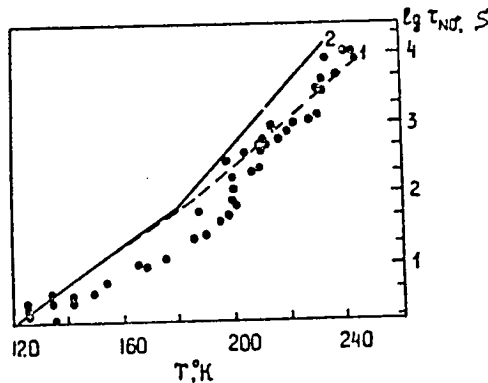


Figure 2. Life-time of  $\text{NO}^+$  ions against clustering ( $\tau(\text{NO}^+) = 1/B(\text{NO}^+)$ ) versus neutral temperature. Points: data from in situ ion composition measurements (ARNOLD et al., 1980), solid curve: calculations, based on theoretical scheme of ion transformation with  $(\text{H}_2\text{O}) = 10^{-6}(\text{M})$ , dashed curve: same with  $(\text{H}_2\text{O}) = 5 \times 10^{-6}(\text{M})$  (Smirnova et al., 1983).

It is pertinent to stress here that such a strong temperature sensitivity of cluster formation efficiency is a vital fact for the existence of a strong temperature control of the electron concentration.

Recently, the annual variations of the efficiency  $B$  of cluster ion formation were calculated using a theoretical scheme and temperature from CIRA model (SMIRNOVA et al., 1983). The results are shown in Figure 3 (curves) together with values of  $B$  estimated from experimental data of ion composition. As it is seen from Figure 3, theoretical calculations based on CIRA model well reproduce the observed features of the annual behavior of  $B$ . Summer  $B$  values are higher than winter ones, the amplitude of summer-to-winter variations being larger at high latitudes.

The arrows in Figure 3 show variations of  $B$  if  $T$  is changed by  $\pm 20^\circ$  from the CIRA values. It is seen that these relatively small changes in  $T$  lead to rather strong effects in  $B$ . Further estimates show that these  $B$  variations both in summer and winter produce nearly equal changes of  $f^+$ . But in summer the variations in  $f^+$  virtually do not influence  $\alpha_{\text{eff}}$  (and so  $[e]$ ) because  $f^+ \gg 1$  so that  $\alpha_{\text{eff}} = \alpha^*(\text{clust}^+)$ . In winter (when  $f^+$  is of the order of 1) the effective recombination coefficient is very sensitive to  $f^+$  variations so that changes in  $f^+$  induced by temperature variations would lead to  $[e]$  variations of the order of factor 2 at middle latitudes and factor 3 in the auroral region.

Thus, day-to-day variations of the electron concentration in winter mentioned above can be accounted for in terms of day-to-day temperature variations in the mesopause region, which are quite able to reach 15-20°. An essential point should be stressed here. The difference in the ion composition between winter and summer conditions leads to quite a different reaction of [e] to small variations of the neutral temperature. So these variations would make nearly no effect in summer, but produce considerable day-to-day variations in winter. During WA events usually a temperature increase is observed which is responsible for the observed decrease of  $f^+$  during WA (see below).

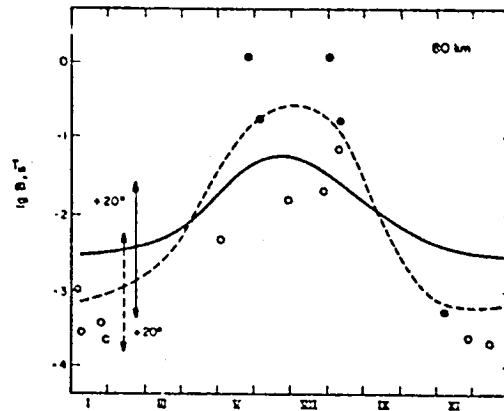
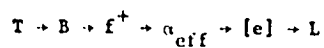


Figure 3. Annual variation of the effectiveness  $B$  of clustered ion formation at 80 km (Smirnova et al., 1983). Dots: values of  $B$ , calculated from simultaneous data on electron concentration and ion composition. Solid and dashed lines: annual variation of  $B$  at middle ( $\approx 40^\circ$ ) and high ( $\approx 70^\circ$ ) latitudes, respectively, calculated with detailed model of clustered ions formation using the temperature from CIRA model. Arrows show the limits of  $B$  if  $\pm 20^\circ$  temperature deviations from CIRA values are used in the calculations.

The role of the humidity variations on  $B$  values also has been considered by SMIRNOVA et al. (1983). The curves in Figure 3 are calculated for  $[H_2O] = 10^{-6}[M]$ . If the  $H_2O$  mixing ratio is enhanced to  $5 \times 10^{-6}$ , the corresponding enhancement of  $B$  is higher in winter (about factor 4) and lower in summer (factor 1.5-2).

Resuming, the above calculations show that the experimentally observed seasonal variations of the ion composition (which, as shown above, leads to the systematic summer-to-winter difference in the electron concentration) can be accounted for by seasonal changes of the mesospheric temperature. The reasonable assumption about the existence of day-to-day temperature variations of  $\pm 20^\circ$  explains the scatter of the [e] data in winter. During WA events the observed temperature enhancement can well account for the detected decrease of  $f^+$  and thus contribute to the [e] increase. Atmospheric temperature is therefore an important parameter strongly influencing the upper D-region ionization-recombination cycle through the channel:



It is widely known that the principal ion production process in the upper D-region in absence of solar flares and corpuscular intrusion is photoionisation of nitric oxide molecules by solar Lyman- $\alpha$  emission. Since nitric oxide is not practically produced in the midlatitude D-region, one may expect that the influence of the chemical processes and the temperature on its concentration should be rather weak. But [NO] should be very sensitive to changes in strato-mesospheric dynamics because it is transport processes that govern the nitric oxide distribution in the D-region. The NO influence on the D-region behavior is strongly confirmed by the fact that during WA events nitric oxide concentration at 70-90 km has been found to be much higher than during normal days (BERAN and BANGERT, 1981).

Calculations, based on rocket experiments in which [e] and the ion composition have been measured simultaneously (DANILOV et al., 1982), also show that in order to account for strong increase of [e] during WA events one has to assume (in addition to the decrease of  $\alpha_{\text{eff}}$  due to decrease of  $f^+$ ) an increase of [NO] up to a factor of 10. The same estimates, on the other hand, show no pronounced difference between average q values for quiet summer and winter days, which means, that for quiet conditions there is no regular seasonal difference in [NO].

The increase of nitric oxide concentration on some winter days giving rise to WA events is the strongest known manifestation of meteorological influence on the D region. Knowing the mechanisms of the influence, we would be able to get information about the dynamics of the mesosphere and lower thermosphere from D-region observations.

There are two main processes which are able to supply NO to the mid-latitude D-region: downward transport from the E region due to eddy diffusion and mean motion, and equatorward transport of NO molecules from the high latitude D-region, where those molecules are formed because of corpuscular intrusion. Estimates show (LAUTER et al., 1976; DANILOV and LEDOMSKAYA, 1982), however, that in order to get a sufficient effect on midlatitude [NO] through the second process one has to have rather strong latitudinal gradient of [NO] of about a factor 10 between mid- and high latitudes, which does not agree with satellite observations. Nevertheless, some correlation between [e] in the D-region and equatorward horizontal circulation has been found (GELLER et al., 1976; HESS and GELLER, 1978).

Thus, the main source of NO in the midlatitude D-region is downward transport from the E-region, where NO molecules are produced in the ion reactions. Concentrations of nitric oxide at 70-90 km depend strongly on the value and the vertical profile of the eddy diffusion coefficient,  $K_t$ . Figure 4 shows [NO] distributions calculated by DANILOV and LEDOMSKAYA (1983b) with various assumptions about the  $K_t$  profile. It is seen from Figure 4 that by varying  $K_t$  in reasonable limits of  $10^5$ - $2 \times 10^7 \text{ cm}^2 \text{ s}^{-1}$  one can get any nitric oxide values in the interval  $10^6$ - $10^7 \text{ cm}^{-3}$ , which means that one can account for any experimentally observed NO variations including increase of [NO] by a factor 3-5 in WA conditions. Not accounted for are only very high [NO] values of the order of  $10^8$ - $10^9 \text{ cm}^{-3}$  reported by some authors during strong WA events. To explain these values in terms of increased eddy diffusion one has to assume very high  $K_t$  values above  $2 \times 10^7 \text{ cm}^2 \text{ s}^{-1}$  which seem to be unrealistic. Further estimates show that enhanced mean motions are effective in transporting [NO] molecules downward to the D-region, when turbulence is weak ( $K_t$  low), but cannot provide essential input to NO downward flux when  $K_t$  is high.

Therefore, turbulence provides the major dynamical mechanisms of meteorological control, influencing nitric oxide distribution, thereby changing the ion production rate q. Thus the eddy diffusion coefficient  $K_t$  might be in principle considered as one of the "governing" meteorological parameters for the D-region.

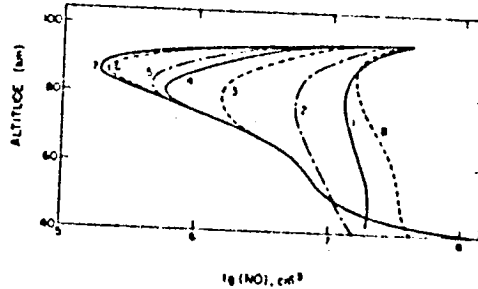


Figure 4. Calculated nitric oxide profiles (DANILOV and LEDOMSKAYA, 1982), using various values and vertical profiles for eddy diffusion coefficient  $K_t$ . Curves labeled 1, 2, 3, 4, 6 are exponential profiles with  $K_t(80 \text{ km}) = 2 \times 10^7, 1.2 \times 10^7, 1.8 \times 10^7 \text{ cm}^2 \text{ s}^{-1}$ , respectively. In these calculations a constant value of  $0.5 \text{ cm s}^{-1}$ , respectively. Curves 5, 7, 8 are profiles with maximum at 90 km and  $K_t(80 \text{ km}) = 2 \times 10^7, 1.2 \times 10^7, 1.8 \times 10^7 \text{ cm}^2 \text{ s}^{-1}$ , respectively. In these calculations a constant value of  $0.5 \text{ cm s}^{-1}$  was accepted for the velocity of the mean downward motion.

Unfortunately our knowledge about the turbulence regime in the middle atmosphere, its nature, sources (e.g., wave dissipation, wind shears), characteristic scales, seasonal variations etc., is rather scarce. Valuable information can be found from mass-spectrometer measurements of the turbopause level  $h_t$  (DANILOV et al., 1979, 1980). In particular it was found that  $h_t$  supposed to be inversely proportional to  $K_t$ , is decreasing with the increase of the neutral temperature at 120 km (DANILOV et al., 1979). This result initially obtained for high latitude measurements, has recently been confirmed for mid-latitude flights. It has been interpreted by KALGIN and POKHUNKOV (1981) as confirmation of the theoretical statement that the value of  $K_t$  near the turbopause should be inversely proportional to the temperature gradient between the mesopause and the turbopause:

$$K_t = (dT/dh)^{-1}_{80-120 \text{ km}}$$

If so, we can try to connect temperature variations observed in WA events with the suggested increase of turbulence. In fact, temperatures at the mesopause level during WA days are 20-50 K higher than during quiet days (e.g., OFFERMANN, 1979; OFFERMANN et al., 1979), but there is no increase of T at turbopause heights, sometimes even some decrease is detected. That means that on WA days  $dT/dh$  at 80-120 km is much lower than on normal days, which can account for higher  $K_t$  values and consequently for higher [NO] in the D-region. This conception is schematically illustrated in Figure 5.

Now, the very important question is for the causes of the above increase of the temperature, and whether this increase is the reason for the enhancement of turbulence as described above, or both temperature and  $K_t$  variations are due to the same initial source. This question is still open, but there is a strong temptation to connect both facts with the dissipation of the wave energy in the upper mesosphere. Unfortunately we still know very little about the mechanisms of wave propagation through the middle atmosphere, about the conditions of its energy dissipation etc., so at the moment it is difficult even to identify these waves - internal gravity, or planetary waves. But it seems worth mentioning (see e.g., DICKINSON, 1968; GELLER, 1981) that the penetration of planetary

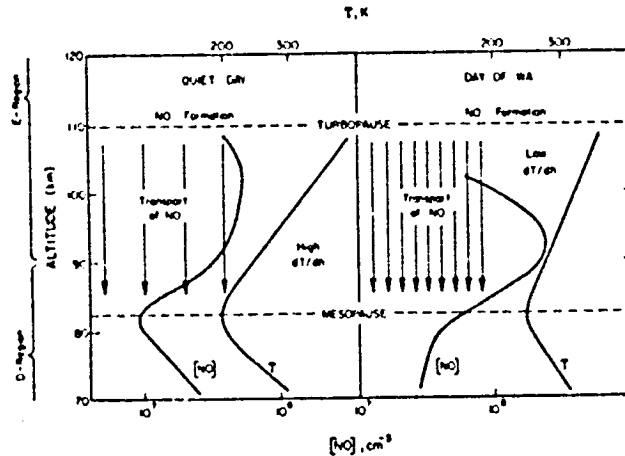


Figure 5. Schematic representation of the processes of NO transport on normal and WA days.

waves through the stratosphere is possible only during periods of west-to-east zonal circulation, which take place only in winter. If that is so and if dissipation of the planetary waves causes the above effects in T and K, then we have at least an explanation why the Winter Anomaly is observed during winter only.

Thus, all the above can be reformulated in terms of our initial task to get information about the middle atmosphere from D-region observations. The regular seasonal variations of electron concentration in the upper D-region give a good indication on the amplitude of summer-to-winter variation of neutral temperature. More detailed information, including water vapor concentration, can be obtained if both [e] and ion composition are measured together. Day-to-day variations in [e] (or L as the more widely available parameter) may provide information about day-to-day changes in T. Days of anomalous winter absorption show that there is an increase of temperature at mesopause heights and an intensification of turbulence at 80-120 km, as well as an increase of nitric oxide concentration in the mesosphere, and presumably an enhancement of wave processes. At the modern stage of our D-region studies the above relations can be used to get more information about the character of temperature variations and the nature and variations of the turbulence and wave processes.

#### REFERENCES

- Arnold, F., D. Krankowsky, E. Zettwitz and W. Joos (1980), *J Atmos. Terr. Phys.*, **42**, 249.
- Bern, D. and W. Bangert (1981), *J. Atmos. Terr. Phys.*, **41**, 1091.
- Danilov, A. D. (1975), *J. Atmos. Terr. Phys.*, **37**, 885.
- Danilov, A. D., U. A. Kalgin and A. A. Pokhunkov (1979), *Space Res.*, **XIX**, 173.
- Danilov, A. D., U. A. Kalgin and A. A. Pokhunkov (1980), *Space Res.*, **XX**, 83.
- Danilov, A. D. and S. U. Ledovskaya (1982), *Ionosfernye Issledovaniya*, No. 32, (in Russian), Izd. Sovetskoe Radio, 45.
- Danilov, A. D. and S. U. Ledovskaya (1983a), *Proc. Inst. Experimental Meteorology* (in Russian), **13**, 102.
- Danilov, A. D. and S. U. Ledovskaya (1983b), *Geomagnetism and Aeronomy* (in Russian), **23**, (to be published).

- Danilov, A. D. and A. G. Simonov (1981), *Geomagnetism and Aeronomy* (in Russian), 21, 932.
- Danilov, A. D. and A. G. Simonov (1982), *J. Atmos. Terr. Phys.*, 44, 567.
- Danilov, A. D., A. G. Simonov, N. V. Smirnova and S. U. Ledonskaya (1982), *Prostranstvenno-vremennaya struktura ionosfery* (in Russian), Moscow, 43.
- Danilov, A. D. and J. Taubenheim (1983), *Space Sci. Rev.*, 34, 413.
- Dickinson, R. F. (1968), *J. Atmos. Sci.*, 25, 984.
- Friedrich, M., K. M. Torkar, K. Spinner, G. Rose, and H. U. Widdel (1979), *Planet. Space Sci.*, 41, 1121.
- Geller, M. A. (1981), *Exploration of the Polar Upper Atmosphere*, (ed. by G. S. Deehr and J. A. Holtet), D. Reidel, Dordrecht, Holland, pp. 1-16.
- Geller, M. A., G. C. Hess and D. J. Wratt (1976), *J. Atmos. Terr. Phys.*, 28, 287.
- Hess, G. C. and M. A. Geller (1978), *J. Atmos. Terr. Phys.*, 40, 895.
- Kalgin, U. A. and A. A. Pokhunkov (1981), in *Ionosfernye Issledovaniya*, No. 34 (in Russian), Soviet Geophysical Committee, p. 66.
- Lauter, E. A., J. Taubenheim, G. Entzian, J. Bremer, G. v. Cossart and G. Klein (1976), *HHI-STP Report No. 7*, Central Institute of Solar-Terrestrial Physics, Berlin-Adlershof, GDR, 84 pp.
- Mitra, A.P. (1974), *Ionospheric Effects of Solar Flares*, D. Reidel, Dordrecht, Holland.
- Mitra, A. P. and J. N. Rowe (1972), *J. Atmos. Terr. Phys.*, 34, 795.
- Offermann, D. (1979), *J. Atmos. Terr. Phys.*, 41, 735.
- Offermann, D., P. Curtis, J. M. Cisneros, J. Satrustegui, H. Lauche, G. Rose and K. Petzold (1979), *J. Atmos. Terr. Phys.*, 41, 1051.
- Reid, G. C. (1977), *Planet. Space Sci.*, 25, 275.
- Smirnova, N. V., A. G. Simonov and A. D. Danilov (1983), *Geomagnetism and Aeronomy* (in Russian), 23, 552.
- Taubenheim, J. (1983), *Space Sci. Rev.*, 34, 397.

N85

20454

UNCLAS

D4

24

# N85-20454

## SYNOPSIS OF MID-LATITUDE RADIO WAVE ABSORPTION IN EUROPE

K. M. Torkar

Space Research Institute of the Austrian Academy of Sciences  
c/o Technical University of Graz  
Inffeldgasse 12, A-8010 Graz  
Austria

M. Friedrich

Department of Communications and Wave Propagation  
Technical University of Graz  
Inffeldgasse 12, A-8010 Graz  
Austria

### ABSTRACT

Radio wave absorption data covering almost two years from Europe to Central Asia are presented. They are normalised by relating them to a reference absorption. Every day these normalised data are fitted to a mathematical function of geographical location in order to obtain a daily synopsis of radio wave absorption. A film of these absorption charts was made which is intended to reveal movements of absorption or absorption anomaly. In addition, radiance (temperature) data from the lower D-region are also plotted onto these charts. No conclusions are drawn; the new procedure to evaluate absorption data is -- at the present stage of processing -- merely intended to stimulate discussion and interest.

### INTRODUCTION

Radio wave absorption in the HF range occurs predominantly in the ionosphere's D-region, i.e. at heights where absorption  $L$  is proportional to both electron density and collision frequency  $\nu$ . Since  $\nu$  is very well predictable via atmospheric pressure (cf. e.g. FRIEDRICH and TOKAR, 1983) it is the electron density  $N_e$  which determines the day-to-day variations of  $L$ . At high latitudes all changes of  $N_e$  are attributable to variations of the ionising fluxes i.e. of charged particles; at low or middle latitudes, however, the fluxes responsible for the formation of the daytime D-region (solar Lyman- $\alpha$ , X-rays, etc.) do not vary drastically, not even in the course of a sunspot cycle. The observed day-to-day variations in (mid-latitude) radio wave absorption by factors of 2 to 3, notably in winter (winter anomaly), are therefore generally attributed to changes in the concentration of nitric oxide (NO), the only component of the middle atmosphere (mesosphere) which can be ionised by the relatively strong solar H Lyman- $\alpha$  line. The following analysis is plausible if one assumes that changes in the NO-concentration are the principal cause for changes of absorption.

### DATA BASE AND NORMALISATION

There have been numerous attempts to study the morphology of winter anomalous absorption (e.g. BEYRON and WILLIAMS, 1976), in recent times notably by SATO (1981) who used  $f_{min}$  data from stations in Europe, the USSR and North America. The aim was to find a connection to geomagnetic activity, but the analysis is severely hampered by the relatively coarse classification of  $f_{min}$ .

In the present treatment we use absorption, i.e. loss of signal strength relative to absorption-free reflection. Both the methods A1 (vertical incidence) and A3 (oblique incidence, i.e. reception of a distant transmitter) are used. Table 1 gives the acronyms of the various data sets, path lengths,

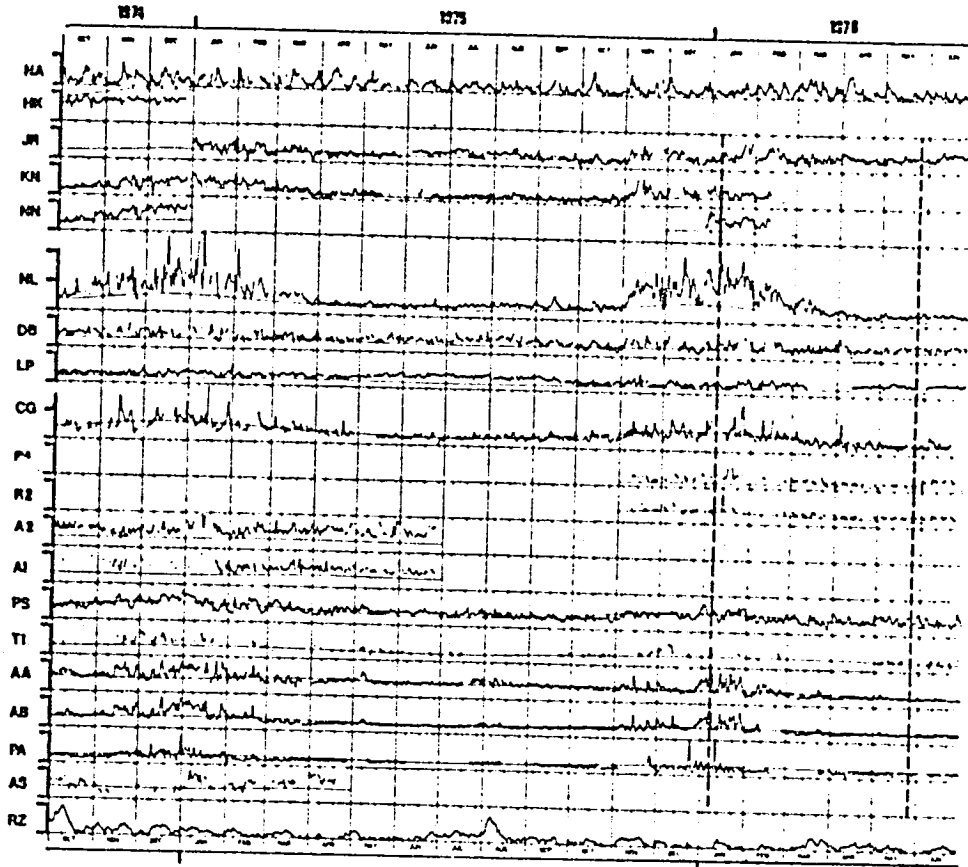


Figure 1. Absorption measurements of the available stations. NA is the daily integrated riometer-absorption at Narssarssuaq, Greenland, and RZ the Zurich sunspot number, all other acronyms are explained in Table 1. Between bars indicates 60 dB, the smooth lines are the simulated reference absorptions and the dashed lines show the days used as examples for absorption patterns (Figure 3).

AA and AB which use the same transmitter but different receivers (distance of the path mid-points ca. 120 km). Hence the observed rapid variations must be considered to be of ionospheric origin and not -- as one might be tempted to believe -- poorly maintained equipment or local interference.

Due to different path lengths, frequencies and the type of measurement (daily integrated absorption  $L_D$ , noon-absorption  $L_{noon}$  etc.) the various data sets show necessarily different seasonal trends and variabilities. Hence the observed absorptions at various locations may be covered up by the above mentioned, expected systematic effects. Therefore a procedure was sought by which in a first approximation these differences can be eliminated. Consequently a reference absorption for each data set and each month was calculated. For this purpose electron densities were computed for the

Table 1.

		frequency MHz	distance km	type	weight		geographic coordinates of midpoint	mean absorption height	
					summer	winter		summer	winter
HK <sup>1)</sup>	Hörby-Kühlungsborn	1.178	225	cos $\gamma$ = 0.2	-	-	55.0N, 12.7E	92.72	90.13
JR	Juliusruh	2.000	-	noon	1.61	0.65	54.6N, 12.4E	91.24	104.08
KN	Kiel-Neustrelitz	2.775	220	cos $\gamma$ = 0.2	0.42	0.75	53.9N, 11.6E	98.50	99.43
NN	Norddeich-Neustrelitz	2.614	395	cos $\gamma$ = 0.2	-	1.05	53.5N, 10.1E	91.25	89.83
NL	Norddeich-Lindau	2.614	296	$\gamma_D$ <sup>2)</sup>	0.93	0.77	52.8N, 8.7E	90.26	98.57
DB	De Bilt	1.850	-	noon	1.53	0.90	52.1N, 5.2E	90.89	96.47
LP <sup>2)</sup>	Luxembourg-Prague	6.090	610	noon	-	-	50.1N, 10.3E	89.02	96.35
CG	Coburg-Craz	2.630	502	$\gamma_D$	1.10	0.96	48.7N, 13.2E	87.69	95.29
R2	Rostov-on-Don	2.000	-	$\gamma_D$	0.87	1.07	47.2N, 39.7E	92.73	93.96
R4	Postov-on-Don	4.000	-	$\gamma_D$	0.48	0.74	47.2N, 39.7E	83.35	83.13
A1	Alma Ata	1.700	-	noon	0.97	1.09	43.3N, 78.9E	88.57	89.55
A2	Alma Ata	2.200	-	noon	1.52	1.36	43.3N, 78.9E	90.70	93.04
PS	Priština-Sofia	1.412	170	cos $\gamma$ = 0.2	0.71	1.26	42.7N, 22.2E	93.37	92.29
T1	Tbilisi	1.700	-	$\gamma_D$	1.02	1.10	41.4N, 44.5E	90.38	92.97
AA	Aranjuez-El Arenosillo	2.830	424	noon <sup>3)</sup>	0.90	1.07	38.6N, 5.2W	87.14	89.51
AB	Aranjuez-Balerna	2.830	374	$\gamma_D$	1.13	1.17	38.4N, 3.2W	88.03	90.45
PA	Patras	)	)	$\gamma_D$	0.87	1.05	38.0N, 23.8E	86.34 <sup>4)</sup>	88.96 <sup>4)</sup>
AS	Ashkhabad	1.800	-	noon	1.04	1.12	37.9N, 58.0E	88.98	89.94
								90.00	93.31

<sup>1)</sup> not used in the further analysis, possibly ground wave propagation

<sup>2)</sup> not used in the further analysis

<sup>3)</sup> monitors the 31 and 49 m broadcast band; appr. linearly related to Rome-Athens on 6.080 MHz (ILIAS and GUPTA, 1979)

<sup>4)</sup> except March 22 to June 30, 1976; cos $\gamma$  = 0.2

<sup>5)</sup> except December 1975 to February 1976;  $\gamma_D$

<sup>6)</sup> applies to Rome-Athens

frequencies and (path mid-point) coordinates. Subject to the availability of the raw data, daily integrated absorption ( $L_p$ , cf. ROSE and WIDDEL, 1977), was used, otherwise values at noon or some constant solar zenith angle were employed. Figure 1 shows the daily values of all stations from October 1974 to June 1976.

The lowest curve is the sunspot number, whereas the uppermost curve represents the average daily riometer absorption at Narsarsuaq (Greenland). The latter is included as a measure of particle influx into the auroral zone, since a connection of charged particle fluxes and mid-latitude absorption has often been sought (e.g. MAENLUM, 1967; TORKAR et al., 1980). However, only the northernmost data (JR) of February and October 1975 possibly show some direct influence of particles. On the other hand, even the relatively large sunspot numbers in August 1975 do not show up as enhanced absorption in any of the data. In most data one can clearly observe the larger absorption in winter, however, all show a larger variability in winter. Of special interest are the data sets

corresponding conditions of each station (noon,  $\cos \chi = 0.2$  or at four typical solar zenith angles  $\chi$  with equal time-spacing for  $L_D$ ) using the ion-chemical model for low solar activity described elsewhere in detail (TORKAR and FRIEDRICH 1983). In this steady-state computation the neutral atmosphere, including the minor species, is taken from other published models, in particular [NO] from RUSCH et al. (1981). Absorption was then computed by a WKB ray-tracing calculation over a spherical Earth. The full SEN and WYLLER (1960) magnetoionic formulae were employed, the magnetic field taken from CAIN et al. (1967) and the collision frequency set proportional to pressure from the AFGL seasonal atmospheric model (COLE and KANTOR, 1978). The proportionality factor of  $6.7 \times 10^5 \text{ m}^2 \text{ s}^{-1} \text{ N}^{-1}$  is the one recommended by FRIEDRICH and TORKAR (1983) based on a number of rocket measurements of  $\nu$ . The reference absorption thus obtained is indicated in Figure 1 as smooth lines. Outside winter one can see reasonably good agreement for the data KN, NL, CG, TI, AA and AB. There is notably an excess of the simulated absorption of HK. This may be due to ground wave propagation at the fairly low frequency (1.178 MHz) of the path which is mainly over sea water. Another feature of the simulated absorption is, that at higher latitudes in summer the observed absorption ([NO]) is consistently higher than in the model (JR, KN, NL, DB, LP and also PS).

For further evaluation the daily absorption values were divided by the corresponding reference absorption. This new quantity (absorption enhancement AE) removes the different sensitivity of the various measurements provided the geometry of the ray (penetration into the ionosphere) is the same.

AE should, therefore, be proportional to an electron density ratio or the square of the ratio of ion production rates; if one assumes that NO and Lyman- $\alpha$  is the dominant production process of the absorbing D-region, AE is equal to  $([NO]/[NO]_{\text{ref}})^2$ .

Before combining all absorption measurements, normalized via AE in the above manner, it was tested to what extent the various data sets measure the same physical phenomenon. Figure 2 shows relative contributions of the various layers of height  $h$  to the total absorption of some of the stations using the reference ionosphere (summer), where  $l_r(h)$  is defined as:

$$l_r = \frac{1(h)}{\int 1(h) dh} = \frac{1(h)}{L}; \frac{dB/km}{dB}; \text{ km}^{-1}$$

One can see that the height regions contributing to absorption differ greatly from station to station. For want of more uniform data, all absorption measurements were nevertheless treated as if they represented the same height regions. Hence an absorption "drift" from e.g. JR to AS could just as well mean a downward motion of enhanced electron (or NO) density at both stations.

#### CONSTRUCTION OF ABSORPTION PATTERNS

The normalized data (absorption enhancement AE) still include variations due to very local effects. Instead of constructing AE-patterns by interpolation between the individual measurements, all AE-values were fitted by analytical functions. The number of locations, or -- more importantly -- the number of simultaneously available measurements, restricts the order of the analytical expression which can be fitted to the data. The simplest form is a plane in general position requiring only three, preferably evenly spaced, points. A somewhat higher level of complexity -- a circular paraboloid -- was chosen which is determined by four parameters, namely location and value of the maximum, and the curvature. This form is employed at the present stage of the analysis; higher orders have been tested, but found to lead to unrealistic excursions. In

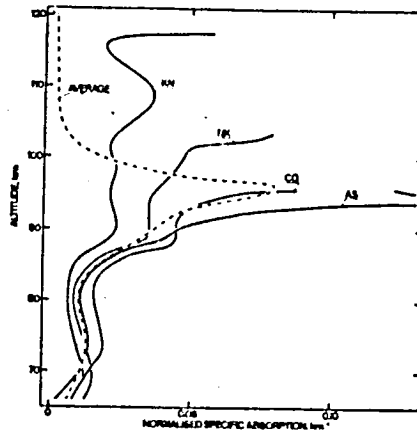


Figure 2. Relative absorption contributions of different heights of some stations together with the average absorption profile of all data sets (summer).

an attempt to account for the different height coverages (cf. Figure 2) weights  $w$  were given to the different data sets according to:

$$w = \frac{1}{\bar{L}} \int \bar{L}^2 dh$$

Here  $\bar{L}$  is the average specific absorption of all measurements divided by the average integral absorption. Its height variation is also shown in Figure 2. Table 1 contains these weights for January and July, but for the further computation these weights were also established for all other months.

Furthermore contained in this table is the mean height of the absorption derived from the same model computations. Those data which are based on  $L_D [= L_0/(1+n)]$  were given additional daily weights according to the quality of the fit  $L = L_0(\cos \chi)^n$  which led to the establishment of  $L_0$  and  $n$ . For every day four parameters were determined by fitting a paraboloid to all  $\log(AE)$ -data by a least-mean-square procedure. In the film contours of absorption enhancement of 0.8, 1.0, 1.3, 1.6 etc. are shown. In order to avoid too rapid fluctuations of the absorption (AE-)patterns, running means of the four parameters are used, i.e. 50% of the day in question and 25% each of the previous and following days.

The curves are fitted to the data in geographic Cartesian coordinates and the contours of constant absorption enhancement then transformed to the projection in which the satellite temperature data are available. In the film only those stations which provided data on the day in question are indicated by small circles. Figure 3 shows two examples where however, all possible stations are indicated with their acronyms. From October 1975 on radiance (temperature) data of the PMR (= Pressure Modulator Radiometer) of the University of Oxford aboard the satellite NIMBUS-6 are available. The weighting function of the highest channel 3000 peaks somewhere just below 80 km. The temperatures at that height are surely not decisive for enhanced electron densities (electron loss rates), but may be an indication of an unstable atmosphere, turbulence and -- in consequence -- of transport of NO into the D-region.

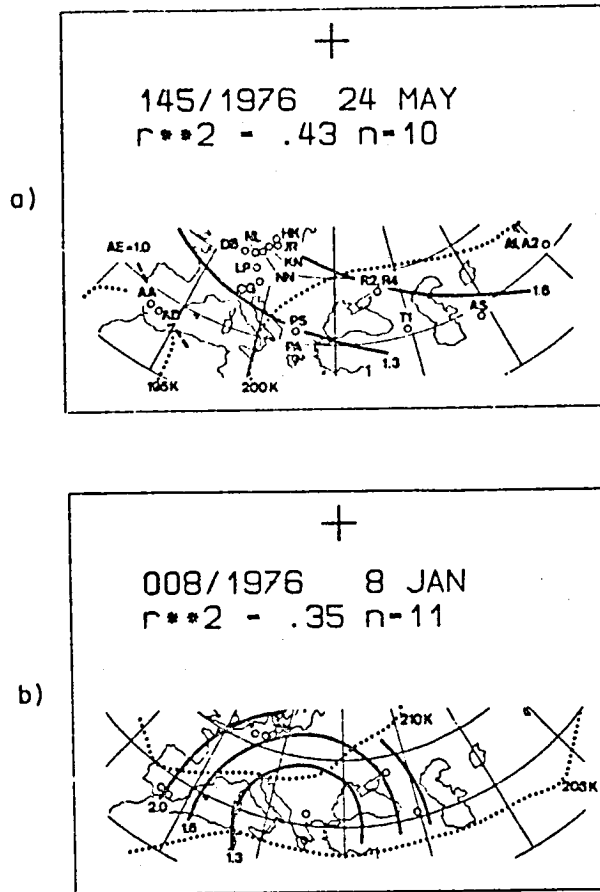


Figure 3. Examples of absorption patterns obtained by fitting an analytical function to the AE values and mesospheric temperatures. (a) typical summer, May 24, 1976, (b) winter anomalous day January 8, 1976.  $r^{**2}$  is the quality of the fit and  $n$  the number of available data for the day.

#### CONCLUSIONS AND IMPROVEMENTS

The quality of the presently available raw data does not permit to draw final conclusions concerning the magnitude or the motions of absorption. More careful screening of the absorption data is envisaged, but also the reference absorption model, which mainly hinges on the adapted [NO]-model, may have to be revised. For the derivation of velocities of absorption patterns it may perhaps suffice to use the running mean as a reference, thereby avoiding errors introduced by an unrepresentative reference absorption.

## ACKNOWLEDGEMENTS

Most of the data used herein were made accessible by the cooperation of other institutions, notably the Heinrich-Hertz-Institut (Berlin), the Max-Planck-Institut für Aeronomie (Katlenberg-Lindau), the World Data Centres in Slough and Moscow, the Astronomical Institute (Prague), the Geophysical Institute Sofia, the Technical University of Denmark (Lyngby) and the University of Athens. The radiance data were generously provided by Dr. C. D. Rodgers of the University of Oxford.

## REFERENCES

- Beynon, W. J. G. and E. R. Williams (1976), *J. Atmos. Terr. Phys.*, 38, 89.  
Cain, S. H., S. J. Hendricks, R. A. Langel and W. V. Hudson (1967), *J. Geomagn. Geoelect.*, 19, 335.  
Cole, A. E. and A. J. Kantor (1978), *Air Force Reference Atmosphere*, AF-GL-TR-78-0051.  
Friedrich, M. and K. M. Torkar (1983), *J. Atmos. Terr. Phys.*, 45, 267.  
Ilias, D. J. and G. P. Gupta (1979), *J. Atmos. Terr. Phys.*, 41, 601.  
Maehlum, B. N. (1967), *J. Geophys. Res.*, 72, 2287.  
Rose, G. and H. U. Widdel (1977), *J. Atmos. Terr. Phys.*, 39, 51.  
Rusch, D. W., R. G. Roble, J.-C. Gerard and A. I. Stewart (1981), in *Handbook for MAE*, Vol. 2 (ed. by S. K. Avery), pp. 442-449.  
Sato, T. (1981), *J. Geophys. Res.*, 86, 9137.  
Sen, H. K. and A. A. Wyller (1960), *J. Geophys. Res.*, 65, 3931.  
Torkar, K. M. and M. Friedrich (1983), *J. Atmos. Terr. Phys.*, 45, 369.

N85

20455

UNCLAS

IONOSPHERIC ABSORPTION ON 1539 KHZ IN RELATION TO SOLAR IONIZING RADIATION

J. Roska

Geophysical Institute  
Czechoslovak Academy of Sciences  
141 31 Prague 4, Czechoslovakia

ABSTRACT

Radio wave absorption data on 1539 kHz for the summer period of 1978-1980 are considered in relation to variations of solar X-ray and Ly $\alpha$  radiation. It is shown that under non-flare conditions Ly $\alpha$  dominates in controlling absorption and that X-rays contribute about 10% to the total absorption. Optimum regression equations show that absorption is proportional to the m-th power of ionizing flux,  $F_{ion}^m$ , where  $m < 1$ . The role of correcting Ly values, measured by the AE-E satellite, is discussed.

It is generally accepted that Lyman- $\alpha$  radiation plays the dominant role in the formation of the D region. But the contribution of different ionizing radiations in the lower ionosphere has not been established too well. In this paper the results of a statistical analysis of A3 absorption data are presented in relation to solar X-ray (1-8 Å) and Lyman- $\alpha$  fluxes. Radiowave absorption data measured on 1539 kHz at the Panska Ves Observatory, Czechoslovakia, (reflection point 50°16'N, 11°47'E, distance 390 km, equivalent frequency, 0.7 MHz) are used. The data set consists of the summer months (June-August) of 1978-1980, separately for the afternoon and forenoon at  $\lambda = 60^\circ$  and  $70^\circ$ . SWF events and absorption data considerably affected by geomagnetic storms have been excluded. X-ray flux data were taken from Solar-Geophysical Data bulletins (1979-1981). In the case of Lyman- $\alpha$  irradiance the question of experimental data is more complicated. The Lyman- $\alpha$  flux values used in this paper were adopted from AE-E satellite measurements (HINTEREGGER, 1981). It is very well known that there are open questions about absolute Lyman- $\alpha$  flux values measured by the AE-E satellite. Figure 1 shows the development of monthly mean values of Zurich sunspot number  $R_z$ , solar flux at 10.7 cm and also Lyman- $\alpha$  flux for the whole period under study. An unexpected enhancement of Lyman- $\alpha$  flux value can be seen at the beginning of 1979. It should also be noted that the values of Lyman- $\alpha$  flux observed during cycle 21 are higher than for cycle 20, and this increase is not matched by corresponding increases in the sunspot number or in the solar flux at 10.7 cm. As BOSSY and NICOLET (1981) have demonstrated, the differences can be explained only by systematic errors and cannot be neglected. We have corrected these Lyman- $\alpha$  flux values in the following way. As can be seen from Figure 1, the ratio of Lyman- $\alpha$  to Lyman- $\beta$  fluxes also significantly increased at the beginning of 1979. If we take into consideration that the Lyman- $\alpha$  to Lyman- $\beta$  ratio decreases in a solar active region (BONNET, 1981), we may claim that this ratio should not increase with increasing solar activity. We can assume that the ratio of Lyman- $\alpha$  to Lyman- $\beta$  is close to its value for average solar activity and has not changed during the whole period studied. We have used this assumption to correct the Lyman- $\alpha$  flux values. As can be seen from Figure 1 the corrected Lyman- $\alpha$  flux values are in better agreement with the development of solar activity. In this study both corrected and uncorrected Lyman- $\alpha$  data were used.

To derive the relation between absorption and ionizing fluxes, we calculate expressions of the type

$$L = A F_x^m + B F_\alpha^m + C$$

where L is radio wave absorption (in decibels), and F is the flux of ionizing radiation, using the least-squares method for all data sets with m between 0.3 -

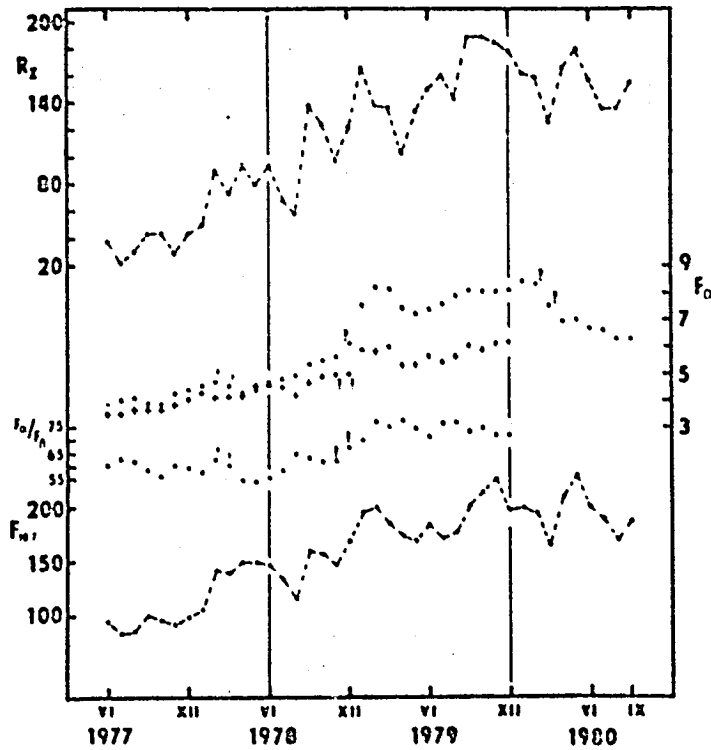


Figure 1. The development of monthly mean values of Zurich sunspot number  $R_z$ , solar flux at 10.7 cm  $F_{10.7}$ , the solar Lyman- $\alpha$  flux  $F_{\alpha}$  (circles, uncorrected values; crosses, corrected values) and ratio of Lyman- $\alpha$  to Lyman- $\beta$  fluxes,  $F_{\alpha}/F_{\beta}$ , over the period 1977-1980. ("?" indicates insufficient number of data.)

2.4. The criterion for estimating the optimum equations is the value of C (about 5 - 10% of the total absorption). All values of m, A, B, C for these optimum expressions are given in Table 1 for uncorrected Lyman- $\alpha$  data and in Table 2 for corrected data. For some data sets it was not possible to derive optimum equations.

Let us first consider the exponent m. Its values are distributed between 0.3 - 1 for the uncorrected data and between 0.35 - 0.8 for the corrected values of  $L_{\alpha}$ . A considerable part of the m values is close to the value of 0.5 to be expected from the equilibrium equation. In all cases in which we were able to derive m for both data sets the exponents m are smaller for the corrected than for the uncorrected data.

This result differs from the results of an analogous analysis of absorption on the frequency 2775 kHz and 1178 kHz for the period 1969-1972 made by LASTOVICKA and BOSKA (1982), where the value of m was evidently  $m > 1$ . The cause of this difference is not clear yet. Ratios of X-ray and Lyman- $\alpha$  con-

Table 1

		60°					70°				
		$m$	A	B	C	$L_x/L_1$	$m$	A	B	C	$L_x/L_1$
1978	a	-	-	-	-	-	0.8	1.7	10.85	3.80	0.04
1979	f	0.75	3.1	10.4	3.7	0.09	-	-	-	-	-
1979	a	0.30	3.90	29.3	10.9	0.08	1.0	1.7	5.8	1.97	0.06
1980	f	0.45	10.4	15.3	6.2	0.36	0.65	5.1	9.3	4.6	0.22
1980	a	0.5	6.6	16.6	8.5	0.20	0.6	3.4	12.5	4.9	0.11

Table 2

		60°					70°				
		$m$	A	B	C	$L_x/L_1$	$m$	A	B	C	$L_x/L_1$
1978	f	0.35	13.6	19.2	5.7	0.37	-	-	-	-	-
1978	a	-	-	-	-	-	0.55	1.7	16.5	4.2	0.04
1979	f	0.45	6.9	19.8	4.23	0.19	-	-	-	-	-
1979	a	-	-	-	-	-	0.8	3.1	10.3	3.9	0.10

contributions to total absorption,  $L_x/L_1$ , for the equations from Table 1 and 2, have been calculated using mean ionizing fluxes for all the individual data sets. The values of  $L_x/L_1$  lie between 0.04 - 0.37 and clearly display the dominant role of Lyman- $\alpha$  radiation in absorption. The typical contribution of X-rays to the total absorption under non-flare conditions is about 10%. For the corrected data sets, the contribution of X-rays is slightly greater than for the uncorrected data. Median values of the correlation coefficients between radio wave absorption and ionizing fluxes are:  $r_{L_1} = 0.33$  and  $r_{L_x} = 0.40$ , respectively. For Lyman- $\alpha$  the correlation is slightly weaker than for X-rays and this result was not significantly influenced by correcting the Lyman- $\alpha$  flux. This is probably due to the Lyman- $\alpha$  variability being small compared to the variability of X-rays.

It can be concluded that the correction of Lyman- $\alpha$  data did not change the results of the analysis significantly. The derived values of the exponent  $m$  are in good agreement with the theoretical assumptions.

## REFERENCES

- Bonnet, R. M. (1981), Space Sci. Rev., **29**, 131.  
 Bossy, L. and M. Nicolet (1981), Planet. Space Sci., **29**, 907.  
 Hinteregger, H. E. (1980), Paper No. C.1.1.6, presented at XXIII COSPAR Meeting, Budapest.  
 Hinteregger, H. E. (1981), Paper No. 2.D.3, presented at IAGA Assembly, Edinburgh.  
 Lastovicka, J. and J. Boska (1982), J. Atmos. Terr. Phys., **44**, 793.  
 Solar Geophysical Data, NOAA, Boulder, Colorado, 1979-1981.

N85

20456

UNCLAS

34  
N85-20456

INDIRECT PHASE HEIGHT MEASUREMENTS IN CENTRAL AND EASTERN  
EUROPE FOR MONITORING D REGION PLASMA

G. v. Cossart

Academy of Sciences of the GDR  
Central Institute of Solar-Terrestrial Physics  
Observatory of Ionosphere Research  
DDR-2565 Kuhlungsborn, GDR

S. V. Pakhomov

State Committee of the USSR of  
Hydrometeorology and Environmental Control  
Central Aerological Observatory  
Dolgeprudny, Moscow Region, USSR

Low-frequency propagation experiments for the investigation of the lower part of the ionospheric D region were at first used by BRACEWELL et al. (1951) at Cambridge in the early fifties. Among these was the method of indirect phase height measurements which has been further developed by LAUTER (1958) at Kuhlungsborn for continuous monitoring of the lower ionosphere. It is based upon field strength measurements of commercial radio transmitters in the frequency range between 50 and 200 kHz at distances from 500 to 1500 km. The field strength records show characteristic diurnal variations with maxima and minima, produced by interference between the ground wave and the ionospherically reflected sky wave, the phase difference between which varies in correspondence to the diurnal variation of the reflection height. The upper part of Figure 1 gives two examples of field strength records on radio frequencies of 164 kHz and 155 kHz at distances of 1023 km and 1359 km, respectively. The variations during forenoon and afternoon are quasi-symmetrical with respect to the real noon at the propagation path midpoint.

From investigations in the LF-range (SMITH, 1973) it is known that the dominant part of downcoming sky wave is the extraordinary component. On the basis of the magneto-ionic reflection condition we can calculate the electron density necessary for reflection of the extraordinary component at a given frequency and angle of incidence. For frequencies ranging from 50 to 200 kHz, these calculated reflection electron densities are between 250 and 550 el cm<sup>-3</sup>. The diurnal height variation of the level where electron density has this given value governs the interference pattern. The height difference corresponding to two successive interference extrema ranges from 2 to 5 km, depending on frequency and propagation path length. The coordination of the individual field strength extrema to corresponding reflection heights is in principle ambiguous, but if two or more simultaneous indirect phase height measurements are available this ambiguity can be removed so that a definite absolute height can be ascribed to each extremum. This coordination can also be achieved by comparison with rocket-measured electron density profiles obtained in the same location.

In the following a very simple approach of interpretation is attempted on the basis of geometric-optic consideration. The lower part of Figure 1 shows an example of height determination from measurements on two frequencies. The times of field strength extrema are referred to the respective solar zenith angles,  $\chi$ , at the propagation path midpoint and coordinated to the corresponding geometric heights. The diurnal variation of the reflection height ranges between 75 and 85 km. The relation between the reflection heights and the logarithm of the Chapman function of  $\chi$  is linear, forming during forenoon and afternoon two straight lines with different slopes. The difference between the forenoon and afternoon branches corresponds to a distinct time difference of about 10

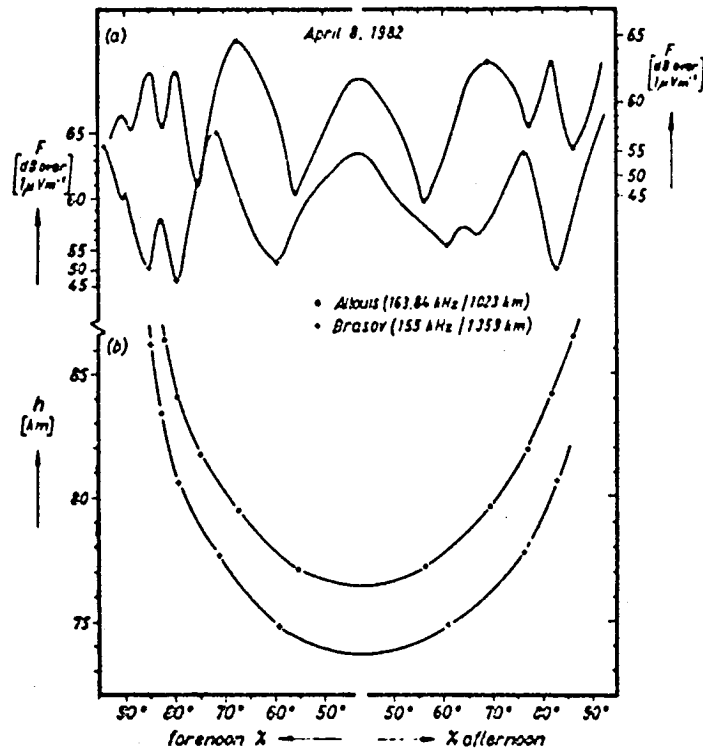


Figure 1. (a) Field strength records of LF signals on long-distance transmission paths at Kuehlungsborn. (b) Diurnal variation of apparent reflection height by coordinating each field strength extremum to its triangulation height.

minutes.

During daytime the normal electron density in the D-region between 70 and 85 km is mainly produced by nitric oxide ionization due to solar Lyman- $\alpha$ -radiation. Molecular oxygen is considered as the main absorber for solar Lyman- $\alpha$ -radiation. On the basis of this concept it can be shown that the height of a level of constant electron density in the D region indeed varies linearly with  $\ln Ch \chi$ , just as does the reflection height in our indirect phase height measurements. The time lag between the forenoon and afternoon values is due to recombination processes in the ionospheric plasma whereas the average of the forenoon and afternoon values approximately represents equilibrium conditions in the D-region. In this case the slope will represent the mean scale height of the neutral atmosphere.

In order to check the validity of this kind of interpretation, field strength measurements on two LF-measuring paths were installed in the Soviet Union, with their path midpoints situated very near to the rocket sounding station Volgograd.

A series of electron density profiles measured at Volgograd by rockets up

to a height of 85 km at different solar zenith angles well confirms the assumption that the reflection height is connected with a fixed value of electron density. Figure 2 shows the height of this reflection electron density obtained by rockets in comparison with the reflection height determined at the same solar zenith angle from indirect phase height measurements. The slope of the regression line does not show the expected 45° angle. The variation of the reflection height in dependence on  $\chi$  is larger than the corresponding change of the fixed electron density level. This result can be explained by variable additional phase changes of the downcoming signal due to variations of electron density below the reflection height. Thus, one has to be aware that the accuracy of phase height determination is somewhat reduced by this effect.

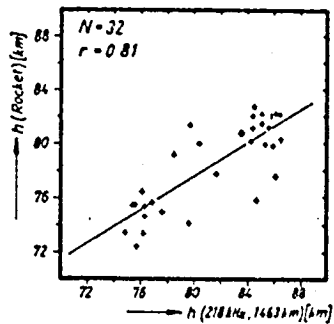


Figure 2. LF reflection height (218 kHz/1463 km) in comparison with corresponding heights derived from rocket-measured electron-density profiles.

An impressive demonstration of the effectiveness of indirect phase height measurements is the appearance of solar flare effects in the records. The strongest observed effects seem to decrease the reflection height by as much as 15 km. But some part of this amount may be also due to a flare-induced additional phase change below the reflection level.

It can be shown that the reflection height depends on the variation of the optical depth for the ionizing solar Lyman- $\alpha$ -radiation; that means it depends on air pressure. It has turned out that an appropriate characteristic for describing the day-to-day variations is the inverse Chapman-function,  $Ch^{-1}\chi$ , of the solar zenith angle value at which the diurnal course of the reflection height crosses a given height level. This quantity is mainly connected with the pressure variation, as confirmed by comparison with the seasonal variation of air pressure measured by rockets.

In Figure 3 the correlation is presented of daily pressure values obtained by rockets at a height of 70 km with corresponding values of  $Ch^{-1}\chi$  during the winter of 1974/75. They are given as deviations from the mean seasonal variation. The result shows a weak but significant correlation. This winter had particularly large variations of air pressure. A similar investigation for other winters did not show such a significant correlation. Thus, it must be assumed that other quantities also influence the  $Ch^{-1}\chi$ -values in the same order of magnitude.

A comparison of the slope of the mean daily variation of reflection height with corresponding temperatures measured by rockets is difficult. The slope

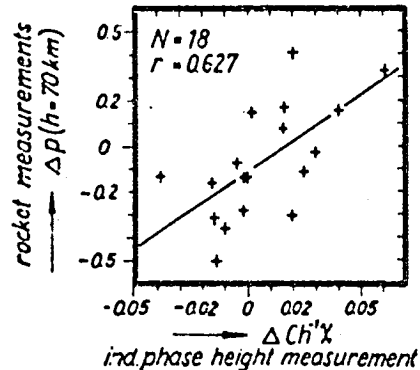


Figure 3. Pressure deviation from seasonal variation in 70 km height in comparison with corresponding  $Ch^{-1}\chi$  values near 78 km height from December 1974 to March 1975.

results from the whole diurnal variation of the reflection height; that means that there is inevitably an averaging over a height range up to 10 km where the vertical temperature profile may considerably vary and likewise an averaging over many hours where also considerable temperature changes may occur. On the other hand, it must be assumed that additional phase changes caused by variations of electron density also influence the slope. Thus, one cannot expect a good correlation between scale heights derived from the slope of the diurnal phase height variation and instantaneous local temperatures measured by rocket. The seasonal variation, however, of the slope is very similar to the seasonal variation of temperature in the altitude around 80 km.

In Figure 4 different data for the winter of 1974/75 are presented in the following manner: The upper curve gives daily values of ionospheric absorption at constant solar zenith angle  $\chi = 78.5^\circ$ . The two curves below show daily values of  $Ch^{-1}\chi$ . They rise when the isobaric surface near 80 km is rising and vice versa. Curve (b) gives  $Ch^{-1}\chi$  values from Eastern Europe and curve (c) from Central Europe. The distance between the path's midpoints is about 2400 km. Both curves show very similar variations, a hint to large-scale pressure variations in this region. The lowest curve of the figure gives some pressure values at 70 km height measured by rockets in Volgograd. The pressure data show similar large variations as those of the  $Ch^{-1}\chi$  values, which confirm the close connection between both of them, as also seen in the figure before. The variation of ionospheric absorption precisely follows inversely the changes of the  $Ch^{-1}\chi$  curves, i.e. large ionospheric absorption is connected with low pressure and vice versa. The high variability in this winter is mainly caused by large-scale changes of pressure.

The results of comparison between indirect phase height measurements and simultaneous rocket soundings in the D-region can be summarized as follows:

- The reflection height approximately varies with the height of a fixed electron density; that means that a continuous patrol of one point of the electron density profile is possible by these measurements.
- The interdiurnal variation of the value of the inverse Chapman function,  $Ch^{-1}(\chi)$ , at the moment of crossing a given reflection height contains

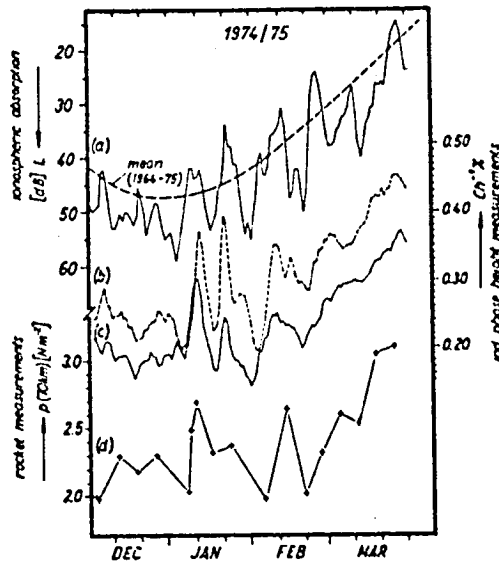


Figure 4. (a) HF-absorption measurements ( $\cos \chi = 0.2$ ) in Central Europe; (b), (c) Ionospheric D-region parameter  $Ch^{-1}X$  from LF indirect phase height measurements in Eastern Europe and Central Europe near the 80-km level; (d) Rocket data of pressure at 70 km height in Eastern Europe in winter 1974/75.

information about day-to-day changes of atmospheric characteristics, mainly air pressure.

- Thus, indirect phase height measurements are a useful completion to rocket measurements, because they allow continuous monitoring of the D-region also between the rocket soundings and, therefore, support the valuation of the rocket results according to the respective background.

#### REFERENCES

- Bracewell, R. N., K. G. Budden, J. A. Ratcliffe, T. W. Straker and K. Weeks (1951), Proc. IEE, part III, 98, 221.  
 Lauter, E. A. and K. Sprenger (1958), Z.f. Meteorol., 12, 205.  
 Smith, M. S. (1973), J. Atmos. Terr. Phys., 35, 51.  
 Bulletin of atmospheric rocket sounding results, issued by: Central Aerological Observatory, Gidrometeoizdat, Moscow.

N85

20457

UNCLAS

N85-20457

39

MEASUREMENTS OF PARTIAL REFLECTIONS AT 3.18 MHz  
USING THE CW-RADAR TECHNIQUE

J. Priese and W. Singer

Academy of Sciences of the GDR  
Central Institute of Solar-Terrestrial Physics  
(Heinrich Hertz Institute)  
DDR-1199 Berlin, GDR

An equipment for measuring partial reflections using the FM-CW-radar principle at 3.18 MHz, recently installed at the Ionospheric Observatory Juliusruh of the CISTP (HHI), is described. The linear FM-chirp of 325 kHz bandwidth is Gaussian-weighted in amplitude and gives a height resolution of 1.5 km (chirp length is 0.6 sec). Preliminary results are presented for the first observation period in winter 1982/83.

INTRODUCTION

A partial reflection experiment was put into operation in December 1982 at Juliusruh (geographic coordinate 54.63°N, 13.38°E, L = 2.62) and is firstly applied to study different D-region parameters such as electron density, height of reflecting layers, and fading periods. This method gives an important enlargement of the well-known groundbased methods such as A1/A3-absorption measurements, indirect phase-height measurements and meteor-wind observations, which are being used in our Institute for diagnostics and monitoring of the mesosphere and lower thermosphere.

INSTRUMENTATION

The functional scheme of the transceiver equipment is given in Figure 1. The chirp signal is generated by an ultra-linear VCO, the frequency ripples of which being smaller than 300 Hz over the whole sweep width (further parameters are listed in Figure 2). High linearity is obtained by matched forming of the controlling voltage following a power series of third order in time (KALASS, 1977; KALASS et al., 1981).

The envelope of the signal amplitude is frequency weighted by Gaussian band-pass-filters in both directions of transmitting and of receiving; the 3 dB-band widths being 66.4 kHz. The Gaussian filters designed by TIMPL (1979, 1980) approximate the ideal Gauss-envelope with ripples smaller 0.2 dB down to -70 dB (the ends of the truncated chirp). The filters are realized by band-passes of 14th order.

The amplified signal is transmitted by an array consisting of 4 x 4 horizontal orthogonal pairs of half-wave dipoles installed approximately  $\frac{1}{8}$  above the dissipative ground ( $n = 30 + j 170$ ); the dipoles of each pair being crossed with a distance of 1 m. A gain of 16.5 dB (for one polarization) referred to the isotropic radiator has been obtained by using the computed values of the attached Sommerfeld-problem (PRIESE and SCHNEIDERHEINZE, 1983) together with the measured current distribution as well as the resulting radiation resistance of each dipole (PRIESE, 1980, 1981). The beam-widths (27° in the E-plane, 28.5° in H-plane) have been measured by means of a helicopter (PRIESE, 1981). The orthogonal arrays are excited in phase quadrature and opposite polarization are obtained by reversing one of the feed systems.

The receiving array is separated about 4 wavelengths from the transmitting antenna and consists of 2 x 2 orthogonal pairs of resonant loops. The sum signal will be amplified by 40 dB in an amplifier of low intermodulation

ORIGINAL PAGE IS  
OF POOR QUALITY

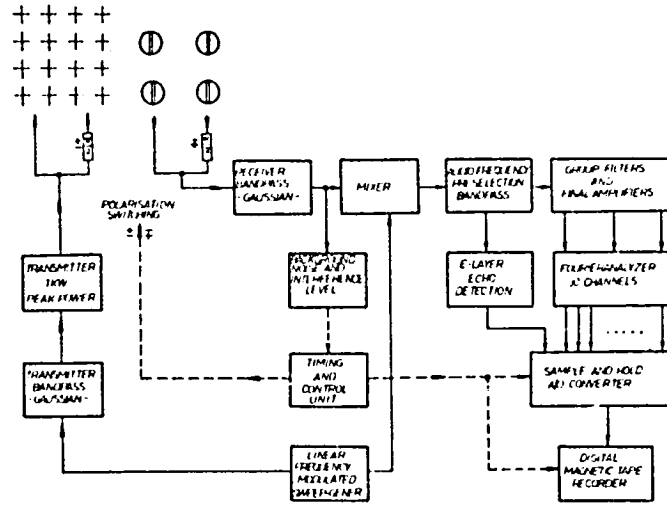


Figure 1. Functional scheme of the transceiver equipment.

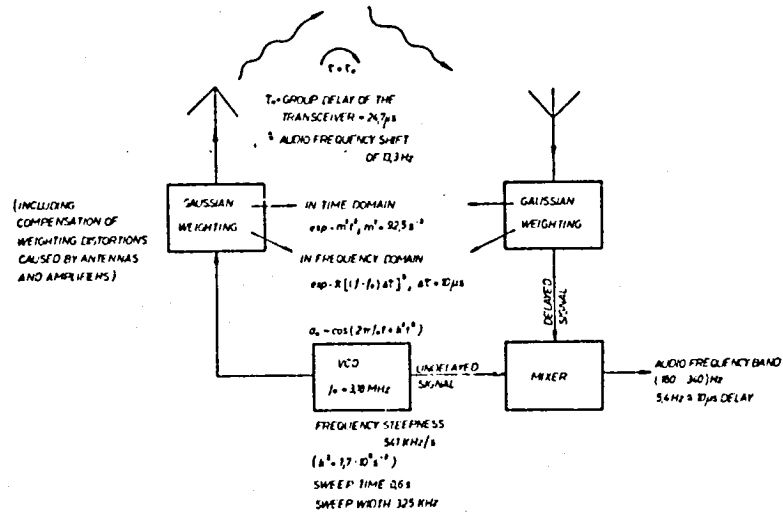


Figure 2. Signal diagram.

distort: (for the first observation period a half-wave dipole could be used only). After mixing of the undelayed with the reflected and therefore delayed signal, the audio frequency components of the mixer spectrum contains the information of height and amplitude of the partial reflection. Following the introduction to chirp theory by KLAUDER et al. (1960) it is well known that an unweighted chirp-process results in an audio frequency spectrum with range-sidelobes of the  $\sin x/x$ -type. A sidelobe-compression is absolutely necessary in order to avoid confusion of the spectra of the partial reflection levels among one another as well as to suppress the sidelobe spectra of the strong E-layer reflection and the mutual coupling between the antennas respectively.

Following a first idea of KLAUDER et al. (1960), Keiser introduced Gaussian weighting as a rigorous method to reduce the sidelobes, and prepared the basic parameters of chirp, filters and transceiver (see reports by BREMER et al., 1973; KALASS et al., 1981). Furthermore, the chirp process results in the important compression gain of the signal compared with a constant-frequency pulse of the same envelope. Power gain  $N$  and delay resolution  $\tau$  are given for an infinite chirp by

$$N = \sqrt{\pi/m} \cdot \Delta\tau, \quad \Delta\tau = \sqrt{\pi} \cdot m/K^2.$$

Based on the desired values of  $\tau = 10 \mu\text{s}$  (corresponding to a height resolution of 1.5 km) and a compression gain of  $N = 43 \text{ dB}$  the signal processing parameters shown in Figure 2 have been derived. Additional efforts have been made to study the effects of sweep truncation as well as of phase and amplitude distortions of the chirp (KALASS et al., 1981).

Last not least, the audio frequency spectrum of a detached partial reflection level is obtained (after some omissions) in the form

$$A_{\text{out}}(f) \sim \exp\left\{-\frac{\pi}{2} \left[N\Delta\tau f - \frac{\tau}{\Delta\tau}\right]^2\right\} = \exp\left\{-\frac{\pi}{2} \left[\frac{f}{5.4 \text{ Hz}} - \frac{\tau}{10 \mu\text{s}}\right]^2\right\}$$

The 3.4 dB width of this spectrum is about 5.4 Hz, so the Fourier-analyzer must have the same frequency resolution and is hardware realized by active low-pass filters of 2.7 Hz bandwidth (KALASS, 1977) following the outputs of the quadrature demodulators. The spectrum of each sweep is analyzed for 30 height channels from 47.5 km to 91 km with a stepsize of 1.5 km. The A/D converter has a resolution of 11 bits. For each sweep the amplitude height profile is recorded on magnetic tape. The data reduction will later be done on an all-purpose KRS 4200 computer.

The equipment has two different modes of operation. In the continuous mode sweeps are transmitted with a repetition frequency of 1.25 Hz, in the intermittent mode 10 consecutive sweeps are emitted at the beginning of each minute. In both modes it is possible to observe either with a fixed polarization (ordinary or extraordinary) or with polarization switching.

#### PRELIMINARY RESULTS

Data have been evaluated for days with high radio wave absorption (winter anomaly) and low absorption in December 1982 and January 1983 to investigate the variability of electron density in winter. For winter anomaly conditions the data of December 24, 1982 and January 12, 1983 are presented. On these days, A3-absorption values on 3 measuring paths exceeded the monthly median value by about 4 to 8 dB and A1-absorption values in the MF-range (2 MHz) by about 6 dB. As example for conditions of low absorption the data of December 27, 1982 and January 21, 1983 are used, when LF-absorption was about 5 dB and MF-absorption about 3 dB below the monthly median (all data for solar zenith angle  $\chi = 78.5^\circ$ ).

In Figure 3, time averaged height profiles (median values) of the amplitudes of the ordinary (o)- and extraordinary (x)-mode are shown for the days mentioned above. The height profiles are smoothed by running averages over 3 successive values. For low absorption the  $A_x$ -height profiles exceed the noise level above 74.5 km and attain a maximum at about 80 km (on Jan. 21 the noise level was enhanced by two times). For winter anomaly conditions, signals exceeded the noise level already at lower heights (on Dec. 24 at 70 km; on Jan. 12 at 67 km). In the height profiles maxima occur on Dec. 24 at 79 km and on Jan. 12 at 76 km. By analysis of the autocorrelation functions for continuous measurements with fixed polarizations, the half-amplitude widths of the autocorrelation functions were found of the order of seconds, increasing with decreasing heights.

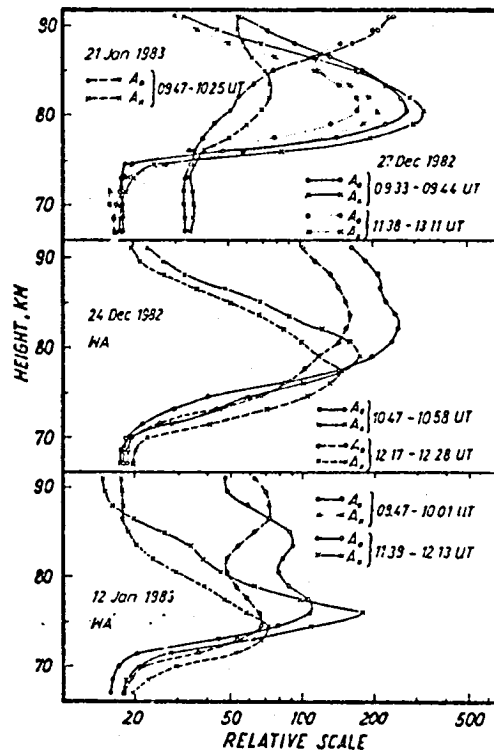


Figure 3. Averaged amplitude profiles of the extraordinary and ordinary component (WA: day with winter anomaly in absorption).

The basic theory for the differential-absorption experiment was given by GARDNER and PAWSEY (1953), modified by BELROSE and BURKE (1964), assuming that observations of weak echoes of high frequency radio waves scattered from the lower ionosphere are caused by Fresnel reflection from discontinuities in the refractive index. Following these papers, the height distribution of electron density has been derived from the observed ratio  $A_x/A_o$  of the backscattered amplitudes of the extraordinary and ordinary magneto-ionic components using the

improved quasi-longitudinal approximation to the exact Sen-Wyller expression of the refractive index after FLOOD (1980). The height profile of monoenergetic collision frequency is assumed as  $\nu_m = 7.5 \times 10^3 \times p$ , the pressure data being taken from CIRA 72 including seasonal variations.

In Figure 4 the derived electron density profiles (solar zenith angles about  $78^\circ$ ) are shown for the data of Figure 3. Noise correction has been performed for the amplitude data by using the noise in the height range 55 to 60 km, where no ionospheric signals are expected. At the upper end of the derived profiles, the electron density values are uncertain by a factor of about 1.5 due to the low signal-to-noise ratio of the extraordinary component.

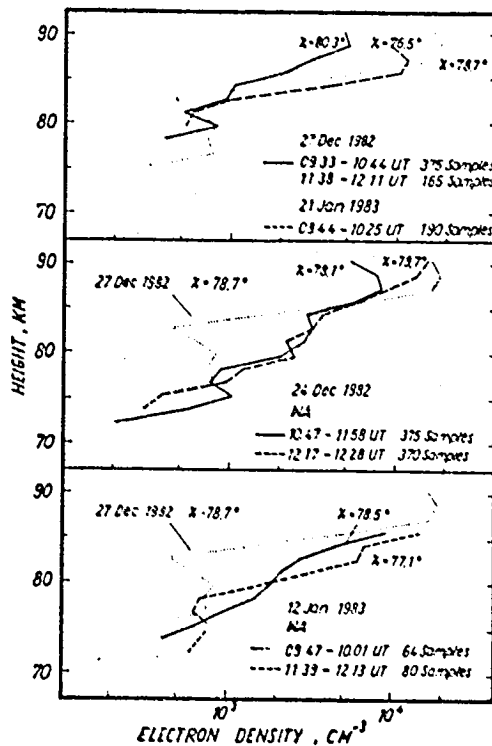


Figure 4. Electron-density profiles for winter conditions using the amplitude data of Figure 3 (WA: day with winter anomaly).

A comparison between the electron density profiles evaluated for high absorption conditions with the profiles derived for low absorption shows a marked increase in electron density between 76 and 85 km in the presence of winter anomaly.

#### CONCLUDING REMARKS

A few examples of preliminary results have been presented, obtained by a new partial reflection equipment using the CW-radar principle during winter

1982/83. For the four days evaluated here it was possible to derive electron density profiles in the height range 72 to 90 km. Under winter anomaly conditions the electron density profiles show a marked increase between 76 and 85 km by a factor of about 2 to 6 compared to days without winter anomaly.

To check the reliability of the derived profiles it will be of interest to compare the observed absorption values in the LF- and MF-range with the theoretical calculated absorption values for these electron density profiles. Before the forthcoming summer observation period the provisional receiving antenna will be replaced by the designed receiving array. In future it is planned to implement a partial reflection drift equipment.

#### REFERENCES

- Belrose, J. S., M. J. Burke (1964), *J. Geophys. Res.*, 69, 2799.  
 Bremer, J., J. Keiser, J. Prieese, W. Singer, J. Taubenheim and E. Weiss (1973), Unpublished report, Central Institute of Solar-Terrestrial Physics, Berlin-Adlershof, GDR.  
 Flood, W. A. (1980), *Radio Sci.*, 15, 797.  
 Gardner, F. F. and J. F. Pawsey (1953), *J. Atmos. Terr. Phys.*, 3, 321.  
 Kalass, D. (1977), Thesis, Hochschule für Verkehrswesen "Friedrich List", Dresden (unpublished).  
 Kalass, D., J. Keiser, A. Himalski, J. Prieese, W. Singer, J.-G. Stangenberg, H. Timpl and W. Vietzke (1981), Unpublished report, Central Institute of Solar-Terrestrial Physics, Berlin-Adlershof, GDR.  
 Klauder, J. R., A. C. Price, S. Darlington and W. J. Albersheim (1960), *Bell System Technical Journal*, 39, 745.  
 Prieese, J. (1980), GDR-Patent WP H01 Q/198373.  
 Prieese, J. (1981), *Nachrichtentechnik/Elektronik*, 31, 372.  
 Prieese, J. and G. Schneiderheinze (1983), NHI-STP Report (in press), Central Institute of Solar-Terrestrial Physics, Berlin-Adlershof, GDR.  
 Timpl, H. (1979), *Nachrichtentechnik/Elektronik*, 29, 188, 283, 458.  
 Timpl, H. (1980), GDR-Patent WP H03 H/206263.



N85

20458

UNCLAS

1 N 85 - 20458

45

ABNORMAL CIRCULATION CHANGES IN THE WINTER STRATOSPHERE,  
DETECTED THROUGH VARIATIONS OF D REGION IONOSPHERIC ABSORPTION

B. A. de la Morena

INTA-CONIE  
Huelva, Spain

ABSTRACT

This paper intends to introduce a method to detect stratospheric warmings using ionospheric absorption records obtained by an Absorption Meter (Method A3). The activity of the stratospheric circulation and the D region ionospheric absorption as well as other atmospheric parameters during the winter anomaly experience an abnormal variation. We have found in our observations a simultaneity in the beginning of abnormal variation in the mentioned parameters, using the absorption records for detecting the initiation of the stratospheric warming. Results of this scientific experience of "forecasting" in the "El Arenosillo" Range, are presented in this communication.

INTRODUCTION

For the last ten years, "El Arenosillo" Range has been participating in international programmes dedicated to the study of winter stratospheric sudden warmings with the launching of meteorological rockets, and with the analysis and distribution of the wind and temperature data recorded, following the rules given by the international scientific community.

The exceptional advantage of a station for the study of the atmosphere with ground-based equipment combined with a rocket launching range, has allowed the simultaneous analysis of the behavior of different parameters of the middle atmosphere during the periods considered as winter anomalies. It confirms that, for the latitude of "El Arenosillo", the abnormal variations of the absorption parameter in the ionospheric D region appear simultaneously with circulation changes (i.e., rotation of direction) of the stratospheric wind that accompany the sudden warmings (MORENA, 1981) as well as a lack of variation of the parameter temperature in the mentioned period of winter anomaly.

Analysing Figure 1a, it can be observed that in the winter period 1975/76 the zonal circulation in the upper stratosphere which presents west component coincides with normal values of absorption for that winter period (from 20th Dec. to 5th Jan., 9th to 18th Jan., and 27th Jan. to 5th Feb.), and on the contrary, the abnormal changes of the zonal circulation to winds of East component correspond to variations of the absorption which are higher than their mean value. On the other hand, the period of winter 1976/77 which was characterized by the absence of circulation changes in the upper stratosphere, showed a normal behavior of the parameter absorption in the ionospheric D region.

Figure 1b is a clear example that the temperature in the stratosphere virtually shows the same variations during unstable periods (as in winter 1975/76) and in periods of circulation stability (as in winter 1976/77).

Based on this, the present experimental study, whose finality is to detect the appearance of winter stratospheric circulation changes in middle latitudes and to follow its development through the observation of the abnormal variations of the ionospheric absorption parameter in D-region, was started. The practical check-up of the mentioned prediction system has been carried out for the last two periods of winter anomaly (1981/82 and 1982/83), using fourteen meteorological rockets Super-Loki, the stratospheric balloons and continuous

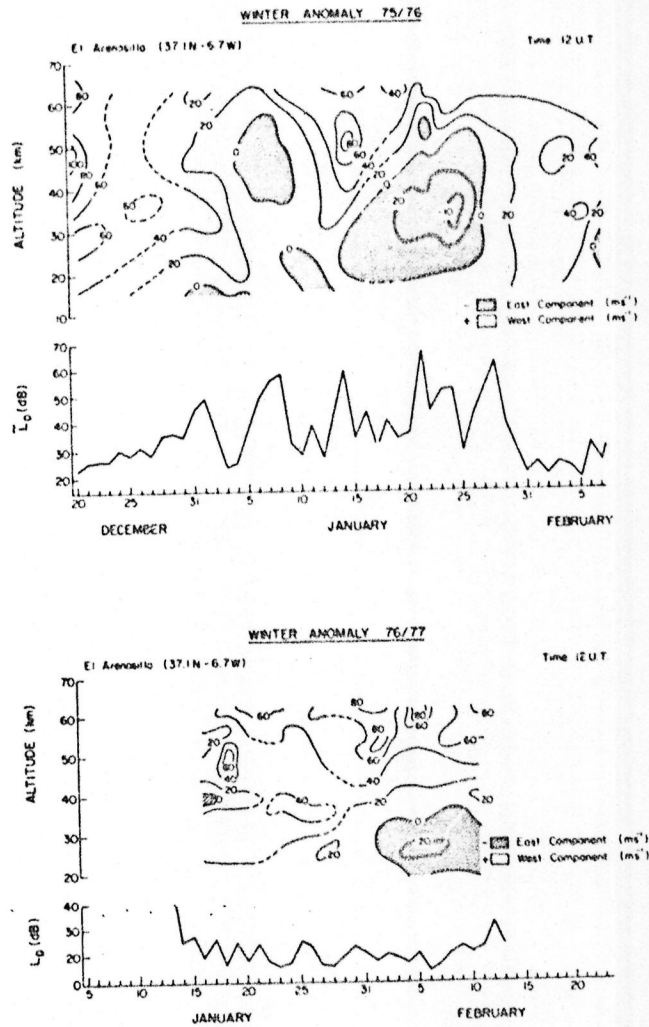


Figure 1a.

records of the A3-Absorption Meter, showing the results given in the following. This study is part of a wide investigation program being developed in "El Arenosillo" that pretends to develop a simple prediction system of the abnormal variations of the parameters characterizing the middle atmosphere through the use of ground-based equipment.

#### ANALYSIS OF THE DATA

The records of wind, temperature, and absorption obtained during the two winter anomaly periods 1981/82 and 1982/83, once again confirm the simultaneous

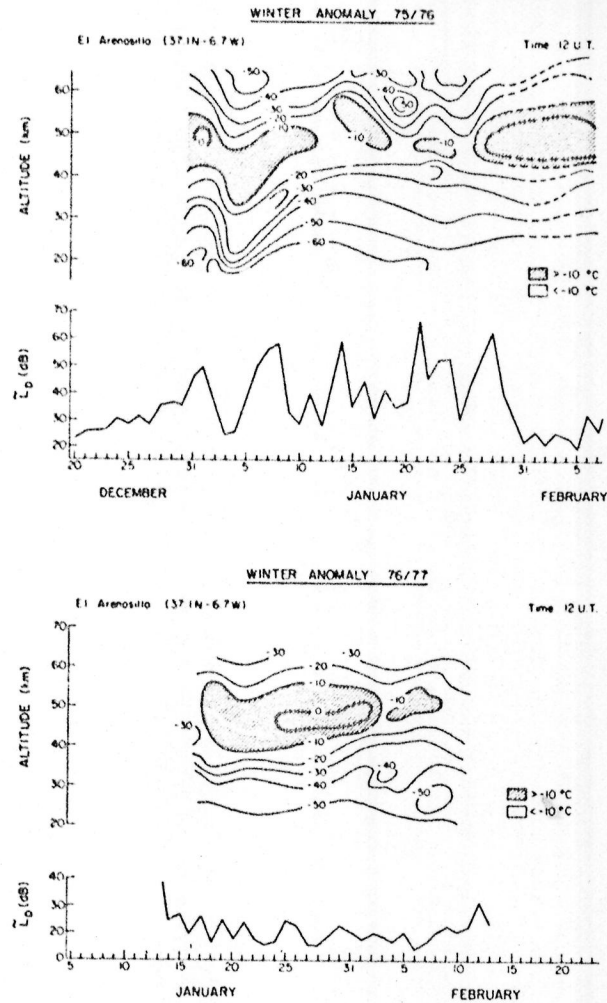
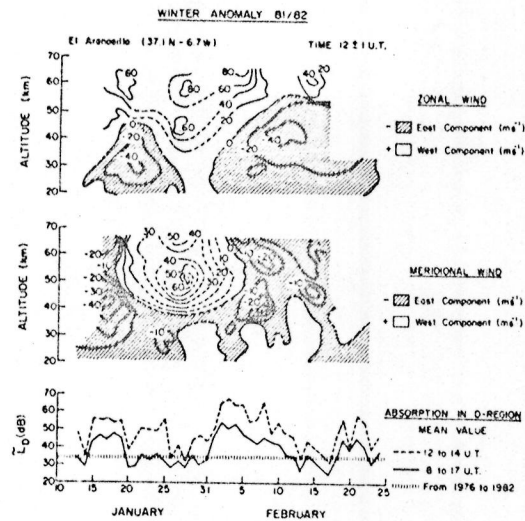


Figure 1b.

appearance of disturbances in the normal behaviour of these atmospheric parameters (Figures 2 and 3). Figure 2 presents a typical winter anomaly with two notable stratospheric changes represented in their meridional and zonal components, being evident in the irregular behavior of the ionospheric absorption in the D-region, with values which are higher than the mean value registered from 1976 to 1982. (We consider the mean value of absorption obtained during the solar cycle, represented by the continuous line, as more significant.)

The periods of maximum absorption coincide with a meridional circulation of North component in the whole stratosphere, while the normal values of absorption



correspond with a wind circulation of East and West component in the upper stratosphere. In this diagram, it is easily seen that the meridional circulation precedes the change of zonal direction to winds of East component. The stratospheric temperature could not be measured during the winter period 1981/82 due to technical problems of the reception system.

Figure 3 analyzes the winter anomaly 1982/83. This was characterized by a period of circulation stability and of absorption, only altered by two weak beginnings of meridional circulation changes in the upper stratosphere, which coincided with sudden increases of ionospheric absorption that were easing off as the zonal circulation was being re-established. Similar as in the winter period of 1981/82, meridional winds of North component preceded the changes of zonal circulation in the upper stratosphere. As expected, the temperature did not experience any notable changes and its behavior was similar to that observed during the winter periods of 1975/76 and 1976/77.

Figure 4 gives a synoptic representation of the direction and intensity of the stratospheric wind during the analyzed periods of winter anomaly 1981/82 and 1982/83, offering a more intuitive image of the base used in this possible prediction system.

It can be observed that when the absorption is higher than the established mean value, a change of meridional direction in the wind circulation of the upper stratosphere begins simultaneously (15th to 19th January 1982, 1st to 7th February 1982, 28th of January to 1st February 1983 and 15th to 17th February 1983). On the contrary, periods of normal absorption indicate that the circulation has been established dominantly in East or West zonal components.

It is important to bring out the processes initiating the circulation change observed during the 28th and 30th of January and 1st of February 1983 by its possible application to the formation theory of the "warmings" through geopotential fluxes, as well as the sudden and big increase of the ionospheric absorption in these days, which reached the highest values recorded in El Arenosillo for the last ten years.

ORIGINAL PAGE IS  
OF POOR QUALITY

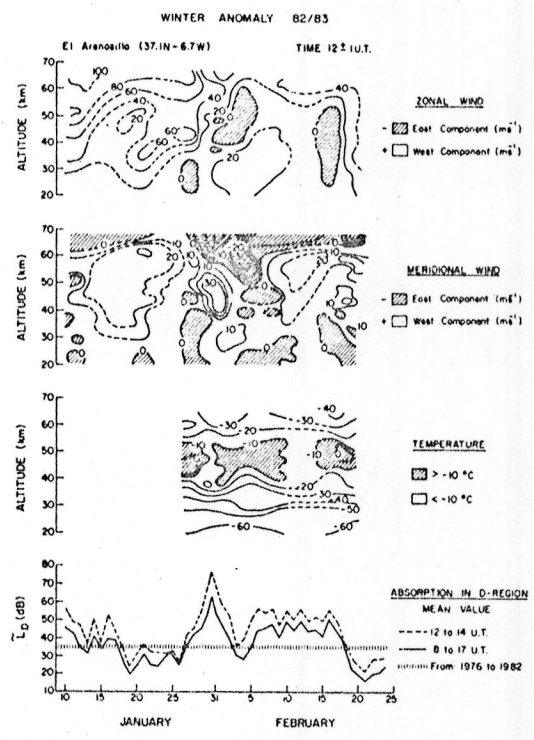


Figure 3.

CONCLUSIONS

- An evident correlation between the behaviour of the absorption parameter in the D-region, and the wind circulation in the upper stratosphere during the periods of winter anomaly is observed.
- Significant increases of absorption indicate the beginning of a circulation instability (turn-round of the wind direction) and the establishment of a meridional component of the wind in the upper stratosphere.
- Normal values of absorption indicate that the circulation is established dominantly in zonal components.
- The mean value of the absorption increases during those winter periods which are characterized by circulation instability.
- Winds of meridional component precede the abnormal change of the zonal circulation.
- Since the stratospheric temperature does not experience any notable variations during the periods of winter anomaly, the system of alert and prediction of sudden warmings (stratalert parts) has great limitations to be used in the middle latitude of El Arenosillo.

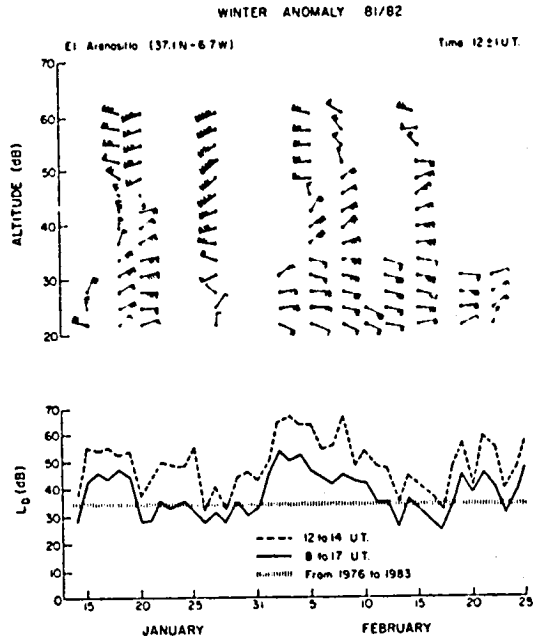


Figure 4a.

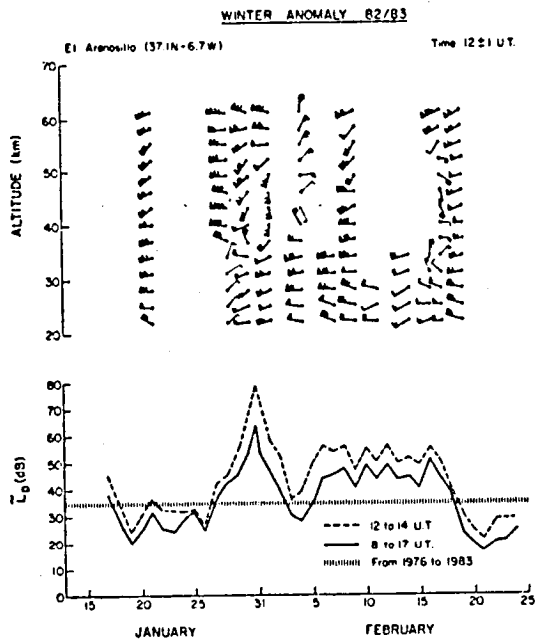


Figure 4b.

ORIGINAL PAGE IS  
OF POOR QUALITY

REFERENCES

- Cisneros, J. M. (1974), I Geophys. Geodesic National Assembly, Spain, Vol. 1, 637.  
de la Morena, B. A. (1981), IV Geophys. Geodesic National Assembly, Spain.

N85

20459

UNCLAS

D9  
52

N85-20459

## WINTER ANOMALY OF THE LOWER IONOSPHERE AND ITS POSSIBLE CAUSES

Z. Ts. Rapoport

Institute of Terrestrial Magnetism  
Ionosphere and Radio Wave Propagation (IZMIRAN)  
142092 Troitsk, Moscow Region, USSR

### INTRODUCTION

It is a well-known fact that in winter the midlatitude lower ionosphere differs considerably from that in summer. This was first discovered as a result of the analysis of ground-based measurements of radio wave absorption in England (APPLETON, 1937). The phenomenon was named the radio wave ionospheric absorption winter anomaly. Later on, we began to speak about winter anomaly of the lower ionosphere, having in mind that a number of parameters of ionized and neutral components of the medium behaves anomalously in winter.

The winter anomaly at midlatitudes shows itself distinctly in MF and HF radio wave ranges. On a long-time average, the maximum value of absorption for a constant solar zenith angle is observed during the winter solstice; it decreases almost to summer values symmetrically towards the equinoctial periods. Another distinctive feature of the winter anomaly is the enhanced day-to-day variability of the absorption in winter compared with other seasons of the year. Beside the general increase of absorption level, called normal winter anomaly (SCHWENK, 1971), there are days and groups of days with excessively high absorption. The zone where the anomaly is observed has a low-latitude boundary below which the anomaly vanishes (see, e.g. LAUTER and SCHANING, 1970; ELLING et al., 1974). It should be also noticed that the magnitude of the effect and the duration of its occurrence decrease with latitude (e.g. RAPOPORT, 1974), that the anomalous region has a cloudy or spotted structure (e.g. SHRESTHA, 1971). The winter anomaly occurs also at high latitudes in the auroral zone in any case but here the effects caused by sporadic energetic particle fluxes are superimposed on those of the winter anomaly (RAPOPORT, 1979).

There have been many attempts to explain the winter anomaly. We should not like to dwell upon all hypotheses suggested. We only want to point out that some scientists regard direct precipitation of energetic particles as the unique cause of the anomaly at all latitudes where it is observed (e.g. SATO, 1981). Other authors assume that the winter anomaly may have also the causes completely independent of particle precipitation, i.e., changes of temperature and gas composition, mainly an increase of nitric oxide density ionized by Lyman-radiation (e.g. OFFERMANN et al., 1982). It seems to us that these opposite stand points do not exclude each other, that they may operate simultaneously, and their relative contribution is different in different cases, as it depends considerably on the latitude of observation (e.g. THOMAS, 1971; BREMER and LAUTER, 1982). We think, next, that the intensity of energetic particle fluxes in the auroral zone and the dynamical structure of the whole middle atmosphere on the levels of the lower thermosphere and mesosphere are definitive for the midlatitude mesosphere conditions. We also think that a correct interpretation of the midlatitude winter radio wave absorption changes is possible only if the whole spatial-time pattern of the event is taken into account. Our analysis is based on data obtained during an integrated experimental program carried out in the USSR in January 1981 and partially in January 1982.

### INTEGRATED EXPERIMENTAL PROGRAM RESULTS

Integrated ground-based and rocket experiments were performed in the USSR in January 1981 and 1982 as a part of the International Middle Atmosphere Program. The rockets M-100B launched in Volgograd ( $\psi = 48.7^\circ\text{N}$ ;  $\lambda = 44.3^\circ\text{E}$ ;

$\phi = 43.1^\circ$ ) provided height profiles of electron density, wind and temperature. Radio wave absorption data obtained by AI method in Volgograd and  $f_{min}$  parameter values obtained at a number of Soviet ionosonde stations were used to determine the situation in the lower ionosphere. The results of these integrated experiments have been presented at the COSPAR Symposium in Ottawa (PAKHOMOV et al., 1982) and in Alma-Ata (PAKHOMOV et al., 1983). The ground-based data showed that absorption in January, 1981 was typical for winter conditions. The geomagnetic field during the whole month was rather quiet. Excessive absorption was observed on January 12-16.

Figure 1 shows electron density altitude profiles ( $N_e(h)$ ) obtained by using the coherent frequency technique on rockets M-100B on the anomalous day of January 14 and on normal days of January 21 and 28 in the morning (Figure 1a) and in the afternoon (Figure 1b), the solar zenith angle being  $\chi = 78^\circ$ . These profiles may be compared with that obtained on January 29, 1980, a day considered as free from the influence of winter anomaly. One may see that  $N_e$  values on quiet winter days (Figure 1a) exceed  $N_e$  values for the day free from anomaly in a considerable altitude range ( $\approx 75$  to  $90$  km), whereas  $N_e$  values are higher on the day of the enhanced absorption than on a day with regular absorption ( $h = 70$  to  $95$  km).

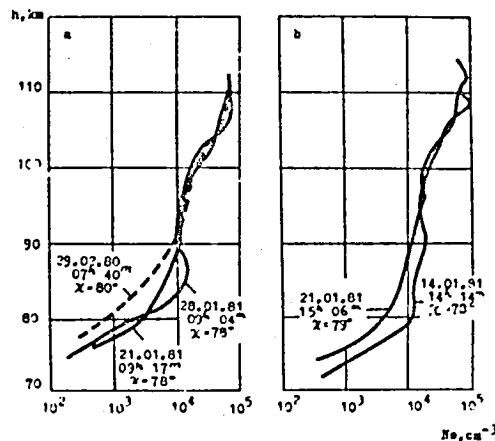


Figure 1. Electron density altitude profiles obtained by coherent frequency technique in Volgograd; solar zenith angle  $\chi = 78^\circ$ . (a) forenoon profiles. (b) afternoon profiles. 14 January is the day of excessive absorption; 21 and 28 January are days of normal winter absorption. The profile obtained on 29 February 1980 at  $\chi = 80^\circ$  is shown for comparison.

Figure 2a shows temperature profiles obtained on January 14, 21 and 28 as well as the CIRA-72 standard profile. The lower part of the figure (b), shows the measured temperature deviations from the corresponding standard profile. The characteristic shape of these  $\Delta T(h)$  curves shows explicitly the influence of atmospheric wave processes on temperature distribution, not only during the excessive absorption but on normal days, too. It should be also noted that the temperature was lower than the standard one on the day of excessive absorption as well as on days of normal winter absorption in the region of enhanced electron density (above  $70$  km). The temperature height distribution on the day

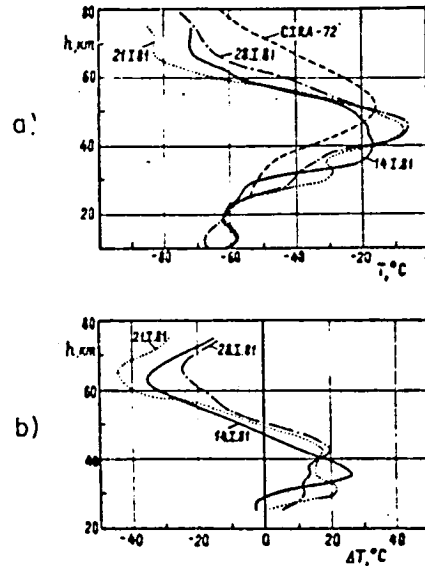


Figure 2. (a) Temperature altitude profiles above Volgograd obtained on 14, 21 and 28 January 1981. The dashed line shows the standard profile CIRA 1972. (b) Altitude profiles of temperature differences  $\Delta T = T_{\text{meas.}} - T_{\text{CIRA}}$ .

with excessive absorption does not show any peculiarities. We should like to call attention to this result, since a rise of the temperature is often considered as one of the most important causes of the winter anomaly because it must reduce the ion clustering rate which, in its turn, must cause a decrease of loss rate and, hence, an increase of electron concentration (see, e.g. SECHRIST, 1967).

The density of hydrated cluster ions which decisively affects the effective recombination effective coefficient in D-region is to a considerable extent dependent on the water vapour content of the medium (see, e.g. SECHRIST, 1970). Figure 3 (FEDYNSKI and YUSHKOV, 1979) displays water vapour density profiles obtained above Volgograd on January 10 and on February 2, 1978. The day of January 10 may be considered as an anomalous one (according to data from Moscow, mean of five near-noon values  $f_{\text{min}} = 2.5$  MHz) while the day of February 2 is a normal one ( $f_{\text{min}} = 1.3$  MHz). One may see that the water vapour density on an anomalous day is considerably lower than on a normal one: at 60 km altitude it is 6 times lower while it is 3.5 times lower at the altitude of 80 km. In this way, it seems that this result confirms the idea that the water vapour is one of the most important factors determining the electron density increase and excessive absorption in D-region. Water vapour density was also measured in January 1982 (Figure 4) -- the profiles have been obtained on 13 and 19 January 1982 at night at  $\chi = 145^{\circ}$  and  $144^{\circ}$ , respectively. Within the measurement accuracy these profiles coincide with that obtained in quiet winter conditions on 2nd February 1978 also shown in Figure 4. Yet, the absorption was rather high on these days in Volgograd (at 2.2 MHz about 50 and 40 dB). This suggests that it was not water but other factors that determined the lower ionosphere conditions during this period.

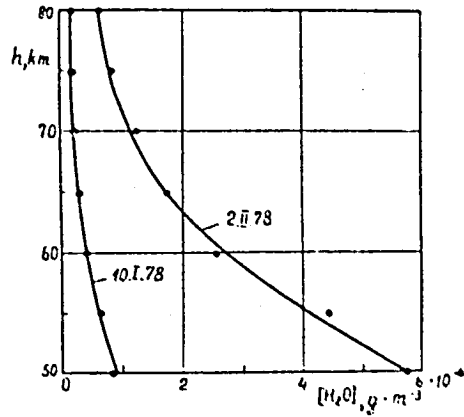


Figure 3. Water vapor density altitude profiles above Volgograd on anomalous (10 January 1978) and normal (2 February 1978) days.

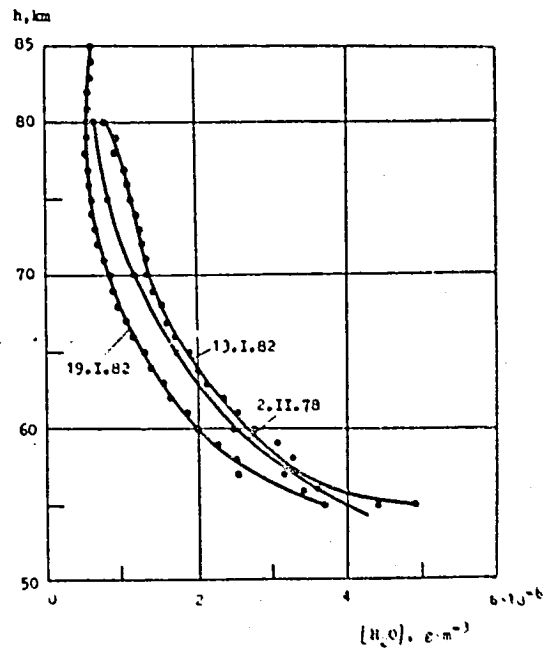


Figure 4. Water vapor density ( $H_2O$ ) altitude profiles above Volgograd on 28 and 19 January 1982 ( $\chi = 145^\circ$  and  $144^\circ$ , respectively). The profile of 2 February 1978 is shown for the sake of comparison.

Thus the experiments in Volgograd in January 1981 and January 1982 show that both the temperature of the mesosphere and the water vapour density may serve only as additional factors and not as decisive factors which determine excessive anomalous winter absorption occurrence at midlatitudes.

DISCUSSION

First of all it should be borne in mind that whatever hypothesis we accept, it should explain all above mentioned peculiarities of the phenomenon. In agreement with other authors (OFFERMANN et al., 1982; BREMER AND LAUTER, 1982) we think that the enhancement of nitric oxide density is the main cause of electron density enhancement in the midlatitude lower ionosphere. We believe that nitric oxide is produced mainly at the ionospheric E region level, with highest rates at high latitudes and particularly in the auroral zone under the influence of precipitating particle (electron) fluxes.

More or less intense particle precipitation occurs permanently in the auroral zone, so that the density of NO caused by this precipitation has all features of the fluxes themselves, namely a very high time variability and spatial inhomogeneity (these features are to a certain extent smoothed out during the air transport). The auroral zone air being rich in NO is transported towards midlatitudes due to a stable winter cyclonic circumpolar vortex. As it moves the nitric oxide produced at high latitudes at an altitude of 90-100 km may be transported by turbulence and vertical motions towards lower altitudes (70-80 km) and it may produce there the above mentioned effects.

As there are no experimental facts which might prove this assumption?

First of all let us consider the data on air circulation.

Constant pressure maps for the North Hemisphere plotted with a one week time resolution for every 5 km in the altitude range 35 km to 60 km are regularly issued by the Central Aerological Observatory (ATLAS, 1982). Figure 5 displays the maps of 60 km altitude for three weeks of January 1981, using geomagnetic coordinates. The dashed circle at a latitude of  $\phi = 67^\circ$  gives a visualization of the auroral zone position. Points at this figure show positions of the observational stations. The wind at these altitudes may be considered as cyclo-geostrophic, so that air is transported along the isobars. One may presume that the circulation picture in general outlines the same at greater altitudes.

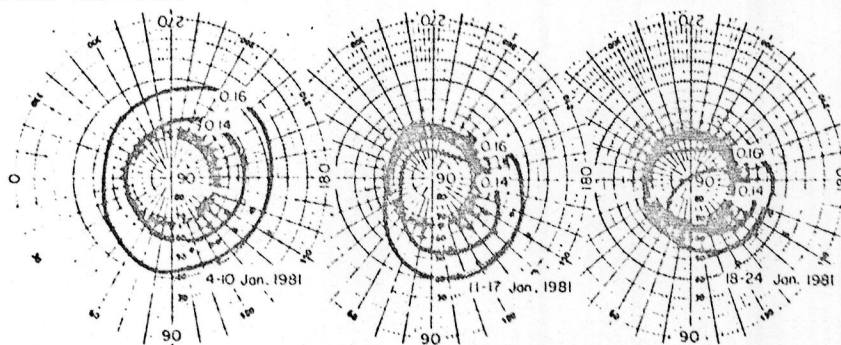


Figure 5. Constant pressure maps (the Northern Hemisphere) for the level of 60 km on 4-10 January and on 18-24 January 1981 (in geomagnetic coordinates). The dashed circle drawn at  $\phi = 67^\circ$  indicates the auroral zone. Each isobar is labelled by its pressure (in millibars).

There is some basis for this assumption. Figure 6 shows velocity and direction of the zonal wind measured by meteor radar in Kuhlungsborn (GDR) (see also GOSSART et al., 1982), at an altitude of about 95 km. One may see that the wind remained westward throughout the whole January which is natural if it follows the cyclonic vortex. Figure 5 shows that the isobars of the week preceding the disturbed days (4-10 January 1981) follow mainly the latitudes below the auroral zone. During the week of 11-17 January including the excessive absorption period they cross the auroral zone almost at halfway. The next week (18-24 January) they pass the auroral zone northward at a considerable portion of their path. It should be especially emphasized that the ionospheric disturbance on 12-16 January was preceded by a solar flare of importance 2N on 9 January with a subsequent weak magnetic storm with a gradual commencement (COSMIC DATA, 1981) followed by an increase of energetic particle precipitation into the lower ionosphere and by an equatorward shift of the auroral zone low latitude boundary. If our hypothesis is valid this should show itself through the time of the disturbance onsets at different stations as well as through the magnitude of the effects itself.

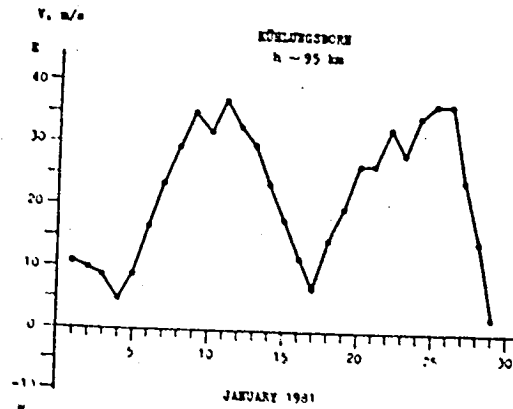


Figure 6. Zonal wind component above Kuhlungsborn in January 1981.

Figure 7a shows  $f_{\min}$  ( $\cos \chi = 0.2$ ) values for a number of Soviet ionospheric stations (Kaliningrad, Moscow, Rostov-on-Don, Arkhangelsk, Gorky, Sverdlovsk, Salekhard, Alma-Ata, Novosibirsk, Yakutsk) during the event of the winter anomalous absorption in January 1981. The character of  $f_{\min}$  variability is different at different stations, nevertheless there is an obvious tendency: the increase of absorption begins earlier at western stations than at eastern ones. This must be so if the disturbance source moves together with the air in the cyclonic vortex, i.e. from west to east.

The quantity  $\Delta f_{\min}$  which is the maximum difference of  $f_{\min}$  values observed on two successive disturbed days has been taken as a measure of the effect's magnitude. This difference versus the longitude of the stations is shown in Figure 7b. One may see that effect decreases as the longitude increases from west to east, following the air moving in the cyclonic vortex. If one takes into consideration a certain space inhomogeneity of the winter anomalous absorption zone, the plot looks rather significant. The stations Moscow and Rostov-on-Don do not fit the general distribution of  $\Delta f_{\min}$ . This may be

partially explained by a more sensitive equipment of the Moscow station, while Rostov-on-Don is the lowest latitude station of all European stations of the Soviet Union. Besides, the growth of  $f_{\min}$  values at these two stations is slower than at other ones, taking more than one day.

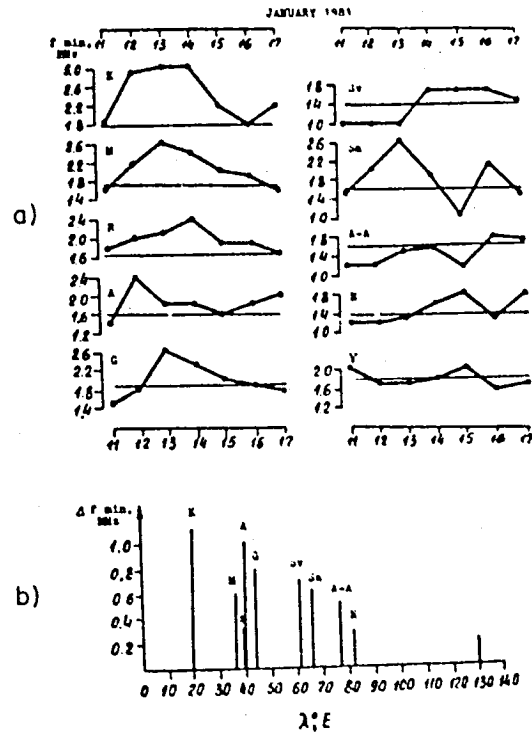


Figure 7. (a)  $f_{\min}$  ( $\cos \chi = 0.2$ ) values at a number of Soviet stations on 11-17 January 1981. The thick horizontal lines show the position of the month by medians. K - Kaliningrad, M - Moscow, R - Rostov-on-Don, A - Arkhangelsk, G - Gorky, Sv - Sverdlovsk, Sa - Salekhard, A-A Alma-Ata, N - Novosibirsk, Y - Yakutsk. (b)  $\Delta f_{\min}$ , the maximum difference of  $f_{\min}$  values for two successive days during the period 11 through 17 January 1981 for the stations shown in Figure 7a.

Midlatitude absorption changes (of  $f_{\min}$  values) compared with constant pressure maps for January 1982 during a normal winter period free of excessive absorption occurrence also reveals a close relation between the two phenomena:  $f_{\min}$  values are greater when the path along the isobars from the auroral zone to the observation station is short than in a case when this path is long (PANKHOMOV et al., 1983).

So, our hypothesis explains all the peculiarities of the phenomenon -- both the normal winter anomaly and the excessive one. In order to verify and to confirm the suggested hypothesis it is necessary to specify the character of circulation on levels of the mesosphere and of the lower thermosphere. Nitric

oxide, water vapour and ozone densities in different geo-heliophysical conditions for different latitudes should be known more precisely, too.

#### REFERENCES

- Appleton, E. V. (1937), Proc. Roy. Soc., A162, 451.
- Atlas, (1982), Atlas of the a.titudinal maps of the 35-60 km layer. Central Aerological Observatory, Gidrometeoizdat (in Russian).
- Bremer, J. and E. A. Lauter (1982), Paper presented at the KAPG Symposium "Meteorological effects in the ionosphere", Sofia, Bulgaria, June, 1982 (unpublished).
- Cosmic Data (1981), Cosmic Data, 1, Nauka, Moscow (in Russian).
- Cossart von G., K. M. Greisiger, K. Sprenger, Yu. I. Portnyagin and I. A. Lysenko (1982), Phys. Solariterr. Potsdam, 18, 77.
- Elling, W., H. K. Geisweid and H. Schwentek (1974), In: Methods of Measurement and Results of Lower Ionosphere Structure, (ed. by K. Rauer), Akademie-Verlag, Berlin, pp. 313.
- Fedynski, A. V. and V. A. Yushkov (1979), In: Low Latitudinal Aeronomical Processes, (ed. by A. P. Mitra), Pergamon Press, Oxford, 263.
- Lauter, E. A. and B. Schaning (1970), J. Atmos. Terr. Phys., 32, 1619.
- Offermann, D., H. C. K. Bruckelmann, J. J. Barnett, K. Labitzke, K. M. Torkar and H. U. Widdel (1982), J. Geophys. Res., 87, 8286.
- Pakhomov, S. V., Z. Ts. Rapoport and V. M. Sinelnikov (1982), Paper presented at the COSPAR Symposium on Solar-Terrestrial Physics (Ottawa, Canada, 1982).
- Pakhomov, S. V., A. K. Knyazev, V. A. Yushkov, Z. Ts. Rapoport and V. M. Sinelnikov (1983), Paper presented at the MAP Symposium (Alma-Ata, USSR, 1983) (in Russian).
- Rapoport, Z. Ts. (1974), In: Methods of Measurements and Results of Lower Ionosphere Structure, (ed. by K. Rauer), Akademie-Verlag Berlin, 305.
- Rapoport, Z. Ts. (1979), Geomagn. and Aeronomy 19, 1042 (in Russian).
- Sato, T. (1981), J. Geophys. Res., 86, 9137.
- Schwentek, H. (1971), J. Atmos. Terr. Phys., 33, 1647.
- Sechrist, C. F., Jr. (1967), J. Atmos. Terr. Phys., 29, 113.
- Sechrist, C. F., Jr. (1970), Radio Sci., 5, 663.
- Shrestha, K. L. (1971), J. Atmos. Terr. Phys., 33, 213.
- Thomas, L. (1971), J. Atmos. Terr. Phys., 33, 157.

N85

20460

UNCLAS



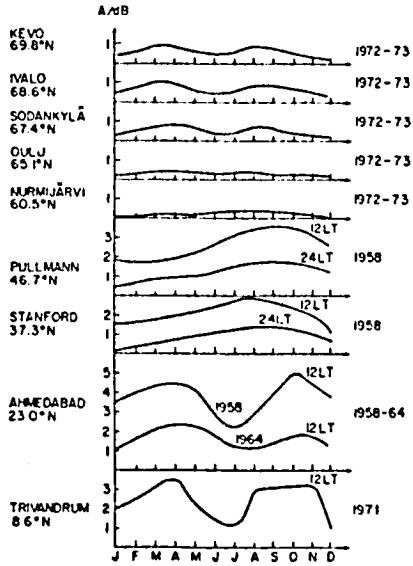


Figure 2. Variation of the total ionospheric absorption measured by riometers at different geographic latitudes in the Northern Hemisphere. For Finnish stations the monthly mean absorption values are used, for the other stations the monthly mean absorption values at 12 and 24 LT.

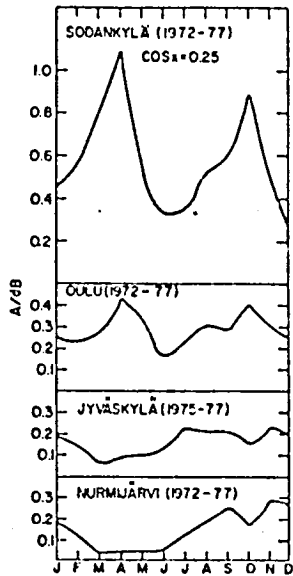


Figure 3. Seasonal variation of ionospheric absorption at constant solar zenith angle.

N85  
20461

UNCLAS

N 85-20461

## WINTER ANOMALY 1982/83 IN COMPARISON WITH EARLIER WINTERS (1960-82)

J. Lastovicka

Geophysical Institute  
 Czechoslovak Academy of Sciences  
 141 31 Praha 4, Czechoslovakia

The winter anomaly in the winter of 1982/83 is compared with the winter anomalies of earlier winters (1960-82) from the point of view of amplitude and timing of the winter anomaly, and geomagnetic and dynamic activity influences. Some evidence of a negative influence of sudden stratospheric warmings on the winter anomaly is given.

Ionospheric absorption of radio waves has been measured continuously since 1960 at the Panska Ves Observatory (Czechoslovakia) by the A3 method. The measurements have been performed on four A3 paths situated in Central Europe (see Table 1).

Figure 1 shows the year-to-year variability of the magnitude of the normal (background) winter anomaly ( $L_w/L_s$  - winter/summer ratio of absorption) over the period 1960-83. The  $L_w/L_s$  ratio is calculated as the ratio of the absorption in the month of maximum winter anomaly to the mean absorption for the summers (June, July) before and after the winter in question. The 1539 kHz data are computed from values measured at  $\chi = 75^\circ$ , other data are mid-day (noon  $\pm 2.5$ h) mean values derived from monthly half-hour median values of absorption reduced to the January solar zenith angle.

The winter anomaly phenomenon occurs every year (Figure 1), but its magnitude displays a pronounced year-to-year variability. The magnitude of the winter anomaly in the last winter (1982/83) appears to be very low and is expected to remain low even after the expected increase of  $L_w/L_s$  when including the forthcoming summer 1983 values.

Figure 2 shows the development of radio-wave absorption at 6090 kHz and 1539 kHz, measured at Panska Ves at  $\chi = 75^\circ$ , and the development of geomagnetic activity in the winter of 1982/83. Unfortunately, the 6090 kHz data were less reliable during this winter due to technical problems. Geomagnetic activity was very high this winter, the highest being observed in February. The monthly medians of absorption (short bold horizontal lines in Figure 2) display a maximum in February as a response to the highest geomagnetic activity. The winter anomaly maximum in February is rather exceptional. It has only been observed in 3 winters of the 23 winters studied, always in relation to high magnetic activity. In spite of high magnetic activity, the main period of the stratospheric warming related reversal of the prevailing zonal wind observed in Central Europe (Collm Observatory - SCHMINDER, 1983) is reflected well in the 1539 kHz absorption in the form of a deep decrease of absorption, as expected.

Summarizing, it can be said that the winter 1982/83 is not suitable for studying a "pure meteorological" winter anomaly because of very high magnetic activity, but it supports my recent conclusion (e.g. LASTOVICKA, 1983) about the negative influence of stratospheric warmings and associated reversals in zonal winds in the upper mesopause region on radio-wave absorption.

There is further evidence of the negative influence of stratospheric warmings on absorption. In winters with major stratospheric warmings (Table 2), the winter anomaly maximum has been observed in a month other than the stratospheric warming maximum. There is only one significant exception -- the most untypical winter of 1979/80 -- when both maxima were observed in February due to

Table 1.

TRANSMITTER	f (MHz)	f <sub>eq</sub> (MHz)	REFLECTION POINT		PERIOD OF RELIABLE WORK
			ψ(N)	λ(E)	
Kiel	2.775	1.0	52°27'	12°27'	1960-1973
Norddeich	2.614	0.8	52°08'	11°00'	1960-1973
Luxemburg	6.090	2.1	50°04'	10°18'	since 1971
Deutschlandfunk	1.539	0.65	50°16'	11°47'	since 1978

Table 2. Winter anomaly maxima in winters with major stratospheric warmings. Dates of stratwarm maxima after FINGER et al. (1979), LABITZKE et al. (1981) and LABITZKE (1981). x - specific distribution of magnetic and stratospheric activity.

WINTER	STRATWARM MAXIMUM	2775 kHz MAXIMUM	2614 kHz MAXIMUM	6090 kHz MAXIMUM	1539 kHz MAXIMUM
62/63	27 Jan	Dec	Dec	-	-
65/66	31 Jan	Dec	Dec	-	-
67/68	1 Jan	Dec	Dec-Jan	-	-
69/70	2 Jan	Dec	Jan	-	-
70/71	7 Jan	Dec	Dec	-	-
72/73	6 Feb	Jan	Dec	Jan	-
73/74	3 Mar	-	-	Jan-Dec	-
74/75	2 Mar	-	-	Jan	-
76/77	4 Jan	-	-	Dec	-
78/79	25 Feb	-	-	Jan	Jan-Dec
79/80	29 Feb	-	-	Feb <sup>x</sup>	Feb <sup>x</sup>
80/81	6 Feb	-	-	Jan	Jan

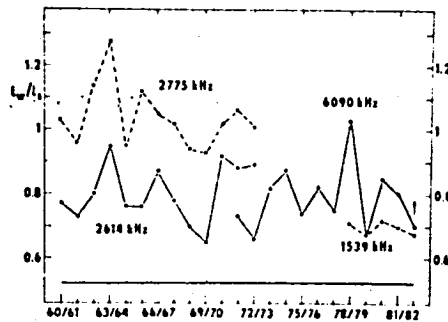


Figure 1. Long-term variability of the magnitude of winter anomaly, 1960-83.  $L_w/L_s$ , winter/summer ratio of absorption, reduced to the same level of the "no-anomaly" absorption ratio (horizontal line at the bottom). Vertical arrow, the 1982/83 value is expected to increase a little after including the summer 1983 values.

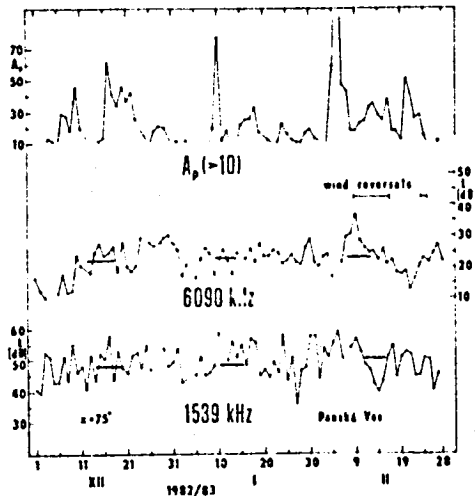


Figure 2. Development of radio-wave absorption at  $\chi = 75^\circ$  and of geomagnetic activity (only  $A_p > 10$  is shown) in the winter of 1982/83. The periods of stratwarm-associated reversals of the prevailing zonal wind in the upper mesopause region (observations at Collm - SCHMINDER, 1983) are shown, too.

specific distribution of geomagnetic activity and minor stratwarms during this winter. The "mutual incompatibility" of the winter anomaly and major stratospheric warming maxima is still more important for winters with the major stratwarm maximum in January. The winter anomaly maximum in winters without a major stratwarm (10 winters) has been observed in January, while in winters with the major stratwarm maximum in January, the winter anomaly maximum has been observed in December (Table 2). Consequently, the occurrence of a major stratospheric warming appears to be followed by a decrease, not an increase, of absorption (i.e. of winter anomaly). This agrees with LASTOVICKA and TRISKA (1982) and LASTOVICKA (1983).

In conclusion it can be said that major stratospheric warmings and related changes in the prevailing zonal wind in the upper mesopause region decrease the magnitude of radio wave absorption and winter anomaly. The winter of 1982/83 supports this conclusion, even if this winter is not suitable for studying a "pure meteorological" winter anomaly due to the very high geomagnetic activity in this winter.

#### ACKNOWLEDGEMENT

I thank Dr. R. Schminder of the Collm Observatory for sending me unpublished wind data.

#### REFERENCES

Finger, F. G. et al. (1979), Stratospheric Warmings 1951-1978, STP and

- Meteorology, Working Doc. III, 90-91, NOAA, Boulder.
- Labitzke, K., R. Lenschow and B. Naujokat (1981), Coordinated study of the behaviour of the middle atmosphere in winter, Handbook for MAP, Vol. 1, 67-75.
- Labitzke, K. (1981), In: UAP Bulletin, Special MAP issue, 8-10, FAA, Washington, July 1981.
- Lastovicka, J. and P. Triska (1982), On the variability of radio wave absorption in central Europe in PMP-1 winters, Paper STP IV.2.8, presented at the Int. Symp. Solar-Terrestrial Physics, Ottawa, May 1982.
- Lastovicka, J. (1983), Winter anomaly and sudden stratospheric warmings, Paper presented at the First All-Soviet Symp. MAP Results, Alma-Ata, February 1983 (in Russian).
- Schminder, R. (1983), Private communication.

N85

20462

UNCLAS

N85-20462

## A MODEL OF THE INFLUENCE OF NEUTRAL AIR DYNAMICS ON THE SEASONAL VARIATION IN THE LOW IONOSPHERE

G. Nestorov, P. Velinov and T. Pancheva

Bulgarian Academy of Sciences  
Geophysical Institute  
1113 Sofia, Bulgaria

## INTRODUCTION

Recently it has become clear that the phenomena in the ionospheric D-region are determined to a great extent by dynamical processes in the strato-mesosphere and lower thermosphere. It is these processes that significantly influence the distribution of the minor neutral constituents and the whole ionic composition of the middle atmosphere, regulating the ionization-neutralization cycle of the D-region. In this respect much attention is paid to the study of the winter anomaly (WA) phenomenon on medium and short radiowaves, in which the meteorological character of the lower ionosphere is most prominent. Significant experimental data about the variations of the electron concentration, N, ion composition, temperature and dynamic regime during WA permit a better understanding of the character of the physical processes in the middle atmosphere. WA is recorded as an abrupt increase of absorption L of the middle and short radiowaves on different winter days caused by a significant growth of N predominantly in the 75-90 km region with a steep gradient in the 80-85 km interval. WA is usually observed at middle latitudes of both the Northern and Southern Hemispheres, and is best recorded in the frequency range  $f_i = f \cos i = 1-2$  MHz, where  $f_i$  is the equivalent frequency of the incident radiowave with a frequency f at angle i. This is confirmed by Figure 1 where we have presented the results of the absorption measurements in the Sofia ionospheric observatory, along the paths

Pristina-Sofia (1412 kHz/170 km;  $f_i = 1.1$  MHz)Greece-Sofia (4050 kHz/320 km;  $f_i = 2$  MHz)All measurements refer to a solar zenith angle  $\lambda = 78.5^\circ$  ( $\cos \lambda = 0.2$ ).

The seasonal variation shown in Figure 1 allows a quantitative estimation of WA magnitude by calculating the excess of the winter absorption value,  $L_w$ , over the summer one,  $L_s$ . In this way the  $L_w/L_s$  ratio, obtained in experimental and theoretical ways, will serve as a criterion for comparing the different physical models of the middle atmosphere.

The purpose of the present report is to evaluate the influence of the neutral wind on the seasonal variation of the electron concentration N for the altitude interval  $90 \leq z \leq 120$  km, where the ratio  $\nu_{in}/\nu_i$ , of the ion-neutral collision frequency,  $\nu_{in}$  and the ion gyrofrequency,  $\nu_i$  decreases from 40 to 1. CIRA-72 is used as a model of the zonal wind.

## THEORETICAL MODEL

The distribution of the electron concentration N in ionospheric regions D- and E- is described by the balance equation:

$$\frac{\partial N}{\partial t} = q - \alpha N^2 - \text{div}(N \vec{v}_e) \quad (1)$$

where q is the electron production rate,  $\alpha$  the recombination coefficient, and  $\vec{v}_e$  the mean electron velocity. Due to the neutrality of electrical charge the following equation holds:

$$\text{div}(N \vec{v}_e) = \text{div}(N \vec{v}_i) \quad (2)$$

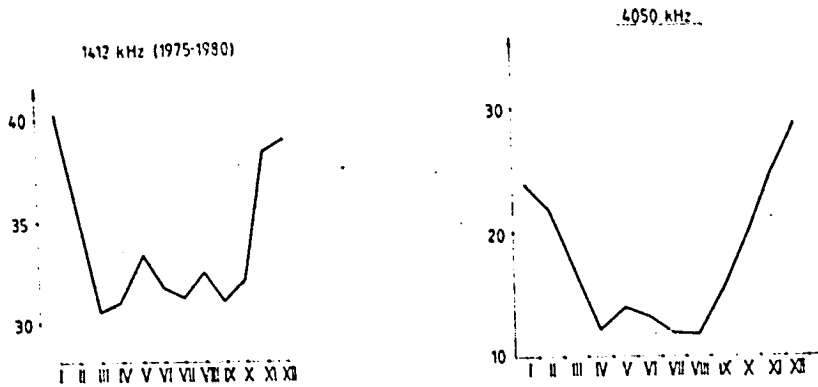


Figure 1a.

Figure 1b.

i.e. ion velocity should be investigated instead of electron velocity. Then, if we assume the three-component model of the ionosphere (neutrals, heavy positive ions and electrons) it becomes necessary to determine the ion drift velocity as a function of the neutral wind, geomagnetic field and  $r_i = v_{in}/v_i$ . If seasonal variations of the neutral wind for different altitudes are known and if the preliminary model for  $q$  and  $\alpha$  is determined and conditioned by ionospheric chemistry in different months, then it is easy to find the seasonal distribution of the electron concentration.

If we neglect the pressure gradient and electric field forces, the macroscopic motion of heavy positive ions in a collisional ionosphere with geomagnetic field is described by

$$d\dot{v}_i/dt = v_{in}(\dot{v} - \dot{v}_i) + (e/m_i)[\dot{v}_i \times \mathbf{B}] \quad (3)$$

where  $e$  and  $m_i$  are the charge and mass of the ions,  $\dot{v}_i$  the ion drift velocity,  $\dot{v}$  the neutral gas velocity, and  $\mathbf{B}$  the local geomagnetic field. Under quasi-steady conditions the ion velocity is determined from (3) as follows:

$$\dot{v}_i = (1 + r_i^2)^{-1} (r_i^2 \dot{v} + r_i[\dot{v} \times \hat{\gamma}]) + (\dot{v} \cdot \hat{\gamma})\hat{\gamma} \quad (4)$$

where  $\mathbf{B} = B_0 \hat{\gamma}$  and  $\hat{\gamma} \cdot \hat{\gamma} = 1$ . From (4) it follows that  $\dot{v}_i$  is strongly influenced not only by the different neutral winds at different altitudes, but also by the strong altitude dependence of  $r_i$ . When  $r_i \gg 1$  there is a full drag of ions by the neutrals, and  $\dot{v}_i = \dot{v}$ . This holds between 60 and 90 km. In the height range from 90-100 to 140 km,  $r_i$  is of the order of 1, and this region is known as the transition region (ANFORD, 1963). There

$$\dot{v}_i = (1 + r_i^2)^{-1} (r_i^2 \dot{v} + r_i[\dot{v} \times \hat{\gamma}]). \quad (5)$$

Finally, when  $r_i \ll 1$ , then  $\dot{v}_i = (\dot{v} \cdot \hat{\gamma})\hat{\gamma}$ .

The quantity of the ion flow is measured by the convergence of the ion velocity. If  $\dot{v}_i$  is given by (5), then

$$\begin{aligned} \text{div } \dot{v}_i &= (1 + r_i^2)^{-1} (r_i^2 \text{div } \dot{v} + r_i(\hat{\gamma} \cdot \text{rot } \dot{v})) + \\ &+ (1 + r_i^2)^{-2} (2r_i \dot{v} + (1 - r_i^2)[\dot{v} \times \hat{\gamma}]) \cdot \nabla r_i \end{aligned} \quad (6)$$

Experiments indicate that the horizontal neutral wind components usually are an order of magnitude or so greater than the vertical component, while the vertical scales appear to be the same for the three components. Hence we can take  $\vec{v} = (v_x, v_y, 0)$ . We use the standard coordinate system in which the x-axis points to geomagnetic east, the y-axis to geomagnetic north, and the z-axis vertically upward. A horizontally stratified ionosphere is assumed. For altitudes 90-100 km, from (5) and (6) follows

$$v_{iz} = [r_i / (1 + r_i^2)] \gamma_y v_x \quad (7)$$

$$v_{iz} / z = [r_i / (1 + r_i^2)] \gamma_y v_x / z + [(1 - r_i^2) / (1 + r_i^2)^2] \gamma_y v_x r_i / z$$

As we are interested in the seasonal course of N for the respective altitudes, we have to solve the quasi-stationary equation (1):

$$dN^2 + [\gamma_y / (1 + r_i^2)] r_i v_x / z + \frac{1 - r_i^2}{1 + r_i^2} v_x r_i / z + r_i p v_x N - q = 0 \quad (8)$$

where the altitude profile of N is taken in the form  $N(z) = N_0 \exp(pz)$  (VELINOV et al., 1974).

In the height range 115-120 km, the full ion velocity or the equation (5) is used. Then the redistribution of electron concentration is influenced not only by the zonal but also by the meridional wind. Then:

$$v_{iz} = [\gamma_y / (1 + r_i^2)] (r_i v_x + \gamma_y v_y) \quad (9)$$

$$\frac{dv_{iz}}{dz} = \frac{\gamma_y}{1 + r_i^2} \left\{ r_i \frac{dv_x}{dz} + \gamma_y \frac{dv_y}{dz} + \frac{1}{1 + r_i^2} \frac{dr_i}{dz} [(1 - r_i^2) v_x - 2r_i \gamma_z v_y] \right\}$$

From (9) it follows that the influence of the meridional wind increases with increasing altitude.

#### NUMERICAL RESULTS

We are interested in the influence of the neutral wind on the seasonal course of absorption of short radiowaves, where the WA is clearly felt. Our attention is drawn by the courses, shown on Figure 1. As some of the radiowaves are reflected below 100 km, other between 100 km and 110 km, it becomes necessary to consider the altitude range from 90 km to 110 km, and to determine mainly the influence of the zonal winds on the seasonal course of N. Assuming that  $L = N$ , we can compare theoretical and experimental results. From CIRA-72 we obtain a monthly value of the zonal wind and wind shear for altitudes 90, 95, 100 and 110 km, for  $\lambda = 40^\circ N$ . We include them in equation (8) and solve it. For altitudes 100 km and 110 km we used data for the meridional wind from MANSON et al. (1981), for January, February and March only. Their influence on N is slight. As the absorption is an integral characteristic, in order to be able to compare the seasonal course of  $L_{1412}$  with the course of N it is necessary to add the seasonal courses of N, influenced by the zonal wind for the altitudes 90, 95 and 100 km (Figure 2). The influence of the zonal wind on WA is obvious, conditioned by the model of  $\mu$  and  $q$ . If the latter increases the winter values of N over the summer values by 16%, then if we add the wind this increase is augmented up to 25%. The experimental results show an increase by 30%. Theoretically obtained seasonal course of N in Figure 2 clearly shows the experimentally obtained secondary maximum in May and minimum in July, as well as the sharp increases of N from October to November, known as "October-effect".

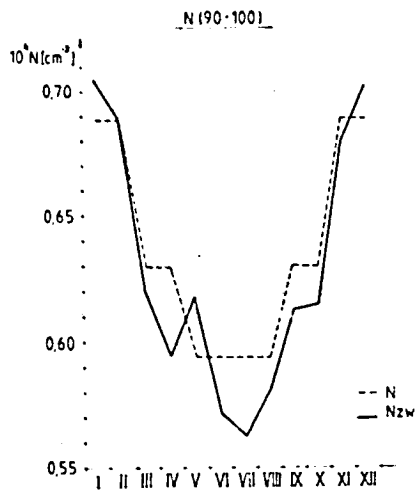


Figure 2.

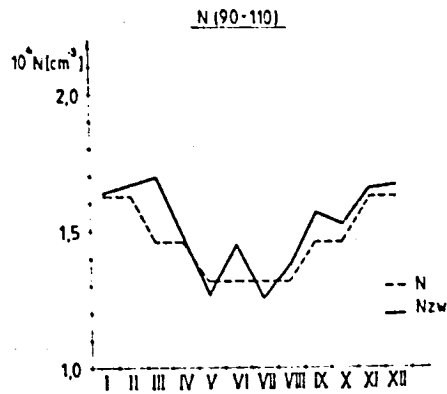


Figure 3.

The same is done for the second radio path,  $L_{4050}$ , and the influence of N by the altitude 110 km is added. Figure 3 shows the seasonal course of the average N. The increases of the winter values are about 38%, but considerably lower than experimentally observed. This may be due to the above mentioned model of  $q$  and  $\alpha$ . The neglect of the influence of the electric field makes itself felt stronger at these altitudes. Figure 3 shows well the summer maximum, which is clearly seen on Figure 1b.

The theoretical results compared with experimental results are encouraging and clearly show the influence of the neutral atmosphere dynamics on the seasonal variation of the electron concentration, N.

#### REFERENCES

- Axford, W. I. (1963), *J. Geophys. Res.*, **68**, 769.  
 Manson, A. H., C. E. Meek and J. B. Gregory (1981), *Handbook for MAP*, Vol. 2, 101, SCOSTEP Secretariat, Urbana, Illinois.  
 Velinov, P., G. Nestorov, and L. Dorman (1974), *Cosmic Ray Influence on the Ionosphere and on Radio Wave Propagation*, Publ. House of Bulg. Acad. Sci., Sofia, pp. 136-142.

N85

20463

UNCLAS

113  
70

# N 85 - 20463

## EXPLANATION OF THE NORMAL WINTER ANOMALY FROM THE SEASONAL VARIATION OF SHORT-WAVE ABSORPTION

P. J. Velinov

Bulgarian Academy of Sciences  
Geophysical Institute  
1113 Sofia, Bulgaria

N. V. Smirnova and V. A. Vlaskov

Academy of Sciences of the USSR  
Polar Geophysical Institute  
Murmansk, USSR

### INTRODUCTION

The frequency dependence of the winter anomaly (WA) of radiowave absorption (LAUTER et al., 1976; FRIEDRICH et al., 1979; VELINOV, 1975; SCHWENK et al., 1978; and NESTOROV, 1965) indicates the altitude range where the considered seasonal variation of absorption,  $L$ , takes place: 75-95 km. In this height region considerable seasonal variations of ionic composition and effective recombination coefficient,  $\alpha_e$ , exist, which can cause seasonal variations of electron concentration,  $N$ , and absorption,  $L$ . In this paper we shall attempt to render a qualitative estimation of the normal WA, i.e. the increased ratio of winter over summer absorption,  $L_w/L_s$ , at medium latitudes  $40^\circ$  and  $50^\circ$ , for solar zenith angles  $\chi = 60^\circ$  and  $75^\circ$ , and compare this with existing experimental data.

### IONIZATION RATE PROFILES

As it is well known, non-deviative radio wave absorption is determined both by the electron density profile,  $N(h)$ , and by the collision frequency. Existing data prove (e.g., SMITH et al., 1978) that the seasonal variation of collision frequency at medium latitudes is insignificant. Therefore the observed increase of  $L_w/L_s$  must appear as a result of enhanced  $N$  under winter conditions. Profiles of ionization rate,  $q(h)$ , needed for the calculation of  $N(h)$ , are shown in Figure 1 for January and July ( $40^\circ N$ ,  $\chi = 60^\circ$ ) at low solar activity ( $F_{10.7} = 90$ ). They are composed of (a) ionization by Lyman- $\alpha$  radiation, calculated by

$$q_{NO}^+ = I_{L\alpha}^m \sigma_{NO} [NO] \exp\{-Ch(x, h) N_{O_2}(h) \sigma_{O_2}\}$$

where  $\sigma_{NO} = 2 \times 10^{-18} \text{ cm}^2$  and  $\sigma_{O_2} = 10^{-20} \text{ cm}^2$ , and

$$I_{L\alpha}^m = 4.3 + 1.5 \times 10^{-2} (F_{10.7} - 80) \text{ erg/cm}^2 \text{ s}$$

(b) ionization of  $O_2(^1\Delta_g)$ , obtained from PAULSEN et al. (1972),

$$q_{O_2}^+ = [O_2(^1\Delta_g)] \times \{0.54 \times 10^{-9} \exp[-2.406 \times 10^{-20} N_{O_2}(h) Ch(x, h)] + 2.615 \times 10^{-9} \exp[-8.508 \times 10^{-10} N_{O_2}(h) Ch(x, h)]\}$$

(c) ionization by X-rays ( $\lambda < 10 \text{ \AA}$ ), found from

$$q(h) = \sum_{\lambda} I_{\lambda}^m k_{\lambda} \sum_{i, \lambda} n_i(h) \exp[-\tau_i N_i(h) \sigma_{i, \lambda} Ch(x, h)]$$



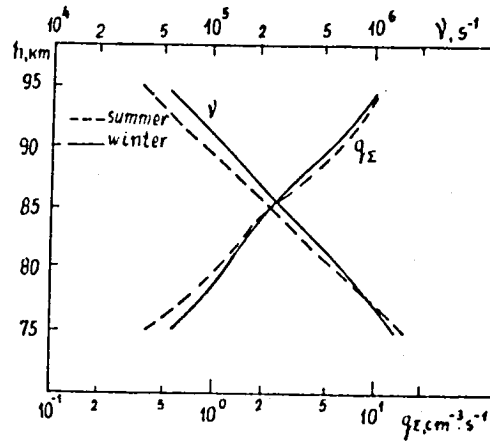


Figure 1.

where  $i = 1, 2$  stands for  $O_2$  and  $N_2$ ,  $k_\lambda$  is the ionization coefficient,  $\sigma_i$  and  $\bar{\sigma}_i$  are the ionization and absorption cross sections, respectively.

#### MODELING OF THE IONIZATION-RECOMBINATION CYCLE

After determining the  $q(h)$  profiles we proceed to determine  $\alpha(h)$  in order to construct  $N(h)$  profiles. Presently, theoretical models of the D region are developed in two directions: Simple models (NITRA and ROWE, 1972) and detailed models (FERGUSON, 1974; REID, 1977). The latter are of great scientific value but a number of processes are still insufficiently known. The main shortcoming of these schemes, however, is in that they require much computer time so that they are unfit for practical use. In view of this it seems necessary to develop a model of ionization-recombination cycle which includes the advantages of the two kinds of models, i.e., relative simplicity under physical suitability (SMIRNOVA, 1982).

The proposed hybrid scheme of ion chemistry is shown in Figure 2. It consists of four ions:  $O_2^+$ ,  $NO^+$ ,  $CI_1^+$ , and  $CI_2^+$  where  $CI^+$  means cluster ions. The simpler cluster ions,  $CI_1^+$ , are formed from the primary ions,  $O_2^+$  and  $NO^+$ , with formation rates  $B(O_2^+)$  and  $B(NO^+)$ , respectively. These rates appear to be effective parameters expressed by the rate constants in the detailed scheme (REID, 1977) and by the concentration of the neutral components involved. The more complex cluster ions,  $CI_2^+$ , are then formed from  $CI_1^+$ . The formation rates are calculated from the formulae:

$$B(NO^+) = r_1[H_2O][N_2] + C^{-1}r_2[N_2]^2r_4[H_2O] + r_6[H_2O](r_r[CO_2][N_2] + C^{-1}r_2[N_2]^2r_3[CO_2]) / (r_{-5}[N_2] + r_5[H_2O])$$

with  $C = r_{-2}[H_2] + r_3[CO_2] + r_4[H_2O]$ , and

$$B(O_2^+) = \frac{k_1[O_2]^2 + v_1[N_2]^2}{(k_2[O] + k_3[O_2(\Delta_g)] + k_{-1}[O_2]/k_4[H_2O]) + 1}$$

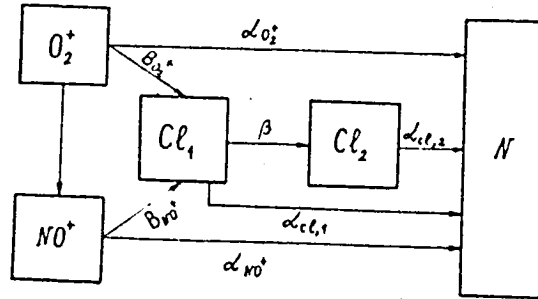


Figure 2.

All the coefficients,  $r_i$ ,  $k_i$ , and  $v_i$ , are temperature-dependent. The temperature dependence of the rates is essentially different (cf. the next section):  $B(\text{NO}^+)$  is proportional to  $T^{-4.4}$ , whereas  $B(\text{O}_2^+)$  is proportional to  $T^{-14}$ .

The advantage of this hybrid quadri-ionic scheme consists in the simplicity of its calculations. The effective recombination coefficient,  $\alpha_e$ , resulting from the ion composition calculated by this scheme, includes both a dependence on  $T$  and on  $[\text{H}_2\text{O}]$ . In Figure 3, calculated  $\alpha_e(h)$  profiles are shown for winter (full curve) and summer (dashed curve).

#### TEMPERATURE DEPENDENCE

The temperature dependence of the lifetime of  $\text{NO}^+$ ,  $\tau_{\text{NO}^+} = 1/B_{\text{NO}^+}$ , in the temperature range 120-230 K, has already been shown here (DANILOV, this volume, Figure 2 on page 19). It was calculated by the formula derived from REID's (1977) model. In that figure, the curve labelled 1 is for  $[\text{H}_2\text{O}] = 1 \times 10^{-6} [\text{M}]$ , curve 2 is for  $[\text{H}_2\text{O}] = 5 \times 10^{-6} [\text{M}]$  with a fixed  $[\text{M}] = 2 \times 10^{14} \text{ cm}^{-3}$ . The full dots are values of  $\tau_{\text{NO}^+}$  determined from simultaneous measurements of positive ion concentration, electron density, and temperature (ARNOLD, 1980). The theoretical temperature dependence of  $B(\text{NO}^+)$  well reproduces ARNOLD's (1980) experimental data. From these data it follows that  $B(\text{NO}^+)$  is approximately proportional to  $T^{-13.9}$  in the range 120-230 K, and to  $T^{-20.4}$  in the range 180-230 K. Comparison of curves 1 and 2 shows that the

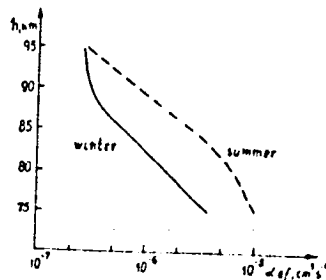


Figure 3.

influence of humidity on  $B(\text{NO}^+)$  is considerable only in the range of high temperatures. The seasonal variations of  $B(\text{NO}^+)$  at medium ( $40^\circ\text{N}$ ) and high latitudes, calculated for temperatures and densities taken from the CIRA-72 model have also been presented here (DANILOV, this volume, Figure 3 on page 20) together with  $B$  values experimentally determined from ion composition measurements (DANILOV and SIMONOV, 1981). The theoretical  $B(\text{NO}^+)$  curves are in good agreement with the data obtained in summer midlatitude experiments. Low  $B$  values under winter anomaly conditions are caused by an increase of  $T$ , which has been measured during the West European Winter Anomaly Campaign and other experiments. Large values of  $B$  in summer high-latitude experiments conducted under disturbed conditions can be explained by a large conversion rate of  $\text{O}_2^+$  ions into  $\text{Cl}^+$  under low summer temperatures. Larger values of  $B$  at the occurrence of noctilucent clouds result from a combination of low temperatures and high humidity.

#### ELECTRON DENSITY AND $L_w/L_s$

$N(h)$  profiles have been calculated with  $q(h)$  as described above, and with  $\alpha_e$  from the hybrid ion composition scheme, taking temperatures and density profiles from the CIRA-72 model, two variants of the water vapor concentration ( $[\text{H}_2\text{O}] = 1 \times 10^{-6} [\text{M}]$  and  $[\text{H}_2\text{O}] = 5 \times 10^{-6} [\text{M}]$ ), and with recombination coefficients  $\alpha_{\text{NO}^+} = 2.3 \times 10^{-7} (300/T)^{0.5}$  and  $\alpha_{\text{O}_2^+} = 1.9 \times 10^{-7} (300/T)^{0.5}$  after MUL and MCGOWAN (1977). The results are presented in Figure 4.  $N(h)$  profiles obtained in this way were used in the calculation of absorption  $L$  of radiowaves at an equivalent frequency of 1 MHz. The results of these calculations are given as winter-to-summer ratio,  $L_w/L_s$ , in Table 1, for  $\alpha_{\text{NO}^+} = 4 \times 10^{-7} (300/T)$  after MUL and MCGOWAN (1977), and for another model with  $\alpha_{\text{NO}^+} = 2 \times 10^{-7} (300/T)$  after LEU et al. (1973). Table 2 gives experimental data of seasonal absorption variations on radio paths with comparable equivalent frequencies. It is remarkable that the higher-latitude paths have a greater degree of manifesting the normal WA than the midlatitude paths. A greater seasonal  $L$  variation of the northern paths may be expected from larger seasonal variations in  $T$ ,  $[\text{NO}]$ , and air density.

#### DISCUSSION

Regardless of the fact that the calculated  $L_w/L_s$  ratios cannot be exactly compared with the experimental data because of the differences in latitude,  $f_{\text{eq}}$ , and  $\chi$ , yet allowing for the tendencies of  $L_w/L_s$  with  $\chi$  and latitude the results obtained in this paper can be considered as fully reasonable. From the fact that the excess of  $L_w$  over  $L_s$  is obtained already with very close  $q(h)$  profiles ( $q_w = q_s$ ) it can be concluded that in order to explain the normal component of the WA, it is not necessary to assume an enhanced ionization rate,  $q$ , but only a decrease of  $\alpha_e$  as a result of a lower

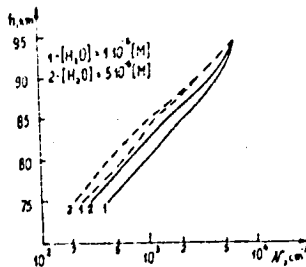


Figure 4.

Table 1

$\alpha(\text{NO}^+), \alpha(\text{O}_2^+)$	Leu, Biondi a. Johnson		Mul and McGowan	
$[\text{H}_2\text{O}]$	$1 \times 10^{-6} [\text{M}]$			
$[\text{H}_2\text{O}]$	$1 \times 10^{-6} [\text{M}]$	$5 \times 10^{-6} [\text{M}]$	$1 \times 10^{-6} [\text{M}]$	$5 \times 10^{-6} [\text{M}]$
$\frac{L_w}{L_s}$ 40°N, $\chi = 60^\circ$	1.5	1.77	1.67	1.96
50°N, $\chi = 78.5^\circ$	2.0	2.12	2.2	2.42

Table 2

f, kHz Radiopath/Distance	$\phi_{\text{refl}}, N^\circ$	$f_e$	$\cos \chi$	$L_w/L_s$
4050 Greece-Sofia/320 km	41.3	2	0.2	1.9
2831 Coburg-Graz/502	49.1	1	0.26	2
2775 Kiel-Neustrelitz/395	53.6	1.9	0.2	1.7
2775 Kiel-Panska Ves/520	52.5	1	0.2;0	1.5; 1.4
2614 Norddeich-Neustr./320	53.9	1.2	0.2;0	2.2; 1.1
1554 Nice-Roburent/80	44	1.5	0.2	1.5
1412 Pristina-Sofia/170	42.7	1.1	0.2	1.4
1223 St. Zagora-Sofia/200	42.5	0.8	0.26	1.2
1178 Horby-Kuhlungsbl./218	54.9	0.8	0.2;0	1.7; 1.2
1730 Lindau Al	52.6	1.7	0.2	1.6
Ushuaia Al	-55	1.7	0.2	2.2

$\text{Cl}^+$  formation rate in winter when temperatures are higher and air densities lower than in summer.

## REFERENCES

- Arnold, F. (1980), *J. Atmos. Terr. Phys.*, **42**, 243.  
 Danilov, A. D. and A. G. Simonov (1981), in: *Ionosfernye issledovaniya No. 34* (in Russian), Soviet Geophysical Committee, 39.  
 Ferguson, E. E. (1974), *Rev. Geophys. Space Phys.*, **12**, 703.  
 Friedrich, M., K. M. Torkar, G. Rose and H. Widdel (1979), *J. Atmos. Terr. Phys.*, **41**, 1163.  
 Lauter, E. A., J. Taubenheim, G. Entzian, J. Bremer, G. v. Cossart and G. Klein (1976), *HHI-STP Report No. 7*, Central Institute of Solar-Terrestrial Physics, Berlin-Adlershof, GDR.  
 Leu, T., M. Biondi and R. Johnson (1973), *Phys. Rev.*, **A7**, 293.  
 Mitra, A. P. and J. N. Rowe (1972), *J. Atmos. Terr. Phys.*, **34**, 795.  
 Mul, P. and M. McGowan (1977), *J. Phys.*, **B12**, 1591.  
 Nestorov, G. (1965), *C. R. Acad. Bulgar. Sci.*, **18**, 919.  
 Paulsen, D. E., R. E. Huffman and J. C. Larabee (1972), *Radio Sci.*, **7**, 51.  
 Reid, G. C. (1977), *Planet. Space Sci.*, **25**, 275.  
 Schwentek, H., W. Elling and M. Peres (1978), *J. Atmos. Terr. Phys.*, **42**, 545.  
 Smirnova, N. V. (1982) in: *Mathematical Modelling of Complex Processes etc.* (in Russian), Acad. Sci. USSR Publ. House, 22.  
 Smith, L. G., E. K. Walton and E. A. Mechtly (1978), *J. Atmos. Terr. Phys.*, **40**, 1185.  
 Velinov, P. (1975), *C. R. Acad. Bulgar. Sci.*, **28**, 1605.

N85

20464

UNCLAS

№85-20464

75

SEASONAL CHARACTERISTICS OF MESOSPHERIC PLASMA AND THEIR TRANSITIONS

E. A. Lauter

Academy of Sciences of the GDR  
Central Institute of Solar-Terrestrial Physics  
Observatory of Ionospheric Research  
DDR-2565 Kuhlungsborn, GDR

The main seasonal features of the middle atmosphere are arising from the different dynamical basic states in winter and summer. The development of the two controversial circulation systems and the also different peculiarities of transition between them in spring and autumn create the completely dominant seasonal variations in strato- and mesosphere. Even in the plasma structures of the mesospheric D-region the seasonal variation is towering above the amplitudes of extraterrestrial influences. Therefore, the conventional monitoring of the D-region by radio wave propagation methods is still important for the exploration of atmospheric processes in mesosphere and lower thermosphere and the modes of action in the stratosphere. Due to the activities of the IGY and IQSY there are now available long series of such data for Middle Europe (50°-60°N) in Ionospheric Bulletins of the MPI Lindau (FRG), ZISTP-OIF Kuhlungsborn (GDR), de Bilt (Netherlands) and Uppsala (Sweden). From standard ionospheric sounding, from A1 and A3 absorption measurements and from winds in the meteor region we know the existence of significant seasonal D- and E-region effects, adhering to equally significant structure changes in the neutral gas in the height region from 20 to 100 km.

We have summarized results about such typical seasonal features in Figures 1 and 2. Following at first the sectors of representation in Figure 1 we may give the following statements:

- (1) In mid-latitudes a pronounced increase of the occurrence probability of the sporadic E-layer exists in summer, lasting from the beginning of May up to the end of August (SPRENGER, 1981) (typical duration time (TDT) of the phenomenon 130 days).
- (2) In the meteor-wind region there exists a regime, which can be described by four seasonal periods (SPRENGER et al., 1974; GREGORY et al., 1982): Two west wind periods correspond to the main development of the stratospheric circulation systems. Representing the upper boundary of the uniform circulation from troposphere to mesosphere in winter, rather stable west winds exist in the 90 km region from late October towards March, culminating in intensity around winter solstice (TDT 140 days). A second west wind period from May to September belongs to a fluctuating thermospheric circulation, existing within and above the cold summer mesopause. Two rather significant transition periods are separating these two wind regimes. The most pronounced one is the wind reversal in spring, i.e. east winds from March 15 till May 10, with a maximum around April 10. The second transition period occurs in autumn between early September and late October with disappearing westerlies and calms in the zonal circulation. Both transition periods are reacting, with significant phase changes in the tidal wind components, on the decrease or reversal of the zonal circulation in the mesospheric wind system below.
- (3) The most remarkable seasonal feature of the D-region is the ionization enhancement in the height region from 80-100 km, the winter anomaly, lasting in our latitude from very late October up to the first days of March (TDT 130 days). It is best observed on frequencies around 1.8 MHz (Figure 1c and Figure 2), which penetrate the whole D-region, when they are reflected at the bottom of the E-layer. An increased electron density gradient at the bottom of the D-

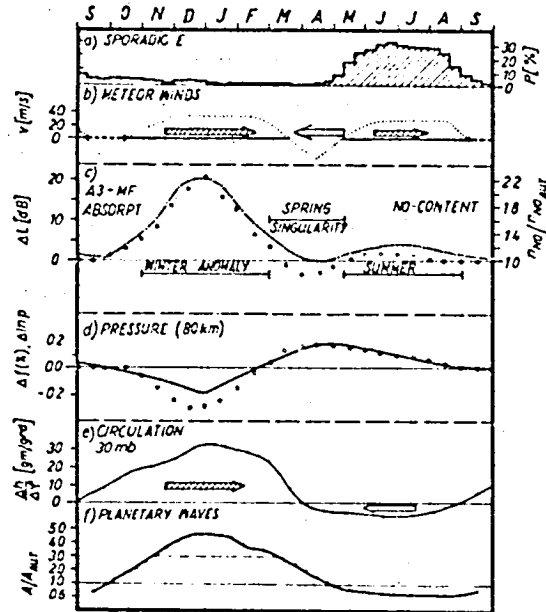


Figure 1. a) Lower thermosphere: probability of E occurrence; b) Meteor winds; c) Upper mesosphere (86 km), high frequency absorption (full line), variation of NO content in respect to Autumn (dots); d) Pressure at 80 km from rockets (full line) and from VLF phase height (dots); e) Circumpolar zonal circulation at 30 mb; f) Planetary wave amplitude at 30 mb.

region accompanies this phenomenon, which is thought to be produced by an enhanced content of nitric oxide in and above the winter-time cyclonic polar vortex. From low-frequency phase height analysis we can find an estimation for the seasonal trend of NO increase in 86 km, relative to normal autumn conditions (LAUTER et al., 1983). The dotted trend in Figure 1c informs us that a NO increase by a factor of 2.5 in this height may describe the anomalous ionization around winter solstice. This extreme ionization enhancement in winter is followed by an ionization deficit in spring, when on all frequencies (Figure 2) an absorption minimum occurs.

(4) In mid-latitudes the pressure at 80 km undergoes a rather continuous variation as to be seen from the Volgograd rocket results (Figure 1d). The winter minimum of pressure corresponds to the maximum of the mesospheric circulation. There is a rather fast transition towards a pressure maximum in spring (April), shifting to late March with greater heights. Analyzed for the same height from VLF reflection height observations, the relative pressure variation (dotted trend in Figure 1d) is in remarkable coincidence with the rocket results, demonstrating also the spring maximum and the small but rather steady pressure decrease over the whole summer up to October, when the drop towards winter level becomes sharper.

(5) The change of the basic states of the middle atmosphere is, of course, seen

best in the circumpolar zonal circulation, expressed in Figure 1e in terms of the gradient of the 30 mb level between 50°N and the pole (geopotential meters per degree of latitude). It is easily seen that the westerlies in winter are rather steeply decreasing towards spring, defining a mean reversal date to easterlies of April 2 for the last 25 years. Contrarily, the autumn reversal is much smoother and more precisely at the very end of August. That means that the winter status of the stratosphere has a typical duration time of 215 days in comparison with the summer status of 150 days. The latter is caused mainly by the radiation transfer of the atmospheric ozone layer and defines the decoupling of meso- and stratospheric energetics from the lower atmosphere. The wind reversal dates in spring are widely fluctuating from year to year obviously in connection with the quasi-biennial wave and preceding major stratospheric warmings, which generally retard the spring reversal (ENTZIAN and LAUTER, 1982).

(6) As a further important parameter of the middle atmospheric dynamics we show in Figure 1f for the 30 mb-level the mean annual trend of the planetary wave amplitude (wave number 1 and 2) relative to its spring and autumn values. It can be seen that the duration of strongly enhanced planetary wave amplitudes (amounting to three times the equinox amplitude) is from the beginning of November to the end of February (TDT  $\approx$  120), comparable with the duration of the winter anomaly. This parameter normally increases rather steadily up to mid-winter, but often fluctuates rather heavily afterwards, especially in connection with stratospheric warmings.

Summarizing the results from Figure 1 we may say, that the annual trends of middle atmosphere parameters do inform us about significant seasonal variations from the stratosphere upwards to the lower thermosphere, but the coupling between the presented parameters is not yet well explored. For example, we expect indeed that the occurrence of sporadic E-layer is connected with wind shears, but we have not yet detected a connection between E-layer and the meteor winds. In the same way we have no clear connection between the tidal structure of the meteor winds and the thermal regime of the mesosphere. On the other hand we know that a significant coupling exists from middle stratosphere to the mesopause region in winter and spring. The development and intensity of the ionospheric winter anomaly is dependent on the development and intensity of the stratospheric-mesospheric circumpolar cyclonic vortex. The winter anomaly, i.e. the enhanced NO-content, disappears rather suddenly when the reversal of the stratospheric wind system occurs, during a major stratospheric warming event as well as in spring. The coupling of the zonal winds in winter is also well detectable up to the meteor region in winter.

Beside the dominating winter features in the middle atmosphere parameters, the significant transitions from winter to summer state in this height region have to be considered. We call these remarkable features the "spring singularity" of the middle atmosphere, which includes:

- The final break-down of the cyclonic stratospheric vortex, i.e. the wind reversal to strato- and mesospheric east winds.
- The disappearance of the upward propagation of planetary waves in the middle stratosphere.
- The pressure maximum in lower and middle mesosphere.
- The total disappearance of the winter NO accumulation in the D-region, a significant minimum of ionospheric absorption.
- The well developed temporal reversal of zonal winds in the meteor zone.

These features of the spring singularity are repeated every year between

middle of March and end of April, announcing the decoupling of the layers from the middle atmosphere. It is well known that the summer state of the middle atmosphere has also some well developed properties (e.g. opposite winds in mesosphere and lower thermosphere, E<sub>s</sub>-layer occurrence). It is much less known that also the D-region has a significant summer status. In Figure 2 we have therefore represented the annual trends of ionospheric absorption on different frequencies. At high frequencies (Figure 2a) the winter maximum dominates, A3 and A1 measurements have the same trend and comparable amplitude. Towards lower frequencies the A3 (245 kHz) semiannual variation is present with maxima in winter and summer and minima in spring and autumn. On low frequencies (f = 200 kHz) a well developed summer maximum of absorption exists, lasting from May to September (TDT - 130 days). This enhanced summer absorption is most remarkably developed on low and very low frequencies. This effect of a very low electron density gradient at the bottom of the D-region is already detectable at sunrise conditions and is lasting over the full day. Separated by the spring singularity, the reversal of the frequency dependence of ionospheric absorption is a very significant indicator for the transition from winter to summer season in the D-region.

A further significant seasonal difference in the plasma state of the mesosphere is the fact, that the influence of solar activity upon D-region is much more pronounced in summer than in winter. From 30 years of D-region observation we find correlations with the solar activity of  $r \geq 0.9$  in summer and  $r \leq 0.6$  in winter months. This gives evidence that the winter D-region structure is much more dependent on the internal atmospheric processes than the summer one.

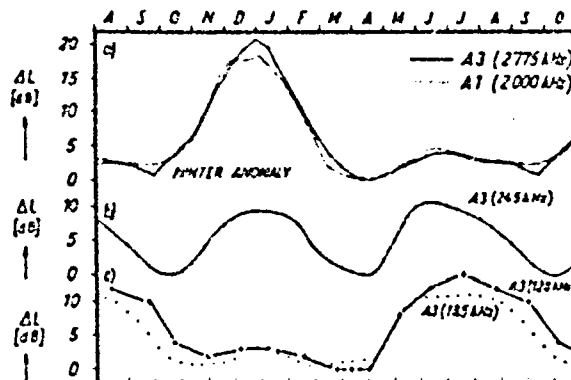


Figure 2. The annual trend of ionospheric absorption on different frequencies.

#### REFERENCES

- Entzian, G. and E. A. Lauter (1982), *Z. Meteorol.*, **32**, 209.  
 Gregory, J. B., C. E. Meek and A. H. Manson (1982), *J. Atmos. Terr. Phys.*, **44**, 649.  
 Lauter, E. A., J. Taubenheim and G. von Cossart (1983), *J. Atmos. Terr. Phys.*, (in press).  
 Sprenger, K. (1981), *Gerlands Beitr. Geophys. Leipzig*, **90**, 305.  
 Sprenger, K., R. Schindler, K. M. Greisiger, D. Kuschner and B. Schaning (1974), *HHI-STP-Report No. 2*, Central Institute of Solar-Terrestrial Physics, Berlin, GDR.

N85

20465

UNCLAS

N85-20465

D15  
79

MIDWINTER DISTURBANCES IN THE MIDDLE ATMOSPHERE

K. Labitzke

Meteorological Institute  
Free University  
Berlin, FRG

The "Middle Atmosphere" is coupled to the troposphere during winter because planetary scale waves can propagate upwards if the prevailing winds are from the west. It is during this time of the year that the well-known "midwinter disturbances" are observed which ultimately affect the whole of the Middle Atmosphere. The mechanism of these disturbances is not completely understood and it will be one key problem to be studied within the MAP (Middle Atmosphere Program).

The large-scale circulation features up to the upper mesosphere will be shown in this paper to demonstrate the synoptic-scale behaviour of the midwinter disturbances. Ground-based and satellite observations will be combined.

The interannual variability of the disturbances will be discussed briefly and it will be shown that the QBO (Quasi Biennial Oscillation) of the equatorial stratosphere appears to modulate the planetary waves during the northern winters, in the troposphere as well as in the Middle Atmosphere.

Figure 1 shows the course of the stratospheric temperatures or radiances over the North Pole during the last winter, 1982/83, and three warming pulses can be clearly distinguished. These warming pulses are also well documented by the rocketsondes launched from Heiss Island/USSR, Figure 2. While the data given in Figure 1 cover only the stratosphere, the rocketsonde data also show the temperature changes in the upper stratosphere, if one considers the situation at the same location and at the same time.

The midwinter disturbances are caused by the amplification of the large planetary-scale waves which propagate upwards from the troposphere through the stratosphere into the upper mesosphere. The horizontal patterns of these waves are shown in Figures 3-6 for a few selected days between 13 and 27 February, 1983, covering the last warming pulse, cf. Figure 1.

While the 30-mbar height fields are based on radiosondes, the upper levels are constructed using thicknesses derived from the SAMS experiment (Stratospheric and Mesospheric Sounder, onboard Nimbus 7). The 1-mbar height fields are based on the SSU experiment (Stratospheric Sounding Unit, onboard the NOAA satellites).

On February 13, 1983, Figure 3, the circulation was relatively undisturbed in the stratosphere and lower mesosphere, i.e., up to the 0.1-mbar level. But a minor warming was present over Eastern Europe, as indicated by the high radiance values of Ch. 27 of the SSU. And consequently, an anticyclone developed, cf. the 0.01-mbar chart in Figure 3, which accounts for a period with winds from the east in the 90-100 km region over Central Europe, as indicated by the low frequency ion drift measurements of the Collm Observatory, cf. Figure 7. When comparing the Collm-data with the 0.01-mbar charts, one has to keep in mind that the planetary-scale waves usually are sloping westwards with height and that the Collm-data belong to a region about 15 km above the 0.01-mbar level.

At the same time the winds were from the west in the whole layer between 58-84 km over Canada, as reported by the partial reflection radar of Saskatchewan, cf. Figure 7.

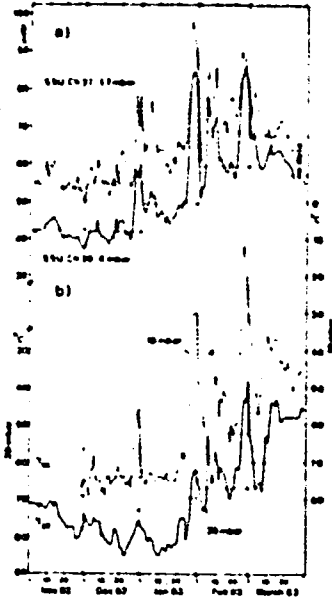


Figure 1. March of radiances and temperatures over the North Pole (horizontal lines are long-term monthly means). a) Radiances ( $\text{mW/m}^2\text{sr cm}^{-1}$ ) of channel 27 and 26 of the SSU, maximum weight around 1.7 and 4 mbar (courtesy Meteorological Office, Bracknell, UK); b) Temperatures ( $^{\circ}\text{C}$ ) at 10 and 30 mbar (data FU Berlin) (from NAUJOKAT et al., 1983).

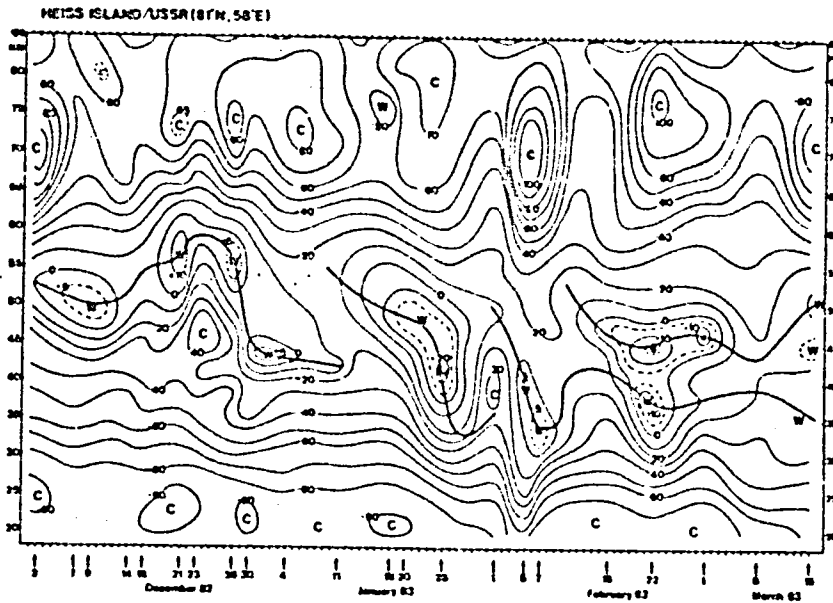


Figure 2. Time height section of rocketsonde temperatures ( $^{\circ}\text{C}$ ) from 2 December 1982 to 15 March 1983 (from NAUJOKAT et al., 1983).

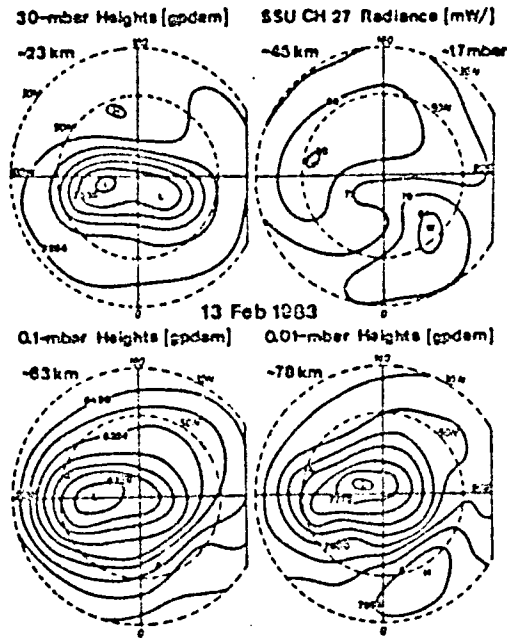


Figure 3.

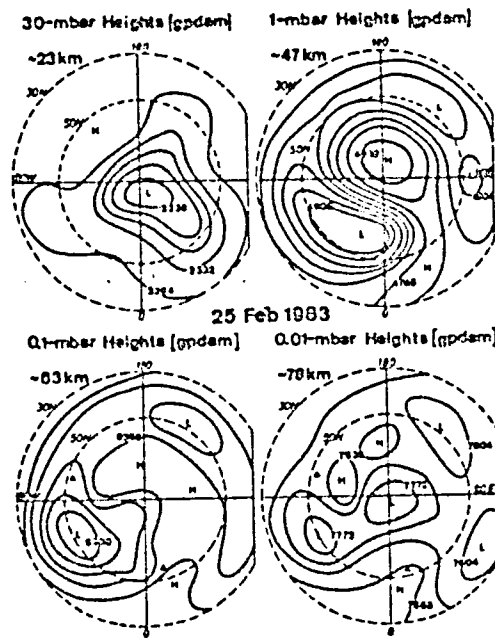


Figure 4.

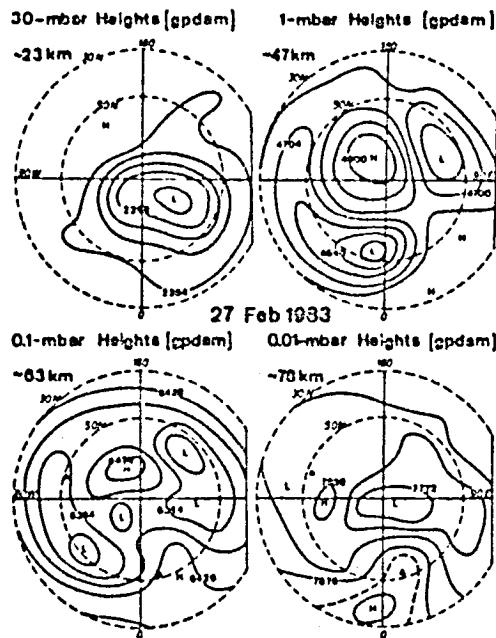


Figure 5.

On 25 February, Figure 4, the third warming pulse of the winter developed, cf. Figures 1 and 2, and its influence is clearly noticeable in the mesosphere. Winds from the east were observed again over Central Europe at about 95 km, and also over Canada at about 60 and 70 km, cf. Figure 7. Here the wind speed had decreased considerably since 13 February, well in agreement with the movement and weakening of the polar vortex.

On 27 February the stratospheric warming reached its peak, Figure 6, with the reversal of the temperature gradient in the stratosphere, concurrently with a cooling in the mesosphere. The resulting height fields, Figure 5, also display a reversal of the circulation in the upper stratosphere over the polar region. The circulation over Central Europe was dominated by a separate anticyclone and the very strong winds from the north reported by the Colla Observatory (not shown) agree with the slope of the anticyclone, Figure 5. The varying winds over Canada (cf. Figure 7) agree with the rather complex circulation systems, Figure 5.

Attempts have been made to show that the large-scale circulation in the mesosphere is similar to the well-known circulation in the stratosphere and that it is possible to study these changes synoptically. For such studies ground-based observations of winds and temperatures can give an important input to the analyses, in addition to the satellite data. However, for the synoptic analyses which concentrate on the large-scale circulation, it is necessary that the prevailing winds (or temperatures) are made available, after the tides have been removed.

The interannual variability of the midwinter disturbances is very large, Figure 8, particularly in the capability of the disturbances to develop into so-called "Major warmings" (\* in Figure 9), i.e., to penetrate into the middle

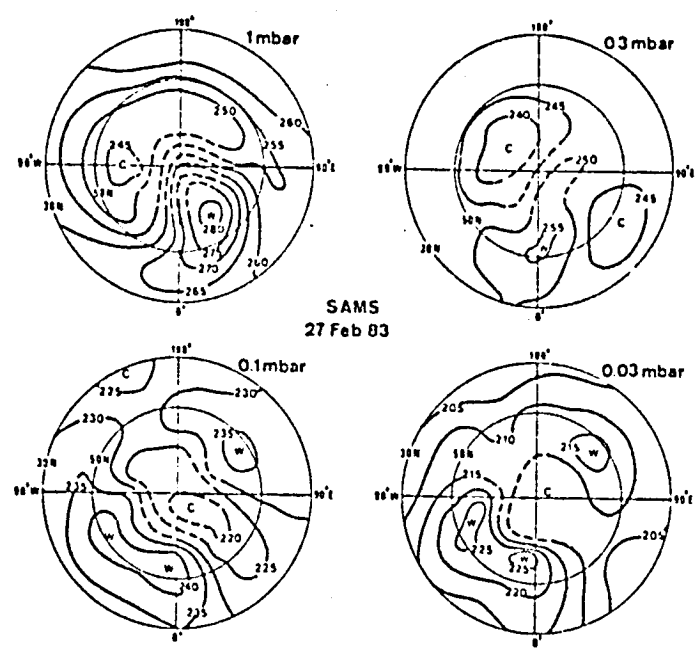


Figure 6. Charts of temperatures (K) retrieved from measurements of the SAMS aboard NIMBUS 7 (courtesy Clarendon Laboratory, University of Oxford, UK) (from NAUJOKAT et al, 1983).

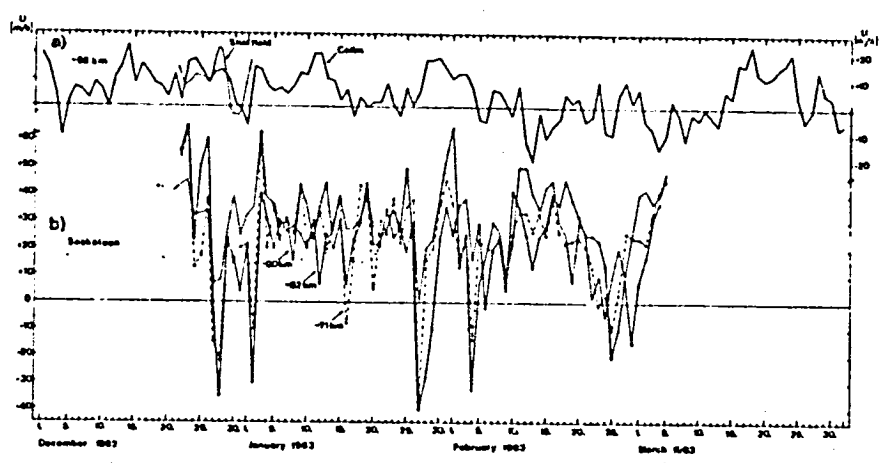


Figure 7. a) Prevailing zonal winds ( $m s^{-1}$ ) around 95 km over middle (51N,13E) and western (53N,2W) Europe measured by low frequency ion drift (courtesy Geophysical Observatory Collm, GDR) and by meteor radar (courtesy Physical Dept., Univ. of Sheffield, UK), respectively; b) Zonal winds ( $m s^{-1}$ ) over Canada (52N, 107W) at three layers (58-66 km layer daily means, 76-84 km layer tidally corrected) measured by partial reflection radar (courtesy University of Saskatchewan, Saskatoon, Canada) (from NAUJOKAT et al., 1983).

ORIGINAL PAGE IS  
OF POOR QUALITY

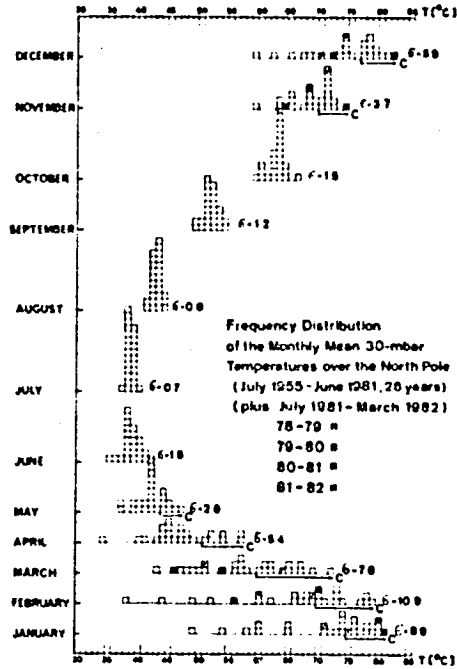


Figure 8. (from LABITZKE, 1983.)

WESTERLY CATEGORY									EASTERLY CATEGORY											
IR	YEAR	NOV	DEC	JAN	FEB	MAR	APR	MAY	FW	R <sub>i</sub>	YEAR	NOV	DEC	JAN	FEB	MAR	APR	MAY	FW	
27	1922/23	CW							early	41	1941/42	CW			M				[late]	
0	1923/24								early	23	1924/25		CW	M					[late]	
74	1925/26		C	C	C	C		C	late	106	1926/27				M				[late]	
203	1927/28	C	C		M	(C)	(C)	(C)	[late]	217	1928/29	CW	CW		C	NFW			early	
146	1929/30	C	CW		C	C			early	68	1930/31		CW		M				early	
39	1931/32		C	C	C	C	C		late	20	1932/33	CW			M	(C)	(C)	(C)	[late]	
18	1933/34	C	C	C	C				early	28	1934/35		CW	C		M			[late]	
18	1934/35	CCW	C	C	C	C			late	104	1935/36		CW		C				late	
111	1935/36		CW	C	C	C			late	81	1936/37	C	C		M			(C)	(C)	[late]
122	1937/38	CCW			M	(C)	(C)		[late]	43	1937/38	CW	C		M			(C)	(C)	[late]
112	1938/39	C			M	(C)			[late]	78	1938/39									early
62	1939/40	C	C	C	C				early	18	1939/40	CW	C	M		(C)			early	
28	1939/40	C	CCW	C	C				early	182	1939/40	CW		C	C	NFW			early	
8	1940/41	C	C	C	C				early										early	
167	1940/41	C	CW	C	NFW				early										early	
114	1940/41	CW	C	C	M		(C)	(C)	[late]										early	
	IC	10 <sup>(1)</sup>	8 <sup>(2)</sup>	10 <sup>(3)</sup>	8 <sup>(4)</sup>	9 <sup>(5)</sup>	4 <sup>(6)</sup>	3 <sup>(7)</sup>			IC	1 <sup>(1)</sup>	3 <sup>(2)</sup>	3 <sup>(3)</sup>	4 <sup>(4)</sup>	2 <sup>(5)</sup>	4 <sup>(6)</sup>	3 <sup>(7)</sup>		
	IH				2	2					IC			3	8					
	INH				1	3	1				IC					4				
	1952/53	C	CCW	C					late	111	1952/53	C	CW						early	

Figure 9. Winters of Figure 8 are grouped according to the case of the zonal winds at the 50-mbar level over the equator (update, LABITZKE, 1982).

stratosphere and to lead to a breakdown of the polar vortex. It is not understood why the winters do develop so differently. One possible explanation appears to be connected with the QBO of the stratospheric winds over the tropics. If one groups the winters according to the equatorial 50-mbar winds in November/December, one can find "Major warmings" (\*) during 57% of the winters belonging to the easterly category, but only during 24% of the winters belonging to the westerly category, Figure 9. And these 24% are winters very close to the solar maximum. (Of course, not enough cases are yet available to put any significance to this result.) But the whole phenomenon is very interesting as it suggests that the stratospheric QBO over the tropics modulates the polar winters, probably through a modulation of the planetary-scale waves of the whole middle atmosphere. This will surely be one important subject to be studied within the NAP.

#### ACKNOWLEDGEMENTS

The timely transmission of data and analyses for the monitoring of the stratosphere during winter (STRATALERT) by the Department of Atmospheric Physics, University of Oxford, UK; by the Meteorological Office, Bracknell, UK; by the Geophysical Observatory Collm, GDR; by the Physics Department, University of Sheffield, UK; and by the Physics Department, University of Saskatchewan, Canada, is gratefully acknowledged.

#### REFERENCES

- Labitzke, K. (1982), J. Met. Soc. Japan, 60, 124-139.  
Labitzke, K. (1983), Advances in Space Research (in press).  
Naujokat, B., K. Petzoldt, K. Labitzke and R. Lenschow (1983), Beilage zur Berliner Wetterkarte, SO 13/83, Meteor. Abh. FU Berlin, Serie B.

N85

20466

UNCLAS

D/6  
86

N85-20466

SPRING CHANGEOVER OF THE MIDDLE ATMOSPHERE CIRCULATION  
COMPARED WITH ROCKET WIND DATA UP TO 80 KM

G. Entzian<sup>1</sup>, D. A. Tarasenko<sup>2</sup>, and E. A. Lauter<sup>1</sup>

1 - Academy of Sciences of the GDR  
Central Institute of Solar-Terrestrial Physics  
Observatory of Ionosphere Research  
DDR-2565 Kuhlungsborn, GDR

2 - USSR State Committee of Hydrology and Control of Natural Environment  
Central Aerological Observatory  
Dolgoprudny, Moscow Region, USSR

The middle atmosphere circulation is governed by two seasonal basic states in winter and summer, twice a year separated by relatively shortlived reversal periods. In this paper we will deal with these seasonal basic states of circulation and the spring changeover period between them.

Figure 1 gives the height profile of the mean zonal wind in winter (December/January) and summer (June/July) as measured by rockets at Volgograd (USSR) completed by ionospheric wind measurements in about 95 km height (Kuhlungsborn and Collm. GDR; SPRENGER et al., 1974). In winter a uniform westwind system exists from the stratosphere up to the lower thermosphere. The maximum wind velocity of 70 m/s is attained at the height of 50 km. In summer there is an eastwind system from the stratosphere up to the upper mesosphere. A maximum of wind velocity of 55 m/s is attained in 70 km, but above 85 km again westwind is established. For comparison, Figure 1 shows also results of CIRA 72 for 50°N. In this reference atmosphere the the winter wind maximum is indeed placed at the correct height, but with 100 m/s it is much too intense. Because CIRA for winter months uses only values of Europe and western Asia a longitude effect should be negligible. Nevertheless, in order to estimate a possible longitude effect the single values at 40 and 50 km height indicate the mean zonal wind (circles) and the mean zonal wind plus the contribution of planetary waves (k=1 and 2; stars) to the zonal wind at the longitude of Volgograd, derived from a harmonic analysis of US-satellite data (NASA) for December/January 1974/75 and 1975/76. From the mean of these two winters only, the actually measured zonal wind is already well represented. Also this result emphasizes that these CIRA values are too high.

During summer, the stratospheric zonal wind is well reflected by CIRA, but the mesospheric wind maximum after CIRA is too low by about 7 km and too weak by about 15 m/s. The lower thermospheric wind values are again relatively well represented by CIRA.

The basic states of geopotential height at 30 mb and their change from one into the other can be seen in Figure 2 for 50°N (latitude mean) and the North Pole. Lower heights at the North Pole than in medium latitudes, as in winter, indicate westwind, higher heights, as in summer, indicate eastwind. The changeover from one state to the other is defined by the crossover of both curves. Its time is determinable with an accuracy of one day, not only in the case of this 13-year mean (1967-1979) but in general also for actual single years. Figure 3 shows the reversal dates defined in this way of the 30 mb level since 1958. The mean reversal date of these 25 years is April 7 with a relatively high variability of ±17.5 days.

An effect of the quasi biennial oscillation can obviously be seen from the alternation of early and late reversals between 1958 and 1967 and again after

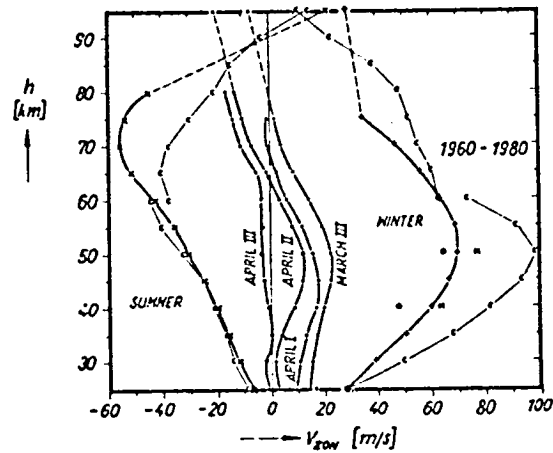


Figure 1. Mean zonal wind from Volgograd rocket data ( $48.7^{\circ}\text{N}$ ;  $44.4^{\circ}\text{E}$ ) during the seasonal basic states: + winter (Dec., Jan.), x summer (June, July) in comparison with CIRA 72 values (c) and US satellite data (o mean zonal wind; \* mean zonal wind plus contribution by planetary waves to zonal wind; and during the spring changeover period ( $\cdot$ ). The experimental data at 95 km are from ionospheric drift measurements at the observatories Kuhlungsborn ( $54.1^{\circ}\text{N}$ ;  $11.8^{\circ}\text{E}$ ) and Collm ( $51.3^{\circ}\text{N}$ ;  $13.0^{\circ}\text{E}$ ).

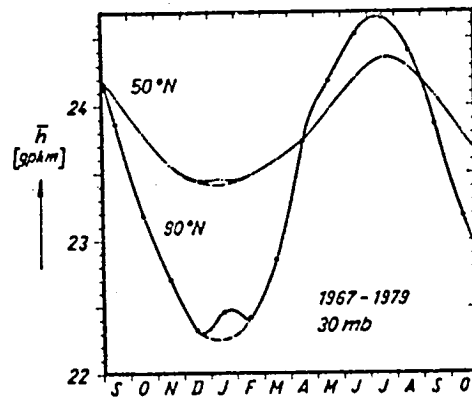


Figure 2. Seasonal variation of the height of the 30 mb level at  $50^{\circ}\text{N}$  zonal average and at the North Pole. Monthly mean values from 13 years (1967-1979). The dashed parts are extrapolations of the autumn and spring branches of the curves, as an estimated behaviour without stratospheric warming effects.

1977. The difference of reversal dates of consecutive years can attain more than one month! Since 1958 a secular trend to earlier reversal dates  $D$  (= day-number)

$$D = -0.52 Y + 132.8$$

( $Y$  = the last two digits of the year) can be observed. Of course this trend can only be the expression of a long-time climatic variation, and at some time the trend will end or even change the direction. Between 1958 and 1980 the above regression is statistically significant by more than 95 per cent, but when including the late reversals of 1981 and 1982 the trend is no longer significant

The small rectangles in Figure 3 indicate periods of late-winter zonal wind reversals. It can be recognized, that in general a late winter zonal wind reversal is followed by a delayed final reversal. For 13 winters without wind reversals, the mean final reversal date is March 29, whereas for 12 winters with wind reversals, the mean final reversal date is April 15. That means the occurrence of a late-winter zonal wind reversal tends to delay the final spring changeover by an average of 17 days in the 30 mb level.

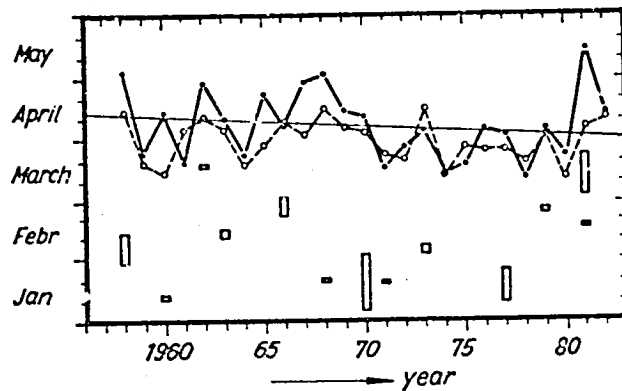


Figure 3. Spring reversal dates of the 30 mb level (·) and the occurrence times of the spring ionization minimum in the lower ionosphere (o). The rectangles indicate periods of late winter zonal wind reversals.

Figure 1 also shows the mean zonal wind height profiles for the last March decade and the three April decades (centered at 25th March, 5th, 15th and 25th April). At the end of March the seasonal changeover begins in the mesopause region and within the next 20-30 days it comes down to the middle stratosphere. With the position of the observing points mentioned above, this result refers to the longitude sector of central and east Europe and to a latitude of about 50°N. Around the middle of April the lower thermospheric east wind attains its most intense value. After that time it breaks down and changes again to westwind, which is then maintained during summer.

Figure 4 investigates if the classification of "early" or "late" spring changeover in the 30 mb level is valid for the whole height profile. For this purpose the mean of zonal wind profiles were evaluated for 4 "early" years (1974, 75, 78, 80) and for 4 "late" years (1967, 68, 69, 70). In the 4 years of

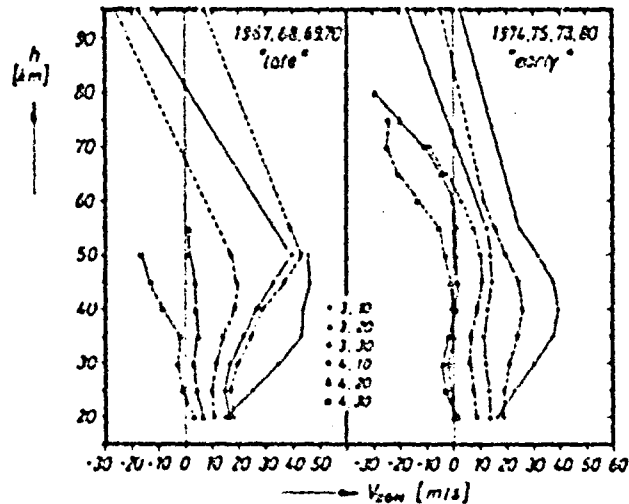


Figure 4. Mean zonal wind profiles (mean of 20 days in each year centered to the given date) over Volgograd, completed by ionospheric drift measurements at 95 km from Kuhlungsborn and Colla, in the cases of 4 years with late and 4 years with early spring changeover in the zonal average of the 30 mb level (see Figure 3).

"early" case the mean changeover date of the 30 mb level (as given in Figure 3) is March 17, and in the "late" case it is April 21, i.e. a difference of about one month. After Volgograd rocket data these reversals at the height of 23 km (about 30 mb) take place on April 17 and May 2, respectively, i.e. a difference of only 15 days. This smaller difference may be an effect of the longitude of Volgograd, but in spite of this smaller effect in the data of Volgograd the "early" and "late" cases can be recovered in almost all heights up to the lower thermosphere and can be identified already about one month before the actual reversal from west- to eastwind in the stratosphere by westwind velocities being smaller in the early case than in the late case.

Because the spring reversal processes are relatively uniform from the stratosphere up to the heights of the lower ionosphere an influence on the ionospheric plasma should be expected. From ground-based absorption and phase height measurements it is known that the electron density passes through a distinct minimum during spring (LAUTER and ENTZIAN, 1983). The occurrence time of this minimum suggests comparison with the reversal dates. The results can be seen in Figure 3. Both parameters are significantly (> 99.9 per cent) correlated with a correlation coefficient of  $r = 0.6$ . Like in the case of final wind reversals the occurrence times of the ionization minima are also delayed in cases of preceding late winter wind reversals: In the mean of the 13 cases without wind reversals the ionization minimum occurs at March 24, in the mean of the 12 cases with wind reversals it occurs at April 5, i.e. 12 days later.

The results confirm the statement made earlier (LAUTER et al., 1976) that during winter a dynamical coupling between different layers exists in the middle atmosphere from the stratosphere up to the lower thermosphere, and that this coupling continues till the final spring reversal.

## REFERENCES

- CIRA (1972), COSPAR International Reference Atmosphere 1972, Akademic-Verlag, Berlin.
- Lauter, E. A. and G. Entzian (1983), Phys. Solariterr. Potsdam, 19, 118.
- Lauter, E. A., J. Taubenheim, G. Entzian, J. Bremer, G. v. Cossart and G. Klein (1976), HHI-STP Report No. 7, Central Institute of Solar-Terrestrial Physics, Berlin-Adlershof, GDR
- NASA, Synoptic analyses 5-, 2-, and 0.4 mb surfaces for July 1974 through June 1976, NASA Reference publication, 1023.
- Sprenger, K., R. Schindler, K. M. Greisiger, D. Kurschner and B. Schaning (1974), HHI-STP Report No. 2, Central Institute of Solar-Terrestrial Physics, Berlin-Adlershof, GDR.

The rocket data were taken from: Bulletin of Atmospheric Rocket Sounding Results, Central Aerological Observatory, Gidrometeoizdat Moscow.

The 30 mb data were taken from: Meteorologische Adhmdlungen Tagliche Hohenkarten der 30 mb Flache, Institute fur Meteorologie der Freien Universitat Berlin-West.



N85

20467

UNCLAS

LARGE-SCALE WINTER-TIME DISTURBANCES IN METEOR WINDS OVER  
CENTRAL AND EASTERN EUROPE

K. M. Greisiger

Central Institute of Solar-Terrestrial Physics  
Observatory of Ionosphere Research  
DDR-2565, Kuhlungsborn, GDR

Yu. I. Portnyagin and I. A. Lysenko

USSR State Committee of Hydrometeorology and Environmental Control  
Institute of Experimental Meteorology  
Obninsk, USSR

As it is well known, in winter a predominant westerly circulation exists in middle and high latitudes from the stratosphere up to the mesopause region (80-100 km), driven by the stratospheric polar west wind vortex. Sudden stratospheric warmings lead to disturbances or even to a breakdown of this vortex with occurrence of easterly winds (LABITZKE, 1981). Such large-scale circulation disturbances can be seen in pressure maps up to mesospheric heights (NAUJOKAT et al., 1983). Moreover, in the mesopause region similar circulation disturbances in periods with stratospheric warmings are also known for a long time from meteor wind and ionospheric drift results (PORTNYAGIN and SPRENGER, 1978). In the present report we investigate daily zonal wind data of the four Pre-MAP-winters 1978/79 to 1981/82 obtained over Central Europe (station Kuhlungsborn, 54.1°N/11.8°E) and Eastern Europe (state Obninsk, 55°N/38°E) by the radar meteor method (D2). Available temperature and satellite radiance data of the middle and upper stratosphere are used for comparison, as well as wind data from Canada (SMITH et al., 1982). The existence or non-existence of coupling between the observed large-scale zonal wind disturbances in the upper mesopause region (90-100 km) and corresponding events in the stratosphere is discussed.

An analysis of wind disturbances in the 90-100 km level above Central Europe in the first Pre-MAP-winter 1978/79 has been already published on the basis of D2 wind results of the station Kuhlungsborn and ionospheric drift (D1) results of the station Collm (GREISIGER et al., 1979). These results will be summarized here only with inclusion of D2 wind data from the station Obninsk in Eastern Europe. As shown in Figure 1 in January and February 1979 three distinct large scale reversals of the zonal prevailing wind ( $V_z$ ) in 90-100 km took place as measured by the D2-method at Kuhlungsborn and Obninsk as well as by the D1-method at Collm (3-days running means are used for smoothing, applied to all winters). In the stratosphere an intense warming of the polar region started after 21 January, proceeding in three pulses and leading to a total breakdown of the circumpolar vortex ("major stratospheric warming") on 23 February (LABITZKE, 1979). The three wind reversals at 95 km occurred some days in advance of the peaks of the warming pulses at the 4 mbar level (SSU Ch 26 data), which in turn occur a little earlier than the peaks in 10 mbar temperature above the North Pole (cf. Figure 1). The period of strongest East wind in the 90-100 km level around 25 February coincided rather well with the breakdown of the polar vortex in the stratosphere, suggesting a strong coupling between the stratosphere and the mesopause region during this major stratospheric warming event.

As reported by SMITH et al. (1982), the zonal circulation in the mesosphere and mesopause region in this winter above Canada, observed at Saskatoon (52°N, 104°W) by the D1-method (partial reflection), did not show a close coupling. There was no reversal near 25 February. Such different behaviour on large scale, however, can be understood through the longitudinal asymmetry in the

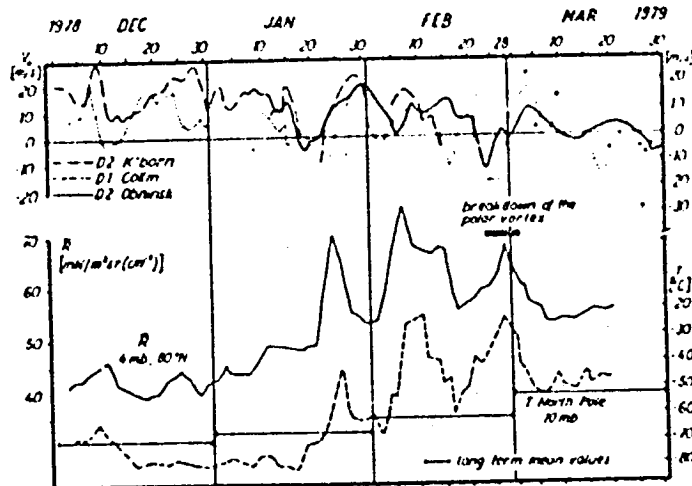


Figure 1.

vertical propagation of planetary waves, which very probably are the primary cause of the coupling.

In winter 1979/80 several circulation disturbances took place again as seen in the zonal prevailing wind data  $V_0$  of Obninsk and Kuhlungsborn (Figure 2). For comparison the situation in the stratosphere is characterized in Figure 2 by the temperature of the 10 mbar level and satellite IR radiance data of 4 and 1.7 mbar over the North Pole (LABITZKE et al., 1980). From 10 January up to 20 February 1980 in the upper stratosphere (4 and 1.7 mbar level) several "minor warmings" occurred, whereas in the middle stratosphere (10 mbar) the temperature above the North Pole was nearly equal or lower than the long-term mean values (Figure 2). At 95 km wind reversals were observed above Central and Eastern Europe around 12 and 24 January followed by a recovery of the West wind circulation and a new weakening after 10 February. Simultaneous D1-wind measurements at Saskatoon also show several wind disturbances but not with such a close temporal connection as for the European region. The mesopause region above Europe seems favorable to indicate large scale winter-time disturbances of the pressure field and corresponding wind field, as already shown for the major stratospheric effect in the first Pre-MAP-winter. At the end of February a "major warming" of the whole stratosphere took place, as seen in Figure 2 by sharp peaks of the radiances and the temperature above the Pole. The zonal wind in the mesopause region now seems to be disturbed simultaneously over the whole Northern Hemisphere with East winds over Europe (Obninsk, Figure 2) and also above Canada around 29 February.

In the third Pre-MAP-winter 1980/81, the stratosphere showed an extreme behaviour (LABITZKE et al., 1981). Beginning with the end of November, strong cooling took place in the polar middle stratosphere, reaching temperatures in December and in the first half of January substantially below the long-term mean values, as shown in Figure 3 for the 10 mbar level. By the end of January a sudden and very strong warming began first in the upper polar stratosphere and a few days later in the 10 mbar level (cf. Figure 3). So the winter 1980/81 in the stratosphere can be clearly divided into two parts, viz., a quiet period up to 20 January and a highly disturbed period after 20 January. In the mesopause

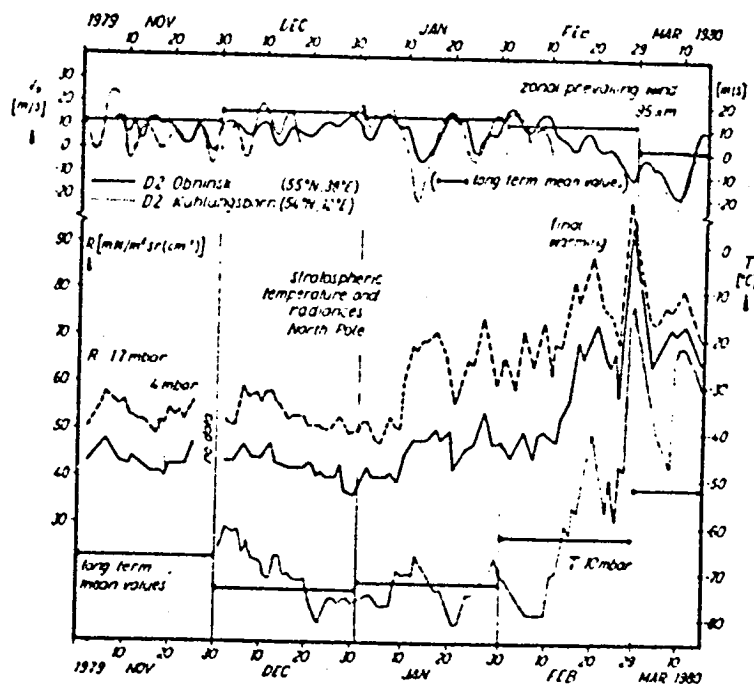


Figure 2.

region, as could be expected from earlier winters, the zonal wind in this second part of the winter was also very disturbed.

During the maximum of the stratospheric warming at the end of January/beginning of February 1981 the strong zonal westerlies at 95 km decreased rapidly and reversed to East wind, practically simultaneously above Central and Eastern Europe (Figure 3), and also above Canada. This confirms the large-scale character of the disturbance and the close coupling with the stratospheric warming event. The first part of the winter 1980/81, though rather quiet with extremely low temperatures in the polar stratosphere showed several disturbances of the zonal wind in the mesopause region, not less intense as during the major stratospheric warming. As shown in Figure 3, simultaneous reversals to East wind above Central and Eastern Europe occur in November and December, and a rapid weakening of the West wind shortly before 20 January. Even stronger disturbances with reversals were observed at Saskatoon at 93 km at about the same periods. That means that in the first part of the winter 1980/81 the zonal circulation in the mesopause region is highly disturbed in a large-scale manner, though the polar stratosphere was rather quiet. One can conclude that these disturbances are probably connected with processes in the mesosphere or in the mesopause region itself. Some indication we have from the radiance data (Figure 3), which show from November to January some little warming peaks which are higher at 1.7 mbar (44 km) than at 4 mbar (38 km).

In January and beginning of February 1981, remarkable wave-like variations of the zonal wind at 95 km with large amplitudes, very similar at both stations, were observed. They seem to be connected with corresponding variations of the

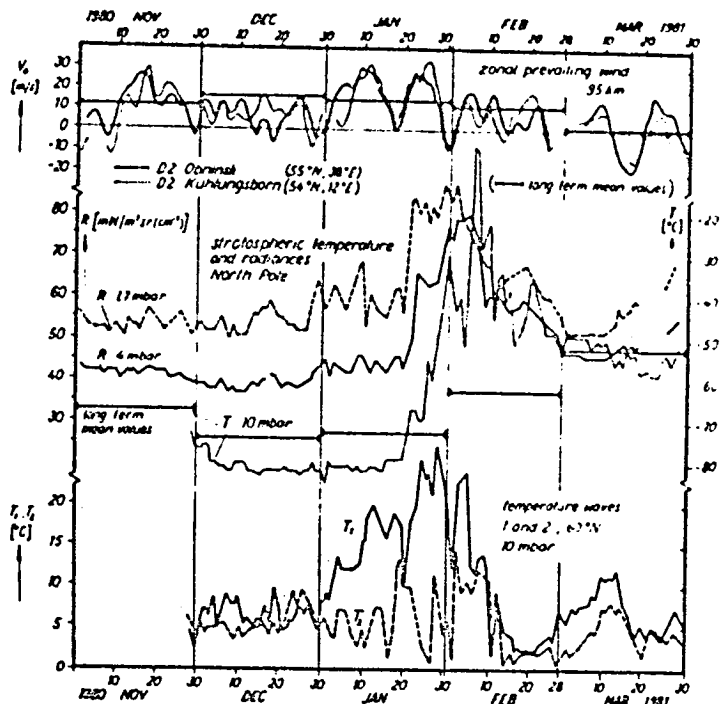


Figure 3.

dominant stationary planetary temperature wave  $T_1$  in the stratosphere at  $60^\circ\text{N}$  (cf. Figure 3). In this respect the stratospheric temperature field was disturbed already before the major warming event (amplification of wave 1 as a precondition of a major stratospheric warming, LABITZKE (1981), and an influence up to the 95 km level at medium latitudes seems to exist.

The fourth Pre-MAP-winter 1981/82 is in some respects similar to the second one. In mid-December a warming in the upper stratosphere (4 and 1.7 mbar) with simultaneous cooling in the middle and lower stratosphere was observed (NAUJOKAT et al., 1982) (cf. Figure 4). The zonal wind at 95 km over Europe is strongly disturbed in December with values below the long-term mean values and some short periods of East winds. In January in the polar stratosphere a strong "minor warming" occurred (NAUJOKAT et al., 1982) with two pulses in the radiances (1.7 and 4 mbar) and 10 mbar temperature around 10 and 25 January (Figure 4). In coincidence with the stronger second pulse we observe an almost simultaneous reversal of the zonal wind above Central and Eastern Europe with an East wind period up to the beginning of February. At Saskatoon at the same time a reversal down to 62 km was recorded which shows the large-scale character of this wind disturbance in connection with the strong "minor warming".

Summarizing our results one can say that in winter during "major warmings" obviously a close coupling exists between the stratosphere and the mesopause region. The temporal and spatial relation between the events in both atmospheric layers can be understood only with informations about the vertical propagation of the pertinent planetary waves as a primary cause of the coupling.

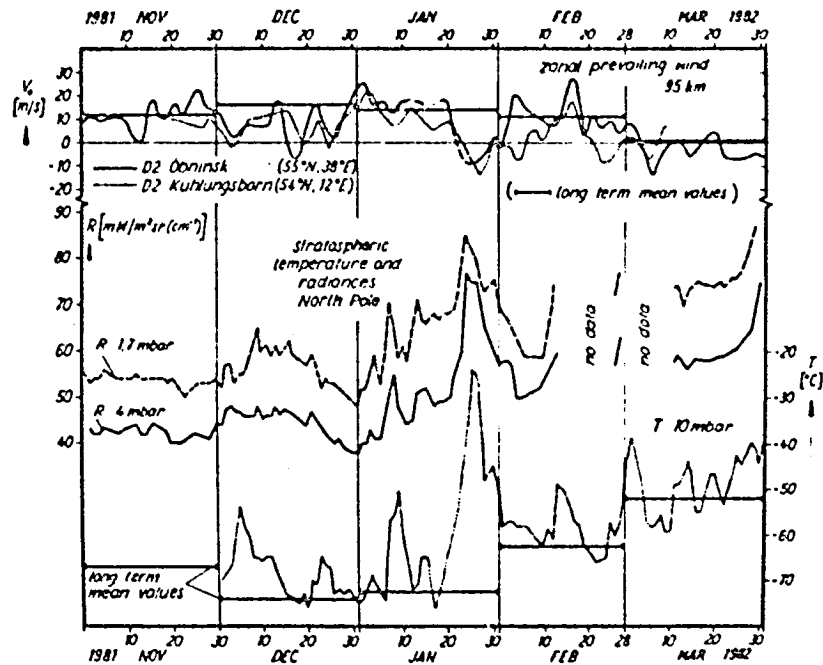


Figure 4.

Not much less intense large-scale zonal wind disturbances in the mesopause region were observed during periods of relatively quiet or even extremely typical winter conditions in the stratosphere. The cause of these disturbances is not clear; it has probably to be sought in the mesosphere or in the mesopause region itself.

## REFERENCES

- Greisiger, K. M. et al. (1979), *Phys. Solariterr.*, Potsdam, **10**, 107.  
 Labitzke, K. (1979), Progress Report for FMP-1.  
 Labitzke, K. et al. (1980), *Beilage Berliner Wetterkarte* 49/80, SO 9/80.  
 Labitzke, K. et al. (1981), *Beilage Berliner Wetterkarte* 81/81, SO 13/81.  
 Labitzke, K. (1981), *Mon. Wea. Rev.*, **109**, 983.  
 Naujokat, B. et al. (1982), *Upp. Atm. Progr. Bull.*, Spec. Issue. **82-2**, August.  
 Naujokat, B. et al. (1983), *Beilage Berliner Wetterkarte* 57/83, SO 13/83.  
 Potnysgin, Yu. I. and K. Sprenger (editors) (1978), *Wind Measurements at Heights of 90-100 km by Ground-Based Methods* (in Russian), Gidrometeoizdat Leningrad.  
 Smith, M. J. et al. (1982), Paper No. C.3.2.2, presented at COSPAR Gen. Assembly, Ottawa.

N85  
204688

UNCLAS

D18  
96

N85-20468

VHF-RADAR OBSERVATIONS IN THE STRATOSPHERE AND MESOSPHERE  
DURING A STRATOSPHERIC WARMING

R. Ruster, P. Czechowsky and G. Schmidt

Max Planck Institute of Aeronomy  
3411 Katlenburg-Lindau, FRG

K. Labitzke

Meteorological Institute  
Free University  
1000 Berlin 33, FRG

The SOUSY-VHF-Radar (lat. 51°N, long. 10°E) was used to carry out measurements during minor and a major stratospheric warming in February and March 1980, respectively. Echoes have been received from the stratosphere up to an altitude of about 30 km continuously during day and night, whereas echoes from the mesosphere were restricted to the daytime and occurred sporadically at different heights within the altitude range from 60 km to 90 km. The three-dimensional velocity vector has been derived from Doppler measurements made in three different antenna beam directions with a height resolution of 1.5 km. In particular the results obtained during disturbed conditions show the change of the zonal winds at mesospheric heights from westerly to easterly. A spectral analysis reveals a diurnal and a weaker semidiurnal tide of the zonal wind component.

This paper has been published in full in: J. Atmos. Terr. Phys., 45, 161. (1983).

N85

20469

UNCLAS

N85-20469

D19  
97

CHANGES IN THE OZONE CONTENT OVER CENTRAL EUROPE DURING REVERSALS  
OF STRATOSPHERIC CIRCULATION IN LATE WINTER

G. Entzian

Academy of Sciences of the GDR  
Central Institute of Solar-Terrestrial Physics  
Observatory of Ionosphere Research  
DDR-2565 Kuhlungsborn, GDR

K. H. Grasnick

Meteorological Service of the GDR  
Main Meteorological Observatory  
DDR-1500 Potsdam, GDR

A superposed-epoch analysis during late winter zonal wind reversals was carried out from 18-year observation series (1963-1980) of the meridional geopotential height gradient in the 30 mb level (latitude mean) and of the ozone content over central Europe.

Figure 1a gives the mean seasonal variation of the meridional geopotential height gradient between 50°N and the North Pole. This parameter is positive during winter, indicating west wind, whereas it is negative during summer, indicating east wind. In some late winters the meridional gradient breaks down to low, sometimes even to negative, values, as for 1977 (dotted curve). Such break-downs are connected with stratospheric warmings. The beginning of these decreases of the meridional gradient, exactly the first day of decreasing during a period which later attains negative values, was taken as key day of the subsequent superposed-epoch analysis. Figure 1b gives the variance of the geopotential height along the 50°N latitude circle. It represents in an integral form the deviation of the wind from a circumpolar zonal flow

$$\sigma = \left[ \frac{1}{2} \sum_{k=1}^{\infty} (A_k)^2 \right]^{\frac{1}{2}}$$

(with  $A_k$  = the amplitude of the k-th planetary wave) i.e., a measure which we may call planetary wave activity. Because the amplitudes of waves  $k > 3$  can be neglected,  $\sigma$  describes mainly the activity of the first 3 modes of planetary waves.

Figure 2a shows the result of the superposed epoch-analysis of 8 cases as given in Table 1.

Table 1. Key days of the superposed epoch analysis.

January 14, 1963	January 5, 1971
February 12, 1966	January 19, 1973
January 2, 1968	January 3, 1977
December 26, 1969	February 14, 1979

The curve through the dots represents the deviation of the meridional height gradient between 50°N and the North Pole from its mean seasonal variation. The gradient decreases and about 12 or 13 days after the key day it attains a minimum of 20 geopotential metres per degree latitude below the normal mean value. The curve of open circles represents the same parameter but between 40° and 60°N, it attains 11 gpm/deg.lat. below normal, about 20 days after the key day. If we formally convert the meridional gradient into zonal wind, we get a reduction of the west wind by 13 m/s and 10 m/s for the mean latitudes of 70°N and 50°N, respectively. After a recovery phase normal values are obtained

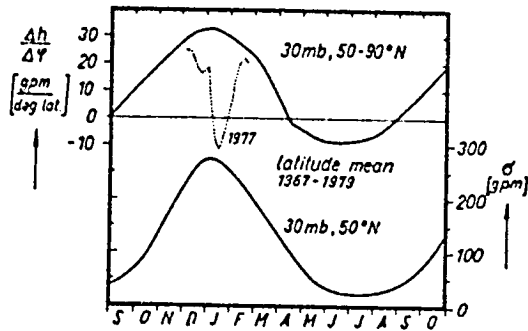


Figure 1. Mean seasonal variation at the 30 mb level (1967 - 1979) of  
 a) the meridional geopotential height gradient between 50° N and the North Pole;  
 b) the variance of the geopotential height along the 50° N latitude circle.

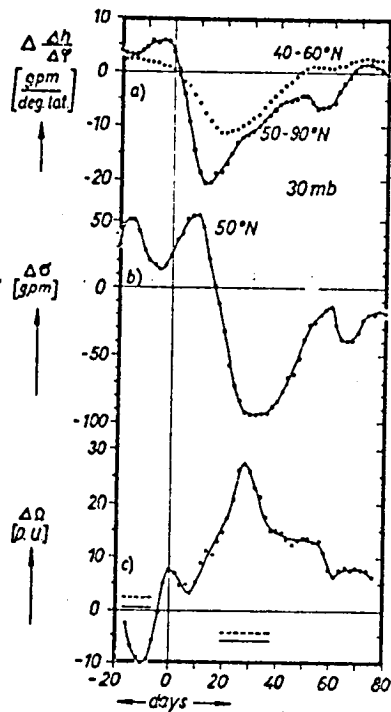


Figure 2. Superposed-epoch analysis of 8 cases of late winter zonal wind reversals between 1963-1980.  
 a) deviation of the meridional height gradient at 30 mb between 50°N and the North Pole from the mean seasonal variation (dots) and between 40° and 60°N (open circles);  
 b) deviation of the variance (planetary wave activity) from the mean seasonal variation;  
 c) deviation of the ozone content over Central Europe from the mean seasonal variation (curve); deviation of the monthly mean of the 8 cases from the long time monthly mean of the ozone content over the tropics (Kodaikanal: dashed horizontal bar, Huancayo: full horizontal bar).

between the 50-th and 60-th day after the key day. Figure 2b shows the behaviour of planetary wave activity. About ten days before the peak of the zonal wind reduction,  $\sigma$  attains a relative maximum and then decreases till the 30-th day, reducing the normal planetary wave activity by almost 100 geopotential metres. Figure 2c gives the deviation of the ozone content over Central Europe from its mean seasonal variation (mean latitude of the 8 stations used: 50°N). It increases and attains a maximum of 27 D.U. (i.e. about 8 per cent) above the normal value, about one month after the key day. This ozone maximum occurs 10 days after the zonal wind minimum and almost simultaneously with the minimum of the planetary wave activity. Because the key days concentrate between the end of January and the middle of February, the ozone effect must be detectable in the seasonal variation, too. Figure 3 gives the seasonal variation of the ozone content over Central Europe with and without zonal wind reversals. In the mean of January to April the ozone content is indeed higher by 18.6 D.U. in years with zonal wind reversals than in the years without. According to the t-test this difference is significant by more than 99.9 percent.

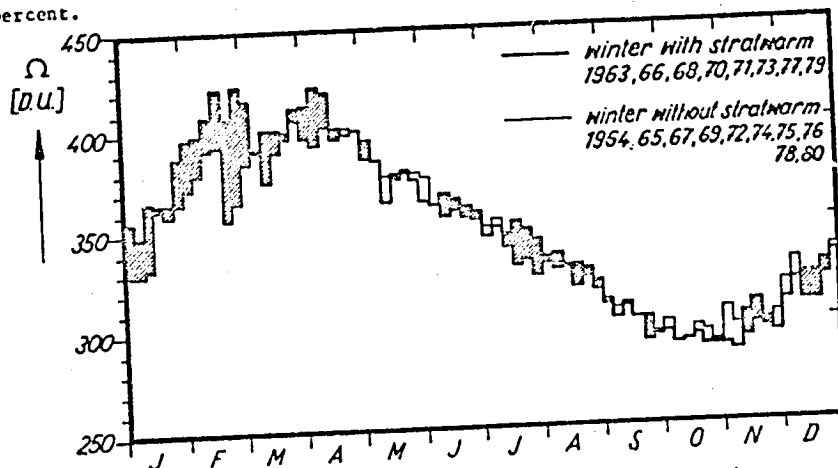


Figure 3. Seasonal variation of the ozone content over Central Europe with and without late winter zonal wind reversals.

In Figure 2c the deviation of the monthly mean from the long time monthly mean of the ozone content over the tropics (stations Kodaikanal 12°N and Huancayo 10°S) is given for the month before and for the month with the wind reversal at medium latitudes. In the month before the wind reversal, there is no significant difference to the normal value, but in the month with wind reversals the ozone content is significantly (on the 95% level) reduced at both stations by 5 D.U. in the mean, i.e., 2.1 per cent below normal. This result can be interpreted as an increase of meridional ozone transport from the tropics to middle latitudes during late winter zonal wind reversals. We have already found such opposite behaviour of the ozone content between the tropics and middle latitudes in the long-time ozone trend of the sixties and seventies, in the solar cycle and in the quasi-biennial-oscillation (ENTZIAN and GRASNICK, 1981). Now it is shown also in periods of some weeks, and in all these cases the meridional transport seems to be the connecting link.

After a theoretical investigation by ROOD (1982) the meridional ozone transport by diabatic circulation is supported by planetary wave transport during stratospheric warmings. In the case of a strong stratospheric warming, Rood expects a decrease of the tropic ozone content by more than 15 per cent,

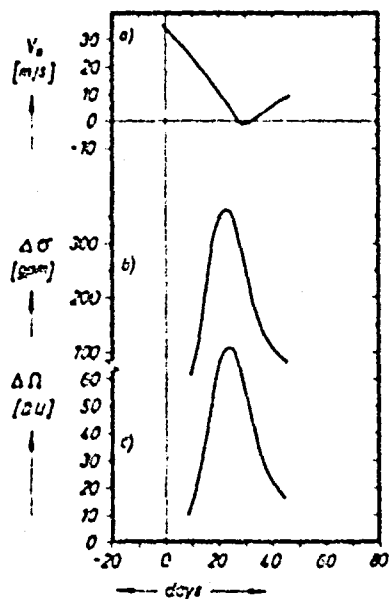


Figure 4. Kawahira's theoretical results of an adopted wave disturbance at 22.5 km beginning at the day zero, converted into parameters comparable with our Figure 2. a) change of zonal wind at 22.5 km as a result of interaction between waves 1 and 2 and the mean flow; b) planetary wave activity ( $k = 1$  and  $2$ ) at 22.5 km; c) ozone content between 10 and 40 km perturbed by planetary waves ( $k = 1$  and  $2$ ).

which is qualitatively in agreement with our experimental result. Generally in contemporary theories the ozone increase in middle latitudes during stratospheric warmings is explained by enhanced efficiency of planetary wave transport, e.g., KAWAHIRA (1982). Figure 4 shows Kawahira's theoretical results converted into a form comparable with our results. After a disturbance at the zero day, planetary waves  $k = 1$  and  $2$  at 22.5 km (near the 30 mb level used by us) reduce the zonal wind by more than 30 m/s, the minimum of zonal wind being reached at the 30th day, i.e., about 10 days later than our experimental result for 50°N. One week before the zonal wind minimum, Kawahira's planetary wave activity at 22.5 km (waves  $k = 1$  and  $2$ ) attains a maximum and simultaneously the ozone content attains also a maximum, of about 70 D.U. above normal. As to the time of ozone maximum, Kawahira's results are in good agreement with ours, though his maximum is twice or three times larger. Our experimental data on planetary wave activity, however, lead to a theoretically unexpected result, because we find, that the ozone maximum is attained during a minimum of that parameter. Therefore it may be suggested that, if planetary waves are responsible for the additional meridional ozone transport during stratospheric warmings, this transport has to take place at heights other than those up to the ozone maximum in the middle latitudes.

#### REFERENCES

- Entzian, G. and K. H. Graenick (1981), *Z. f. Meteorol.*, 31, 322.  
 Kawahira, K. (1982), *J. Meteorol. Soc. Japan*, 60, 831.  
 Rood, R. B. (1982), The effect of stratospheric warmings on the zonal mean ozone distribution, Paper no. STP IV, 3.7, presented at XXIV COSPAR Plenary Meeting, Ottawa.

The 30 mb data were taken from *Meteorologische Abhandlungen, Tagliche Hohenkarten der 30 mb Fläche*, Institut für Meteorologie der Freien Universität, Berlin.

The ozone data were taken from *Ozone data for the world*, publ. by the Atmospheric Environment Service, Dept. of the Environment, in co-operation with the WMO, Downsview, Ontario, Canada.

N85

20470

UNCLAS

SOME ASPECTS OF GENERAL CIRCULATION AND TIDES IN THE MIDDLE ATMOSPHERE

A. I. Ivanovsky

State Committee of Hydrometeorology and  
Control of the Natural Environment  
Moscow, USSR

From 80 km altitude upwards, a change in the character of mean zonal circulation compared with stratospheric and mesospheric circulation has been observed by many investigators. Firstly, in radio meteor sounding data from an average level near 95 km in middle latitudes, a semi-annual wind variation was found. While in the main seasons (summer and winter) a westerly wind is observed here, in the interseasonal periods the wind weakens sharply or even reverses into easterly wind. The circulation features of the meteor zone have been discussed in detail in the monograph by PORTNYAGIN and SPRENGER (1978). The recently available possibilities to obtain vertical profiles of the wind from radio meteor data in the altitude range 80-110 km have shown that the features of annual variation at 95 km reflect a sign reversal of the circulation near 100 km. While below 80 km a westerly circulation is found in winter, and an easterly circulation in summer, above 100 km the circulation is easterly in winter and westerly in summer. This can be clearly seen in Figure 1, taken from the monograph by KOKIN and CAIGEROV (1981). The fact of this circulation reversal in itself was not surprising, since it had been mentioned in many papers and monographs. However, it is surprising inasmuch as in none of the theoretical models (e.g., SCHROEBEL and STROEBEL, 1978; CLUSHAKOV et al., 1979; DICKINSON et al., 1977) this circulation reversal was obtained.

Analysis of mean daily winds at altitudes above 200 km, determined from radiowave incoherent scatter data, again showed a normal monsoon circulation, as seen in Figure 2 (EMERY, 1978). Thus, one may come to the conclusion that between 100 and 200 km, possibly nearer to 100 km, a layer of anomalous circulation must be situated, at least in middle latitudes.

The understanding of mechanisms which are responsible for the circulation "anomaly" in this height region appears to be of extraordinary interest and importance. Obviously, one had to take into account mechanisms which are usually not considered in hydrodynamics. Let us write the equation of motion taking into account the presence of a charged component of the atmospheric gas, the presence of the Earth's magnetic field, and the existence of the electric potential field (DOKUCHAEV, 1959; CLUSHAKOV, 1975):

$$2 \cdot [\nabla \dot{v}] = - \nabla p - \dot{e} + \frac{1}{c} [j \cdot \dot{B}] \quad (1)$$

The appearance of a quantity which is new for hydrodynamics, viz., the current density,  $j$ , requires additional equations to close the system of hydrodynamic equations. Usually this can be done by writing  $j$  in Ohm's law under conditions of anisotropic conductivity due to the Earth's magnetic field:

$$j = \dot{\sigma} \dot{E} \quad (2)$$

$$\dot{E} = \nabla \phi + \frac{1}{c} [\dot{v} \cdot \dot{B}]$$

$\dot{\sigma}$  - conductivity tensor

$\phi$  is the electric field potential, the nature of which will be discussed below, and  $\frac{1}{c} [\dot{v} \cdot \dot{B}]$  is the electric induction. For large-scale and rather slow processes ( $T > 1$  hour), space charge may be considered as quasi-stationary, i.e.,

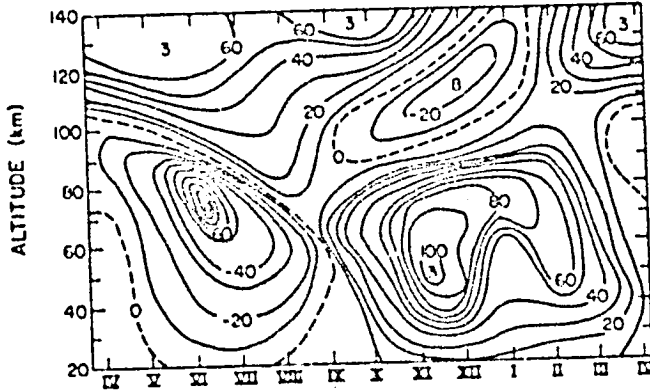


Figure 1. Height-season variation of the prevailing zonal wind in middle latitudes. Solid curve-computed data, dashed curve-experiment.

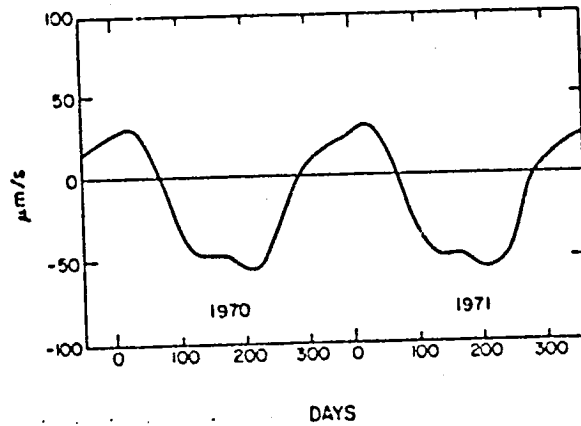


Figure 2. Annual variation of prevailing wind at 300 km altitude over Millstone Hill from incoherent scatter data

$$\text{div } \mathbf{j} = 0 \tag{3}$$

This equation appears to close the system. DOKUCHAEV (1959), neglecting the electric potential field, has shown that the electrodynamic force,  $\mathbf{j} \times \mathbf{B}$ , can be divided into the ion friction, in the form of dry (Rayleigh) friction with coefficients  $\frac{\sigma_1 B_0^2}{c^2}$  for zonal and  $\frac{\sigma_1 B_z^2}{c^2}$  for meridional components, and the magnetic rotary force, coinciding in its sense with the Coriolis force, so that the effective rotation of the Earth may be written in:

$$\omega' = \omega - \frac{\sigma_2 B_0 B_z}{2 c^2 \cos \theta}$$

Here,  $\sigma_1$  is Pedersen conductivity,  $\sigma_2$  is Hall conductivity, and

$$R_0^2 = B_z^2 + B_0^2$$

The  $\sigma_2$  value has a distinct maximum at 110-120 km altitude, and a considerable diurnal variation. In daytime, according to some data, the sign of  $\omega'$  in the 110-130 km region can become opposite to the sign of  $\omega$ . If this reversal of the sign  $\omega'$  took place both in day and night, then, according to the geostrophic relation for large-scale slow processes, with the sign of pressure gradient remaining unchanged, the wind sign would reverse in this altitude region. This is the simplest hypothesis to explain the circulation "anomaly". But, unfortunately, what is most possible, the Coriolis force compensation takes place far from always, and the "anomaly" level of 110-130 km is too high to correspond to experimental facts.

Another hypothesis is connected with peculiarities of the solar UV heating rate altitude profile (see Figure 3). As seen from this figure, the volume heating source decreases with altitude everywhere except for the 90-105 km altitude region where it increases. This anomaly in the heating source profile draws one's attention to an attempt to explain the circulation "anomaly".

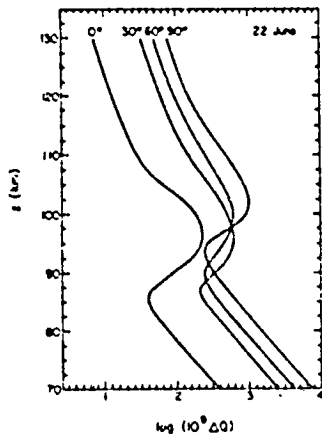


Figure 3. Vertical variation of UV heating rate in the atmosphere for summer solstice conditions at different latitudes.

Having written the system of hydrodynamic equations for a zonal case (without longitudinal dependence) and represented viscosity and heat conduction terms in the form of Rayleigh friction and Newtonian cooling, by means of substitutions one can obtain the equation for pressure latitudinal variations as a function of height

$$\frac{d^2 p}{dx^2} + \frac{dp}{dx} - \Pi p = \frac{\gamma - 1}{\gamma \chi} \frac{dq}{dx} \quad (4)$$

Where  $dx = \frac{dz}{H}$ , and  $q$  is a volume UV radiation heating source.

$$\Pi = \frac{\eta}{\chi} \frac{gH}{a^2 \tau_0^2} \lambda \frac{R}{\nu g} \left( \frac{\partial T}{\partial z} + \Gamma \right)$$

$\eta$  is the Rayleigh friction coefficient,  $\chi$  is the Newtonian cooling coefficient,

$\epsilon_0 = 2$ , other symbols are the standard ones. By substitution of  $p = Pe^{-x/2}$ , equation (4) is obtained in the form:

$$\frac{d^2 p}{dx^2} - b^2 p = \frac{\gamma - 1}{\gamma X} e^{x/2} \frac{dq}{dx}; \quad b^2 = \frac{1}{4} + 1$$

In the simplified case of absence of the Earth's influence, Green's function of the left-hand side operator is equal to:

$$G(x, \xi) = \frac{1}{b} \exp(-b|x-\xi|)$$

Then the solution is written in the form:

$$P(x) = \frac{\gamma - 1}{\gamma X_0} \int_{-\infty}^{\infty} e^{-b|x-\xi|} e^{\xi/2} \frac{dq}{d\xi} d\xi$$

For sufficiently large values of  $b$ , the integral kernel assumes the character of a delta function, and  $P(x)$  will alter its sign together with the alteration of the sign of  $\frac{dq}{d\xi}$ . The sign alteration of the latter quantity, as mentioned above, takes place in the 90-105 km altitude region. Together with this, the circulation sign will naturally change. In the hypothesis suggested the question of the value of  $b$  is very important. In order that this value is adequately large, it is necessary that the Rayleigh friction coefficient should be much greater than the Newtonian cooling coefficient. The high level of thermal stability also contributes to an increase of  $b$ . It is possible that the large value of  $b$  is a specific quality of the mesosphere and thermosphere. Obviously, the mechanism suggested at least partly explains the appearance of the "anomaly" circulation near 100 km.

However, one does not manage to explain the "anomaly" up to the 120-130 km altitude by means of this mechanism, and we will address again the equation (1), taking into account the electric potential field.

Strange as it may seem, the complex case of self-consistent calculation of hydrodynamic characteristics jointly with the electric field for tidal waves has already been done by GLUSHAKOV et al. (1979, 1980, 1981), but the simpler case of zonal stationary flow has not been examined. Let us fill the gap by presenting the results in this paper, in a simplified form only.

Integrating (3) over  $z$  in infinite limits (in fact, in a thin ionospheric layer) supposing that  $j$  vanishes outside the ionospheric layer, we obtain the expression

$$\frac{1}{a \sin \theta} \frac{\partial}{\partial \theta} \sin \theta \int_{-\infty}^{\infty} j_0 dz = 0 \quad (6)$$

It follows from this that  $\sin \theta \int_{-\infty}^{\infty} j_0 dz = C$ , but the integral current must not flow over the Pole, because this would mean non-zonality. Therefore,  $C$  must be zero, i.e.,

$$\int_{-\infty}^{\infty} j_0 dz = 0.$$

Expressing  $j_0$  in terms of Ohm's law, taking into account zonality of the problem, and making some simplifications conditioned by numerical estimates for altitudes less than 130 km, one can obtain

$$E_0 = \frac{B_p \bar{U}_r}{c} \cos \theta$$

$$\bar{U}_r = \frac{1}{\Gamma_1} \int_{-\infty}^{\infty} \sigma_1 U_r dz; \quad \Gamma_1 = \int_{-\infty}^{\infty} \sigma_1 dz \quad (7)$$

Here geostrophic wind is determined by

$$U_r = \frac{1}{ca} \frac{1}{\rho} \frac{\partial p}{\partial \theta}$$

For  $\bar{U}_r = 30$  m/s and  $B_p = 0.5$

$$E_0 = 1.5 \cos \theta \quad \left[ \frac{mV}{m} \right]$$

This electric field is adequate to influence strongly the wind. Noncomplex, but expanded calculations yield the expressions

$$U = U_r - \frac{2}{\sqrt{1+3\mu^2}} \frac{\Delta l}{l_0} \bar{U}_r \quad (8)$$

$$V = - \frac{l_0 \omega'}{1_0 \frac{1}{2} \mu^2 + v^2} \left( U_r - \left( 1 + \frac{\Delta l}{l_0} \frac{2}{\sqrt{1+3\mu^2}} \right) \bar{U}_r \right)$$

Here,  $l_0 = 2\omega'$  ( $\omega'$  - the Earth's effective rotation),

$$v = \frac{\sigma_1 B_p^2}{\rho c^2}; \quad \Delta l = \frac{\sigma_2 B_p^2}{\rho c^2}; \quad \mu = \cos \theta$$

Assume that  $U_r$  increases with height.  $\bar{U}_r$  is the result of averaging  $U_r$  over height, with  $\sigma_1(z)$  as a weighting function having a pronounced maximum near 140 km; so that  $\bar{U}_r \approx U_r(z = 140 \text{ km})$ . Apparently, below this level, as seen from (8), the sign of  $U$  and  $V$  may reverse with respect to  $U_r$ .

Let us now discuss the current state of tidal theory. Historically it has developed in a way that investigations were made independently in two altitude regions: below 100 km, where dissipative forces are negligible and above 100 km, where these forces are essential.

By 1970 the theory for the region below 100 km was summarized in the monograph of CHAPMAN and LINDZEN (1970). All calculations were based on tidal energy sources connected with the solar UV radiation absorption computed by BUTLER and SMALL (1963). Though explaining many experimental facts, the theory appeared to be incompetent to explain facts connected with semidiurnal tide seasonal variations in mid-latitudes.

In the last decade, theory of tidal seasonal variation has been greatly developed. IVANOVSKY and SEMENOVSKY (1971) pointed out that for the mean zonal circulation, different from the air shell rotation as a whole, the so-called "equivalent depth" in the classic tidal theory depends in a complex way on the seasonal variation of the circulation index. It is important to emphasize that the circulation character in the stratopause region (50 km) influences the tidal seasonal variations in the meteor zone.

Further development of the theory was aimed at improvements of the

numerical technique of solving linear equations, taking into account high-latitude profiles of the background zonal wind and temperature by means of the perturbation method (LINDZEN, 1974; WALTERSCHEID et al., 1979, 1980). These calculations qualitatively confirmed the results of Ivanovsky and Semenovskiy, but did not address solving the tidal seasonal variation problem.

A revision of calculations of tidal energy sources and their seasonal variations appeared to be extremely important in the theory (FORBES and GARRETT, 1978, 1979). The maximum of the source appeared to be greater than that of BUTLER and SMALL (1963), and the altitude region of maximum values was narrower. While in BUTLER and SMALL's (1963) sources the Hough mode (2,2) prevailed for the new sources, in certain seasons, the modes (2,4) and (2,5) are essential.

WALTERSCHEID et al. (1980) made tidal calculations for a new source already. So it seemed that all the necessary work had been done to complete the tidal seasonal variation theory in the altitude region up to 100 km.

A paper by KAIDALOV (1979) disproved this opinion. Kaidalov drew attention to the fact that the perturbation method used by LINDZEN (1974) and WALTERSCHEID et al. (1979, 1980) is good for tidal modes which do not change their character when propagating upward or being trapped. In contrast, the main modes of the semidiurnal tide are on the boundary between propagating and trapped ones, being trapped in one altitude region but propagating in others, the boundaries between these regions being dependent just on the height-latitude distribution of mean zonal wind and temperature. Zero-order approximation in the perturbation theory, not taking into account effects of background wind and temperature for all approximations, defines the tidal waves character as trapped or propagating and leads to inadmissibly large errors in the tide calculation. KAIDALOV (1979) developed a numerical technique to solve the tidal model, taking into account seasonal variations of background wind and temperature without the short-comings of the perturbation method.

Considering tides above 100 km, we will limit ourselves to a few problems arising here. In its most complete form, modelling of tidal variations in the thermosphere is based on the equation of motion (1), Ohm's law (2), the equation of quasistationary space charge (3), together with the equations of energy and continuity. Usually, all variations are examined in linear approximation. Dissipative forces are molecular and turbulent heat conductivity, and ion friction. The contribution of molecular and turbulent friction is estimated to be insignificant, at least, up to the 200-250 km height.

In a majority of theoretical investigations the electric potential field is excluded and, as a rule, a torsional effect by the magnetic rotary force compensating the Coriolis force is neglected. This means that, instead of self-consistent examination, combining hydrodynamic equations with electrodynamic equations, a purely hydrodynamic approach is used (e.g., GARRETT and FORBES (1978)).

Taking into account the electric field and magnetic rotary force generates a series of new effects. Estimation of conclusions with regard to these effects, using experimental data, permits one to evaluate more reasonably their contribution to the tide formation in the thermosphere.

Partial or even complete compensation of the Coriolis force by the magnetic rotary force at 110-130 km altitudes would result in the formation of sharp wind maxima at these altitudes. In numerical experiments this maximum is well pronounced, as it can be seen in Figure 4, taken from theoretical papers by GLUSHAKOV et al., (1979, 1981). After excluding the magnetic rotary force the effect vanishes. These wind maxima are also well observed in luminous trail experiments (ANDREEVA et al., 1981).

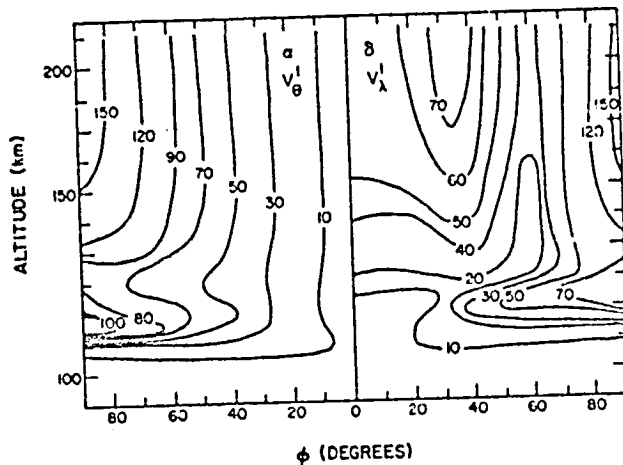


Figure 4. Height-latitude cross-section of the amplitude of zonal (a) and meridional (b) tidal wind diurnal component. In the 120 - 130 km altitude region at high latitudes tidal wind amplitude maxima are clearly seen.

It is of interest to connect the sporadic layer  $E_s$  appearance with this wind maxima. This is especially interesting as, according to the calculation, the height of wind maximum increases from lower towards higher latitudes, as it is observed for the height of the layer  $E_s$ .

Calculations show that taking into account the electric field may appear to be essential in the tidal wind pattern at altitudes above 130-140 km. This can be seen from Figure 5. It should, however, be mentioned that the electric field contribution in the tidal wind formation essentially depends on the electron concentration model assumed. The increase of electric field contribution to the tidal wind formation is caused by the fast increase with height of the electric forces term  $\frac{dV}{dt}$  [ExB]. A sharp growth of the  $\sigma_1/\rho$  value with height begins near 125-130 km, and this quantity reaches approximately a constant value near 160-180 km. On the other hand, the forces term connected quasi-linearly with the pressure gradient also increases with height, prevailing over the electric force below 140 km, but being inferior to it at altitudes above 140 km.

Calculations by GLUSHAKOV et al. (1979, 1981) show that in the formation of semidiurnal tidal winds in the region from 100 to 200 km, tidal oscillations propagating from the mesosphere prevail. These propagating oscillations influence also the rather considerable variations of relative temperature at the altitude near 110 km both for diurnal and, especially, for semidiurnal tides. Estimations of the electric field contribution may be considered to be valid only, if not only the thermodynamic parameters, but also the calculated electric field corresponds to direct measurements. Estimations of the electric field connected with the dynamo-effect have been made from drift velocities of ions in the ionospheric F<sub>2</sub> layer. In Figure 6 a comparison of the electric fields calculated theoretically and derived from drifts measurements according to data of incoherent radiowave scatter data (RICHMOND et al., 1980) is presented. It shows qualitative similarity of these fields.

Calculations made and their comparison with experiment remove a shadow of doubt about the considerable contribution of the electric field in the formation

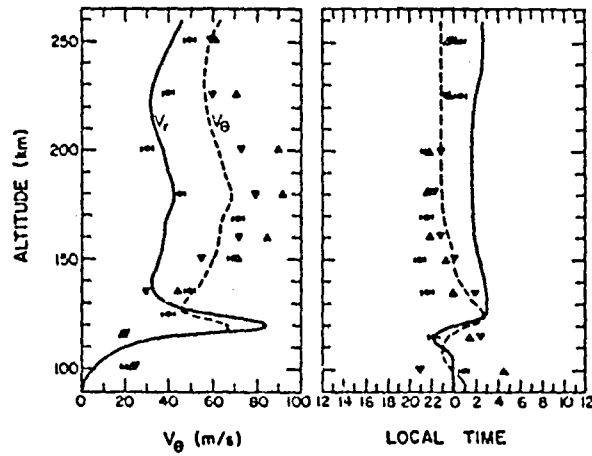


Figure 5. Vertical profile of tidal wind diurnal component amplitude (a) and phase (b):  
 — without electric field accounted for  
 - - - with electric field accounted for  
 $\Delta, \nabla, \oplus$  experimental data

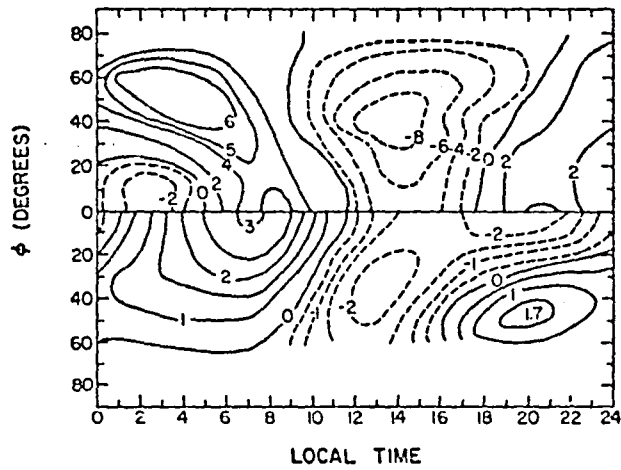


Figure 6. Time-latitude variation of electric field. At the top: theory, at the bottom: empirical model of RICHMOND et al. (1980).

of tidal oscillations of thermospheric parameters. However, only first steps have been made in the investigation of these new effects, and further efforts are needed in this direction.

## REFERENCES

- Andreeva, L. A., I. V. Elashova, L. A. Katasev, O. F. Kluev and A. D. Hananyan (1981), in: Problems in Solar-Atmospheric Relations, Gidrometeoizdat, Moscow, pp. 53-66 (in Russian).
- Butler, S. T. and K. A. Small (1963), Proc. Roy. Soc., A274, 91.
- Chapman, S. and R. Lindzen (1970), Atmospheric Tides, D. Reidel, Dordrecht/Holland.
- Dickinson, R. E., E. C. Ridley and R. G. Roble (1977), J. Atmos. Sci., 34, 178.
- Dokuchaev, V. P. (1959), Izvestiya Acad. Sci. USSR, Geophys. Ser., 5, 783.
- Emery, B. A. (1978), J. Geophys. Res., 83, 5704.
- Forbes, J. M. and H. B. Garrett (1978), Geophys. Res. Lett. 5, 1078.
- Forbes, J. M. and H. B. Garrett (1979), Rev. Geophys. Space Phys., 17, 1951.
- Garrett, H. B. and J. M. Forbes (1978), J. Atmos. Terr. Phys., 32, 657.
- Glushakov, M. L. (1975), Geomagn. i. Aeronomiya, 15, 266.
- Glushakov, M. L., G. V. Gridchin, V. N. Dulkan, A. I. Ivanovsky and L. A. Cherepanova (1979), in: Regional Structure of Dynamical Processes of the Middle Atmosphere, (in Russian), Izd. Ilim, Frunze, pp. 25-36.
- Glushakov, M. L., V. N. Dulkan and A. I. Ivanovsky (1979), Geomagn. i. Aeronomiya, 19, 663, 857.
- Glushakov, M. L., V. N. Dulkan and A. I. Ivanovsky (1980), Geomagn. i. Aeronomiya, 20, 62.
- Glushakov, M. L., V. N. Dulkan and A. I. Ivanovsky (1981), Geomagn. i. Aeronomiya, 21, 845.
- Ivanovsky, A. I. and Yu. V. Semenovskiy (1971), Izvestiya Acad. Sci. USSR, Ser. Atmosph. and Ocean Physics, 7, 246.
- Kaidalov, O. V. (1979), Trudy IEM, 2, 3.
- Kokin, G. A. and S. S. Gaigerov (editors) (1981), Meteorology of the Earth's Upper Atmosphere, (in Russian), Gidrometeoizdat, Leningrad, 270 pp.
- Lindzen, R. S. (1974), J. Atmos. Sci., 31, 1421.
- Portnyagin, Yu. I. and K. Sprenger (editors) (1978), Wind Measurement at 90-100 km Height by Ground-Based Methods, (in Russian), Gidrometeoizdat, Leningrad, 197 pp.
- Richmond, A. D., M. Blanc, B. A. Emery et al. (1980), J. Geophys. Res., 85, 4648.
- Schoeberl, M. R. and D. F. Strobel (1978), J. Atmos. Sci., 35, 577.
- Walterscheid, R. L. and S. V. Venkateswaran (1979), J. Atmos. Sci., 36, 1623, 1636.
- Walterscheid, R. L., J. G. De Vore and S. V. Venkateswaran (1980), J. Atmos. Sci., 37, 455.

N85

20471

UNCLAS

D21  
110

N 85 - 20471

ASPECTS OF PLANETARY WAVE TRANSPORTS IN THE MIDDLE ATMOSPHERE

G. Schmitz

Academy of Sciences of the GDR  
Central Institute of Solar-Terrestrial Physics  
Observatory of Ionosphere Research  
DDR-2565, Kuhlungsborn, GDR

ABSTRACT

The heat and momentum flux due to standing planetary waves in the stratosphere has been calculated on the basis of satellite data. The convergence of these fluxes has been investigated and shows an apparent heating and acceleration of the mean zonal state. The Eliassen-Palm flux divergence calculation shows that the mean zonal state is effectively decelerated. Furthermore the interaction between ultra-long waves and waves  $k = 4 - 15$  in the troposphere has been investigated for a winter period and has been discussed in connection with the geopotential wave one amplitude, which increases before a stratospheric warming event occurs.

The investigation of processes which determine the deviation of the zonally averaged temperature and wind field from radiation equilibrium is a central question in stratospheric dynamics. LEOVY (1964), HOLTON and WEHRBEIN (1980) in their model calculations take into consideration a linear drag that produces a deceleration proportional to the mean zonal wind, while SCHOEBERL and STROBEL (1978), DETHLOFF and SCHMITZ (1982) additionally consider the momentum transport by planetary waves. On the basis of a stationary model, Dethloff and Schmitz showed that the planetary wave influences on the mean state are small above the stratopause. In the following at first the standing momentum and heat flux and the divergence of the Eliassen-Palm flux is investigated. Furthermore the wave  $k = 4 - 15$  projection on the ultra-long waves in the troposphere preceding the occurrence of a stratospheric warming has been calculated.

The data basis is the monthly mean standard 500, 200 mb topographies of the European Meteorological Bulletin, the 100, 50, 30, 10 mb topographies from Obninsk, the synoptical bulletin and the 5, 2, 0.4 mb data source are the NOAA NMC maps for the winter 1974/75 where meteorological rocketsonde and satellite radiance data are used for analyses. The high topographies are given once a week only. The momentum and heat fluxes are calculated from the planetary wave amplitudes and phases. In the following the mean December values for the two years will be discussed. In Figure 1 the amplitude of planetary wave one is shown. The maximum of wave one appears at 70°N at a height of about 35 km with 800 gpm. Figure 2 shows the meridional standing momentum transport due to the sum of waves  $k = 1 - 3$ . The momentum transport has high values in the jet region of the upper troposphere and at a height of 50 km in middle latitudes. The meridional heat transport of the waves  $k = 1 - 3$ , given in Figure 3, also has largest values in the stratosphere, the two fluxes being essentially determined by the wave one contribution.

These shortly discussed fluxes are the basis for a determination of the interaction between ultra-long waves and mean zonal circulation, according to the Eulerian zonally-averaged momentum and thermodynamic equation. The interaction of the zonally averaged state with the planetary waves is explained through the convergence of momentum and heat fluxes. The effective acceleration and heating rates, resulting from these terms, have been calculated for the monthly mean December of the years 1974, 1975. The largest acceleration appears in high latitudes at 35 km with about  $12 \text{ ms}^{-1}/\text{day}$ . The convergence of the meridional heat flux seems to give strong heating rates of about  $4^\circ\text{K}/\text{day}$  at high latitudes and at a height of 40 km, but cooling in middle latitudes. These

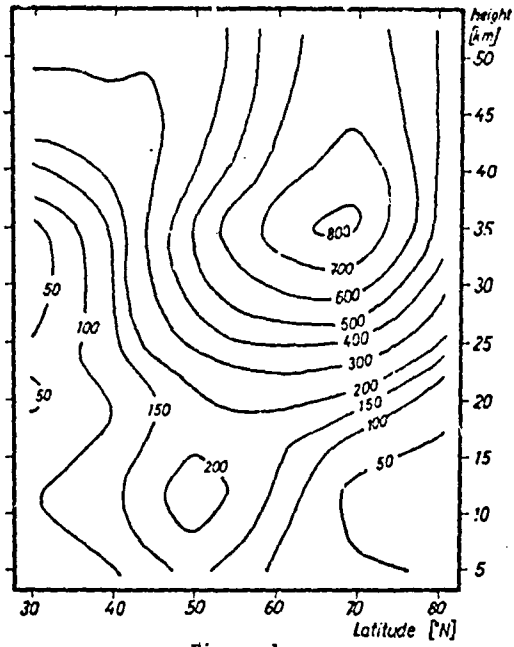


Figure 1.

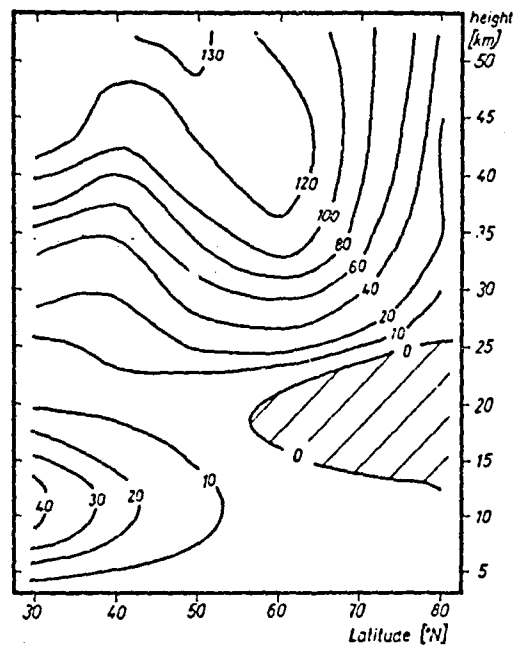


Figure 2.

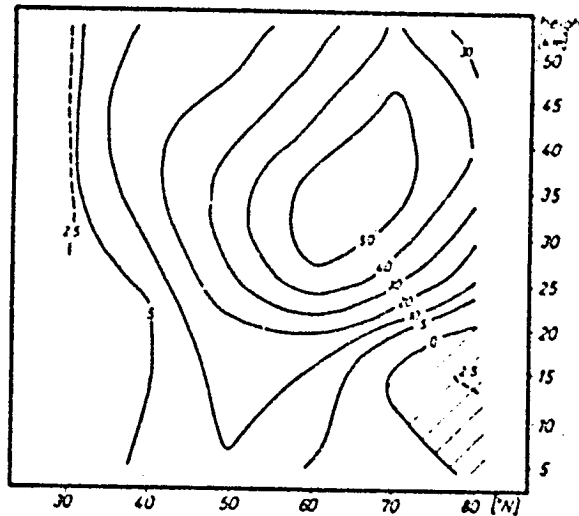


Figure 3..

values are lower than those given by GELLER (1982), because here we discuss the standing part of fluxes only. The calculated effective dynamical heating rates in the stratosphere are approximately equal to the diabatic heating rate. From the nonacceleration theorem of CHARNEY and DRAZIN (1961) and ANDREWS and MCINTYRE (1976) is known that one obtains misleading physical information when discussing the influences of the planetary wave momentum or heat fluxes alone, because steady planetary waves without dissipation or internal forcing do not force the zonal mean state. EDMON et al. (1980) propose the use of residual mean equations for a discussion of the net effect of planetary waves fluxes on the mean flow. The waves are introduced into this system only through the divergence of the Eliassen-Palm flux in the residual zonal momentum equation. Figure 4 shows the Eliassen-Palm flux divergence for the standing waves as a mean value of December 1974/1975. The EPF divergence has negative values at a latitude of  $40^{\circ}$ - $60^{\circ}$ N of the stratosphere, whereas the divergence term of the Eulerian zonal momentum equation is positive so that the mean zonal state is effectively decelerated, in contrast to an acceleration in the Eulerian picture. GELLER (1982) discussed this relation for the data of January 1979 where he found a zonal mean state acceleration which is reduced by a factor 2 when calculated from the EPF divergence. If we discuss the December mean consisting of only 8 weekly values at 5, 2, 0.4 mb as a stationary solution, then the residual meridional flow is induced to balance the EPF divergence.

Furthermore we have investigated the connection between standing and transient fluxes and their spectral characteristics on the data basis of the winter period 1970/71. The results suggest a relation between the zonal mean ultra-long  $k = 1 - 3$  and the  $k = 4 - 15$  wave transport. One possibility for such a relation is that this process is conducted via the mean zonal state, the other is the nonlinear interaction between ultra-long waves and waves  $k = 4 - 15$ . We shortly discuss the latter conception further, because it seems that the time variability of ultra-long waves in the stratosphere is also connected with this process. Furthermore the question arises whether the high increase of the amplitudes of geopotential wave one or two in the troposphere before a stratospheric warming is related to the interaction between ultra-long and waves  $k = 4 - 15$ . This question has been investigated by calculating the projection of

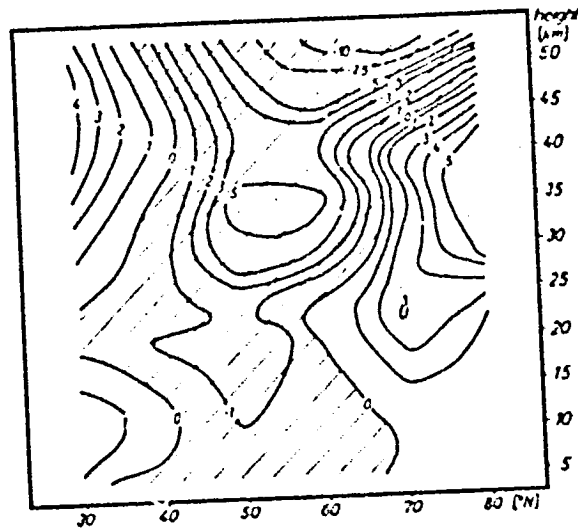


Figure 4.

nonlinear interaction of baroclinic waves with wavenumbers 4 - 15 on the ultra-long waves at 200 mb.

The wave transport terms  $u^*v^*$ ,  $v^*v^*$ ,  $u^*u^*$  have been investigated. These transports appear in the momentum equations and excite or dissipate ultra-long waves. The symbol (---) stands for the waves 1, 2, 3 and (---) for the baroclinic wave  $k = 4 - 15$  contributions. So we discuss for example  $(v^*v^*)_1$  as the interaction between the waves  $k = 4 - 15$  and the wave  $k = 1$ . Figure 5 gives the standing plus transient wave  $k = 4 - 15$  projection on the wavenumbers  $k = 1, 2$  for the transport  $v^*v^*$ . The interaction with wave 1 appears much stronger than that for wave  $k = 2$ . It will be interesting to determine the importance of this source for an interpretation of standing ultra-long waves in models.

Figure 6 shows the geopotential wave one amplitude in the period from December 1970 to January 1971 at 200 mb. Around 5-8th December at 55°N, 20th December at 50°-70°N, and about 15th January at 75°N we observed an acceleration of wave-one amplitude. For the winter 1970/71 the warming was observed around 10th January and it seems that this warming was stimulated by the amplitude acceleration at about 25th December. This acceleration is a necessary prerequisite for the development of a stratospheric warming. Figure 7 shows the baroclinic wave projection  $(v^*v^*)_1$  on the wavenumber  $k = 1$  at 200 mb. The thickened isolines for the wave projection terms are larger than the monthly mean total value by a factor of two. Comparison of the curves shows that in middle or high latitudes periods of strong baroclinic wave interactions with wave 1 correspond with periods of large wave amplitude accelerations. Furthermore the net acceleration of geopotential wave amplitudes was estimated on the basis of the divergence of the transports  $u^*v^*$  and  $v^*v^*$  in the meridional momentum equation. For the mentioned time periods one obtains at 50°N an acceleration of about 50-100 gmp/day which is a reasonable value in mechanistic models to describe a stratospheric warming.

In summarizing, it seems that the time variability of ultra-long waves in the stratosphere is also determined by interaction with baroclinic waves in the upper troposphere.

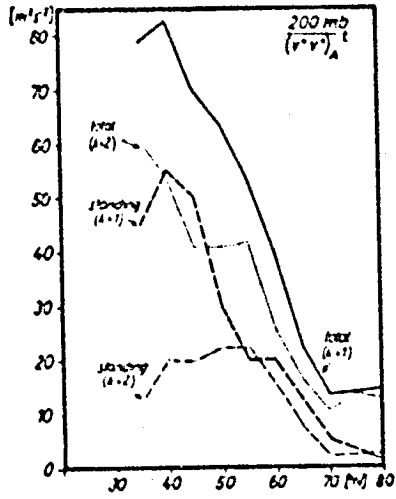


Figure 5.

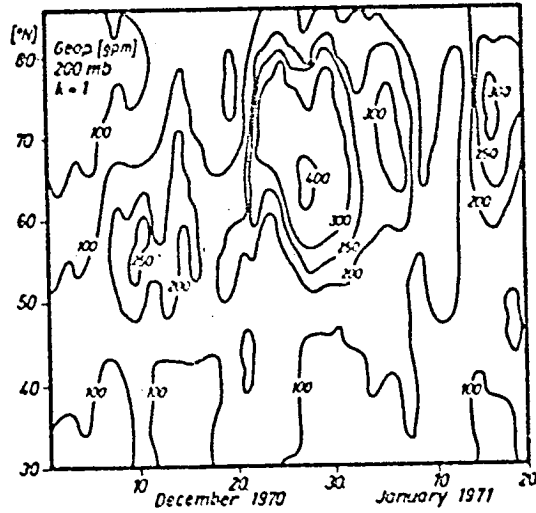


Figure 6.

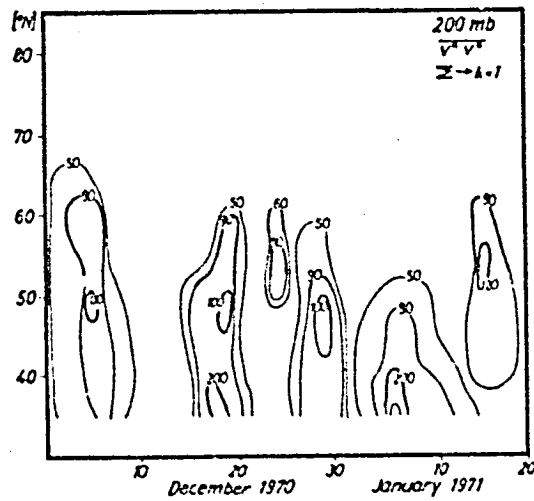


Figure 7.

## ACKNOWLEDGEMENT

I thank Dr. N. Grieger and W. Kruger for their efforts in the preparation of the observational results.

## REFERENCES

- Andrews, D. G. and M. E. McIntyre (1976), *J. Atmos. Sci.*, **33**, 2031.  
 Charney, J. G. and P. G. Drazin (1961), *J. Geophys. Res.*, **66**, 83.  
 Dethloff, K. and G. Schmitz (1982), *Phys. Solariterr., Potsdam*, **18**, 91.  
 Edmon, H. J., B. J. Hoskins and M. E. McIntyre (1980), *J. Atmos. Sci.*, **37**, 2000.  
 Geller, M. A. (1982), Dynamics of the middle atmosphere, Tutorial lecture delivered at the Fifth International Symposium on Solar Terrestrial Physics in Ottawa, Canada.  
 Schoeberl, M. R. and D. F. Strobel (1978), *J. Atmos. Sci.*, **35**, 577.

N85

20472

UNCLAS

D22

N85-20472

116

COUPLING BETWEEN THE THERMOSPHERE AND THE STRATOSPHERE:  
THE ROLE OF NITRIC OXIDE

G. Brasseur

Institut d'Aeronomie Spatiale de Belgique  
3, Avenue Circulaire  
B-1180 Brussels, Belgium

ABSTRACT

Two-dimensional model calculations reveal that the chemical conditions at the stratopause are related to the state of the thermosphere. This coupling mechanism can be partly explained by the downward transport of nitric oxide during the winter season and consequently depends on the dynamical conditions in the mesosphere and in the lower thermosphere (mean circulation and waves). In summer, the photodissociation of nitric oxide plays an important role and the thermospheric NO abundance modulates the radiation field reaching the upper stratosphere. Perturbations in the nitric oxide concentration above the mesopause could therefore have an impact in the vicinity of the stratopause.

As indicated for example by DANILOV and TAUBENHEIM (1983), the behavior of the D-region is significantly different in summer and in winter. During the first of these seasons, the electron density seems fairly dependent on the solar zenith angle while, during the winter, considerable day to day variations completely mask any control of the ionosphere by solar or geophysical parameters. Furthermore, as reported already by APPLETON in 1937, anomalous increases in absorption of high frequency radio waves occur during certain groups of winter days. Even outside these irregular winter anomaly events, the absorption and consequently the electron concentration appears to be considerably higher in winter than in summer. Since the quiet time ionization in the D-region is due primarily to the action of the solar Lyman- $\alpha$  radiation on nitric oxide molecules, the understanding of the lower ionosphere and its probable control by dynamical processes requires a detailed understanding of the NO distribution in the mesosphere.

In order to achieve such a study, a two-dimensional model with coupled chemical and dynamical processes has been constructed. This model ranges from 40 to 100 km altitude and from the North to the South pole. Dynamical parameters such as the meridional circulation and the eddy diffusion tensor are prescribed. In particular, the two-dimensional eddy components are taken from EBEL (1980) but, as indicated hereafter, some changes have been introduced in several model runs in order to estimate the sensitivity of the dynamical activity in the lower thermosphere on the calculated concentration values. This model which is in many aspects similar to the model developed by SOLOMON et al. (1982) and which is described in detail by BRASSEUR and DE BAETS (1983), considers the most important chemical and photochemical processes related to the odd oxygen, odd nitrogen and odd hydrogen species as well as the positive and negative ions and the electrons. This paper will deal essentially with the behavior of nitric oxide below 100 km.

Nitric oxide is produced in the stratosphere by the oxidation of nitrous oxide ( $N_2O$ ) in the presence of the electronically excited atomic oxygen  $O(^1D)$ . An additional source, essentially at high latitude, is due to the action of the cosmic rays. In the thermosphere, ions which are produced by solar EUV and X rays as well as by particle precipitation, especially in the auroral belts (relativistic electron precipitation, solar proton events, etc.) lead to the formation of NO molecules. Direct dissociation or dissociative ionization of  $N_2$  is another source of NO. Calculations made by RUSCH et al. (1981) indicate that each ion pair formation produces 1.3 nitric oxide mole-

cules. Consequently the thermospheric NO production rate will be controlled by the solar and geomagnetic activity. In the present paper, only quiet conditions will be considered. Downward transport of nitric oxide from the thermosphere will depend on the strength of the vertical exchanges and of the chemical stability of NO in the mesosphere. As indicated by Figure 1, the nitric oxide flux is directed downwards in the whole mesosphere during the winter when the lifetime of NO is long and the  $K_{zz}$  values are large, indicating that thermospheric nitric oxide could reach the stratosphere and interact with the ozone layer. Comparisons of calculated and observed  $O_3$  density for different solar activity levels (SOLOMON and GARCIA, 1983) give indirect evidence for such a  $NO_x$  transport above  $60^\circ N$  during the winter.

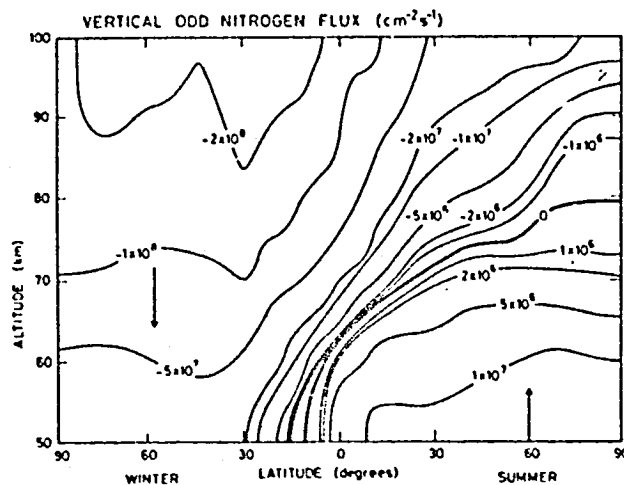


Figure 1. Meridional distribution of the vertical flux component of nitric oxide calculated with the exchange coefficients suggested by Ebel (1980).

During the summer season, the downward transport by eddy diffusion is weak and is even slowed down by the upward meridional circulation. The loss of NO by photodissociation and recombination is intense and is even enhanced by the fact that the lower temperature in the vicinity of the summer mesopause reduces the rate of the  $N(^4S) + O_2$  reaction (reformation of NO after its photodissociation) and thus favors the  $N(^4S) + NO$  reaction (destruction of odd nitrogen). Therefore no dynamical coupling between the thermosphere and stratosphere appears in summer and the nitric oxide flux is directed upwards during this period of the year. However, as pointed out by FREDERICK et al. (1983), the absorption of the UV radiation by variable thermospheric NO could modulate the radiation field reaching the lower mesosphere and the upper stratosphere and consequently modify the dissociation rate of nitric oxide in the  $\delta$  bands at these levels. The magnitude of this effect appears however to be probably smaller than the 11 year variability of the solar irradiance. Figure 2 shows the calculated distribution of the nitric oxide concentration for winter and summer conditions. It can be seen that nitric oxide is present in winter and that the concentration minimum at the mesopause level is very weak during this season.

In order to estimate the sensitivity of the NO distribution on the strength

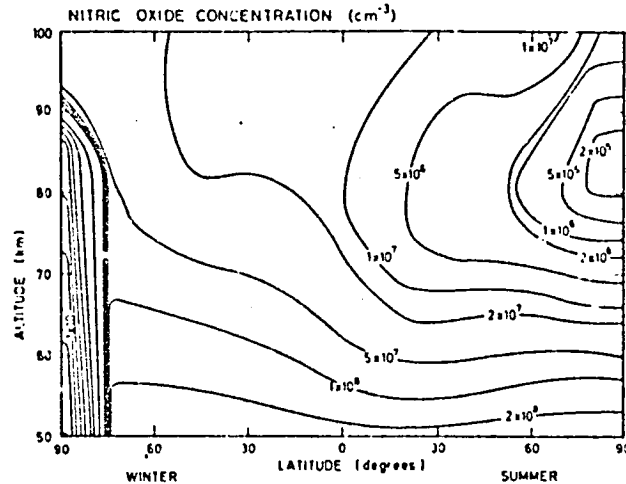


Figure 2. Meridional distribution of the nitric oxide concentration calculated with the exchange coefficients suggested by Ebel (1980).

of the vertical transport, the  $K_{zz}$  values have been decreased in the thermosphere by a factor which is uniform with latitude. Three cases have been considered: case 1 refers to the Ebel's values, case 2 to a very slow diffusion coefficient  $K_{min}$  and case 3 to an intermediate value. Figure 3 shows the 3 corresponding profiles for summer and winter mid-latitude. The  $K_{zz}$  profile suggested by ALLEN et al. (1981) to explain observed atomic oxygen distributions by their 1-D model is also indicated.

The nitric oxide mixing ratio and flux at the stratopause for the two extreme cases (1 and 2) are shown in Figure 4a and b. These figures indicate again that a coupling between the thermosphere and the stratosphere is possible essentially during the winter. The strength of the coupling as well as the

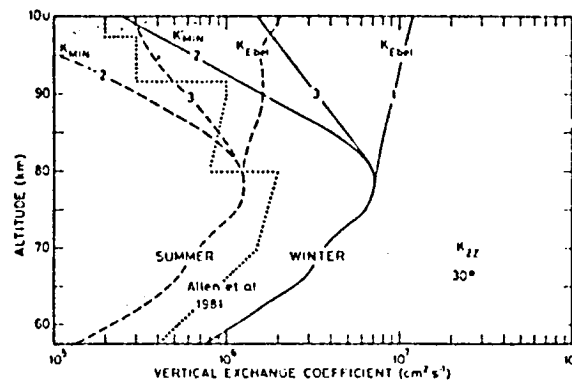


Figure 3. Different vertical exchange coefficients  $K_{zz}$  adopted in the model calculations. Vertical distributions represented at 30° latitude for winter and summer conditions. The profile used by ALLEN et al. (1981) is also indicated.

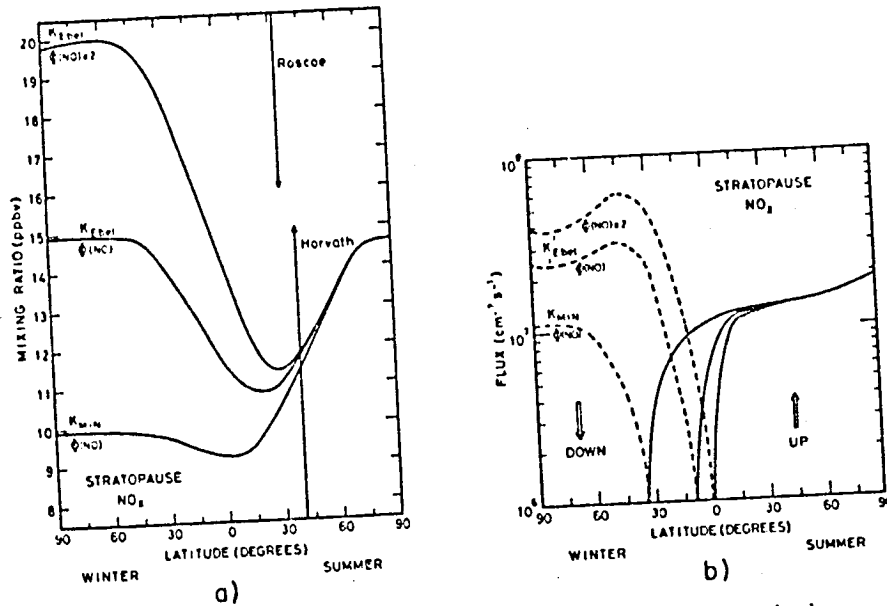


Figure 4a. Latitudinal and seasonal distribution of the nitric oxide mixing ratio calculated at the stratopause (50 km altitude) assuming different conditions:  $K_{Ebel}$  refers to the exchange coefficients suggested by Ebel;  $K_{min}$  to the smallest vertical eddy diffusion depicted in fig. 3; (NO) refers to an upper boundary flux conditions corresponding to quiet solar conditions (Solomon, private communication, 1981) and (NO)  $\times$  2 to the imposed flux which has been multiplied by 2.

Figure 4b. Same as in fig. 4a but for the nitric oxide vertical flux.

latitude of the border between the downward and the upward NO exchange regions varies with the adopted  $K_{zz}$  profile and with the downward flux imposed at the upper boundary (which reflects the integrated NO production above this level and consequently the solar and geomagnetic activity). In order to estimate this last effect, the nitric oxide flux at 100 km has been uniformly doubled. The corresponding impact on the stratopause NO is also indicated in Figures 4a and b.

Comparisons between observed and calculated nitric oxide profiles are not straightforward since the measured concentrations exhibit large variations. This variability might partly be attributed to instrumental errors but it also reflects the large changes occurring in the real world. It seems however that most observations show a concentration minimum near 85 km altitude ( $10^6$  to  $10^7$  cm<sup>-3</sup>) but that this minimum is considerably weaker during the winter ( $5 \times 10^6$  to  $5 \times 10^7$  cm<sup>-3</sup>). Observations made during winter anomaly events (BERAN and BANGERT, 1979) show large NO densities and a vertical profile indicating almost perfect mixing conditions (and consequently strong vertical exchanges between 50 and 80 km).

The comparison between available data and the calculated profiles obtained

with the 3 different transport coefficients suggests that case 3 (intermediate  $K_{zz}$ ) is somewhat more representative of most nitric oxide observations than the other eddy diffusion profiles. The corresponding meridional distribution of NO is shown in Figure 5 and should be compared with the results depicted in Figure 2. It should be remembered that these model results refer to average seasonal and diurnal conditions. The magnitude of the diurnal variation of NO at selected altitude and at 30 degrees latitude can be estimated from Figure 6.

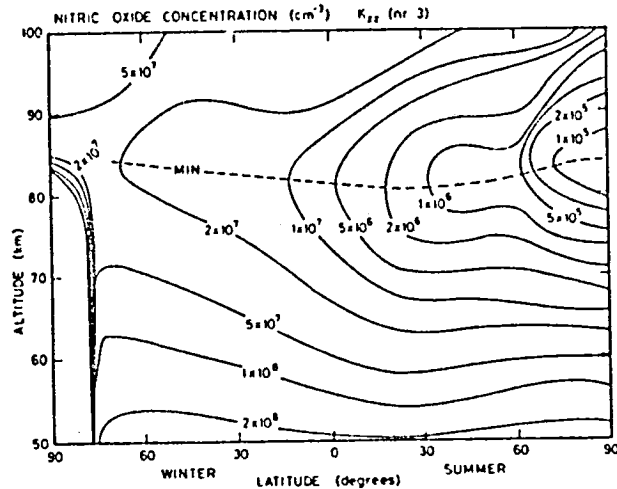


Figure 5. Meridional distribution of the nitric oxide concentration calculated with the intermediate values of  $K_{zz}$  (case 3) and Ebel's values for  $K_{yy}$  and  $K_{yz}$ .

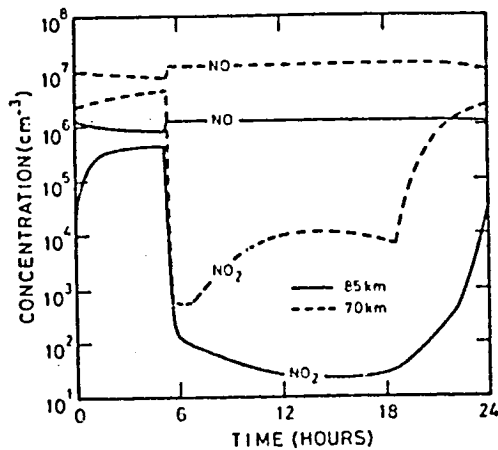


Figure 6. Diurnal variation of nitric oxide and nitrogen dioxide calculated at 70 and 85 km altitude for spring conditions and 30 degrees latitude. The total  $\text{NO}_x$  concentration is assumed to be  $1.2 \times 10^7$  and  $1.2 \times 10^6 \text{ cm}^{-3}$  at 70 and 85 km, respectively.

Finally, the electronic concentration which is derived from the NO distribution shown in Figure 5 and which is obtained from a detailed ionic model is represented in Figure 7. It can be seen that the concentration of electrons is considerably higher in winter owing to the fact that the nitric oxide density is larger during this season and that the temperature and consequently the effective electron loss are higher in the winter hemisphere. The model explains thus satisfactorily the observed higher radio wave absorption during wintertime (which is sometimes called the regular component of the winter anomaly) but cannot explain the causes of the irregular components of such anomalous events since the calculations are performed with seasonal averages of temperature, diffusion coefficients and wind components. Satellite data might provide indications on the relative role played by nitric oxide and by the temperature in the appearance of sudden anomalous absorption events.

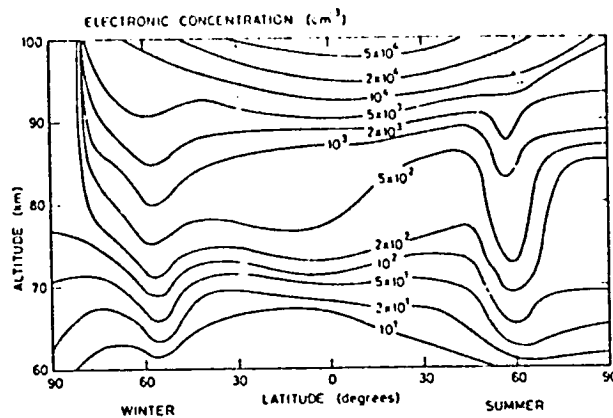


Figure 7. Meridional distribution of the 24 hours averaged concentration of electrons calculated with the NO distribution shown in figure 5. These values correspond to solar quiet conditions.

#### REFERENCES

- Allen, H., Y. L. Yung and J. W. Waters (1981), *J. Geophys. Res.*, **86**, 3617.  
 Appleton, E. (1937), *Proc. Roy. Soc.*, **A162**, 451.  
 Beran, D. and W. Bangert (1979), *J. Atmos. Terr. Phys.*, **41**, 1091.  
 Brasseur, G. and P. De Baets (1983), Minor constituents in the mesosphere and lower thermosphere, in preparation.  
 Danilov, A. D. and J. Taubenheim (1983), *Space Sci. Rev.*, **34**, 413.  
 Ebel, A. (1980), *J. Atmos. Terr. Phys.*, **42**, 617.  
 Frederick, J. E., R. B. Abrams and P. J. Crutzen (1983), The delta-band dissociation of nitric oxide: A potential mechanism for coupling thermospheric variations to the mesosphere and stratosphere, submitted to *J. Geophys. Res.*  
 Rusch, D. W., J. C. Gerard, S. Solomon, P. J. Crutzen and G. C. Reid (1981), *Planet. Space Sci.*, **29**, 767.  
 Solomon, S., P. J. Crutzen and R. G. Roble (1982), *J. Geophys. Res.*, **87**, 7206.  
 Solomon, S. and R. R. Garcia (1983), Transport of thermospheric NO to the upper stratosphere, preprint.

N85

20473

UNCLAS

## ATMOSPHERIC-PROFILE IMPRINT IN FIREBALL ABLATION-COEFFICIENT

Z. Ceplecha and P. Pecina

Astronomical Institute of the Czechoslovak Academy of Sciences  
251 65 Ondrejov Observatory, Czechoslovakia

During the past two decades three different projects for registration of meteoric fireballs were put into operation using multistation photographic technique. They have yielded data on several hundreds of fireball trajectories, some of them with deep atmospheric penetration down to heights of 20 kilometers. The immediate results of multistation photograph of a fireball are the relative distances along the trajectory,  $l_{obs}$ , and the heights,  $h_{obs}$ , measured at each shutter time-mark,  $t$ , (shutter breaks of the image). The precision of one value of  $l_{obs}$  is of the order of several tens of meters. There are usually many tens of independent points (breaks) available for long fireball trajectories with independently measured  $l_{obs}$  and  $h_{obs}$ . We need a good theoretical relation for a least-squares solution of  $l=l(t)$  or  $h=h(t)$ , where  $l$  is the theoretically given distance along the trajectory and  $h$  the height. Until recently there were no adequate formulae expressing theoretically the distance along the fireball trajectory,  $l$ , as function of  $t$ . We have been able to find such formulae and moreover to find their general form for any atmospheric profile used.

The motion and ablation of a single non-fragmenting meteor body can be expressed by the following set of differential equations first presented by HOPPE (1937):

$$\frac{dv}{dt} = -\Gamma A \rho_d^{-2/3} \rho_m^{-1/3} v^2 \quad (1)$$

$$\frac{dm}{dt} = -\frac{\Lambda A}{2\zeta} \rho_d^{-2/3} \rho_m^{2/3} v^3 \quad (2)$$

$$\frac{dh}{dt} = -v \cos z_p \quad (3)$$

where  $v$  is the velocity,  $m$  the mass,  $h$  the height of the meteoroid,  $\rho$  the air density at any time instant  $t$ . The parameters are:  $\Gamma$  the drag coefficient,  $\Lambda$  the heat-transfer coefficient,  $A$  the shape factor:  $A = S m^{2/3} \rho_d^{2/3}$ , where  $S$  is the head cross-section and  $\rho_d$  the density of the meteoroid,  $\zeta$  is the energy necessary for ablation of one unit of mass and  $z_p$  is the angle between the fireball trajectory and the vertical. The ablation coefficient, is defined by

$$\sigma = \frac{\Lambda}{2\zeta\Gamma} \quad (4)$$

and the shape-density coefficient,  $K$ , by

$$K = \Gamma A \rho_d^{-2/3} \quad (5)$$

To solve the system of equations (1) to (3), we have to assume a physical profile of the atmosphere. Until now everybody working in the field of physical theory of meteors and its application to observations solely used the assumption of exponential decrease of the air density with height corresponding to an isothermal atmosphere:

$$\rho = \rho_c \exp(-bh) \quad (6)$$

where  $b$ , the air density gradient, was assumed constant as well as the zero-level air-density,  $\rho_c$ . Moreover, the solution of the system (1) to (3) was known only in the form of  $v=v(\rho)$ :

$$\bar{E}_1\left(\frac{1}{6} \sigma v_\infty^2\right) - \bar{E}_1\left(\frac{1}{6} \sigma v^2\right) = \frac{2K \rho m_\infty^{-1/3} \exp\left(\frac{1}{6} \sigma v_\infty^2\right)}{b \cos z_R} \quad (7)$$

where  $v_\infty$  is the initial velocity (before entering the atmosphere) and  $m_\infty$  is the initial mass and  $\bar{E}_1(x) = \int_x^\infty \frac{\exp(-u)}{u} du$  is the exponential integral. Thus numerical differentiation of directly observed distances along the fireball trajectory,  $l_{obs}$ , was necessary to get  $v_{obs}$  for application of formula (7) to observations. Such an indirect method yielded ablation coefficients and initial velocities with standard deviations much larger than corresponding to the accuracy of the measured distance,  $l_{obs}$  so the accuracy of the observed quantities was far from being utilized fully.

Recently we have proposed a solution of the system (1)-(3) in a closed form expressing  $l=l(v(t))$ :

$$t - t_0 = -\frac{2}{b \cos z_R} \int_{v_0}^v \frac{\exp\left(\frac{1}{6} \sigma x^2\right) dx}{x^2 \left[ \bar{E}_1\left(\frac{1}{6} \sigma v_\infty^2\right) - \bar{E}_1\left(\frac{1}{6} \sigma x^2\right) \right]} \quad (8)$$

$$l - l_0 = \frac{1}{b \cos z_R} \ln \left[ \frac{\bar{E}_1\left(\frac{1}{6} \sigma v_\infty^2\right) - \bar{E}_1\left(\frac{1}{6} \sigma v^2\right)}{\bar{E}_1\left(\frac{1}{6} \sigma v_\infty^2\right) - \bar{E}_1\left(\frac{1}{6} \sigma v_0^2\right)} \right] \quad (9)$$

Here  $v_0$ ,  $l_0$  are the velocity and the distance at the point  $t=0$  from where the relative time is counted. The integration variable is denoted  $x$ . The equations (8) and (9) hold under the assumption (6). The observed values,  $l_{obs}$  and  $h_{obs}$  for each independent time instant,  $t$ , can be fitted to equations (8) and (9) by the least-square method and the parameters  $l_0$ ,  $v_0$ ,  $v_\infty$ ,  $\sigma$  can be determined.

In applying our formulae (8) and (9) to observations of fireballs we started to suspect much greater importance of the air density profile for the resulting values of the parameters than it was assumed previously, when the simplistic approach to the air density profile with a constant air density gradient was assumed as correct. Our solution of (1) to (3) for a general air density profile has the form

$$t - t_0 = \int_{l_0}^l v^{-1} dl \quad (10)$$

$$\frac{\bar{E}_1\left(\frac{1}{6} \sigma v_\infty^2\right) - \bar{E}_1\left(\frac{1}{6} \sigma v^2\right)}{\bar{E}_1\left(\frac{1}{6} \sigma v_\infty^2\right) - \bar{E}_1\left(\frac{1}{6} \sigma v_0^2\right)} = \frac{\int_h^\infty \rho dh}{\int_{h_0}^\infty \rho dh} \quad (11)$$

where  $h_0$  is the height at the time instant  $t_0$ . Among other parameters  $v_\infty$  and  $\sigma$  can be determined by the least-square method to fit the observations to (10) and (11).

Details on both solutions (8), (9) and (10), (11) can be found in two recent papers (PECINA and CEPLECHA, 1983, 1984) together with outlines of the numerical procedures and of the computer programs used. The ablation

coefficients and initial velocities computed for 10 Prairie Network and one European Network fireballs for the isothermal atmosphere (1962) and for the seasonal atmosphere (1966) are compared in Table 1. Graphical comparison of ablation coefficients computed for the isothermal atmosphere and for the seasonal atmosphere are plotted in Figure 1. The following results are evident.

- a) The computed ablation coefficient is strongly dependent on the atmospheric model used. Differences by using a simplistic isothermal atmosphere are up to factor of two.
- b) The standard deviations when using a seasonal atmosphere are significantly smaller than for the simple isothermal model.
- c) The initial velocity differs also far outside the standard deviations for the majority of cases and the values from the seasonal atmosphere are better. This has astronomical significance in computing the orbits.

The main conclusion is evident. The generous assumption of simple atmospheric model used up to now for theoretical considerations of meteoroid penetration into the atmosphere and for computational applications to fireballs yields incorrect results. At least, the density profile of "Monthly atmospheres" should be used (CIRA, 1972) for any future theoretical and experimental applications to get any reliable data on ablation coefficients and initial velocities of fireballs with good dynamic data. Analysing ablation coefficients computed for many fireballs of different structure and composition of their meteoroids, we could better recognize different types of bodies and their average characteristics. Then, using the average statistical value of the ablation coefficient for each separate structural and compositional group of fireballs, we could determine details of the instant air density profile of the Middle Atmosphere at the particular moment of any fireball with good dynamic data and moreover the local disturbance by large meteoric bodies. And in this direction we want to contribute to studies of the Middle Atmosphere in the near future.

#### REFERENCES

- CIRA (1972), COSPAR International Reference Atmosphere 1972, Akademie Verlag, Berlin.
- Pecina, P. and Z. Cepelcha (1983), Bull. Astron. Inst. Czechosl., 34, 102.
- Pecina, P. and Z. Cepelcha (1984), Bull. Astron. Inst. Czechosl., 35, No. 1 (or 1983, No. 6).
- U.S. Standard Atmosphere (1962), Washington
- U.S. Standard Atmosphere Supplements (1966), Washington

Table 1. Comparison of ablation coefficient,  $\sigma$ , and initial velocity,  $v_{\infty}$ , computed with constant air density gradient,  $b$ , and with seasonal air density profile.

Fireball Number	$\sigma$ $\text{s}^2/\text{km}^2$		$v_{\infty}$ km/s		Height Interval km
	$\sigma \exp(-bh)$	Seasonal Atmosphere	$\sigma \exp(-bh)$	Seasonal Atmosphere	
FN39057	0.0229	0.0195	14.339	14.350	74
	$\pm 0.0009$	$\pm 0.0005$	$\pm 0.006$	$\pm 0.002$	36
FN39060	0.007	0.018	31.94	31.81	91
	$\pm 0.003$	$\pm 0.002$	$\pm 0.06$	$\pm 0.04$	50
FN39065	0.0362	0.0316	17.303	17.332	68
	$\pm 0.0009$	$\pm 0.0006$	$\pm 0.009$	$\pm 0.004$	34
FN39078	0.0634	0.0604	10.975	10.982	62
	$\pm 0.0031$	$\pm 0.0013$	$\pm 0.011$	$\pm 0.003$	41
FN39404	0.0396	0.0303	15.319	15.346	79
	$\pm 0.0007$	$\pm 0.0007$	$\pm 0.006$	$\pm 0.004$	28
FN39405	0.0465	0.0451	14.405	14.385	70
	$\pm 0.0017$	$\pm 0.0009$	$\pm 0.011$	$\pm 0.003$	46
FN39434	0.0269	0.0146	14.289	14.317	69
	$\pm 0.0009$	$\pm 0.0007$	$\pm 0.004$	$\pm 0.002$	27
FN39469A	0.0132	0.0176	26.39	26.42	95
	$\pm 0.0020$	$\pm 0.0016$	$\pm 0.04$	$\pm 0.02$	56
FN39729C	0.0107	0.0109	27.890	27.823	72
	$\pm 0.0004$	$\pm 0.0002$	$\pm 0.029$	$\pm 0.009$	43
FN39820A	0.0208	0.0212	24.617	24.611	80
	$\pm 0.0003$	$\pm 0.0002$	$\pm 0.006$	$\pm 0.003$	39
EN290181	0.059	0.031	11.578	11.611	64
	$\pm 0.006$	$\pm 0.004$	$\pm 0.011$	$\pm 0.004$	33

\* Different average values of  $b$  were used corresponding to different height intervals for particular fireballs and to the U.S. Standard Atmosphere (1962).

Seasonal atmosphere were taken from U.S. Standard Atmosphere Supplements (1966).

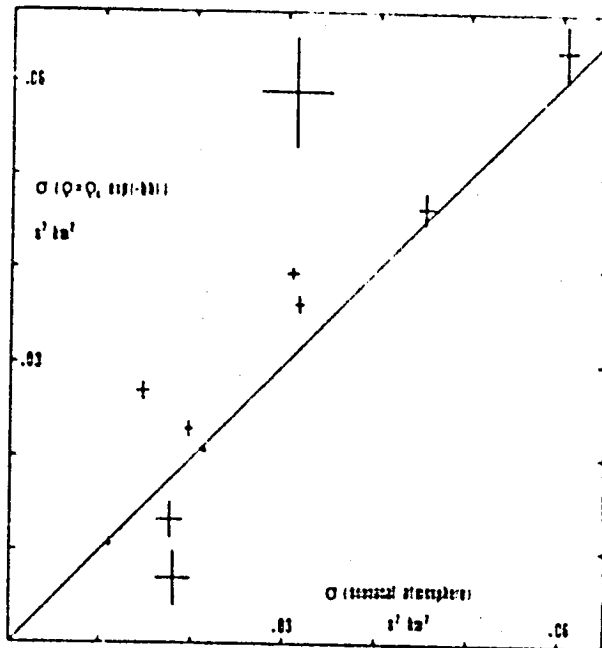


Figure 1. The average ablation coefficient,  $\alpha$ , computed from the simple isothermal atmospheric model ( $\alpha = \alpha_0 \exp(-bh)$ ) is plotted against the average ablation coefficient computed from the seasonal atmospheric model. Bars are the standard deviations. The 45° line marks equal values of  $\alpha$  from both computations.

N85

20474

UNCLAS

85-20474

127

METEOR WIND RESULTS FROM ATLANTA, U.S.A., AND RAMEY, PUERTO RICO

R. G. Roper

School of Geophysical Sciences  
Georgia Institute of Technology  
Atlanta, Georgia 30332

ABSTRACT

Results obtained using the French (CNET) Meteor Wind Radar at Ramey, Puerto Rico (18°N, 67°W), and the Georgia Tech Radio Meteor Wind Facility in Atlanta, U.S.A. (34°N, 84°W) are presented and compared. Prevailing wind, diurnal and semidiurnal wind amplitudes are considerably larger over Ramey than over Atlanta, but the mean zonal circulation over Atlanta is more characteristic of the equatorial circulation than winds measured by stations at higher mid-latitudes. The value of continuous observations, with a height resolution of  $\pm 2$  km, is again emphasized, as is the need for the application of several techniques, groundbased, in-situ and satellite, if projects such as the MAP GLOBMET are to succeed in delineating the global meteorology of the mesopause.

INTRODUCTION

The Georgia Tech Radio Meteor Wind Facility is located in Atlanta (34°N, 84°W), and has been in operation since August, 1974. The system has been described by ROPER (1975), and results pertaining to both prevailing winds and tides using data from the four years 1974-1978 have been published by ROPER (1978 a,b), SALBY and ROPER (1980), BOLAS and ROPER (1981), and AHMED and ROPER (1983). No data is available for the period August 20, 1978 through July 14, 1980, when both transmitter and receiving sites were relocated (but still remained within a kilometer of their previous positions).

The French (CNET) Meteor Wind Radar, described by GLASS et al. (1978), was installed at a site near Aguadilla, Puerto Rico, during the summer of 1977. The site (18°N, 67°W, see Figure 1, from MATTHEWS et al., 1981) is located approximately 44 kilometers west-north-west of the 430 MHz Thomson scatter radar and other facilities at the National Astronomy and Ionosphere Center, Arecibo Observatory. The CNET radar has been described by various authors as the Aguadilla Radar, the Punta Borinquen Radar, and, as in this paper, the Ramey Radar. Only the zonal component of the wind at meteor heights is measured.

The Arecibo Thomson scatter radar has provided meteor zone wind measurements (MATTHEWS, 1976) prior to the installation of the Ramey meteor wind radar. However, Arecibo is a multi-use facility, and cannot be dedicated to any one task for more than a few days at most.

Other meteor radars have been operated in the tropics. In a pioneering effort, BABADZHRANOV et al. (1970) reported meteor winds from Mogadishu (2°N, 45°E) for the period 22-29 September, 1968. The University of the West Indies has provided useful data from Jamaica (18°N, 77°W) as reported by ALLEYNE et al. (1974) and SCHOLEFIELD and ALLEYNE (1975).

Figure 2 (from MATTHEWS et al. 1981) is included to show the excellent agreement between the winds measured simultaneously at Ramey (H) and Arecibo (TS) between 0900 and 1600 hours, August, 1978.

EQUATORIAL WINDS

Before the Ramey radar was taken over by Georgia Tech in 1978, the Groupe Radar Meteorique of CNET had conducted several campaigns, each of which lasted

got these reports



LONG PERIOD VARIATIONS OF THE ZONAL WIND  
BORINGUEN -AUG-SEPT 1977

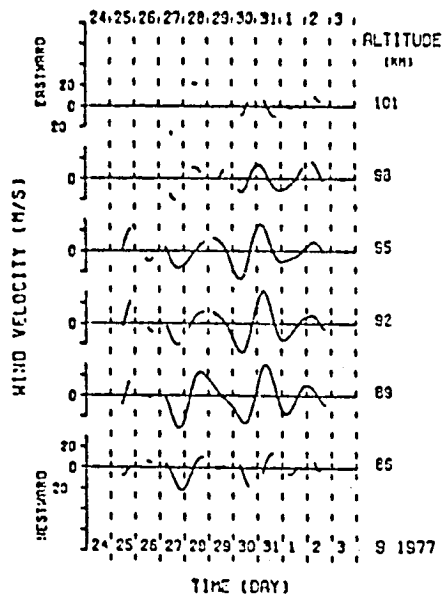


Figure 3.

DIURNAL TIDE  
BORINGUEN -AUG-SEPT 1977

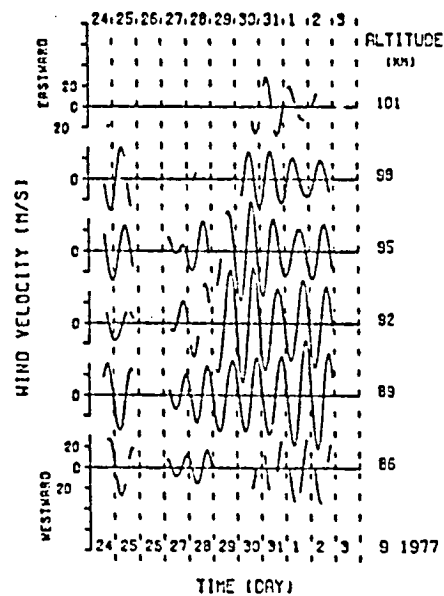


Figure 4.

Figure 5 illustrates the variation with time of the 12-hour zonal component, with an apparent modulation of the 12-hour periodicity at approximately 7 days.

Figure 6 presents the zonal prevailing, 24- and 12-hour component amplitudes for the period March 17-24, 1979. These results, the first produced under Georgia Tech operation of the system, are somewhat controversial, in that the large amplitudes in all three components on March 21 (which accompany a zonal wind reversal from easterly to westerly above 90 km) appear anomalous.

RAMEY AND ATLANTA WINDS: FEBRUARY - JUNE, 1981

Figure 7 details the monthly mean winds determined for the period February through June 1981, the only period for which long term means are available simultaneously from both sites. Some problems were encountered at both sites during the period because of F region backscatter folding back into the meteor region (range ambiguity). This phenomenon is a problem only at times of high sunspot activity, and is not present for most of the sunspot cycle.

While winds are weaker over the "midlatitude" station (Atlanta is 34°N), strong winds and shears in both height and time are characteristic of the equatorial (Ramey, 18°N) winds. However, as has been noted previously in Atlanta data, if one simply characterizes the zonal mean wind in terms of "easterly" or "westerly" circulation, it would appear that Atlanta is on the fringe of the equatorial circulation, since its "spring reversal" appears much later than is normally the case for midlatitude stations.

SEMI-DIURNAL TIDE  
BORINDUEN - AUG-SEPT 1977

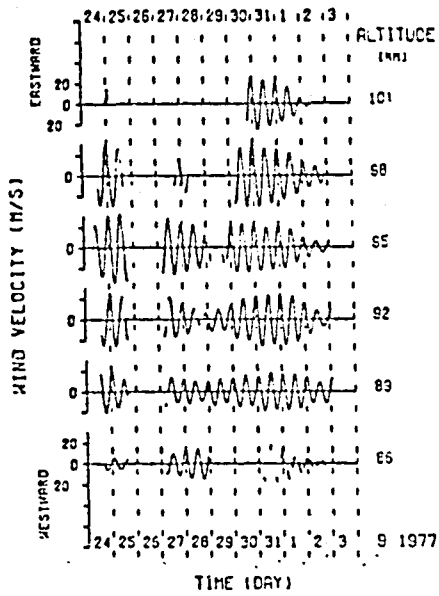
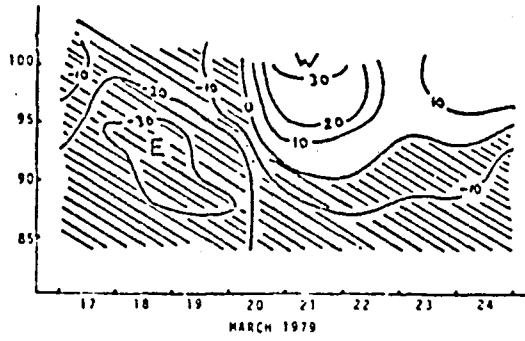
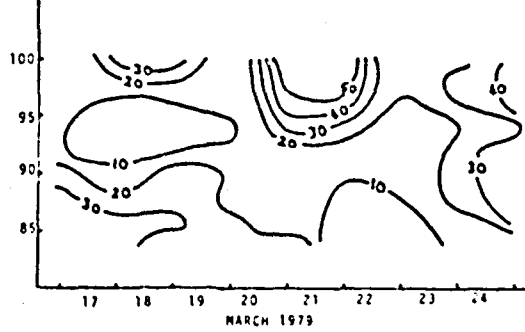


Figure 5.

RAMEY (18 N, 67 W) ZONAL WIND



RAMEY (18 N, 67 W) ZONAL DIURNAL WIND AMPLITUDE



RAMEY (18 N, 67 W) ZONAL SEMIDIURNAL WIND AMPLITUDE

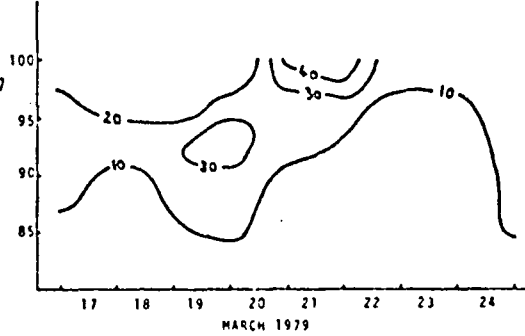


Figure 6.

## ZONAL MEAN WIND - 1981

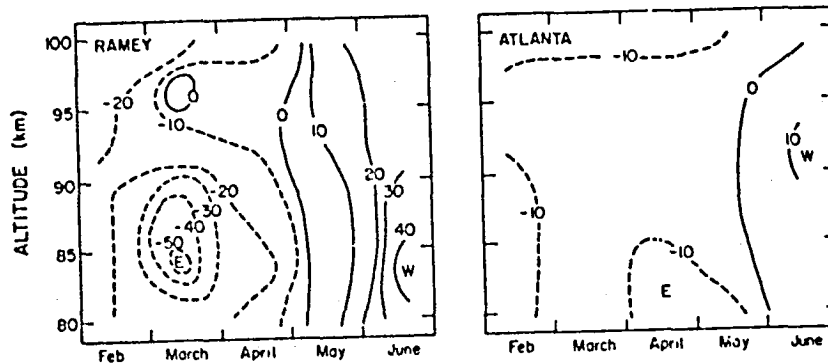


Figure 7.

Figures 8 and 9 of the diurnal and semidiurnal amplitudes, respectively, have not been analyzed in detail but are included to emphasize the much larger tidal amplitudes observed at Ramey compared to Atlanta.

## MESOPAUSE CIRCULATION VARIABILITY

Figure 10, which demonstrates the correlation between wind reversals over Atlanta and midwinter polar stratospheric warmings (discussed in detail in DOLAS and KOPER, 1980) is included to emphasize the need for continuous monitoring of the variation of the wind with height, which is required for a full understanding of the circulation at mesopause altitudes. This region does exhibit characteristics of a synoptic meteorology.

Obviously, the results produced by one or two stations are not of much use in determining the global nature of this synoptic meteorology. In order to further this aim, a cooperative program has been set up under the auspices of the Middle Atmosphere Program to further the cooperation which has been carried out since 1970 in the IAGA Global Radio Meteor Wind Studies Project, and the URSI/IAGA Coordinated Tidal Observations Program, which included incoherent

## DIURNAL AMPLITUDE - 1981

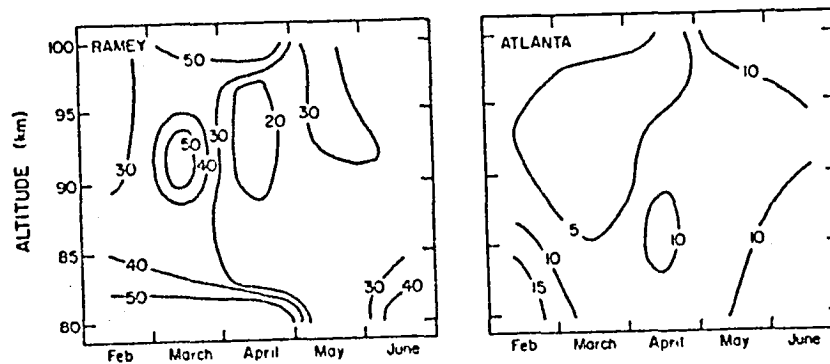


Figure 8.

SEMI-DIURNAL AMPLITUDE - 1981

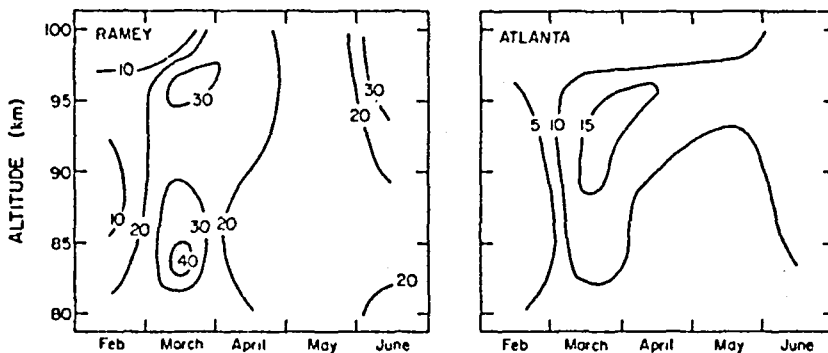


Figure 9.

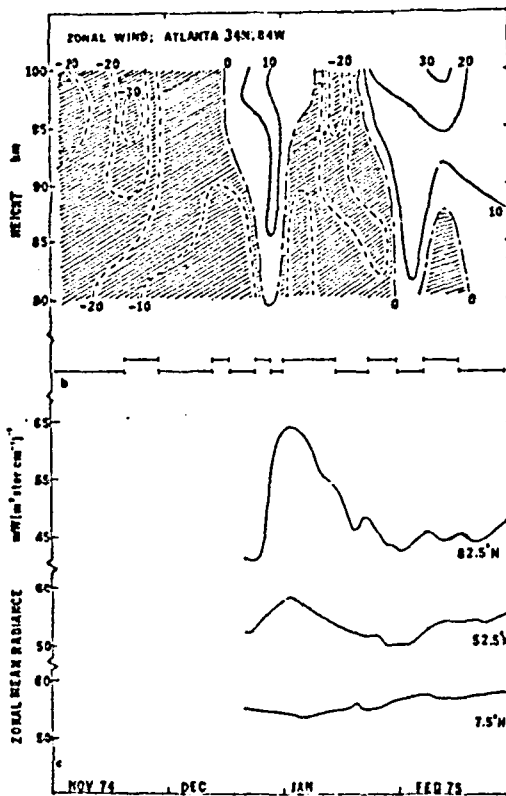


Figure 10.

scatter radar results. This MAP project, GLOEMET (Global Meteor Observations System; for details see MAP Handbook No. 7, p. 20), while oriented towards meteor research, is seeking the cooperation of experimenters using many different techniques (partial reflection drifts, mesospheric scatter radars, lidar, rockets, satellites, etc.) to contribute to the atmospheric dynamics portion of the program, since all available data will be needed if a truly global picture of upper mesosphere/lower thermosphere circulation is to be realized.

#### ACKNOWLEDGEMENTS

The research reported here has been supported by the Atmospheric Research Section of the National Science Foundation, which also contributed towards travel funds for the author's attendance at this meeting.

#### REFERENCES

- Ahmed, M. I. and R. G. Roper (1983), The diurnal and semidiurnal oscillations in meteor winds over Atlanta, *J. Atmos. Terr. Phys.*, (in press).
- Alleyne, H., W. Keenlside, G. S. Kent, J. W. MacDougall and A. J. Scholefield (1974), Observations of atmospheric tides over Jamaica using three different techniques, *J. Atmos. Terr. Phys.*, 36, 171.
- Babadzhanov, P. B., B. V. Kalchenko and V. V. Fedynsky (1970), Meteor winds over the equator, *Izv. Akad. Nauk SSSR.*, 9, 33.
- Dolas, P. M. and R. G. Roper (1981), Prevailing wind in the meteor zone (80-100 km) over Atlanta and its association with midwinter stratospheric warming, *J. Atmos. Sci.*, 38, 182-188.
- Glass, M., R. Bernard, J.-L. Fellous and M. Massebeuf (1978), The French meteor radar facility, *J. Atmos. Terr. Phys.*, 40, 923-931.
- Matthews, J. D., M. P. Sulzer, C. A. Tepley, R. Bernard, J.-L. Fellous, M. Glass, M. Massebeuf, S. Ganguly, R. Harper, R. A. Behnke and J. C. G. Walker (1981), A comparison between Thomson scatter and meteor radar wind measurements in the 65-105 km altitude region at Arecibo, Planet, Space Sci., 29, 341-348.
- Matthews, J. D. (1976), Measurements of the diurnal tides in the 80 to 100 km altitude range at Arecibo, *J. Geophys. Res.*, 83, 505.
- Roper, R. G. (1975), The measurement of meteor winds over Atlanta, *Radio Sci.*, 10, 363-369.
- Roper, R. G. (1978a), Winds from the Atlanta (34°N, 84°W) radio meteor facility, *J. Atmos. Terr. Phys.*, 40, 891-893.
- Roper, R. G. (1978b), Radio meteor winds over Atlanta (34°N, 84°W) August 1974 - December 1977, Final Report on Contract E-16-668, NSF Grant No. ATM75-14414, July.
- Salby, M. L. and R. G. Roper (1980), Long period oscillations in the meteor region, *J. Atmos. Sci.*, 37, 237-244.
- Scholefield, A. J. and H. Alleyne (1975), Low latitude meteor wind observations, *J. Atmos. Terr. Phys.*, 37, 273.

N85

20475

UNCLAS

D25  
N85-20475BASIC FEATURES OF GLOBAL CIRCULATION IN THE  
MESOPAUSE-LOWER THERMOSPHERE REGION

Yu. I. Portnyagin

Institute of Experimental Meteorology  
USSR State Committee of Hydrometeorology  
and Control of Natural Environment  
Obninsk, USSR

Circulation models, which cover heights up to the turbopause, i.e., practically up to the natural upper border of the homosphere, play an important part in the studies of general features of global atmospheric circulation. At present there are a number of circulation models for the height range up to 100-120 km. For the heights above the upper limit of standard radio sounding (~30 km) these models are based on rocket sounding data, with non-systematized data of meteor radar observations and ionospheric drift measurements used only in particular cases.

Meanwhile as continuous 24-hour meteor radar wind measurements convincingly indicate the resultant wind at 70-110 km (mesopause-lower thermosphere region) is a superposition of daily prevailing wind and of the winds originating from diurnal and semidiurnal variations of atmospheric parameters. And significant day-to-day and seasonal variations are observed in amplitudes and phases of diurnal and semidiurnal wind oscillations.

Thus average velocities of prevailing wind at 70-110 km can be obtained reliably enough only on the base of the methods which allow for daily and shorter period observations of resultant wind velocities with further selection of diurnal wind velocity means from the data obtained. These are first of all the radar meteor trail technique (D2 technique, according to URSI classification) and some versions of ionospheric methods of spaced receiver drift measurements (D1 technique), such as partial reflection method, drift measurements in the long-wave range, etc. But earlier circulation models for the heights of mesopause-lower thermosphere developed from D1 and D2 measurements were based on scanty data.

By now D1 and D2 techniques have been used and are being used for observations at a lot of stations located in the high, middle and low latitudes of both hemispheres. The systematical wind velocity measurements with these techniques make it possible to specify and to refine earlier mesopause-lower thermosphere circulation models. With this in view we have made an effort to obtain global long-term average height-latitude sections of the wind field at 70-110 km using the analysis of long-period D1 and D2 observations. Data from 26 meteor radar and 6 ionospheric stations were taken for analysis.

Observational periods at different stations do not always completely coincide and in several cases they even do not overlap. Thus the wind field model based on these data can be considered as a long-term average (climatic) model with the accuracy characterized to a first approximation by monthly mean velocity variance  $D$  resulting from year-to-year variations of the velocities. The estimates from long-period measurements at Heis Island, Molodezhnaya Station, in Kuhlungsborn, Obninsk, Jodrell Bank and Adelaide have shown, that on the average the value  $\sigma_1 = \sqrt{D_1}$  can be taken as  $\sigma_1 = 7$  m/s (for the Northern Hemisphere  $\sigma_1 = 5$  m/s, for the Southern  $\sigma_1 = 9$  m/s).

An important point in developing the model was the assumption of zonal mean approximation being acceptable for a climatic description of the wind regime in mesopause-lower thermosphere. The assumption was established on the comparison

of seasonal variation of zonal and meridional wind velocities at observational stations closely spaced along latitudes but significantly different with respect to longitude.

Figure 1 a,b,c,d shows monthly mean velocities of zonal ( $v$ ) and meridional ( $u$ ) winds for the stations located in two latitudinal belts of the Northern Hemisphere:  $52^{\circ}$ - $57^{\circ}$ N and  $45^{\circ}$ - $50^{\circ}$ N. ( $52^{\circ}$ - $57^{\circ}$ N latitude belt includes the stations: Jodrell Bank ( $2^{\circ}$ E), Kuhlungsborn-Collm ( $12^{\circ}$ E), Obninsk ( $38^{\circ}$ E), Kazan ( $49^{\circ}$ E), Tomsk ( $85^{\circ}$ E), Badary ( $102^{\circ}$ E) and Saskatoon ( $107^{\circ}$ W);  $45^{\circ}$ - $50^{\circ}$ N: Budrio ( $12^{\circ}$ E), Kiev ( $31^{\circ}$ E), Kharkov ( $30^{\circ}$ E), Volgograd ( $44^{\circ}$ E) and Khabarovsk ( $135^{\circ}$ E)). It is easily seen, that despite the significant differences in longitude the features of seasonal variations of wind parameters remain essentially similar at all the stations. The respective variance of values over longitude  $D_{\lambda}$  is characterized by  $\sigma_{\lambda}^{E,W} = 7$  m/s,  $\sigma_{\lambda}^{NS} = 5$  m/s, which is comparable with  $\sigma_i$ .

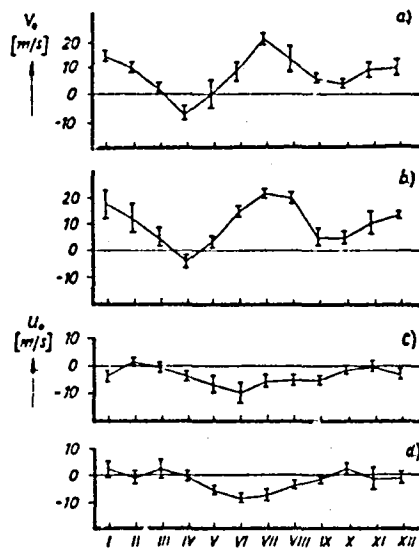


Figure 1. Seasonal variation of zonal ( $u_0$ ) and meridional ( $v_0$ ) components of the prevailing wind velocity at 95 km height, averaged over various longitudes for the two latitudinal zones:  $52^{\circ}$ - $57^{\circ}$ N (a,c),  $45^{\circ}$ - $50^{\circ}$ N (b,d).

It is necessary to point out that at a number of stations distributed well enough over the latitudes the measurements were taken with equipment enabling the measurement of altitude wind profiles in the height range of 70-110 km. (Kiruna,  $68^{\circ}$ N; Saskatoon,  $2^{\circ}$ N; Garchy,  $48^{\circ}$ N; Atlanta,  $35^{\circ}$ N; Punta Borinquen,  $18^{\circ}$ N; Townsville,  $18^{\circ}$ S; Adelaide,  $35^{\circ}$ S; Birdlings Flat,  $44^{\circ}$ S). As for the rest of the stations, measurements refer to the average meteor zone  $\sim 95$  km and make it possible to specify the character of latitudinal dependence of wind velocities in the cross sections obtained.

Besides, for the 70-80 km height range, rocket measurements were also used. Comparison has shown the monthly mean wind velocities from rocket data to exceed

(by 15-50%) those from D1 and D2 measurements. Basic regularities of seasonal variation however show a good qualitative agreement for all the three methods.

Height-latitude sections of zonal wind field were constructed as follows. For each month of the year wind velocity means obtained from experimental evidence were plotted on a two-dimensional coordinate grid over the range of  $90^{\circ}\text{N} < \phi < 90^{\circ}\text{S}$ ,  $70 \text{ km} < h < 110 \text{ km}$ . Isotachs were drawn on the obtained height-latitude sections taking account of the data plotted, and in some cases the data were smoothed within the range of acceptable errors in mean values. The experimental evidence available showed quite good agreement and on the whole enabled the basic circulation systems to be identified and their seasonal transformations to be traced.

Monthly mean wind velocities at height-latitude grids with a height step  $\Delta h = 2 \text{ km}$  and a latitude step  $\Delta \phi = 5^{\circ}$  were taken from the obtained monthly mean height-latitude sections by means of interpolation. The latitude dependence at each height level was approximated by a Fourier series up to the fourth harmonic, used to estimate latitudinally smoothed values for  $V(\phi, z)$ . Height-latitude sections of the zonal wind field constructed in this manner are presented in Figures 2-5. They show that the spatial structure of the zonal wind field has a number of regularities and undergoes appreciable seasonal variations. These regularities are briefly discussed below for the main seasons of the year.

#### December, January, February (Figure 2)

Zonal component sections of the prevailing wind for winter in the Northern Hemisphere and summer in the Southern Hemisphere exhibit five basic dynamical structures.

- (1) A region of westerlies in the Northern Hemisphere, dynamically connected with the strato-mesospheric winter low. An additional circulation cell develops in the upper part of this dynamic structure.
- (2) A region of high-latitude easterly circulation in the lower thermosphere of the Northern Hemisphere.
- (3) A low-latitude region of easterly circulation.
- (4) A region of easterlies in the Southern Hemisphere.
- (5) A westerly circulation cell in the Southern Hemisphere.

#### March, April, May (Figure 3)

These are the months of the seasonal reconstruction of the circulation in the meteor zone. They are characterized by the following dynamic structures:

- (1) A region of easterly circulation in the Northern Hemisphere.
- (2) A region of westerly circulation in the Northern Hemisphere.
- (3) A low-latitude region of easterlies.
- (4) A region of westerlies in the Southern Hemisphere.

#### June, July, August (Figure 4)

The height-latitude structure of the zonal wind field in these months is to some extent similar to that in December-February in the hemispheres with respective seasons. However, the circulation patterns in the summer (Northern) and winter (Southern) hemispheres possess some peculiarities which distinguish them from similar seasonal structures of the circulation in December-February. The following dynamic structures are clearly seen.

- (1) A region of easterly circulation in the Northern Hemisphere.
- (2) A region of westerly circulation in the lower thermosphere of the Northern Hemisphere.

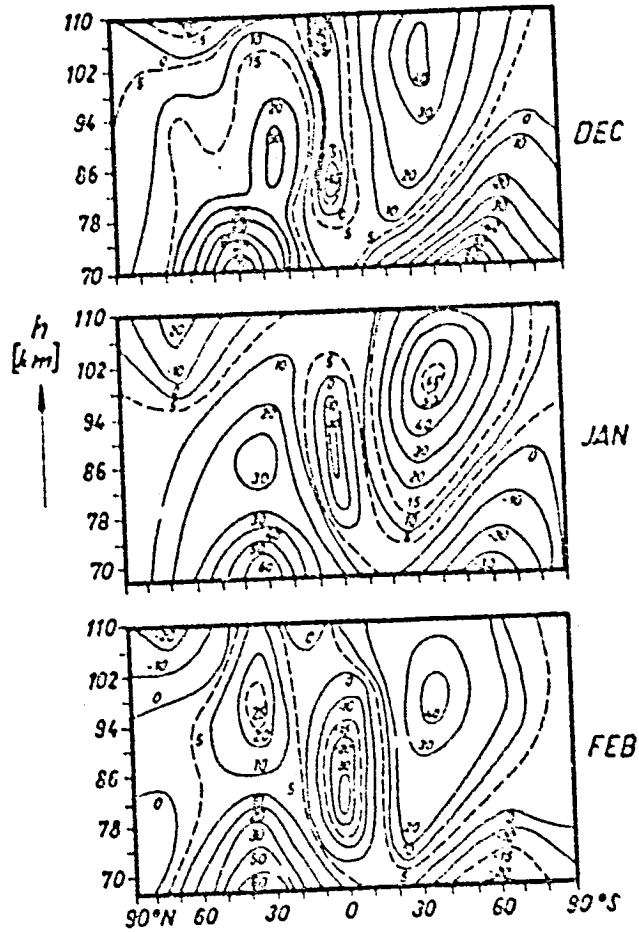


Figure 2: Height-latitude structure of the zonal wind field (m/s) for December-February (a-December, b-January, c-February; positive values are westerly wind).

- (3) A large region of westerlies in the Southern Hemisphere.
- (4) A region of easterly circulation in the lower thermosphere of the Southern Hemisphere which couples to the zone of low-latitude easterlies. Such field structure of easterlies in the winter Southern Hemisphere differs from the structure of easterlies in the winter Northern Hemisphere described above.

September, October, November (Figure 5)

November can be ranked among the months of steady circulation. In September/October, several transformations of the circulation systems take place.

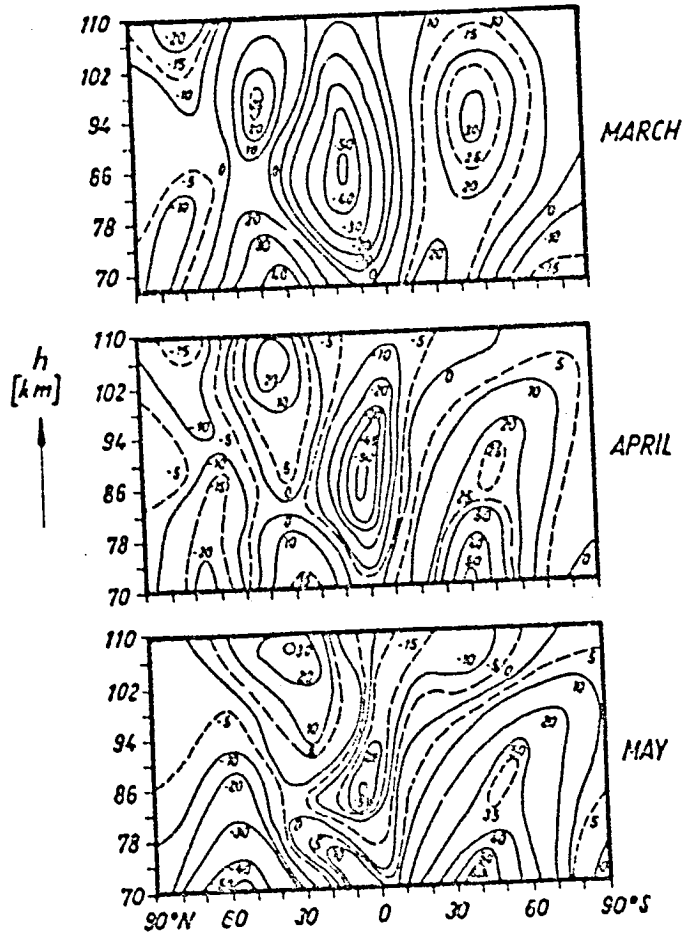


Figure 3. Height-latitude structure of the zonal wind field (m/s) for March-May (a-March, b-April, c-May).

The cross sections considered above reveal that despite some analogy in seasonal variations of basic dynamic structures in the Northern and Southern Hemispheres a complete mirror symmetry, suggested earlier, is not observed. The circulation systems of the Southern Hemisphere are distinguished from the systems of the Northern Hemisphere by a number of features. The most significant peculiarity of the circulation in the Southern Hemisphere is permanently larger values of wind velocities as compared to those for respective seasons of the Northern Hemisphere.

The height-latitude section, shown in Figures 2-5 represent an empirical zonal mean model for the zonal wind field in the meteor zone of the atmosphere, which describes climatic regime of the zonal wind at 70-110 km heights.

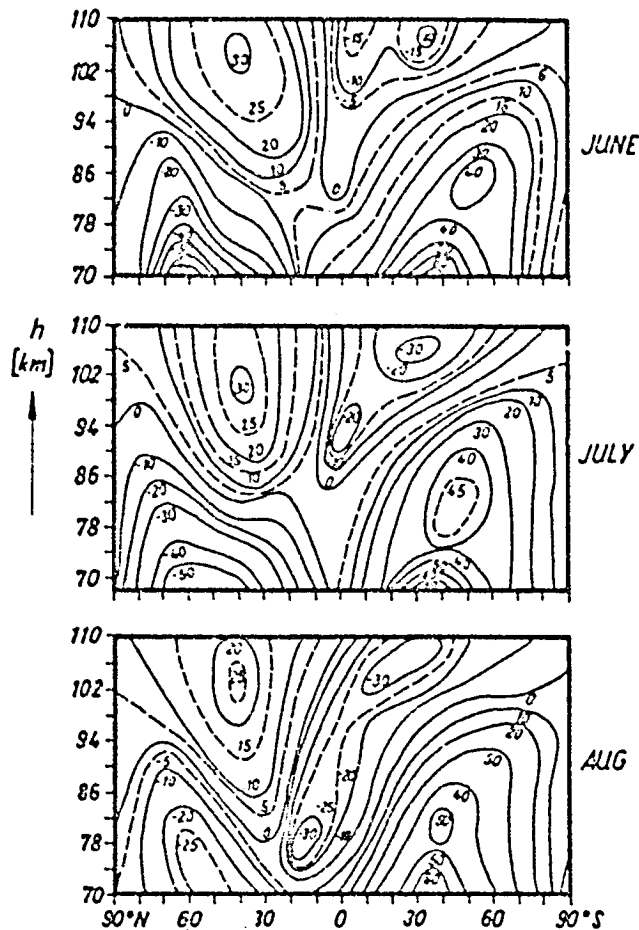


Figure 4. Height-latitude structure of the zonal wind field (m/s) for June-August (a-June, b-July, c-August).

In contrast to the data on zonal wind, statistically reliable data on the latitudinal structure of the ageostrophic meridional wind are mostly available for 95 km height. We have made an effort to parameterize Reynolds viscous stresses in the equation of motion for the meridional wind using the data on meridional wind velocities at 95 km and the height-latitude sections of mean zonal wind. The main contribution into the divergence of Reynolds stresses is proved to be given by the terms associated with the vertical eddy transport of the momentum. The resulting expression for meridional wind  $u_0$  is as follows:

$$u_0 = K_{\text{eff}} \left( \frac{1}{H} \frac{\partial v}{\partial z} - \frac{\partial^2 v}{\partial z^2} \right) \cdot (2\epsilon \cos \theta)^{-1} \quad (1)$$

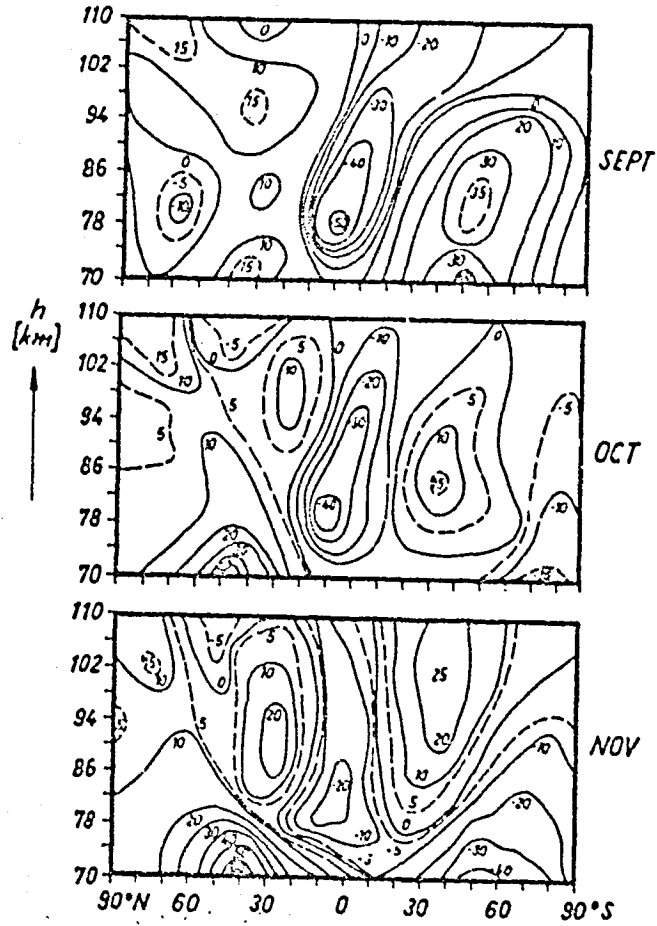


Figure 5. Height-latitude structure of the zonal wind field (m/s) for September-November (a-September, b-October, c-November).

where  $K_{eff}$  is a value with the dimension of the diffusion coefficient,  $v_0$  is the zonal wind velocity,  $Z$  is the height measure in the log-isobaric system of coordinates,  $H$  is the scale height,  $\Omega$  is the angular velocity of the Earth's rotation, and  $\theta$  is the colatitude. Using equation (1) for parameterization is justified by the fact that for seasons with steady circulation (winter, summer) at 95 km height there is a significant correlation between experimental values

of  $u_0$  and the value of  $\Gamma = \left( \frac{1}{H} \frac{\partial v_0}{\partial Z} - \frac{\partial^2 v_0}{\partial Z^2} \right)$ , which was obtained from height-

latitude sections of the zonal wind field. An important point here is that the changes in the sign of  $u_0$  with latitude are followed by similar changes in the sign of the parameter  $\Gamma$  and as a result  $K_{eff}$  is essentially positive at all the latitudes (except at the latitudes near the equator, where parameterization (1) is not valid). At about 95 km, according to our estimates  $K_{eff} \approx 10^3$

$m^2/s$ , which is in agreement with other data at the heights above 100 km  $K_{eff}$  reaches the value of eddy diffusion coefficient at the level of the turbopause. The dependence of  $K_{eff}$  on height, normalized to  $K_{eff}$  at 95 km height, is considered here to be the same for all latitudes. Taking into account the values of  $K_{eff}$  obtained for various heights and latitudes from the data on the vertical and latitudinal structure of the zonal mean wind field applied to equation (2) we calculated the values of ageostrophic meridional wind velocities in the zonal mean approximation.

Figure 6 presents height-latitude sections of the ageostrophic meridional wind field for January (a) and July (b), obtained by the method discussed above. It clearly shows that on the average at all heights of the Northern meteor zone the wind is southerly in January and northerly in July, which agrees with the average movement of air masses from the summer hemisphere to the winter one.

In January, a region of northern winds is distinctly marked in the equatorial latitudes of the lower thermosphere. The picture is different, however, in July. While the regions of southern winds are well pronounced in the low and high latitudes, another region of southern winds is observed in the middle and subtropical latitudes of the Southern Hemisphere. On the whole,

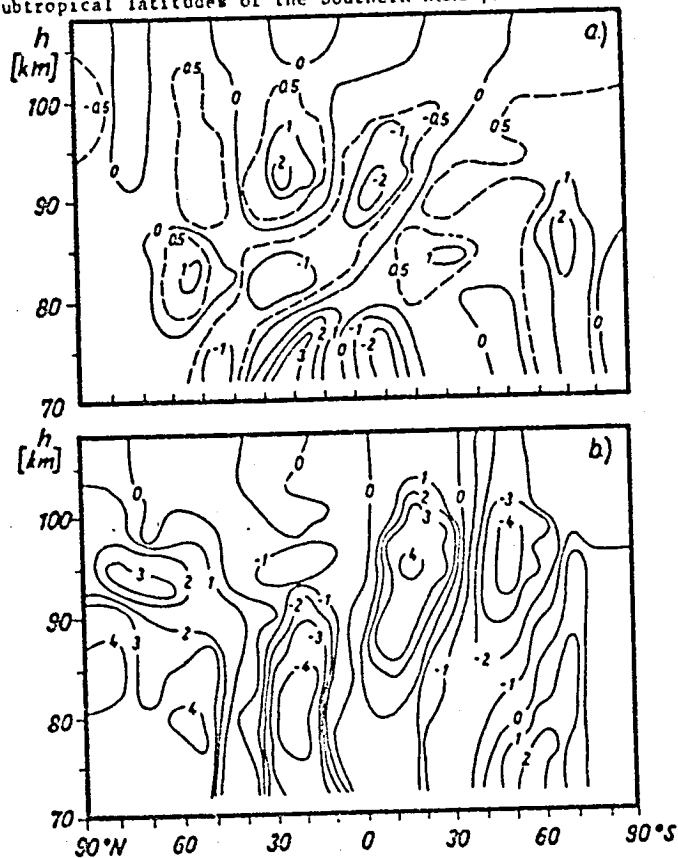


Figure 6. Height-latitude structure of the meridional wind field for January (a) and July (b).

however, the height-latitude sections of the meridional wind field given here should be considered as estimates which mostly give information about the sign of the meridional wind and to a lesser degree characterize the absolute velocities at the heights significantly different from 95 km.

Meridional wind calculations were used to obtain respective values of vertical wind  $w_0$  by means of integrating the continuity equation.

Calculation results of field  $w_0$  are shown in Figure 7 (a,b). They show that at 75-105 km heights there are rather large-scale structures of upward and downward flows, which can significantly affect many physical processes in this height interval and in particular the processes important for understanding D and E region aeronomy and formation of the mesopause thermal structure. The zones of downward and upward winds alternating along the latitude indicate there are global circulation cells in the meteor zone of the atmosphere. The most significant are direct circulation cells connected with the ascent of air masses in low latitudes and descent in middle latitudes. Indirect cells are likely to exist along with the direct ones in the middle latitudes. Despite a rather complicated structure of the vertical winds in the meteor zone of the atmosphere their regularity is clear.

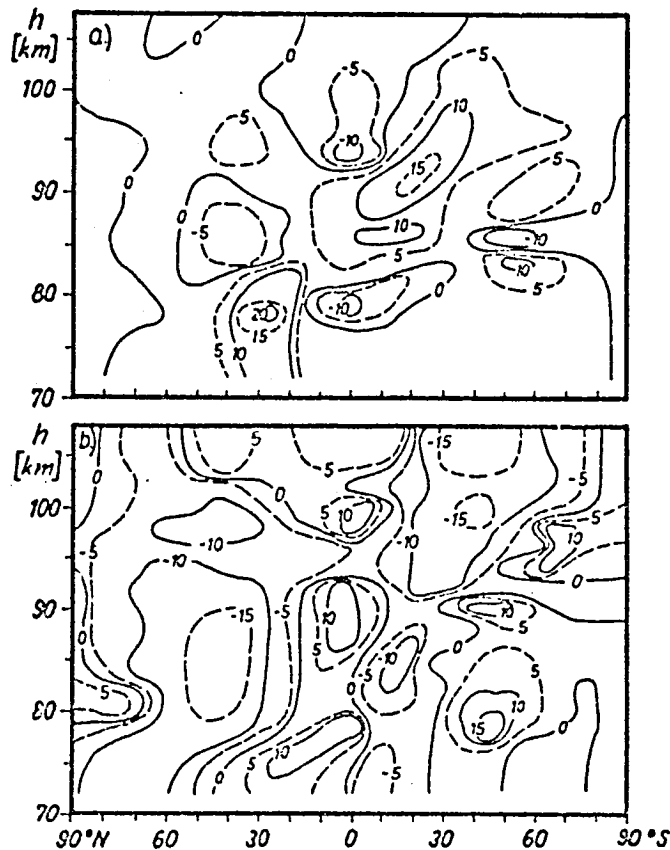


Figure 7. Height-latitude structure of the vertical wind field for January (a) and July (b).

N85

20476

UNCLAS

N85-20476

26

143

WINDS AND WAVES (4 MIN - 11 YRS) IN THE UPPER MIDDLE ATMOSPHERE  
(60-110 KM) AT SASKATOON, CANADA (52°N, 107°W):  
M.F. RADAR (2.2 MHz) SOUNDINGS 1973-1983

A. H. Manson, C. E. Meek and J. B. Gregory

Institute of Space and Atmospheric Studies  
University of Saskatchewan  
Saskatoon, Sask., S7N 0W0 Canada

INTRODUCTION

The Saskatoon MF Radar has been operating since 1968, but in its present continuous-sounding, real-time processing mode since June 1978: 2.2 MHz; 50 kw, 20  $\mu$ s pulse; 7.5 Hz pulse rate; 1 profile every 5 min; 32 heights, 49, 52 ---- 142 km. The real-time "full correlation analysis" is made possible by converting the 8-bit amplitudes to binary (0,1) with respect to the mean in 30 sec blocks: partial correlations formed by the AND instruction are accumulated continuously for the whole record; cross-correlograms and autocorrelations result. In a second microcomputer the "proper" peaks are selected and their amplitudes and positions are found; these data plus the mean autocorrelogram are then used to calculate the velocities and pattern parameters -- the method is efficient and of high quality (MEEK and SOIFERMAN, 1979; MEEK, 1980; MEEK et al., 1979, GREGORY et al., 1979).

Most of the atmospheric data shown here were obtained since 1978. Prior to that time the limitations of computing systems usually allowed only noon data (1 hr) each day -- our interest has always been on the full climatology of the region. However now that we operate continuously each day, waves with periods from 10 min to 5 years are available for study: gravity waves (GW), tides, planetary waves (PW) and circulation effects. We will show examples of all of these.

MEAN WINDS AND LONG PERIOD ( $\lambda$ 10d) OSCILLATIONS

The basis for most analyses are 1h mean winds at 3 km intervals (Figure 1): such plots reveal the mean wind and its variations, the 24- 12-h tides, and G.W. fluctuations. The basic analysis is to fit a mean, and 24- 12-h harmonics to each 24-h of data; and then obtain means for monthly (30-d) and (sometimes) 10-d intervals.

Zonal and meridional cross-sections (10-d averages) are available for all years, but we show 1980 (Figure 2). Comparisons with CIRA (1972) demonstrate the need to update that model: e.g. October, May, June (EW) are usually stronger than CIRA; December weaker. Magnitudes may differ by factors of 2-3 within the vortex (GREGORY et al., 1981; MANSON et al., 1981a). Important differences from an expanded data set (GROVES, 1969) also exist: his reversed zonal flow above 90 km appears too strong, probably due to tidal contamination. More seriously the meridional flow at Saskatoon is inconsistent with Groves and also simple circulation models that require poleward/equatorward flow above 80 km in winter/summer to be consistent with the thermal winds. The role of gravity waves in depositing momentum and balancing the Coriolis torque is being actively studied at Saskatoon -- winter is a puzzle because of the equatorward flow above 85 km.

The 12-, 6-, 3-mth oscillations (Figure 3) are consistent with the zonal cross-sections, and are stable from year to year (MANSON et al., 1981b). Our results (12-6-mth) are consistent with CIRA below 100 km, but differences above are probably due to tidal contamination in CIRA. By using good quality noon data the strengths of the summer and winter mesospheric vortices have been

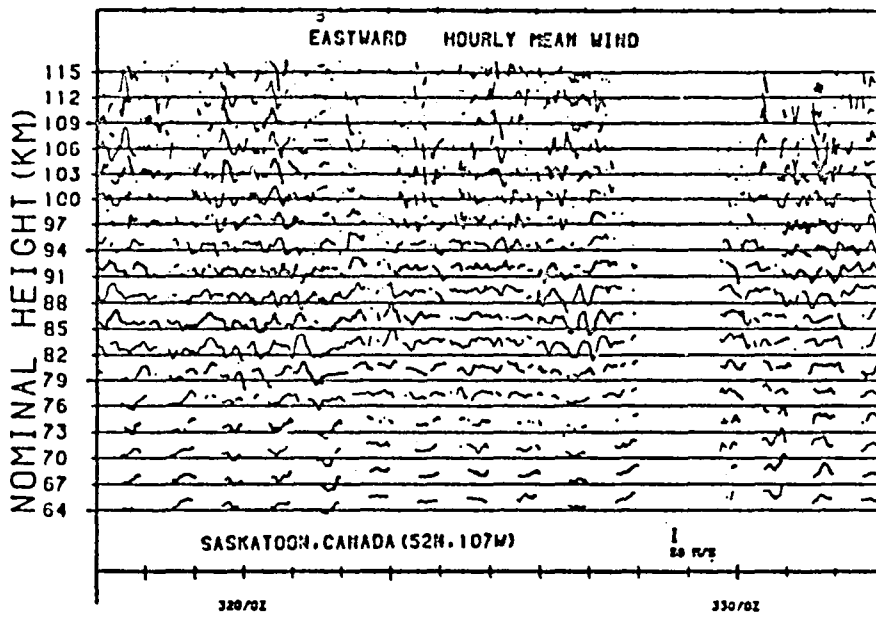


Figure 1. Winds during the November 1981 ICMUA Tidal campaign (-5 km).

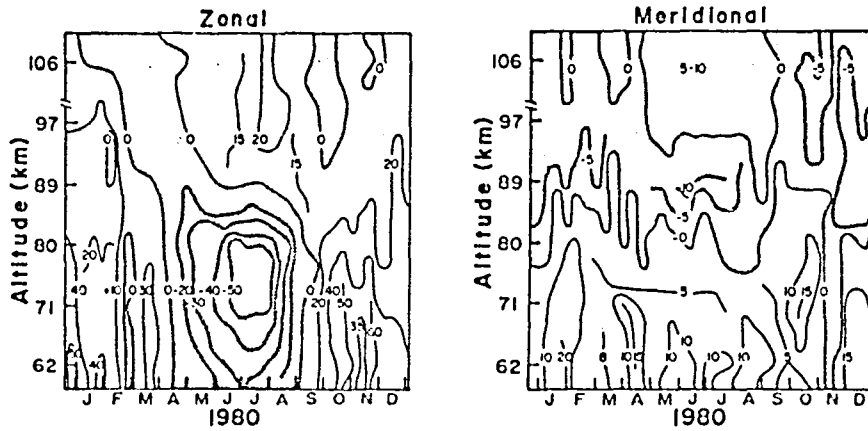


Figure 2. Zonal and meridional winds (10-d averages used): 1980.

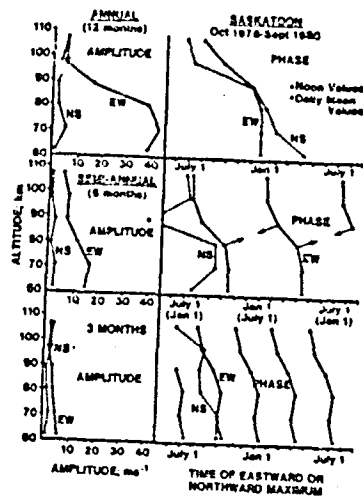


Figure 3. Long period oscillations.

studied from 1974 -- the vortices have strengthened by factors of  $>2$ , largest in winter, as the sunspot number has increased (GREGORY et al., 1981). This effect is believed to be independent of, or not caused by, tidal fluctuations.

Finally fluctuations of the mean winds and tides occur during STRATWARMS (MANSON et al., 1981a,c; SMITH et al., 1982). There are frequently oscillations with periods of several days up to  $\sim 100$  km, as well as strong reversals of the zonal flow below  $\sim 80$  km. We are involved with DYNAMICS/SWAMP of MAP.

Comparisons of hourly and monthly mean winds from the Radar and from rocket data (e.g. GREGORY et al., 1981) obtained from Primrose Lake (340 km NW), show excellent agreement. These data, and the nature of the wind field discussed here, demonstrate the quality of the winds data from the M.F. radar.

#### SPECTRAL ANALYSIS (10d - 6h)

Various forms of analysis have been applied to the continuous hourly data, divided into  $\sim 30$ d (monthly) sets. The result of a swept-frequency covariance calculation is shown in Figure 4, for a typical winter month (February 1981). The 12-h tide is dominant, and 24-, 8-, 6-h tidal oscillations grow with altitude. There are strong oscillations of 16d period also, possibly associated with the STRATWARM of 1981. Seasonal variations are shown in the Fourier analysis for 89 km (Figure 5): the 24-/12-tide becomes larger/smaller in summer months; and 2.1, 5-d oscillations are evident especially, but not exclusively, in summer. These oscillations and others with periods of 1.25 - 16d are frequently observed; these are consistent with the planetary normal modes investigated by SALBY (1981). Careful study of the spectra also show the presence of 16h ( $16.2 \pm .7$ ) and 10h ( $9.7 \pm .4$ ) oscillations which may be due to the modulation of the 12-h tide by the 2.1d wave (MANSON et al., 1982).

The P.W. oscillations are being compared with meteor-radar winds from Monpazier (France) during 1979/1980, and there is excellent agreement between the occurrence of such oscillations, and also their amplitudes and vertical wavelengths (J. L. Fellous - private communication, to be published).



## TIDES (12- 24-h)

The monthly semi-diurnal tides evidence a clear seasonal variation in their characteristics (MANSON et al., 1981a,c). Figure 6 shows the so-called spring-equinoctial months of March, April, May. March is typical of a winter month, with short vertical wavelengths and large amplitudes (Nov-March are winter-like). May is summer-like in phase, and its wavelength is usually intermediate between winter (43:6 km) and summer (180:90 km) (MANSON et al., 1982; MANSON et al., 1983). The transitions from winter to summer-like states (June-August) are very regular and rapid being centered on March 30 and November 1-10 and requiring only 15d. A summary of these features is shown in Figure 7. Sophisticated non-classical theoretical models like that of WALTERSCHEID and DEVORE (1981) and FORBES (1982b) produce some of these features, e.g., longer wavelengths in summer (2,2 mode dominant) and shorter in winter ((2,3)-(2,5) modes effects); but their phases and the magnitudes, rapidity and regularity of the seasonal changes are not explained. Comparisons with French (J. L. Fellous) and New Zealand (M. J. Smith, G. J. Fraser) data show basically similar behaviour to the Saskatoon 12-h tide. The daily tidal fluctuations are discussed elsewhere (MANSON et al., 1982): possible causes are non-migrating tides, local tidal forcing and gravity-wave coupling.

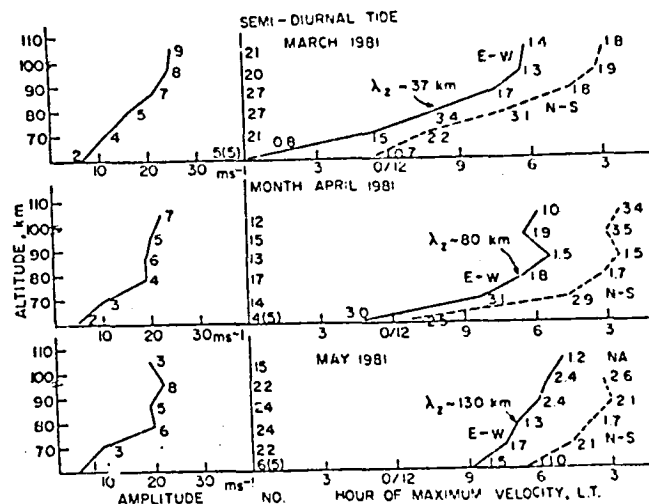


Figure 6. Semi-diurnal tides (amplitudes are arithmetic means; s.d. shown).

The 24-h tide is more irregular on a daily or monthly basis. Theory (e.g. FORBES 1982a), suggests that modes such as the evanescent  $S_{-1}$ ,  $S_{-2}$  and propagating  $S_1$  should be present. There is actually a seasonal variation, with longer wavelengths in summer months, and a distinct phase variation (Figure 8), which theories have not successfully predicted. The New Zealand data for 1978-1980 (M. J. Smith, G. J. Fraser - private communication, to be published) shows a similar seasonal morphology. I am closely involved in ATMAP (MAP) and the ICMUA Tidal Working Group.

## GRAVITY WAVES (4 min - 6 h)

Ever since the elegant and perceptive paper of C. O. HINES (1960) on

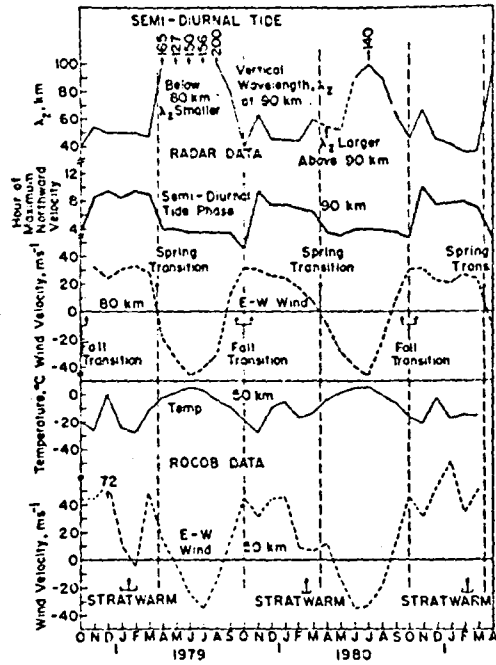


Figure 7. Semi-diurnal tidal variations.

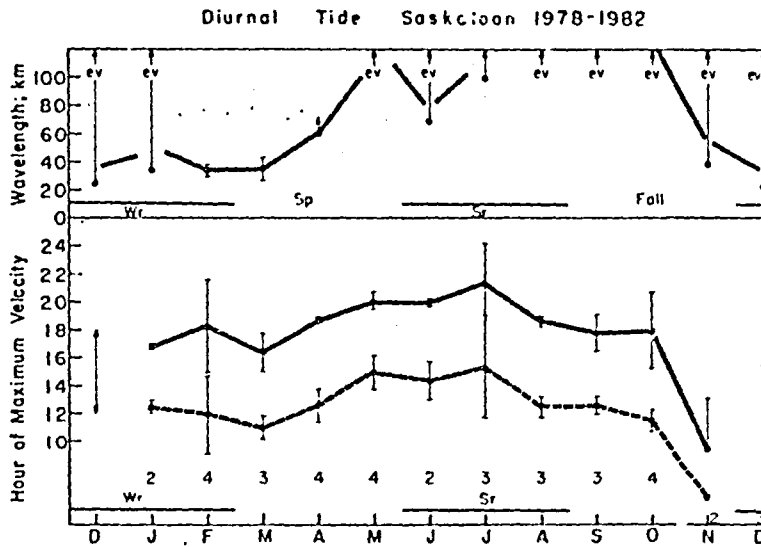


Figure 8. Diurnal tide variations.

gravity waves their presence and importance in the atmosphere has become increasingly obvious. At Saskatoon plots of the 5 min wind vectors reveal fluctuations clearly related to internal gravity waves: the use of 1-h means to filter out the shorter periods is therefore very important.

Special observations were carried out in 1978/1979: six 3h campaigns with 1 min sampling times (FANSO et al., 1981d). These data showed that short period waves ( $5 \text{ min} \leq T \leq 90 \text{ min}$ ) were present in all seasons; the wave oscillations also revealed polarization, consistent with the absorption or reflection of G.V. with phase velocities parallel to the mean flow. We show in Figure 9 (right) profiles of the r.m.s. gravity wave oscillations, the energy scale heights  $h_0$ , and the corresponding energy dissipation ( $\epsilon_0$ )/group velo-

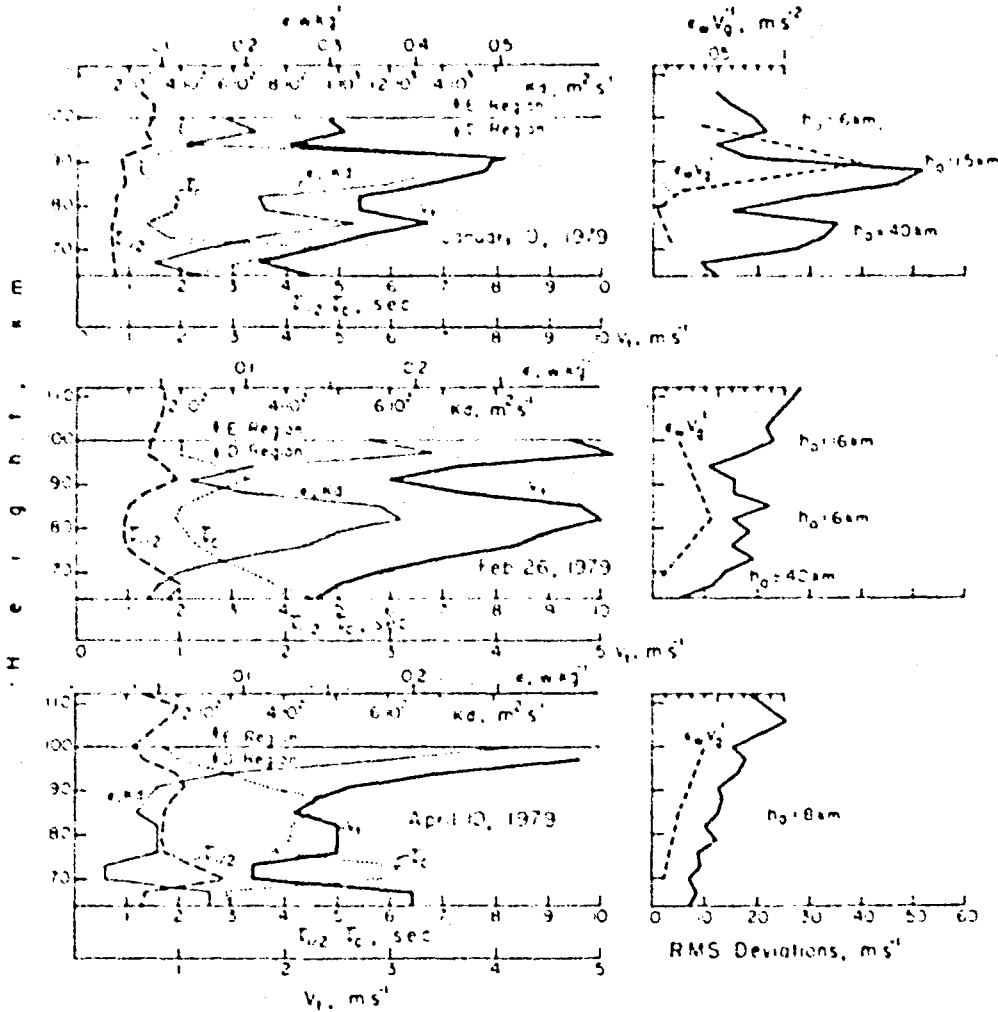


Figure 9. Energy dissipation by turbulence ( $\epsilon_0$ ) and eddy diffusion ( $K_d$ ).

city ( $V_g$ ):  $1 < V_g < 10$  m/s. The profiles of  $\epsilon$  ( $\sim 0.05$ - $0.3$  W/kg) agree well with those derived independently from  $\tau_c$  (fading time seen by a moving observer):  $V_r$  is the s.d. of the random velocity of the scatterers assuming isotropic turbulence; and  $\epsilon$ ,  $K_d$  the energy dissipation by turbulence and eddy diffusion respectively (ZIMMERMAN and MURPHY, 1977). Values of  $K_d$  (200-600  $m^2/s$ ) compare well with other observations.

We have earlier data, which also illustrates interactions between the G.W. and the mean flow. Variations of the heights of maxima for the r.m.s. deviations of the wind correlate very well with heights of reversal of the mean flow, on a monthly basis, 1972-74 (MANSON et al., 1975, 1976). This is consistent with G.W. whose phase velocities are antiparallel to the direction of the main vortex (40-80 km), which reach the reversal height, and then experience critical levels. Large amplitudes and eventual dissipation result, and their momentum is deposited into the flow. The importance of such a process has only recently become evident, as zonal and meridional cross-sections from observation (Figure 2) and circulation models have appeared. As discussed by LINDZEN (1981) and others, some momentum deposition is required to close off the summer and winter vortices and balance the considerable coriolis torque. As noted before, the winter equatorward flow (>80 km) is a problem, as its torque would be additive to any GW momentum deposition!

Finally for several years we have compared the energy densities of FW, Tides and GW (MANSON et al., 1981a,c). Near 80 km all waves are comparable, with GW (<1h) largest; but by 100 km their order (increasing) is FW; tides; GW (>1.5h), GW (<1.5h): values are largest in winter and late summer. Estimating vertical group velocities, the values of  $c$  are  $\sim 10^{-3}$ - $10^{-2}$ ;  $<0.05$ ;  $\sim 0.1$  W/kg, respectively.

Considerable effort is now going in to measuring GW characteristics with a spaced winds system (GRAVNET), to contribute to the MAP GRAYMAP project. This should help our understanding of all scales of motion in the upper middle atmosphere.

#### REFERENCES

- Forbes, J. H. (1982a), *J. Geophys. Res.*, **87**, 5222.  
 Forbes, J. H. (1982b), *J. Geophys. Res.*, **87**, 5241.  
 Gregory, J. B., C. E. Meek, A. H. Manson and D. G. Stephenson (1979), *J. Applied Met.*, **18**, 682.  
 Gregory, J. B., C. E. Meek and A. H. Manson (1981), *Atmosphere-Ocean*, **19**, 24.  
 Gregory, J. B., C. E. Meek and A. H. Manson (1981), Report No. 5, Dynamics Group, I.S.A.S., University of Saskatchewan, Saskatoon, Canada  
 Groves, G. V. (1969), *J. Brit. Interplanet. Soc.*, **22**, 285.  
 Pines, C.O. (1960), *Can. J. Phys.*, **38**, 1441.  
 Lindzen, R. S. (1981), *J. Geophys. Res.*, **86**, 9707.  
 Manson, A. H., J. B. Gregory and D. G. Stephenson (1975), *J. Atmos. Sci.*, **32**, 1682.  
 Manson, A. H., J. B. Gregory and D. G. Stephenson (1976), *J. Atmos. Terr. Phys.*, **38**, 143.  
 Manson, A. H., C. E. Meek and J. B. Gregory (1981a), *J. Geophys. Res.*, **86**, 9615.  
 Manson, A. H., C. E. Meek and J. B. Gregory (1981b), *J. Geomag. Geoelectr.*, **33**, 613.  
 Manson, A. H., J. B. Gregory and C. E. Meek (1981c), *Planet. Space Sci.*, **29**, 615.  
 Manson, A. H., J. B. Gregory and C. E. Meek (1981d), *J. Atmos. Terr. Phys.*, **43**, 35.  
 Manson, A. H., C. E. Meek, J. B. Gregory and E. K. Chakraborty (1982), *Planet. Space Sci.*, **30**, 1283.

- Manson, A. H., C. E. Meek and J. B. Gregory (1981), *J. Atmos. Sci.* (in press).
- Meek, C. F., A. H. Manson and J. B. Gregory (1979), *J. Atmos. Terr. Phys.*, 41, 251.
- Meek, C. E. and J. Soifermon (1979), A real time ionospheric drift system, Dynamics Group Report, ISAS, University of Saskatchewan, Saskatoon, Canada
- Meek, C. F. (1980), *J. Atmos. Terr. Phys.*, 42, 835.
- Salby, M. L. (1981), *J. Atmos. Sci.*, 38, 1827.
- Smith, M. J., J. B. Gregory, A. H. Manson, C. F. Meek, R. Schminder, D. Kurschner, and K. Labitzke (1982), *Space Research*, COSPAR, Ottawa.
- Walterscheid, R. L. and J. G. DeVore (1981), *J. Atmos. Sci.*, 38, 2291.
- Zimmerman, S. P. and E. A. Murphy (1977), *Dynamical and chemical coupling*, D. Reidel, Holland, p. 35.

N85

20477

UNCLAS

## THE DYNAMICS OF IONOSPHERIC D-REGION OVER EAST SIBERIA

E. S. Kazimirovsky

Siberian Institute of Terrestrial Magnetism  
Ionosphere and Radio Propagation  
Irkutsk, USSR

## ABSTRACT

Some main results of experimental investigations of the dynamical regime of the ionospheric D-region over East Siberia are presented. Regular measurements of horizontal ionospheric drifts by the radio method of closely spaced receivers, using a long wavelength transmitter operating at a frequency of 200 kHz, have been carried out near Irkutsk, USSR, since 1975. The seasonal and inter-annual variations of prevailing wind (zonal and meridional), and amplitudes and phases of semi-diurnal tides are investigated. Evidence is presented to show the response of D-region dynamics to stratospheric windings. Planetary and gravity waves are found in the wind field. Comparison with results of analogous measurements in Central Europe (Collm, CDR) reveals a longitudinal effect on the dynamical regime of the mid-latitude lower thermosphere.

The structure, composition and radiative properties of the middle atmosphere cannot be completely understood without full consideration of the role of atmospheric motions on all scales. Relatively little is known about the large-scale circulations in the 60 to 100 km region, their interaction with ionospheric phenomena, and their role in vertical transport of trace species.

There is observational evidence for the broad spectrum of motions in the D-region. These include zonal and meridional mean motions, planetary waves, tides, gravity waves, synoptic scale motions, turbulence. The most important results of measurements (structure and composition) include the finding that the lower ionosphere exhibits not only a solar but also a strong non-solar control which is partly of meteorological nature.

The Middle Atmosphere Program (MAP) involves the investigation of the global wind field in the height range 15-120 km and, in particular, in the upper mesopause region. This region (85-95 km) has until presently been comparatively poorly understood, while its dynamics and structure determine the manner of interaction between lower-atmospheric meteorological phenomena and ionospheric processes. We believe that continuous monitoring of the dynamical regime of the ionospheric D-region is one of the most urgent tasks of the upper atmosphere physics.

There are some significant difficulties with undertaking of such monitoring. Most of the experimental data have been obtained from rocket experiments, meteor trail radars, spaced-receivers (DI) using vertical pulse radar (including partial reflections) and a modification of the DI method which includes the use of broadcasting longwave transmitter signals, reflected by the lower ionosphere during the nighttime. The last method offers some advantages (comparatively simple equipment, no additional radio noise sources) and in principle measures the horizontal drift velocity of ionospheric irregularities. But there are good reasons for interpreting these measurements as an information on the neutral meteorological wind in the reflection region (85-95 km). This method has been calibrated by independent radar meteor and rocket wind measurements and its physical efficiency is proven.

The available regular experimental information about the midlatitude ionospheric wind has until recently been confined solely to the American (GREGORY

and MANSON, 1975) and European (PORTNYAGIN and SPRENGER, 1978) continents. There were no data on the dynamical regime of the lower thermosphere for the Asian continent. For the investigation of the general atmosphere circulation at ionospheric heights and of local behavior of the dynamical regime over East Siberia, regular wind measurements have been made by the D1 method (200 kHz) near Irkutsk (USSR) since 1975. The method we apply yields the wind velocity averaged over 30 minutes. The volume of data ( $\sim 13 \times 10^3$  half-hourly values) permits to assess with great confidence the average characteristics of prevailing winds, of amplitudes and phases of the semidiurnal tide, and the spectrum of planetary and internal gravity waves.

Observations are possible only at night (the data interval, depending on season, is 8-16 hours long). The instrumentation and processing techniques have been described by KAZIMIROVSKY and KOKOUROV (1979).

It is evident that the wind velocity modulus in the region under investigation is quite stable. Most of the values are within the range of 20-60 m/s so that a wind velocity of 40 m/s can be considered typical for this region. It should be noted that this value is in good agreement with wind measurements at similar heights made in Canada (GREGORY and MANSON, 1975) and Australia (STUBBS and VINCENT, 1973).

Both during summer and winter, the eastward wind prevails, but during equinoxes the westward wind. The seasonal variation of the velocity is not very large, maximum values of the zonal velocity being observed during solstices. The spring reversal of circulation is as a rule longer than the autumn reversal (KAZIMIROVSKY and KOKOUROV, 1979; KAZIMIROVSKY et al., 1979; KAZIMIROVSKY, 1981).

These winds exhibit both seasonal and interannual variability. Interannual variability is most pronounced during equinox periods and is associated with the circulation reversal in the upper mesospheric region. The winter regime (November-December) is most stable, although some interannual variability in winter is also indicated. These variations, we believe, should be interpreted as a consequence of the effect of stratospheric warmings (the number and intensity of which are different for the same months of different years) and as a possible effect of variations of solar and geomagnetic activity.

In fact the dependence on solar cycle of both prevailing and tidal wind in the height region between 90 and 100 km during winter, as found at first by SPRENGER and SCHMINDER (1969) from ionospheric drift measurements in the LF range, has been confirmed by PORTNYAGIN et al. (1977) by similar results from radar meteor wind measurements. GREGORY et al. (1980) has revealed a complex pattern of trends in zonal and meridional flow. The 11-year cycle response of seasonal zonal flow was shown to vary with altitude. Speeds increase from solar minimum to maximum by factors of 2-4. Response in the upper mesosphere and lower thermosphere was present in summer as well as winter.

We have found also from our drift measurements that zonal prevailing wind increased from 1975 to 1981, but not so fast as in Canada and Europe. This may be connected with the lower geomagnetic latitude of our observatories.

In addition we found a strong coupling between the dynamical regime of the region under investigation and stratospheric temperature. We can track stratospheric warming effects upon the ionospheric dynamics up to E-region winds (KAZIMIROVSKY et al., 1982).

We have investigated stratosphere-ionosphere coupling both for the winter solstice and for the spring circulation reversal. During the periods of sudden stratospheric warmings there are effects in the ionospheric D-region dynamics

1-2 days after the time of maximum temperature at the 30-mb level. The velocity modulus increases, the southward transport gets stronger, the amplitude of the semidiurnal tide for the meridional wind increases too, and the zonal wind decrease and even changes its sign. In winter the meridional wind is more sensitive to stratospheric temperature variations but during spring reversal the zonal wind is. Statistical analysis allows us to find out that for the most prevailing wind directions at the 85-95 km level we have almost always the same regime of stratospheric pressure and temperature. We found that the most favorable conditions for coupling from below occur in winter, when stratospheric zonal winds get weaker and the meridional extent of disturbing processes increases. The character of coupling varies not only from year to year but also from one warming to the other and is determined by the height and location of anticyclones generation.

Simultaneously with our measurements, a coordinated study of upper atmospheric winds has been carried on by the same method in Central Europe (Geophysical Observatory Collm, GDR). Cooperative analysis of the data (SCHMINDER et al., 1978a, 1978b, 1979, 1980) shows a difference in the wind field despite the fact that geographical latitudes of both stations are nearly equal and the procedure of data treatment is practically the same. We can find longitudinal effects manifested in a distinct character of histograms for the wind direction, a systematic excess of the prevailing zonal wind in East Siberia in comparison with Central Europe, a weaker semidiurnal tide during winter months over East Siberia, and different periods of equinoctial reversal of the circulation (spring reversal is observed respectively later and autumn reversal earlier over Siberia than those over Europe), etc. Thus, we have obtained the experimental evidence for a change of the midlatitude general atmospheric circulation at ionospheric D-region heights not only with season but also with region. We may interpret this as an effect of the dependence of the lower ionospheric dynamics on the climatic characteristics of the region under investigation and on the state of the lower atmosphere.

The reasons for real geophysical variations of the monthly mean values have been discussed by PORTNYAGIN et al. (1978) and attributed to synoptic fluctuations of wind velocities having periods of several days. Such synoptic fluctuations are associated with strato-mesospheric warmings and planetary wave propagation. In addition to these processes we believe that variations of the reflection height, which are associated with variations of the character of the vertical distribution of ionization, may also be significant. Regrettably, we lack information about the three-dimensional global distribution of D region ionization. We lack even a complete two-dimensional picture for any height. Evidence for the electron density in the D region is deduced from rocket profiles and data obtained by the method of partial reflection. Large seasonal differences and variation from year to year are observed. Longitudinal gradients in the distribution of electron density in the D region are also possible (in the ionospheric F region these effects are well documented). This will lead to variations of the radio wave reflection height in the long wavelength range at different radio frequencies and at different locations and even at one frequency and one location during different years. We also know that in the mesosphere region, the dynamical regime can vary rapidly with altitude.

Therefore, it is clear that although the morphological study of the space-time variations of the dynamical regime on the basis of coordinated programs using the radiophysical methods is of great value, these measurements alone cannot reveal unambiguously the cause of the variations observed without simultaneous careful control of the reflection height with an accuracy of the order of a few kilometers. There is a need to organize complex experiments combining remote sensing and in situ rocket methods of measurements of all parameters of the plasma in the height range under investigation.

Essential part of the dynamical regime of the ionosphere with the exception of the prevailing wind and tides are the planetary waves and internal gravity waves. We studied the spectrum of these waves on the basis of our wind measurements in the upper mesopause region (KAZIMIROVSKY and CHERNOBROVKINA, 1979; KAZIMIROVSKY et al., 1980) and found waves with prevailing periods from 20 to 80 minutes in zonal and meridional wind variations. From the daily values of the prevailing velocity and amplitude of semidiurnal tide, we determine with high statistical reliability the presence of maxima in the spectrum corresponding to periods 50-60, 32-34, 27-30, 22, 16-19, 10-13, and 4-8 days. The wide range of prevailing periods may be explained by the nonstationarity of the processes being studied. Actually, a special kind of dynamical spectral analysis confirmed the change of the wind field spectrum with the time.

In conclusion, we may say that we have obtained some new information about the dynamical regime of the ionospheric D-region over East Siberia. This information can be used to improve atmosphere models, such as CIRA-72, which have neglected longitude differences above 60 km. For the Middle Atmosphere Program, morphological study of space and time variations of the dynamics, based on coordinated observations by a network of stations using the radar-meteor and spaced receiver methods, is invaluable.

#### REFERENCES

- Gregory, J. B. and A. H. Manson (1975), *J. Atmos. Sci.*, **32**, 1667.
- Gregory, J. B., A. H. Manson and C. E. Meck (1980), International Symposium on Middle Atmosphere Dynamics and Transport, Urbana, Ill.
- Kazimirovsky, E. S. and V. D. Kokourov (1979), *The Ionospheric Motions*, Novosibirsk, Science Publishing House, 344 pp. (in Russian).
- Kazimirovsky, E. S. and V. D. Kokourov (1979), *J. Geomagn. Geoelectr.*, **31**, 195.
- Kazimirovsky, E. S., V. D. Kokourov and E. I. Zhovty (1979), *J. Atmos. Terr. Phys.*, **41**, 867.
- Kazimirovsky, E. S. (1981), *J. Geophys. Res.*, **86**, 9626.
- Kazimirovsky, E. S., G. V. Vergasova, G. Ya. Khachikjan and M. P. Rudina (1982), *J. Atmos. Terr. Phys.*, **44**, 913.
- Kazimirovsky, E. S., and N. A. Chernobrovkina (1979), In: *Issledovaniya po geomagnetizmu, aeronomii i fizike Solntsa*, Izd. Nauka Moscow, **19**, 373 (in Russian).
- Kazimirovsky, E. S., N. A. Chernobrovkina and N. V. Larionov (1980), in: *Issledovaniya po geomagnetizmu, aeronomii i fizike Solntsa*, Izd. Nauka Moscow, **51**, 147 (in Russian).
- Portnyagin, Yu. I., O. V. Kaidalov, K. M. Greisiger and K. Sprenger (1977), *Phys. Solariterr.*, Potsdam, **5**, 91.
- Portnyagin, Yu. I., and K. Sprenger (editors) (1978), *Wind Measurements at 90-100 km by Ground-Based Methods*, Hydrometeoizdat, Leningrad, 340 pp. (in Russian).
- Schminder, R., E. S. Kazimirovsky et al. (1978), *Zeitschr. f. Meteorol.*, **28**, 62.
- Schminder, R., E. S. Kazimirovsky et al. (1978), *Geomagn. i Aeronomiya*, Moscow, **18**, 936 (in Russian).
- Schminder, R., E. S. Kazimirovsky et al. (1979), *Meteorology and Hydrology*, Moscow, **11**, (in Russian).
- Schminder, R., K. M. Greisiger, E. S. Kazimirovsky et al. (1980), *Phys. Solariterr.*, Potsdam, **12**, 92.
- Schminder, R., D. Kurschner, E. S. Kazimirovsky and V. F. Petruchin (1982), *Geomagnetism i Aeronomiya*, Moscow, **22**, 782 (in Russian).
- Sprenger, K. and R. Schminder (1969), *J. Atmos. Terr. Phys.*, **31**, 217.
- Stubbs, T. J. and R. A. Vincent (1973), *Austral. J. Phys.*, **25**, 645.

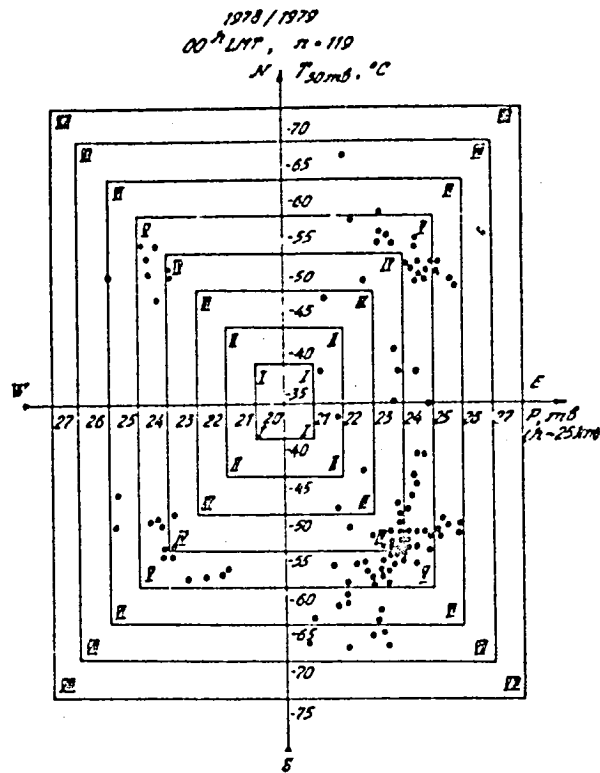


Figure 1. Map of the midnight wind direction distribution in the ionospheric D region for different thermobaric zones. Winter, 1978/1979.

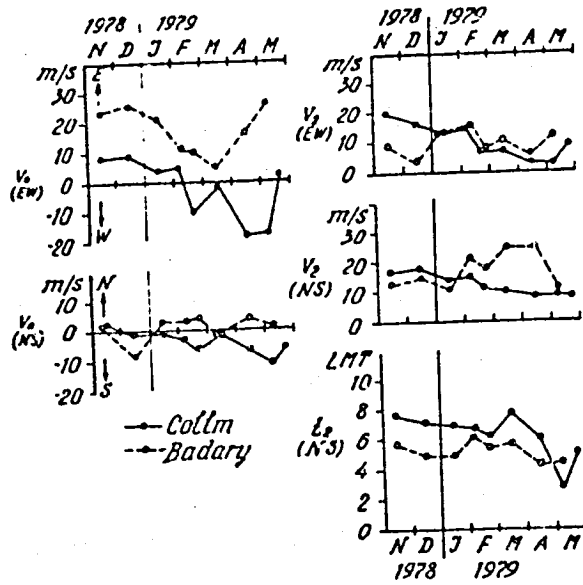


Figure 2. Longitudinal effects in the results of upper atmospheric wind measurements (D1, 85-95 km) obtained over Central Europe and East Siberia: seasonal variations (November 1978 - May 1979) of the wind field parameter in the upper mesopause region.  $V_0$  m/s - prevailing wind, positive towards E and N, respectively;  $V_2$  m/s - amplitude of the semidiurnal tide;  $t_2$  (LMT) - phase of the meridional semidiurnal tidal wind component defined as the local mean time of the occurrence of the northward maximum.

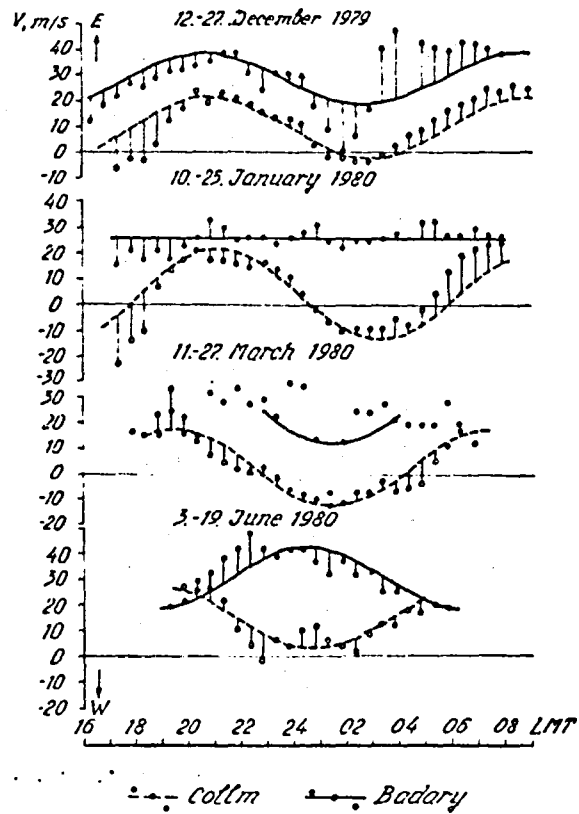


Figure 3. Longitudinal effects in the results of upper-atmospheric wind measurements (D1, 85-95 km) obtained over Central Europe and East Siberia: mean nighttime variations of the measured wind, zonal component.

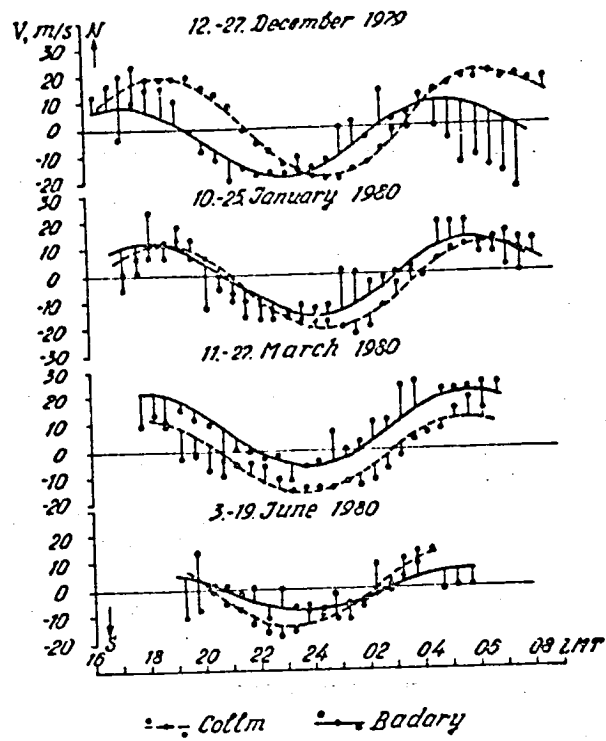


Figure 4. Mean nighttime variations of the measured wind (D1, 85-95 km), meridional component.

N85

20478

UNCLAS

D23  
160

N85-20478

MEASUREMENT OF THE VERTICAL GRADIENT OF THE SEMIDIURNAL  
TIDAL WIND PHASE IN WINTER AT THE 95 KM LEVEL

R. Schminder and D. Kurschner

Karl Marx University Leipzig  
Department of Physics  
Collm Geophysical Observatory  
DDR-7261 Collm, GDR

ABSTRACT

When supplemented by absolute reflection height measurements, low frequency wind measurements in the 90-100 km height range become truly competitive in comparison with the more widely used radar meteor wind observations. For example, height profiles of the wind parameters in the so-called meteor zone can be obtained due to the considerable interdiurnal variability of the average nighttime reflection heights controlled by geomagnetic activity.

The phase of the semidiurnal tidal wind is particularly height-dependent. The measured vertical gradient of  $1/4$  h/km in winter corresponds to a vertical wavelength of about 50 km.

Wind measurements in the upper atmosphere, at heights between 90 and 100 km, have been carried out at the Collm Geophysical Observatory of Karl Marx University Leipzig for a number of years now. These measurements use the closely-spaced receiver method and three measuring paths, on 179, 227, and 272 kHz. They take place every day between sunset and sunrise, i.e., nightly. A night in this sense may last as long as 18 hours in winter. Both the measurements and their evaluation are completely automatic, and the prevailing winds and tides are separated.

This technique has a number of advantages which, apart from being able to assign wind readings to accurate heights, could be described as follows:

- (1) Daily measurements can be made over longer periods with comparatively simple equipment and give very good information at low cost.
- (2) Wind measurements are possible on several measuring paths from one point. This gives representative data on the average wind conditions over large areas such as Central Europe, from one observatory. The transmitters are broadcasting stations which can be used free of charge over decades and whose operation is guaranteed by governments. That means we need no powerful transmitters of our own, and interference is avoided.
- (3) Wind variations with very short periods can be studied because of the high measuring density of one reading per minute and measuring path, or even more. For example, the average in 1982 was 1.7 reading per minute on 272 kHz; eight readings per minute are possible over shorter periods of time.
- (4) The zonal and meridional wind components can be measured at the same time and in the same volume in the upper atmosphere.
- (5) The wind records are available on-line. Automatically operated equipments allow the parameters of circulation to be provided with a time delay that is determined and limited only by the period of tidal winds and which is acceptable for a synoptic meteorology of the upper atmosphere; and
- (6) The whole arrangement lends itself to mobile use easily, so that an entire measuring network could be standardized on this basis.

Problems have so far been encountered in determining the reference height since these are not pulse measurements at vertical incidence but measurements on continuous-wave transmitters at oblique incidence. It was possible to calculate the reflection height from the electron density profiles only in the past, and there was no way to determine interdiurnal or short-time height variations. This handicap was overcome last year with the help of a new method developed by Korschner at our observatory. The absolute value of the reflection height is obtained from the time delay between the sky wave and the ground wave transmission of respective modulation bursts in the frequency range around 1,600 Hz, and this is presently done on the 179 kHz measuring path. Beyond our application, the method could be used in all cases where ionospheric research is conducted with the aid of the sky wave component from l. f. broadcasting transmitters. One example is A3 absorption measurements.

When l. f. ionospheric drift measurements are supplemented in this manner they become competitive with the radar meteor wind method, and this all the more since the advantages of the latter are hardly used to the full in any field. The only disadvantage of the method is that l. f. drift measurements are restricted to the night hours so that problems arise in determining the diurnal tidal wind component which is, however, small anyway in medium and higher latitudes.

To give an example of the results that can be obtained with this method, we would like to present our wind measurements of December 1982 and January 1983 and draw a few conclusions. The transmitter distance is 170 km for the 179 kHz measuring path, 460 km for 227 kHz, and 400 km for 272 kHz. The reflection points are over Central Europe near 52°N and 15°E and are about 200 km apart at a height range between 90 and 100 km. The average integral measuring density was more than 3 values per minute.

Figure 1 shows the results of the wind measurements for an individual night in December 1982, at the top for the zonal component, below for the meridional component. The mean nighttime reflection height is 90 km. The table gives a survey of the results obtained from the harmonic analysis of the wind records for each night during the two months, using the averages from all three measuring paths. As it is seen, the zonal prevailing wind is mostly directed toward the east, and the meridional prevailing wind toward the south. Even a cursory look at the table shows that there is a close connection between the phase position of the semi-diurnal tidal wind and the measured height - great heights are equivalent to an early phase, and vice versa.

Figure 2 shows the average daily wind variation at two average height levels of 90 and 100 km for December 1982. The wind and height values have been arranged hourly, in two groups below and above 94.5 km. We can see a clear phase difference in the semi-diurnal tidal wind which is somewhat above two hours for a height difference of 10 km.

Using the analyses for individual days from the table, one can calculate exact regression lines. An example would be this particular phase of the semi-diurnal tidal wind. Figure 3 shows the regression lines for all three measuring paths for the zonal component only, and for the average from all three paths, in the latter case for the zonal and meridional components. The vertical gradient of the phase results from the slope of the regression line on 179 kHz and is a quarter-hour per kilometer, or 7°/km. This is equivalent to a vertical wavelength of about 50 km.

The slope seems to fall off slightly as the equivalent frequency is reduced. This apparent reduction results from the fact that the absolute heights are only measured on 179 kHz and the reflection height variations are smaller for a steeper  $N(h')$  profile and lower equivalent frequencies. The

3



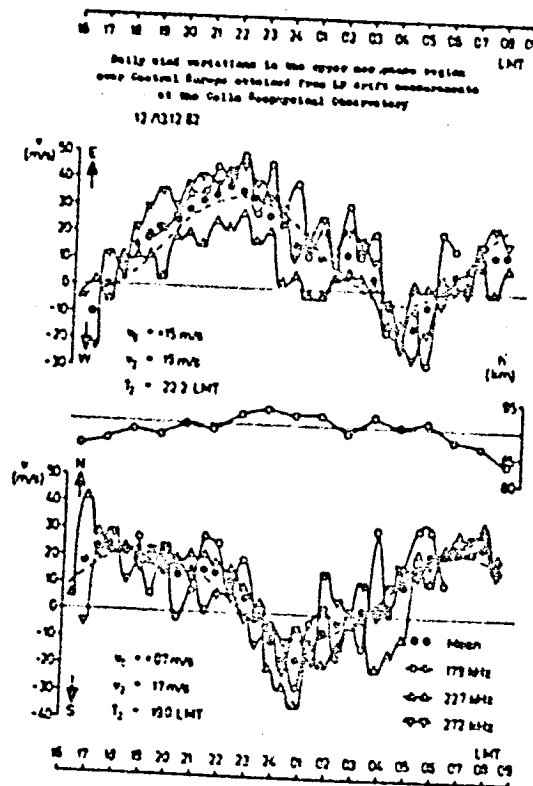


Figure 1. Daily wind variations in the upper mesopause region over Central Europe obtained from LF drift measurements at the Colla Geophysical Observatory.

equivalent frequency is 140 kHz for the 179 kHz measuring path, 115 kHz for the 277 kHz measuring path and 70 kHz for the 227 kHz measuring path.

It is typical for values of the vertical gradient of the phase of the semi-diurnal tidal wind to be in the range of a quarter-hour per kilometer, and such values are found even where the usable height range increases upward in the presence of magnetic storms. The reflection heights depend largely on geomagnetic activity. To calculate a regression line we used the sum of the  $K_1$  values for the six three-hour intervals from 15 to 9 hours UT. It turned out that in the range from  $K_1 = 10$  to  $K_1 = 30$  the height increases by a half kilometer for each unit that is added to the sum of  $K_1$ .

During stratospheric warming effects in the upper mesopause region when the prevailing zonal wind direction is reversed, the vertical gradient of the phase of the semi-diurnal tidal wind is also 15 min/km, but the sign is quite opposite: the phase is shifting from the evening to midnight hours with increasing reflection height, just now observed during the last event in February 1983.

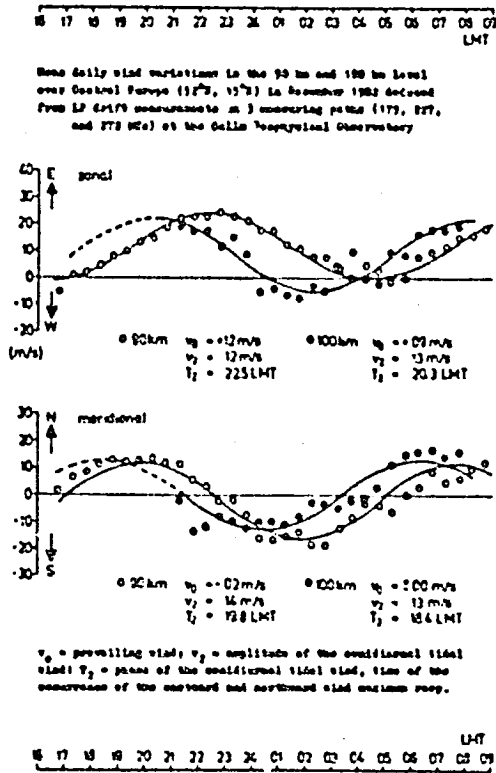


Figure 2. Mean daily wind variations in the 90 km and 100 km level over Central Europe (52°N, 15°E) in December 1982 deduced from LF drift measurements on 3 measuring paths (179, 227, and 272 kHz) at the Colla Geophysical Observatory.  $v_0$  - prevailing wind;  $v_2$  - amplitude of the semidiurnal tidal wind;  $T_2$  - phase of the semidiurnal tidal wind, time of the occurrence of the eastward and northward wind maximums, respectively.

Table 1. Results of upper atmosphere wind measurements over Central Europe obtained from LF drift measurements on 179, 277, and 272 kHz at the Collm Geophysical Observatory.

Height	December 1982						January 1983						Symbols		
	zonal			meridional			zonal			meridional					
	$v_0$	$v_2$	$T_2$	$v_0$	$v_2$	$T_2$	$v_0$	$v_2$	$T_2$	$v_0$	$v_2$	$T_2$		$h'$	
01./22.	+16	26	22.6	+12	10	19.2	90	+15	18	22.2	-09	18	19.2	92	$v_0$ (m/s) = prevailing wind, positive towards E and W resp.
07./23.	+36	16	21.8	+36	17	19.3	91	+14	13	22.4	-08	10	17.6	92	
01./24.	+11	19	20.0	-79	22	18.9	96	+09	29	19.8	-12	10	18.4	93	
04./25.	+32	20	18.7	+34	14	16.7	137	+06	23	21.2	-01	21	18.4	94	amplitude of the semidiurnal tidal wind
05./26.	+27	22	20.3	-01	20	18.5	95	+27	13	22.1	-10	14	20.1	92	
06./27.	+06	15	21.6	-09	18	19.2	95	+05	19	21.8	-07	13	19.6	89	
07./28.	+03	25	19.2	00	17	17.9	103	+06	25	22.2	-03	18	19.2	83	$T_2$ (LMT) = phase of the semidiurnal tidal wind, defined as the time of the occurrence of the eastward and northward wind maximum resp.
21./29.	+29	15	20.2	+36	10	17.4	104	+13	15	21.3	-05	18	18.4	95	
09./10.	+07	18	22.8	-02	13	21.2	93	+12	12	20.1	-01	10	17.6	103	
10./11.	03	20	21.1	+23	10	18.8	100	+20	25	17.8	+01	02	16.6	102	tidal wind
11./12.	+11	17	21.0	-05	20	18.3	96	+20	07	21.2	-06	14	19.4	93	
12./13.	+15	19	22.2	+07	17	19.0	97	+11	21	21.9	+01	22	19.1	92	
13./14.	+23	10	02.5	+10	09	22.5	88	+10	21	22.0	-07	20	19.9	94	$T_2$ (LMT) = phase of the semidiurnal tidal wind
14./15.	+29	17	22.7	-09	12	22.2	89	+01	16	22.9	-04	13	18.1	94	
15./16.	+16	06	22.9	-02	11	18.9	93	+07	23	22.4	-03	21	17.1	9	
16./17.	+13	04	19.8	03	10	18.9	99	-01	22	21.0	-16	16	17.2	95	tidal wind, defined as the time of the occurrence of the eastward and northward wind maximum resp.
17./18.	+09	15	20.4	-07	15	19.7	96	+04	14	20.4	-06	10	18.5	97	
18./19.	+08	18	21.0	-03	17	19.1	93	03	21	22.3	03	10	18.0	101	
19./20.	+04	14	22.9	03	13	20.6	93	+02	20	22.6	-28	09	18.0	100	tidal wind, defined as the time of the occurrence of the eastward and northward wind maximum resp.
20./21.	+12	13	22.7	+03	05	19.9	95	+22	14	21.6	-11	18	17.7	97	
21./22.	+03	14	18.6	+10	06	18.5	97	+09	16	21.1	-17	15	18.8	91	
22./23.	+17	08	23.5	+01	18	21.5	89	+01	19	22.1	-10	15	17.9	94	tidal wind, defined as the time of the occurrence of the eastward and northward wind maximum resp.
23./24.	+18	09	21.9	-27	16	23.7	89	-03	12	19.5	-06	10	18.8	95	
24./25.	+14	16	23.1	-08	17	23.5	90	+27	28	21.0	-06	19	18.8	100	
25./26.	+09	20	2.8	-09	15	23.1	91	+21	27	20.9	-02	12	19.4	98	tidal wind, defined as the time of the occurrence of the eastward and northward wind maximum resp.
26./27.	+13	13	22.1	+01	15	20.0	90	+06	16	22.5	+01	11	20.7	94	
27./28.	+14	09	21.3	-09	14	18.7	93	+18	20	21.4	+09	14	20.3	92	
28./29.	+11	11	00.3	-17	15	19.4	91	+18	12	22.4	+15	04	22.3	96	tidal wind, defined as the time of the occurrence of the eastward and northward wind maximum resp.
29./30.	+12	21	02.0	-06	15	20.5	93	+19	10	22.0	-02	13	20.4	91	
30./31.	-01	27	22.5	-01	13	19.9	93	+15	13	21.8	-02	14	20.9	95	
31./21.	-07	11	22.4	+11	06	15.3	93	+11	12	17.5	-02	12	17.8	102	

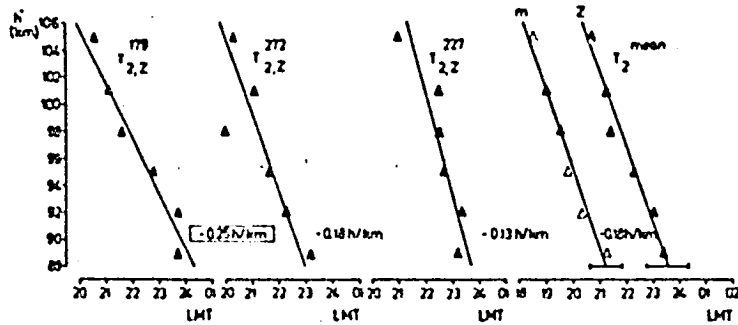


Figure 3. The vertical gradient of the phase  $T_2$  of the semidiurnal tidal wind in December 1982 and January 1983 deduced from LF drift measurements on 3 measuring paths (179, 277, and 272 kHz) and from reflection height measurements on 179 kHz over Central Europe at the Collm Geophysical Observatory (z - zonal component, m - meridional component).

## MEDIUM FREQUENCY RADAR OBSERVATIONS IN THE MIDDLE ATMOSPHERE

P. Czechowsky, G. Schmidt and H. Kopka

Max Planck Institute of Aeronomy  
D-3411 Katlenburg-Lindau, FRG

## ABSTRACT

In November 1982 the HEATING and the PRE (Partial Reflection Experiment) facilities near Tromsø (Norway) were operated together in a pulsed mode as a radar system to investigate structures in the middle atmosphere. For the first time, echoes from the upper troposphere and stratosphere have been detected on a frequency of 2.75 MHz.

The paper will be published in full in: Journal of Atmospheric and Terrestrial Physics.

N85

20479

UNCLAS

## STRATWARM EFFECTS IN THE IONOSPHERIC D-REGION WIND FIELD

G. V. Vergasova

Siberian Institute of Terrestrial Magnetism  
Ionosphere and Radio Wave Propagation (SibIZMIR)  
Siberian Branch of the USSR Academy of Sciences  
Irkutsk, USSR

## ABSTRACT

An analysis is made of the wind field structure in the strato-thermosphere over Eastern Siberia during the winter stratwarms of 1975-1977. It is found that coupling between dynamical processes in the stratosphere and lower thermosphere is effected through changes of the temperature regime of the atmosphere. The circulation regime both in the stratosphere and lower thermosphere depends on location of the source of perturbations that cause stratospheric warmings. The effect of warming-induced perturbations on the dynamics of above- and underlying layers and the meridional extent of the processes are determined by the altitude and region where anti-cyclones originate. In conditions of a warmer stratosphere, there is a considerable loss of wind stability in the ionospheric D-region. A time delay of 1 to 2 days of lower-thermosphere processes is found to occur with respect to stratospheric processes of temperature variation at 30 mb level.

We have investigated the ionospheric circulation parameters and the meteorological conditions at the troposphere and stratosphere. Wind measurements in the D-region were carried on at the SibIZMIR since 1974. We believe that there is a response of D-region dynamics to the stratospheric processes, especially to the stratospheric warmings. We have found (VERGASOVA, 1978; VERGASOVA and KAZIMIROVSKY, 1979) high correlation between D-region winds and temperature variations at the 30 mb level during stratospheric warmings. As a rule we had zonal wind reversals from westerly to easterly, increasing of southward wind or even reversal of the meridional wind, and increase of semidiurnal tide amplitude. The response of the wind field is delayed by 1-3 days after the maximum of temperature at the stratosphere ( $T_{max}$ ). The cross-correlation coefficients for ionospheric wind and stratospheric temperature were sometimes very high (-0.95).

The results derived by the superposed epoch method provide an average pattern of the interaction of the D-region dynamical regime with stratospheric temperature, reveal delay effects but do not give us any details about effects of each individual warming. We have been interested in examining the extension of the influence of each individual warming on the ionospheric dynamics, without limiting our attention only to temperature, but using the entire set of parameters varying during the perturbation (pressure, temperature, wind velocity, wind direction, zonal and meridional winds).

We have examined seven warmings, including also local ones, observed over Eastern Siberia since December 1975 through March 1977 (VERGASOVA, 1981). In order to evaluate the variation of the D-region wind structure as a function of the wind profile shape in the troposphere, we constructed the maps of the wind field in the tropo-, strato- and thermosphere and incomplete wind profiles (data on the height range 30 to -85 km are missing and the linear interpolation has therefore only a conventional character).

To evaluate the effect of each individual warming a preliminary meteorological analysis was made. We considered the region giving rise to anti-cyclones, connected with the warming wave, the height of their upper boundary, further propagation of a warm region and warming-induced changes in

the stratosphere at 30 mb level over Eastern Siberia. For example, during the warming of 31 December 1975 through 25 January 1976 there occurred a penetration of a warm region from the Atlantic anti-cyclone into high and temperate latitudes (CAO BULLETIN; BUGAEVA and RYAZANOVA, 1978). The Atlantic anti-cyclone was a strong one, with its upper boundary above 70 km. In the stratosphere at the end of December a kind of a three-cell baric field appeared. Over the poles there is an observable cyclone with depressions extending into the Eurasian and American continents while over the northern parts of the Pacific and Atlantic Oceans, two active anti-cyclones occurred with high upper boundary. There were no strong winter warmings in the stratosphere but there were some local warmings.

At Irkutsk the warming attained its maximum stage on 6 January, the temperature at 30 mb level increasing by about 20°C. The formation of anti-cyclones had significantly increased the dynamical instability in 20-60 km layers, which is apparent from Figure 1, showing wind field maps for the tropo-, strato- and thermosphere. In the stratosphere this dynamical instability occurs as a decrease of the modulus  $|v_x/v_y|$  (ratio of the zonal to meridional components), i.e., as an increase of meridionality with increasing temperature and pressure in the stratosphere. In the period of interest the disturbed region ( $h \sim 70$  km) was rather close to the lower thermosphere and may influence the ionospheric D region dynamics (Figure 1). We have seen the significant decrease and reversal of the zonal flow and a significant increase and reversal of the meridional component of the wind. Figure 2 shows the influence of temperature and pressure fluctuations at a height  $h \sim 25$  km upon the wind profile structure in the tropo-strato-thermosphere. For the higher values of temperature and pressure the profile seems to be narrower, approaching the vertical axis. These changes are connected with a decrease of the "velocity gradient" ( $\text{grad}_h v$ ) of zonal and meridional flows when temperature increases. The "velocity gradient" for the incomplete wind profiles may roughly be estimated as a velocity difference at the ionospheric D-region and at 30 mb level, attributable to a relevant height difference of 60 km. This is particularly typical of the zonal flow.

A change of the modulus of the ratio of the zonal to meridional wind component  $|v_x/v_y|$  for 30 mb level and in the ionospheric D-region, as the warming evolves, is illustrated in Figure 3. For comparison this figure also shows the state of the thermobaric field at  $h \sim 25$  km for each of the two measurement times. For the maximum warming phase this ratio is minimal. Thus, at the highest values of pressure and temperature in the stratosphere in winter, meridional flows predominate both below (at  $h \sim 25$  km) and above (in the ionospheric D region). For this warming the action of perturbation maybe penetrates even above the ionospheric D region.

The analysis of the seven warmings permits the following conclusions:

- (1) Evidently winter tropo-, strato- and thermosphere circulation systems are affected by a common source of perturbations that generate stratospheric warmings.
- (2) The character of meteorological impact varies not only from year to year but also from warming to warming.
- (3) The circulation regime both in the stratosphere and in the lower thermosphere depends on localization of the source of perturbations that cause stratospheric warmings. The force of action of the warming-induced perturbations on the dynamics of above- and underlying layers and the meridional extension of processes depend on the altitude and localization of anticyclones. Similar inferences have been reached by BUTKO et al. (1978).

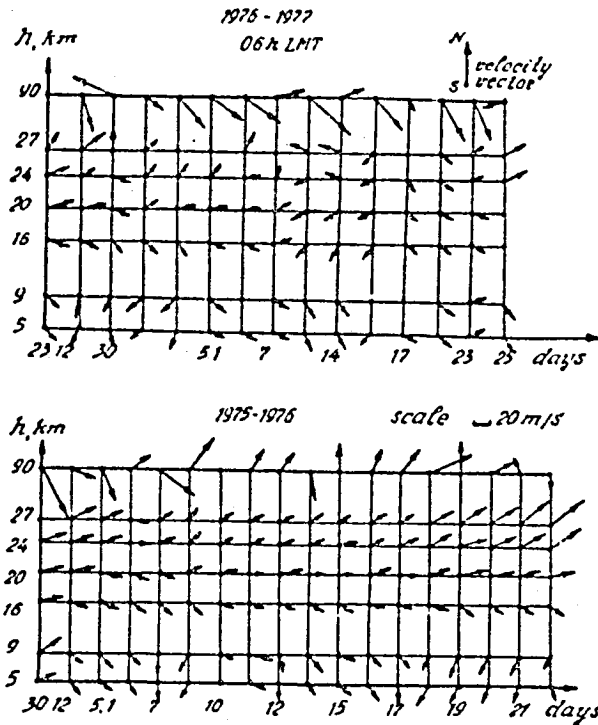


Figure 1. Maps of tropo-strato-thermospheric wind field during the warmings: 31 December 1975 through 25 January 1976 (bottom) and 17 December 1976 through 20 January 1977 (top) at 0600 LMT.

(4) The experimental data obtained over Eastern Siberia confirm the theoretical prediction of CHARNEY and DRAZIN (1961), that the winter provides most favorable conditions for perturbations to propagate upwards from below because at that time in the stratosphere strong zonal flows are weakened and the meridional extension of processes grows. The decrease of the modulus of the ratio of the zonal to meridional wind components (Figure 3) is illustrative in this regard.

We may assume that the energy of perturbations through planetary waves, can be relayed also into higher ionospheric heights, thus causing relevant changes in its dynamical regime.

In April 1976 when a local-scale warming was observed only over Eastern Siberia, D-region winds and E and F2 region drifts were simultaneously measured by the D1 method. The experimental data thus obtained proved the possibility of meteorological control of the dynamical regime of the ionospheric D and E regions. (The correlation coefficient of the zonal component of the wind velocity in the D region with stratospheric temperature is 0.77 and that for the E region is 0.95, see Figure 4. We had, however, no effects in the ionospheric F region dynamics (VERGASOVA and KAZIMIROVSKY, 1980).

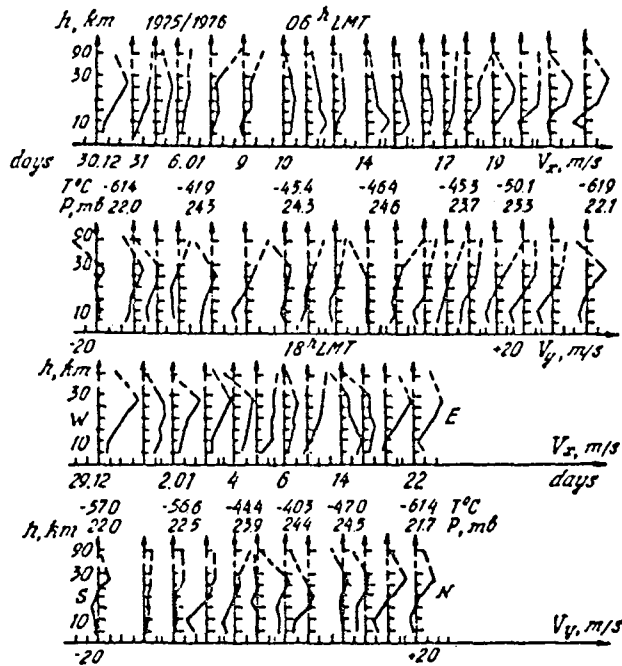


Figure 2. Zonal and meridional wind profiles for the warming 31 December 1975 through 25 January 1975.

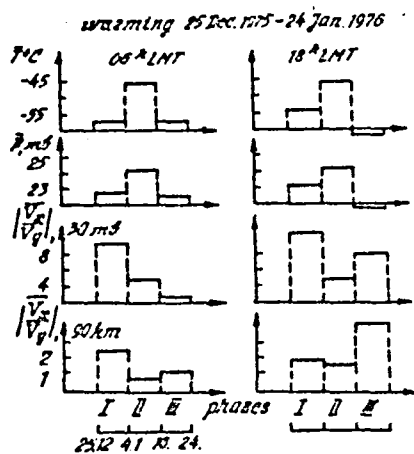


Figure 3. T, P,  $|\overline{V_x/V_y}|_{30mb}$  and  $|\overline{V_x/V_y}|_{90km}$  for different phases of the warming 25 December 1975 through 24 January 1976: I - initial phase, II - main phase, III - recovery phase.

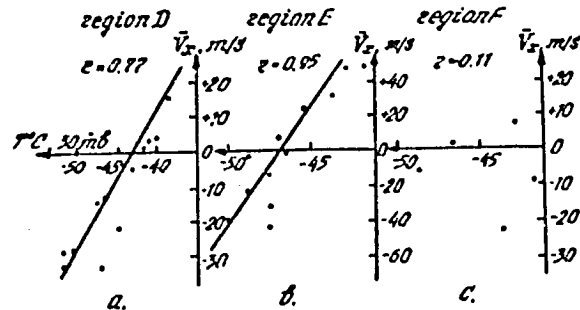


Figure 4. Correlograms for zonal and 30-mb level temperature.

On the basis of the experimental results obtained we can draw a general conclusion that during periods of very strong perturbations of the thermal field of the type of sudden winter stratospheric warmings the structure of the dynamical regime in the D and E regions of the ionosphere over Eastern Siberia is largely influenced by the meteorological situation from below.

#### ACKNOWLEDGEMENT

I would like to thank my colleagues from Ionospheric Dynamics Laboratory (SibIZMIR). Special thanks are due to Prof. E. S. Kazimirovsky for many pieces of valuable advice and comments.

#### REFERENCES

- Bugayeva, I. V. and L. A. Ryazanova (1978), *Trudy CAO, Moscow*, 140, 48.  
 Butko, A. I., L. A. Ryazanova and K. E. Speransky (1978), *Trudy CAO, Moscow*, 140, 76.  
 CAO Bulletin: Results of rocket sounding of the atmosphere, Central Aerological Observatory, GUGMS, vol. 9-13, 6.  
 Charney, J. G. and P. Drazin (1961), *J. Geophys. Res.*, 66, 83.  
 Vergasova, G. V. (1978), In *Issled. po geomagnetizmu, aeronom. i fizike Solntsa*, Moscow Nauka, 44, 163-170.  
 Vergasova, G. V. (1981), In *Issled. po geomagnetizmu, aeronom. i fizike Solntsa*, Moscow Nauka, 55, 62-72.  
 Vergasova, G. V. and E. S. Kazimirovsky (1979), In *Regional structure of dynamical processes of the middle atmosphere*, Frunze Ilim, 74-86.  
 Vergasova, G. V. and E. S. Kazimirovsky (1980), In *Issled. po geomagnetizmu, aeronom. i fizike Solntsa*, Moscow Nauka, 51, 178-183.

N85

20480

UNCLAS

N 85 - 20480

D 30  
171

OROGRAPHIC DISTURBANCES OF UPPER ATMOSPHERE EMISSIONS

N. N. Shefov and N. N. Pertsev

Institute of Physics of the Atmosphere  
Academy of Sciences  
Moscow, USSR

ABSTRACT

There are some increases of the temperature of the hydroxyl emission ( $\Delta T \sim 20$  K,  $z \sim 90$  km) and of the intensity of the 6300 oxygen emission ( $\Delta I/I \sim 20$  per cent,  $z \sim 250$  km) for the lee of the mountains at distances about 150 km in the case of the latitudinal direction of the wind ( $U \sim 10$  m/s) at the 3000 m level.

Airflow motions over mountains may be one of the possible processes of generation of wave disturbances penetrating into the upper atmosphere (HINES, 1974; LINDZEN, 1971). The purpose of this paper is to study the penetration of orographic disturbances into upper atmosphere. Airplane measurements of emission variations of hydroxyl and atomic oxygen 6300 Å near the Northern Ural mountains were made. Several nocturnal flights have been carried out in March, 1980 and January - February, 1981 at heights about 3000 m along 64° northern latitude in the Ural region. Spectrographs SP-48 with electronic image converters registration for Oh ((9,4) and (5,1) bands - 7700 - 8100 Å) and OI (6300 Å) emissions were used. The zenith region was observed, and exposure time was 2 minutes. This corresponds to averaging of the emission intensities along the airplane trace over a distance of 10 km. Simultaneous measurements of atmospheric temperature variations at the flight altitude have also been made. Data during 13 nights were obtained. The direction of wind was west to east during 5 nights, east to west during 4 nights, and nearly meridional during the rest of the cases. During some nights observations were disturbed and blended by aurora. These data were withdrawn.

In Figure 1 mean variations of the increments of hydroxyl emission rotational temperature  $\Delta T_{90}$  and relative intensity of oxygen emission 6300 Å for meridional and latitudinal wind directions are shown. A distinct increase of hydroxyl emission temperature (maximum intensity level is about 85-90 km) and of oxygen emission intensity (maximum intensity level is about 250-270 km) is clearly seen in the lee of the mountains at distances up to 300 km. There are wave disturbances in the atmospheric temperature with wavelengths about 10-50 km and amplitudes up to 0.4 K in the case of latitudinal direction of the wind at 3000 m level.

A comparison of various characteristics of the lower and upper atmospheric parameters of the measured data is shown in Figure 2. Circles represent the 1980 data, and dots those for 1981. It should be emphasized that numbers of dots and circles are not the same on all figures as for several flights there are no simultaneous data of hydroxyl and oxygen emissions.

Figure 2 shows that there are some connections between processes at the various altitudes. The horizontal distances,  $X_{90}$  and  $X_{250}$ , of the maximum disturbance of emissions are the same in many cases. However, there are some data of 1980 (circles) when  $X_{90}$  is greater than  $X_{250}$ . At these times orographic effects were observed to the west of the Ural because of westward wind. The observed decreases of the  $X_{250}$  compared to  $X_{90}$  may be explained by an eastward zonal component of the thermospheric wind for this season and diurnal period (HILLER, 1981; SEMENOV, 1982).

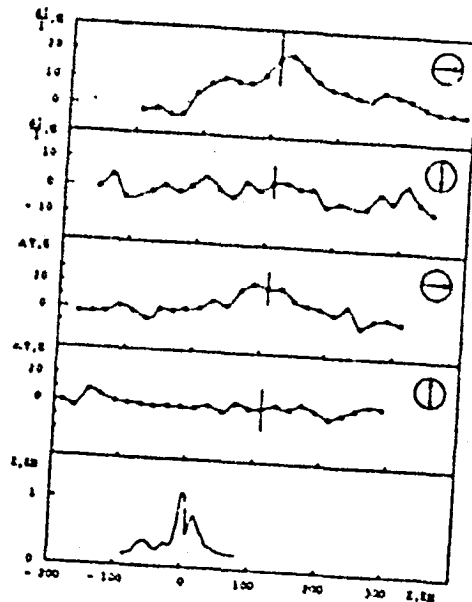


Figure 1. Mean variations of increments of hydroxyl rotational temperature  $\Delta T_{00}$  near 90 km, and relative intensity  $\Delta I/I$  of the 6300 Å oxygen emission near 250 km, in dependence on the distance  $X$  from the Northern Ural mountains along the geographic parallel (about  $66^\circ N$ ) for various wind directions (shown by arrows,  $U \sim 10$  m/s). The vertical lines are error bars.

It is also notable that there are correlations between the velocity  $U$  of wind at the flight altitude and the measured values of  $X_{90}$  and  $X_{250}$  for the observed limits of  $U$ , as well as correlations between the halfwidths of the regions of disturbed emissions,  $\Delta X_{90}$  and  $\Delta X_{250}$ .

The dislocation of Ural mountains and a mesospheric temperature disturbance region reveal some criteria of interconnection between processes in the lower and upper atmosphere and allow to analyse the results of the temperature variation measurements at the flight altitude near 3000 m, distorted by the Doppler effect caused by airplane movement (velocity is about 60-90 m/s).

There are standing and propagating waves in the wave disturbances, as obtained by a harmonic analysis of measured time series of temperatures at the height of 3000 m. The existence of a standing wave has been revealed from the phase coincidence of the waves relative to ground surface during consecutive flights over the mountains. Amplitudes  $\Delta T$ , horizontal wavelengths  $\lambda_x$  and periods  $\tau$  for the standing waves observed on January 26, 1981 in the eastward lee of the mountains are given in Table 1. Some estimations of corresponding values of the vertical wavelengths  $\lambda_z$  for standing waves and also the group velocity components  $C_x^g$  and  $C_z^g$  in the ground system obtained from the dispersion relation are also presented in Table 1. The wind velocity was 14 m/s. According to HINES (1974), wave disturbances with such parameters can penetrate up to the mesopause.

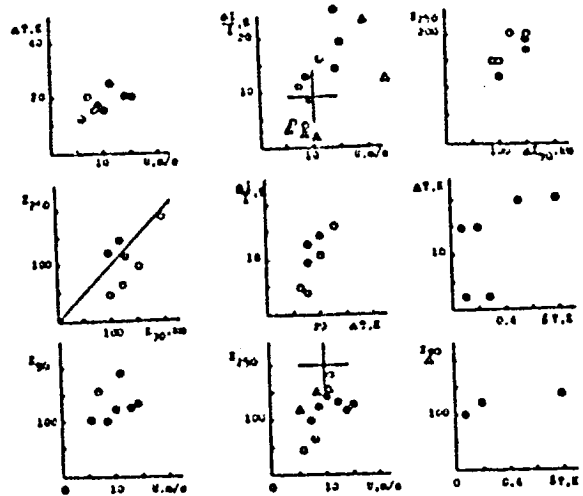


Figure 2. Comparisons of measured data:  $X$ , horizontal distance of the maximum increments of the upper atmospheric emission parameters,  $\Delta X$ , halfwidth of disturbed region  $\Delta T_{90}$  and  $\Delta I/I$ , mean amplitudes,  $U$  wind velocity and  $\Delta T$  temperature disturbance amplitudes at the 3000-m level. Circles represent data of 1980, dots are data of 1931. The cross is the result for the Hawaiian Islands, triangles are the same for Yokosuka (see the text).

For all these examples the horizontal components of the group velocity  $C_g^x$  are directed downwind, the vertical components  $C_g^z$  are directed upward and their values are almost equal. Such wave disturbances may reach the mesopause within 4-8 hours. According to the measurements, disturbances in the upper atmospheric emissions were observed during the whole period of night measurements (i.e., about 7 hours usually). The values of vertical energy fluxes  $F_z = \overline{\delta P \cdot \delta W/2}$  ( $\delta P$  and  $\delta W$ , being amplitudes of pressure and vertical velocity) for measured temperature amplitudes  $\Delta T$  were computed on the basis of linear theory. The results are also included in Table 1.

It follows from Figure 2 that the values of disturbances at various levels of the atmosphere depend upon the wind velocity in the lower atmosphere. One can note that there is approximate proportionality between the temperature increments,  $\Delta T_{90}$ , at the height near 90 km (and also the relative increments of the 6300 emission,  $\Delta I/I$ ) and the wind velocity,  $U$ . Such type of correlation is in agreement with theoretical estimations of the orographic disturbance amplitude in the upper atmosphere (near 90 km) in certain limits of used parameters (BLANK, 1980).

It is interesting to compare the obtained results with the observed data of the emission behaviour in the vicinity of other mountain ranges. Measurements of the spatial distribution of the 6300 emission intensity near the Hawaii Islands (ROACH et al., 1964; ROACH and GORDON, 1973) revealed a stable spot structure very similar to the geographic structure of these islands. From this fact Krassovsky suggested that the observed emission morphology is caused by

Table 1. Parameters of four wave trains of standing waves for January 26, 1981.

QUANTITY	1	2	3	4
Period $\tau$ , Min	12.2	13.5-2.5	19.3	23.4
Horizontal Wavelength $\lambda_x$ , km	8.5-0.9	9.5-1.0	13.8-1.2	16.3-1.7
Vertical Wavelength $\lambda_z$ , km	14.0-0.9	9.2-2.2	7.1-0.9	6.9-0.8
Horizontal Group Velocity $C_x^E$ , m/s	7.3-3.3	5.8-2.5	2.9-1.1	2.0-0.9
Vertical Group Velocity $C_z^E$ , m/s	5.5-1	5.8-1	5.0-1	4.3-1
Temperature Amplitude $\Delta T$ , K	0.05	0.09	0.08	0.08
Pressure Amplitude $\Delta P$ , Pa	1	2	2	2
Amplitude of Vertical Velocity $\Delta W$ , m/s	0.1	0.2	0.2	0.2
Vertical Flux of Energy $F_z$ , erg/cm <sup>2</sup> s	70	200	200	200

ographic disturbances penetrating into the upper atmosphere (SEMENOV et al., 1981). Supposing that the expected amplitude of such disturbances is proportional to the square of the mountain height (BLANK, 1980), the data for the Hawaii mountains (~3000, 4000 and 4200 m) after reduction to the altitude (~900 m) of the Ural have been represented by a cross in Figure 2. The size of the cross corresponds to the uncertainty of the data of the horizontal dimension of the observed emission region (ROACH et al., 1964, 1973), and of the wind in the troposphere, which was assumed to be equal to the seasonal mean for this geographic region. Nevertheless there is a satisfactory agreement between these data.

There are also some examples of simultaneous variations of emissions of atomic oxygen 5577 Å ( $z \sim 100$  km) and 6300 Å, observed in Japan (MISAWA et al., 1981). Analyses of the meteorological situation in the troposphere showed that there was wind flowing from west to east with a velocity about 10 m/s at the isobaric levels 850 mbar and 700 mbar. In this case the relief of Honshu Island may be adopted as a single mountain with a height of about 3000 m and a horizontal dimension about 280 km, with its center located about 150 km from the observing station Yokosuka. The observed intensity variations of 6300 Å emission can be reduced for mountain height in the same way as in the case of Hawaii Islands. The results are represented on Figure 2 by triangles. They are in satisfactory agreement with the other data. Of course it would be necessary to take into account the hydroxyl rotational temperature data which unfortunately are absent in the paper of MISAWA et al. (1981).

The nature of the 90 km level emission disturbance differs from that for the 250 km level. The increase of the temperature at 90 km is caused by dissipation of waves, generated by the airflow over the mountains. The

disturbances at heights about 250 km rise possibly as a result of some dynamical transfer from 90 km up to 250 km level, maybe in consequence of a piston effect. The increase of the disturbance region dimension in case of the 6300 Å emission intensity compared with that of the 90 km level is obviously the result of an increase of the diffusion rate at greater altitudes. According to the experimental data the mean ratio of the disturbance region dimensions is about 1.5.

Using the temperature increment at 90 km level one can conclude that the total energy of the disturbance observed along the X axis (in the case of 10 m/s velocity, Figure 2) is

$$\Delta E = \frac{3}{2} N k H \int T_{90} dx \sim 1.6 \cdot 10^{12} \text{ erg/cm}$$

where N is the particle density of the atmosphere, H is the thickness of the disturbance layer, k is Boltzmann's constant. With a disturbed region dimension of about 150 km, we get the energy density  $10^5 \text{ erg/cm}^2$ . The average time for generating a stable disturbance is obviously several hours. Since the recorded variations in the mesopause and thermosphere have existed during the whole period of the flight, the lifetime may be estimated to be  $10^4$  s. Therefore the vertical energy flux of the orographic disturbance is about  $10 \text{ erg/cm}^2$  s. On the other hand, the measured amplitudes of the temperature variations at the flight level give a vertical energy flux of about  $10^2 \text{ erg/cm}^2$  s according to the linear wave theory (see Table 1). Such estimations show that heating of the layer near the mesopause takes a small part of mountain lee wave energy.

The authors would like to thank Prof. V. I. Krassovsky for his advice and attention to this work.

#### REFERENCES

- Blank, A. D. (1980), *Izv. Acad. Sci., USSR Atmospheric and Oceanic Physics*, 16, 643.
- Hiller, H. (1981), *Planet. Space Sci.*, 29, 579.
- Hines, C. O. (1974), *The Upper Atmosphere in Motion*, AGU, Washington, D.C.
- Lindzen, R. S. (1971), *Tides and gravity waves in upper atmosphere*, in *Mesospheric Models and Related Experiments*, (ed. G. Fiocco), D. Reidel, pp. 122-130.
- Misawa, K., I. Takeuchi, Y. Kato and I. Aoyama (1981), *Ann. Geophys.*, 37, 549.
- Roach, F. E. and J. L. Gordon (1973), *The Light of the Night Sky*, D. Reidel, Dordrecht, Holland.
- Roach, F. E., W. R. Steiger and W. E. Brown (1964), A summary of one year of observations of 6300 Å airglow at Haleakala, *Technical Report of Inst. Geophys.*, HIG-64-16.
- Semenov, A. I. (1982), *Geomagnetism and aeronomy, USSR*, 22, 497.
- Semenov, A. I., M. V. Shagaev and N. N. Shefov (1981), *Izv. Acad. Sci., USSR, Atmospheric and oceanic physics*, 17, 982.

N85

20481

UNCLAS

D31  
176

N85-20481

## TWILIGHT INTENSITY VARIATION OF THE INFRARED HYDROXYL AIRGLOW

R. P. Love, K. L. Gilbert and R. J. Niciejewski

Department of Physics  
The University of Western Ontario  
London, Canada N6A 3K7

The vibration rotation bands of the hydroxyl radical are the strongest features in the night airglow and are exceeded in intensity in the dayglow only by the infrared atmospheric bands of oxygen. Since their discovery over thirty years ago, the bands have been the basis of many studies of the behaviour of the region near the mesopause such as its temperature, composition and the effect of gravity waves.

One aspect of the hydroxyl airglow behaviour which has not been well studied is the variation of intensity during evening twilight. There are two reasons for this:

- (1) Scattered sunlight has made ground-based measurements only possible when the sun is more than 6° below the horizon. Thus the only measurements available have been from aircraft or balloons.
- (2) The rapid changes which occur at twilight require a time resolution of a few minutes. Few airglow spectrometers have the sensitivity to provide this time resolution while maintaining the good spectral resolution required to discriminate satisfactorily against the scattered sunlight contribution.

Using a ground-based Fourier Transform Spectrometer, we have been able to make hydroxyl intensity measurements as early as 3° solar depression. As will be seen below, models of the twilight behaviour show that this should be sufficient to provide measurement of the main portion of the twilight intensity change. Our instrument is equipped with a liquid nitrogen-cooled germanium detector whose high sensitivity combined with the efficiency of the FTS technique permits spectra of the region 1.1 to 1.6  $\mu\text{m}$  at high signal-to-noise to be obtained in two minutes. The use of a polarizer at the entrance aperture of the instrument reduces the intensity of scattered sunlight by a factor of at least ten for zenith observations.

### RESULTS

Three spectra of the region of the 4-2 and 3-1 OH bands are shown in Figure 1. Some of the individual lines of the bands can be readily identified in the spectrum taken at 3.02° solar depression and the remainder of the band is clearly visible by 5.49°. The feature at 6320  $\text{cm}^{-1}$  is the 0-1 band of the infrared atmospheric system of oxygen.

We have prepared a computer model of the behaviour of the hydroxyl intensity for comparison with the observations. Although the model is relatively simple, it is not possible to provide more than a brief outline here. Excited hydroxyl radicals are assumed to be produced exclusively by



Ozone is produced by



and destroyed through photodissociation by sunlight

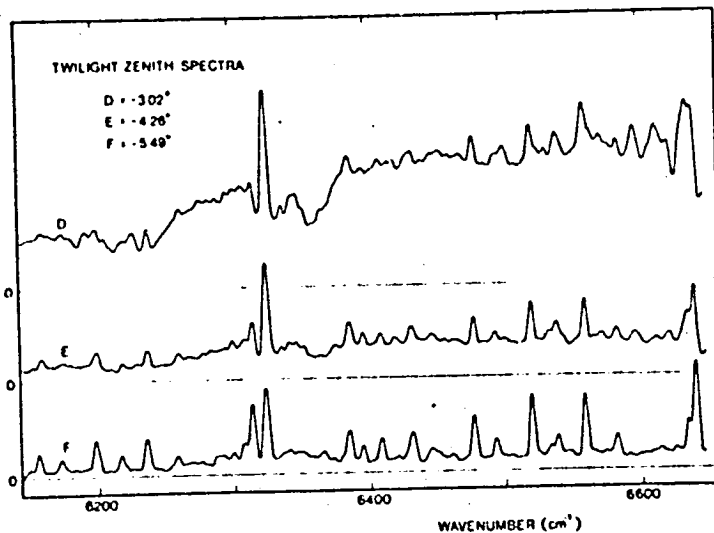
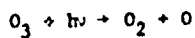


Figure 1.



as well as by process (1). At evening twilight, the cessation of process (3) leads to an increase in the ozone concentration and hence in the hydroxyl production rate. The extent of this increase depends on the atomic hydrogen profile assumed. We have assumed an initial hydrogen profile with a peak of  $1.6 \times 10^8$  atoms/cm<sup>3</sup> at 85 km. The model has also been run with various multiples of this profile. One important feature of the model is that the photodissociation rate as a function of altitude is recalculated at each step to allow for the increase in the ozone concentration.

The model calculation and observations taken on an evening in March are shown in Figure 2. The observations have been normalized to give agreement at large solar depressions. The agreement of the observation with the model is quite good although the fit is better with a model calculation for which the atomic hydrogen concentration is doubled. Data for three other spring nights is available. For two of these, the increase is comparable to the night shown. On the third, only partial data is available due to cloudy conditions at the start of the observing period. The increase observed is more rapid and fits the model calculation for the normal hydrogen profile.

#### DISCUSSION

We have shown the feasibility of making ground-based observations of the evening twilight increase in hydroxyl excitation. The principal value of such observations is the information they provide on the hydrogen atom concentration near the mesopause, a quantity for which there is only scanty data available.

Preliminary data are consistent with hydrogen atom concentrations at 85 km in the range  $1.5 - 3 \times 10^8$  cm<sup>-3</sup>.

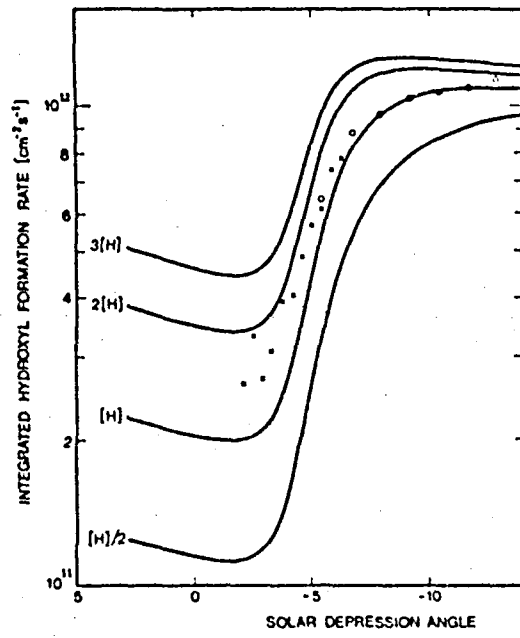


Figure 2.

N85

20482

UNCLAS

N85-20482

D32  
179

INVESTIGATION OF AERONOMIC PROCESSES ON THE BASIS  
OF IONOSPHERIC SPORADIC E

P. Bencze

Geodetic and Geophysical Research Institute  
Hungarian Academy of Sciences  
H-9401 Sopron, Hungary

INTRODUCTION

The vertical sounding of the ionosphere by means of radio waves is even nowadays the most widely used method of ionospheric research. From the parameters scaled from ionograms only the characteristics of the sporadic E layers are directly related to dynamical processes. It is now generally accepted that at mid-latitudes E<sub>s</sub> ionization is produced by wind-shear in the lower thermosphere.

It is also known that the lower thermosphere is an important region of the atmosphere, processes of which affect almost the whole atmosphere. Namely, in the lower thermosphere forms the "surface" called the homopause separating the homosphere from the heterosphere, respectively the turbopause, the boundary between the turbosphere and the diffusion region. The turbopause is defined as the altitude where the coefficient of turbulent diffusion equals the coefficient of molecular diffusion which increases with increasing height. The changes of the height of the turbopause result in variations of the composition of the neutral gas in the upper atmosphere. The altitude changes of the turbopause are mostly connected with variations of the turbulent diffusivity. At the same time, turbulent diffusion is also one of the factors establishing the vertical transport of atmospheric constituents produced in the thermosphere to the mesosphere and vice versa.

Realizing these two facts a method has been developed, by means of which the characteristics of turbulence can be determined on the basis of E<sub>s</sub> parameters.

METHOD AND DATA USED IN THE INVESTIGATIONS

It has been assumed that the wind-shear theory of mid-latitude sporadic E is valid. First, the ion-convergence is computed by means of the formula (REDDY and MATSUSHITA, 1968)

$$\frac{dv_{iz}}{dz} = -\alpha_{eff} n_{max} \left( \frac{n_0^2}{n_{max}^2} - 1 \right)$$

where  $v_{iz}$  is the vertical component of the ion drift velocity,  $\alpha_{eff}$  is the effective recombination coefficient outside of the stratification,  $n_{max}$  and  $n_0$  are the maximum electron density within the layer, respectively the electron density in absence of the layer. The maximum electron density of the E<sub>s</sub> layer is obtained from the measured blanketing frequency  $fbE_s$ . The electron density, appearing in the absence of the layer, that is the background electron density is computed by means of formulas defining ionospheric models (e.g., RAWER and RAMAKRISHNAN, 1972). In these relations the maximum electron density of the E layer was calculated from the simultaneously measured  $foE$  value, considering the measured virtual height  $h'E_s$  as height of the E<sub>s</sub> layer. Then, the vertical shear of the horizontal wind is determined by means of the equation

$$\frac{du}{dz} = - \frac{1 + \left(\frac{v_{in}}{\omega_i}\right)^2}{\frac{v_{in}}{\omega_i} \cos I} n_{\text{eff}} n_{\text{max}} \left(\frac{n_0}{n_{\text{max}}} - 1\right)$$

where  $v_{in}$  and  $\omega_i$  are the ion-neutral collision frequency, respectively the ion gyrofrequency,  $I$  being the magnetic dip angle. The ion-neutral collision frequency has been computed from the formula given by CHAPMAN (1956). The number density of the neutral gas, necessary for the determination of the ion-neutral collision frequency has been obtained from CIRA (1972).

For the determination of turbulent parameters, first the gradient Richardson-number

$$R_i = \frac{\frac{\partial \theta}{\partial z}}{\frac{1}{g} \left(\frac{\partial u}{\partial z}\right)^2}$$

is computed, where the vertical gradient of the potential temperature has been determined on the basis of CIRA (1972). According to the investigations of WOODS (1969) turbulence sets in, if the value of the gradient Richardson number is less, than 0.25. Testing the fulfillment of this condition, the vertical turbulent wind  $w$  is calculated by means of the relation (DEACON, 1959)

$$w = [-0.15 (R_i)^{1/2} + 0.08]u$$

where  $u$  is the horizontal wind velocity. The latter can be computed from the thermal wind equation using atmospheric models, or measured values are used.

The turbulent diffusivity is determined by means of the formula

$$K = \frac{\langle w^2 \rangle}{\left(\frac{1}{g} \frac{\partial \theta}{\partial z}\right)^{1/2}}$$

given by ZIMMERMAN and MURPHY (1977). This relation is valid, if the vertical turbulent spectrum is inertial and limited to the buoyant limited scale. Since the dimensions of inhomogeneities in the  $E_s$  layer, inferred from the wave length of radio waves reflected from the layer are between 1.5 and 15 m, this condition is fulfilled also in our case.

For the illustration of the quality of the data, obtained by means of this method, the  $E_s$  parameters of the ionospheric stations Bekescsaba, Hungary (46°40'N, 21°10'E) and Juliusruh, GDR (54°38'N, 13°23'E) have been used. Further, the horizontal wind velocity has been determined from the drift velocity measured with the spaced receiver method in Kuhlungsborn, GDR (54°07'N, 11°46'E), extrapolating the data to the height of the  $E_s$  layer.

#### RESULTS AND CONCLUSIONS

Figure 1 shows the turbulent diffusivity deduced from ionospheric sporadic E in different altitudes above the ionospheric stations Bekescsaba and Juliusruh. Here the wind data measured by means of the spaced receiver method in Kuhlungsborn were used assuming that the horizontal wind velocity does not significantly change with latitude. In the Figure the values of turbulent diffusivity given by other authors are also given. It can be seen that our results agree very well with the data of other experiments.

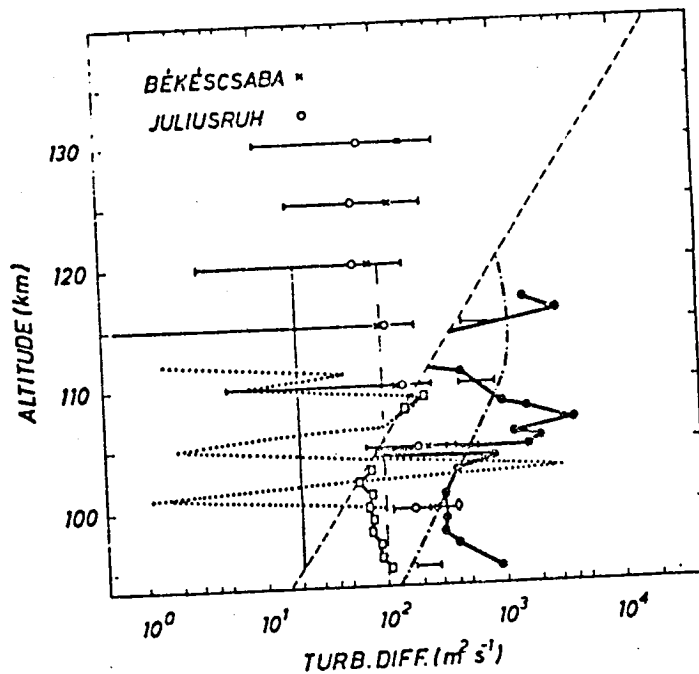


Figure 1.

In Figure 2 the seasonal variations of the turbulent diffusivity deduced from  $E_s$  parameters in different altitudes above the ionospheric station Bekescsaba are shown. Here again the drift velocity measured in Kuhlungsborn was used. The turbulent diffusivity displays below 115 km a seasonal variation with maxima in the equinoctial months and minima in summer respectively in winter. Above 115 km a seasonal variation with a minimum in summer and a maximum in winter appears. It should be mentioned that the seasonal variation of the turbulent diffusivity agrees with that obtained by ROPER (1966) from radio-meteor wind-shear observations.

An attempt has also been made to determine the variation of the turbulent diffusivity during and after geomagnetic disturbances. The turbulent diffusivity was obtained this time by computing the horizontal wind velocity from the thermal wind equation. The mean variations of the turbulent diffusivity below and above the turbopause (100 km, resp. 120 km) during and after 12 geomagnetic disturbances of the year 1973 are shown in Figure 3. It can be stated that the change of the turbulent diffusivity below the turbopause is opposed to that appearing above the turbopause. Since the turbulent diffusivity increases below the turbopause during geomagnetic disturbances, this would indicate a rise of the turbopause and composition changes in accordance with theoretical considerations (SINHA and CHANDRA, 1974) and satellite measurements (PROLSS, 1960).

## REFERENCES

- Chapman, S. (1956), *Nuovo Cim* 4, Ser. 10, Suppl. No. 4, 1385.  
 CIRA (1972), Akademie Verlag, Berlin.

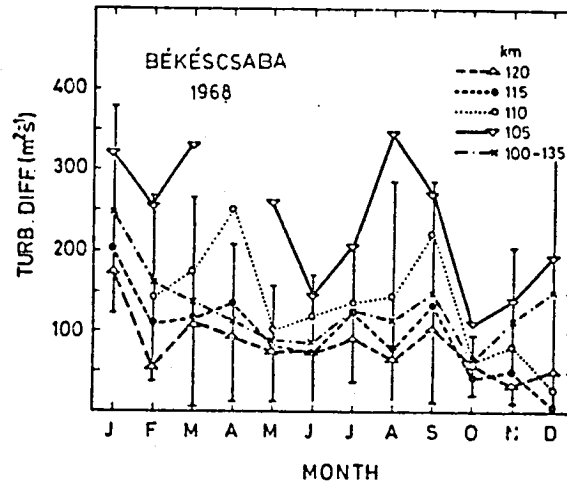


Figure 2.

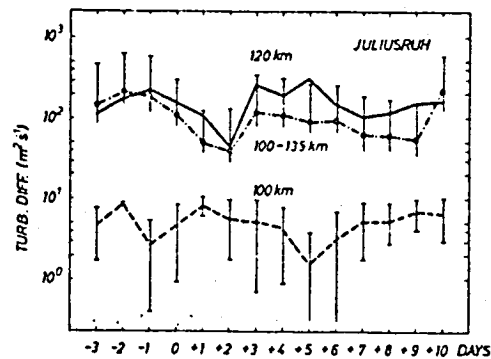


Figure 3.

- Deacon, E. L. (1959), Intern. J. Air Pollution, 2, 92.
- EHI Geophysical Data, (1968, 1973), Akad. Wiss DDR, Zentralinst. f. Solar-Terr. Physik, Berlin.
- Ionospheric Data Békéscsaba (1968, 1973), Central Inst. Meteorology, Budapest.
- Pross, G. W. (1980), Rev. Geophys. Space Phys., 18, 183.
- Rawer, K. and S. Ramakrishnan (1972), Tentative Tables of Electron Density and Excess Electron Temperature for Temperate Latitude, Arbeitsgruppe f. Physik. Weltraumforschung, Freiburg.
- Reddy, C. A. and S. Matsushita (1968), J. Atmos. Terr. Phys., 30, 747.
- Roper, R. G. (1966), J. Geophys. Res., 71, 5785.
- Sinha, A. K. and S. Chandra (1974), J. Atmos. Terr. Phys., 36, 2055.
- Woods, J. D. (1969), Radio Sci., 4, 1289.
- Zimmerman, S. P. and E. A. Murphy (1977), In: Dynamical and Chemical Coupling Between the Neutral and Ionized Atmosphere, eds. B. Grandal and J. A. Holtet, D. Reidel Publ. Co., Dordrecht-Holland, p. 35.

N85

20483

UNCLAS

N 85-20483

D-33  
183

SPACE AND TIME VARIATIONS AND TURBOPAUSE DYNAMICAL STRUCTURE

O. G. Ovezgeldiyev, L. P. Korsunova and Yu. Karadzshayev

Physico-Technical Institute  
Turkmen SSR Academy of Sciences  
15 Gogol St  
744000 Ashkhabad, USSR

Studies of different characteristics of turbulence in middle atmosphere are being carried out at present by means of MST-radars, by partial reflections (up to 100 km), radar and photographic observations of meteor trails (80-100 km), and also by rocket (80-140 km) and grenade (30-90 km) measurements. The least studied level here is a turbopause - a transitional zone between the regions of turbulent and non-turbulent motion at the height of more than 100 km. At the same time, regular ionospheric observations of the sporadic E layer make it possible to get information of the turbopause behaviour.

Indeed, the  $E_s$  layer is the only large-scale formation in the midlatitude ionosphere whose parameters are for the most part determined by dynamical characteristics of the middle atmosphere (GERSHMAN et al., 1976). The region of most frequent occurrence of  $E_s$  coincides with the zone of wind shears maxima (OVEZGELDIYEV et al., 1976), wind shears being the sources of hydrodynamic turbulence at  $h > 100$  km. Thus, the conditions of  $E_s$  formation and those of dynamical stability conservation prove to be interconnected, a fact which allows us to consider  $E_s$  to be a natural indicator of the turbopause.

An important property of  $E_s$  is transparency, caused by the scattering of radio waves at small-scale irregularities of electron density, those are from random turbulent motions (GERSHMAN and OVEZGELDIYEV, 1973). The increase of turbulence intensity leads to the increase of  $E_s$  inhomogeneity extent and to the increase of the scattered energy part. It leads to the increase of  $E_s$  transparency range ( $f_h/f_o$ ). We say in this respect that the value of the transparency range is a measure of the turbulence intensity at the height of the sporadic layer. Thus, studying  $E_s$  behaviour one can realize some of the characteristics of lower thermosphere turbulence. These statements are confirmed by investigating the dynamical structure of the turbopause by means of a spectrum analysis method.

To illustrate the above mentioned, see Figure 1 where the profiles of  $E_s$  transparency range are given for Ashkhabad, the data having been obtained by hourly observations in 1957-65 at daytime (solid line). The dotted line represents the probability of  $E_s$  occurrence at various heights. A common feature for all profiles is the transparency increase at the height of 90-100 km, indicating turbulence intensification at this height level. Since a transparency range of less than 0.1 (in relative units) is induced by radio wave reflection from a thin layer but not by a scattering on the irregularities (KORSUNOVA, 1974), its corresponding height indicates a level where turbulence does not play any significant part, i.e., the turbopause. It is evident that the height of maximum  $E_s$  occurrence coincides with this level within a few kilometers.

Time spectra of the critical frequency  $f_oE_s$  and blanketing frequency  $f_bE_s$  for the records of a spaced chain of ionosphere vertical sounding stations have been studied by means of a maximum entropy method, while coherence spectra were analysed with the Blackman and Tukey method (KARADZSHAYEV, 1982). It has been found out that the frequency parameters spectrum of  $E_s$  within the range of 1-10 cycles/h is discrete with one or two maxima (Figure 2). The first, a low frequency maximum with  $T=40$  min, is of larger amplitude, stable and

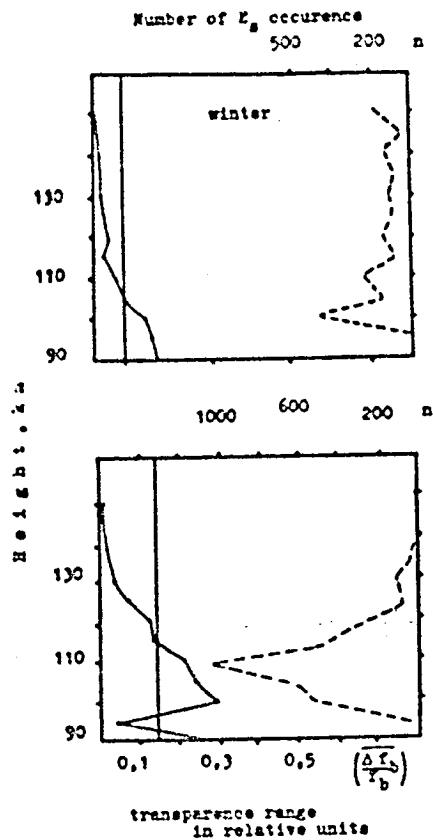


Figure 1. Height profiles of  $E_s$  occurrence and transpance range  $\left(\frac{\Delta f}{f_b}\right)$  for Ashkhabad.

exists permanently; the second one with  $T=10$  min is less stable, occurs irregularly and more often so within  $f E_s$  spectra. Further, the first maximum corresponds to a higher level of coherence which decreases as the distance between the stations increases. Analysing these results in terms of the theory of  $E_s$  formation at mid-latitudes, one can conclude that the low-frequency maximum is induced by cellular eddies, usually interpreted as wind shears with horizontal dimensions of not more than 300 km. Irregularity, small amplitude and low coherence in the range of the second maximum are indicative of the fact that turbulence must be its only source. Horizontal dimensions of the corresponding eddies, which are about 40 km, may be regarded as an indication of the outer scale of turbulence. A corresponding spectrum of turbulence in the region of the outer scales is defined by the expression  $E(k) \sim k^{-3}$ .

Figure 3 shows diurnal variations of (a) the most probable heights of  $E_s$  and (b) transpance range characterizing the behaviour of the turbopause height and of turbulence intensity for summer solstice conditions. It is obvious that

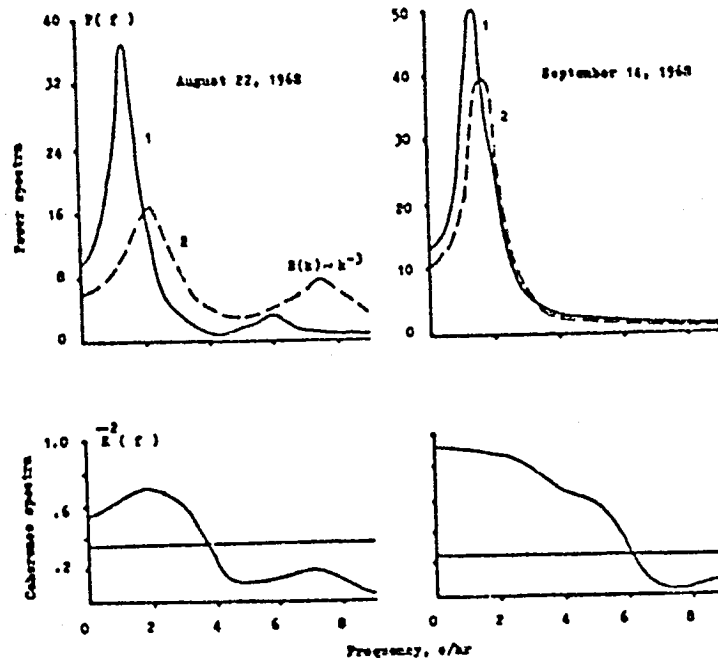


Figure 2. MEM power spectra  $f_{\alpha} E_{\alpha}(1)$ ,  $f_{\beta} E_{\beta}(2)$  and coherence spectra of these parameters.

at mid-latitudes  $h_T$  varies with a semi-diurnal period, reaching its maximum at 0600 and 1800 LT with an amplitude of  $\sim 10$  km. As it is clear from transparency range variations, turbulence intensity varies with a diurnal period, reaching its maximum at night. The amplitude of variations from day-time till night is by a factor of 3.

Annual variations of the above-mentioned turbopause parameters for night hours are represented in Figure 4 where the vertical lines give the dispersion when computing the average. Figure 4 shows that the character of  $h_T$  variations depends upon latitude. At  $<50^{\circ}\text{N}$  the turbopause height varies with an annual period, increasing in summer and decreasing in winter. At  $>50^{\circ}\text{N}$  besides a summer maximum there exists a winter maximum as well. The amplitude of variations increases with latitude, but does not exceed 7 km. Turbulence intensity has a semi-annual variation with maxima at solstices, the winter maximum amplitude increasing as the latitude increases. Circles in the figure represent the results of the turbopause height measurements in the rocket experiments and a small-scale turbulence (1-5 km) intensity, defined by the fading meteor trail reflections for the corresponding latitudes (TEPIN, 1976; VON ZAHN, 1970; SCHOLZ and OFFERMANN (1974); ROSENBERG et al., 1973); GOLOMB, 1974; SCHAEFFER, 1969; TRINKS et al., 1978). It may be noted that there exists a satisfactory agreement in the order of values of the turbopause height and with the character of the annual variations of turbulence intensity, measured by different methods. Regularities of the turbopause space and time variations deduced, are also characteristic of the southern hemisphere stations, situated in other longitudinal zones.

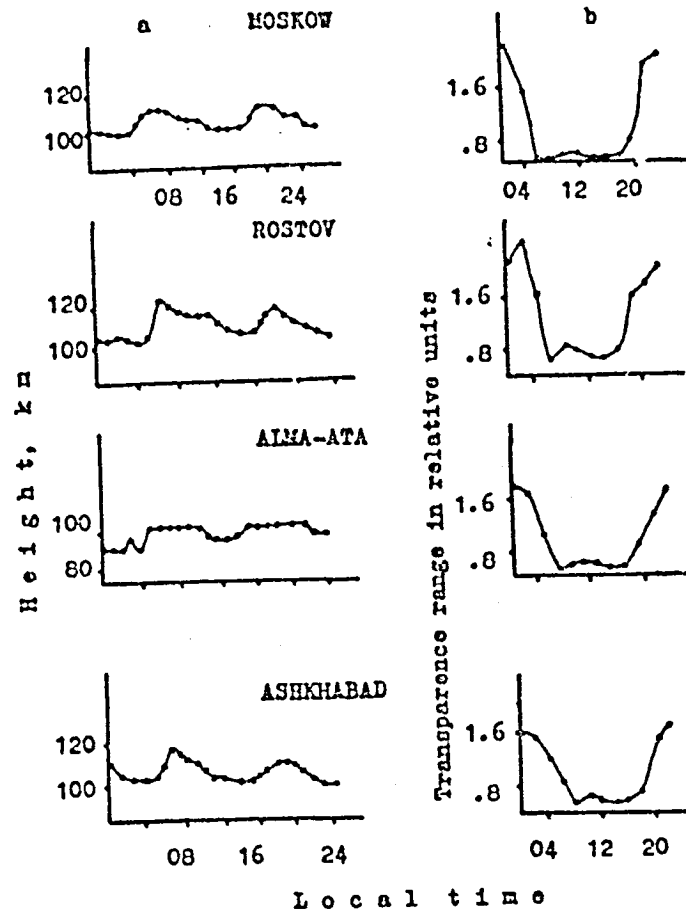


Figure 3. Diurnal variations of the most probable heights of  $E_s$  ( $\overline{hE_s}$ ) and transparency range  $\left(\frac{\Delta f_b}{f_b}\right)$  for summer solstice.

Thus, from the above, one can come to the following conclusions:

- (1) turbulence intensity is higher at night than in the daytime;
- (2) the height of the turbopause in latitudes 30-60°N is higher in summer than in winter and at equinoxes;
- (3) variations of the intensity of the turbulent processes are characterized as semi-annual, with maxima at solstices and minima at equinoxes;
- (4) the amplitude of both turbopause parameters increases as the latitude increases.

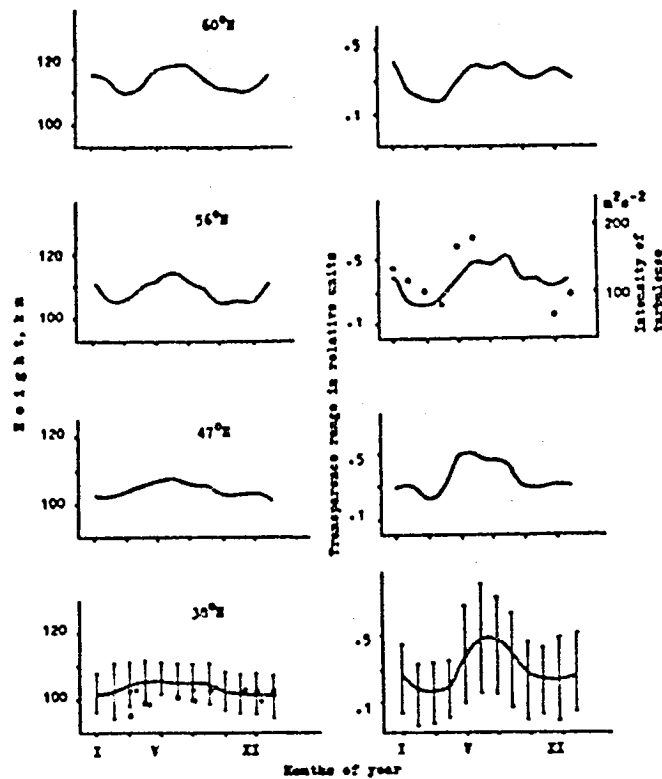


Figure 4. Annual variations of the turbopause heights and intensity of turbulence for nighttime. Circles refer to the results of rocket measurements.

#### REFERENCES

- Gershman, B. N., Yu. A. Ignatiev and G. N. Kamenetskaya (1976), Formation Mechanisms of Ionospheric Sporadic Layer E<sub>s</sub> at Different Latitudes, "Nauka", Moscow.
- Gershman, B. N. and O. G. Ovezgeldiyev (1973), Proc. Academy of Sci. of the USSR, Ser. Phys.-Tech., Chem. and Geol. Sciences, 4, 35.
- Golomb, D. (1974), Space Res. XIV, 103, Akademie-Verlag, Berlin.
- Karadzhayev, Yu. (1982), Proc. Academy of Sciences of the USSR, Ser. Phys.-Tech., Chem. and Geol. Sciences, 2.
- Korsunova, L. P. (1974), Geomagn. and Aeronomy, 14, 160.
- Ovezgeldiyev, O. G., L. P. Korsunova and T. I. Bivaltseva (1976), Geomagn. and Aeronomy, 16, 358.
- Rosenberg, N. W., D. Golomb, S. P. Zimmerman, W. K. Vickery and J. S. Theon (1973), Space Res., XIII, 435, Akademie-Verlag, Berlin.
- Schaefer, E. (1969), J. Geophys. Res., 74, 3488.
- Scholz, T. G. and D. Offermann (1974), J. Geophys. Res., 79, 307.
- Teptin, G. H. (1976), Structure of the Low Thermosphere, Kazan. Univ.
- Trinks, H. et al. (1978), J. Geophys. Res., 83, 2169.
- Von Zahn, U. (1970), J. Geophys. Res., 75, 5517.

N85

20484

UNCLAS

D34  
188

# N 85 - 2048.4

## THE HIGH-LATITUDE D-REGION DURING ELECTRON PRECIPITATION EVENTS

J. K. Hargreaves\*, P. N. Collis\* and A. Korth\*\*

\*Department of Environmental Sciences, University of Lancaster  
Bailrigg, Lancaster, England.

\*\*Max-Planck-Institut für Aeronomie, Postfach 20,  
D-3411 Katlenburg-Lindau 3, FRG.

The paper is concerned with the fluxes of energetic electrons entering the high-latitude atmosphere during auroral radio absorption events, and with their effect on the electron density in the auroral D region. We attempt to calculate the radio absorption during precipitation events from the fluxes of energetic electrons measured at geosynchronous orbit, and then consider the use of absorption measurements to indicate the magnetospheric particle fluxes, and the production rates and electron densities in the D region.

Although riometers have been operated at high latitudes since the International Geophysical Year of 1957-58, and despite a general acceptance that in the auroral zones they register the effects of energetic electrons which reach the D region during precipitation events, there has persisted a lack of hard evidence on the cause-and-effect relationships involved. It has not been clear, for example, which part of the electron spectrum causes most of the auroral radio absorption, or how exactly one can account for the absorption quantitatively from knowledge of the electron spectrum. Further, it has not been established whether radio-absorption measurements using riometers can serve to indicate the magnetospheric fluxes, the fluxes reaching the atmosphere, or the resulting electron density distribution in the lower ionosphere - though useful results from rockets have recently been published concerning the last point (Friedrich and Torkar, 1983; Miyazaki et al., 1981). Considering the advantages of the riometer technique as an auroral monitor (simplicity and continuity of operation, and suitability for use in a network), and an increasing tendency to combine riometer data with measurements from other ground-based techniques such as cameras and magnetometers in auroral studies, it would be a great advantage to have a more specific interpretation of riometer data. The comparison which we attempt here therefore has a practical aspect as well as the scientific one.

There are several links in the chain of events connecting magnetospheric particles with auroral radio absorption:

Particle fluxes at geosynchronous orbit  
↓  
Ionospheric particle precipitation  
↓  
Electron production rate  
↓  
Electron density profile  
↓  
Radio absorption profile  
↓  
Total radio absorption.

The ionospheric production rate has been calculated from the incoming spectrum of energetic electrons using the method of Rees (1963). The conversion of an electron-density profile to an absorption profile is straightforward given an appropriate neutral-atmosphere model, and the final integration to total absorption is trivial. Since there are uncertainties about the ionospheric loss rates linking production rate to electron density, we may be able to narrow the

possibilities here; however, it turns out that there are also major effects in the relation between magnetospheric particles and those reaching the ionosphere.

Penman et al. (1979 a, b) attempted to calculate auroral radio absorption using particle data from the geosynchronous ATS-6. Those data included electron energies only up to 80 keV, and one result of the investigation was that although the 40-80 keV band was important in auroral absorption production, extrapolation of the spectrum suggested that the 80-160 keV band should also be important. Although reasonable agreement between calculated and observed absorption was obtained for some events, the smaller events presented greater difficulty.

The present study uses the medium-energy charged-particle spectrometer on GEOS-2, which covers the energy range 15-300 keV. The detector reception angle is rectangular,  $\pm 2^\circ$  by  $\pm 3^\circ$ , and the standard data processing sorts the fluxes into bins according to pointing angles (with respect to the geomagnetic field, whose orientation is known from the magnetometer) of  $0^\circ - 5^\circ$ , then every  $10^\circ$ , up to  $175^\circ - 180^\circ$ . There are 15 energy ranges, the energy being determined by pulse height analysis. The events studied were selected using the University of Lancaster riometer network in Scandinavia. To try to ensure that the GEOS footprint was close to the ground stations events were only used if there was similarity of time variation between the absorption event and the satellite particle flux, and if the absorption event was fairly uniform over the riometer network. The absorption was calculated from the measured  $0^\circ - 5^\circ$  fluxes for 37 occasions between September 1978 and June 1979, two thirds of them during the winter months. The absorption measured at 30 MHz ranged between 0.1 dB and 6.0 dB. Initially, a height profile of the effective recombination coefficient,  $\alpha_e$ , was assumed on the basis of published literature.

Calculations of the absorption assuming that the measured  $0^\circ - 5^\circ$  flux is indeed the flux precipitated into the atmosphere give values that are about right for large events but are consistently over-estimates for the small events. Taking the ratio  $R = A_{\text{obs}}/A_{\text{calc}}$ , where  $A_{\text{obs}}$  and  $A_{\text{calc}}$  are respectively the observed and calculated absorption values, it is found that the variation of R with  $A_{\text{obs}}$  is well represented by a relation

$$R = 1.15 \tanh (A_{\text{obs}}/3.3).$$

The use of the function  $\tanh$  is purely empirical and at this stage has no significance other than that it fits the data. The constant 1.15, whose value in any case depends on the magnitude of  $\alpha(h)$ , represents the fact that wide-beam riometer data tend to overestimate the true (or zenithal) absorption because of the obliquity of some of the received cosmic-noise signals. Its precise value is not germane to the present analysis. We note in passing that of the data points about one-third represent daytime (i.e. sunlit ionosphere) and two-thirds night (dark ionosphere), but the same procedure works equally well for both sets and it appears, therefore, that solar illumination has no significant effect.

It seems likely that the departure of R from a constant value stems from the assumption that the flux recorded by the GEOS detector within pointing angles  $0^\circ - 5^\circ$  is the flux actually precipitated into the atmosphere. The theory of pitch-angle diffusion given by Kennel and Petscheck (1966) shows that there will be a distribution of pitch angles within and just outside the loss cone. Since the theoretical loss cone in our case is  $2.6^\circ$ , the detector will record particles outside the loss cone that do not reach the atmosphere. How serious this is depends on the pitch angle diffusion coefficient, D. If D is sufficiently large we have strong diffusion, with the loss cone re-filling rapidly and an almost uniform distribution of pitch angles. In this extreme

the  $0^\circ - 5^\circ$  flux indeed represents the flux in the loss cone. But if  $D$  is small, diffusion is weak and there will be a hole in the pitch-angle distribution, a depletion to which the  $\pm 2^\circ$  by  $\pm 3^\circ$  detector is relatively insensitive.

Calculations based on the Kennel and Petscheck theory have been carried out to predict the response of the detector as functions of pointing angle and diffusion coefficient, and by going back to the raw particle data examples have been found which tend to confirm that the loss cone is more depleted (relative to the region just outside the loss cone) for weak absorption events than for stronger ones.

For an  $\alpha$ -type loss process the radio absorption should be proportional to the square root of the production rate. We therefore identify the term  $\tanh(A_{\text{obs}}/3.3)$  with  $(F_p/F_m)^{1/2}$ , where  $F_p$  is the flux precipitated (i.e. within the  $2.6^\circ$  loss cone) and  $F_m$  is the  $0^\circ - 5^\circ$  measured flux. From this relation it is seen that  $F_p/F_m$  exceeds 50% if  $A_{\text{obs}} > 3$  dB, but is only 10% if  $A_{\text{obs}} = 1$  dB. To get the ratio over 90%, approaching an isotropic particle distribution therefore, the observed absorption must exceed 6 dB. Absorption events as large as this are infrequent. (During the whole IMS period of 4 years there were only about 35 events  $> 6$  dB in Scandinavia). It seems, therefore, that most auroral absorption events occur under conditions of less than strong diffusion.

It is also possible to relate the magnitude of the absorption event to that of the diffusion coefficient. Values range between about  $1 \times 10^{-2} \text{ s}^{-1}$  to  $3 \times 10^{-5} \text{ s}^{-1}$  from strong to weak absorption events.

Having derived a method for calculating the radio absorption from particle fluxes measured at geosynchronous orbit, we now consider what absorption measurements using a riometer can tell us about magnetospheric particles and about D-region electron densities, and what reliance can be placed on such estimates. For this purpose the precipitating electrons are considered in energy bands 20-40 keV, 40-80 keV, 80-160 keV and 160-320 keV. Plots of the energy flux within a given band and over pointing angles  $0^\circ - 5^\circ$  show the association with the measured radio absorption to be best for the 40-80 keV and 80-160 keV energy bands. The band 160-320 keV show no significant association, indicating that these particles do not usually produce much auroral absorption. For the 40-80 keV and 80-160 keV bands it appears that the measured auroral absorption provides a worthwhile indicator of the energy flux if the absorption exceeds 2 dB. Below that level it places an upper limit on the energy fluxes. Equations have been derived for these relationships, both for  $0^\circ - 5^\circ$  and for trapped ( $85^\circ - 95^\circ$ ) particles. No day-night difference is evident.

The procedure has been carried through to estimates of electron-ion production rates and electron densities, both as a function of height in the D region. As an example, the estimated production rate ( $Q$ ) at  $85 \text{ km}$  is related to the 30 MHz absorption ( $A$ ) by  $Q = 4620 A^2$ , where  $Q$  is in  $\text{cm}^{-3} \text{ s}^{-1}$  and  $A$  is in dB. The scatter of the data points suggests that a prediction using this formula would be correct to within a factor of 2 on 95% of occasions. In converting production rates to electron densities several profiles of the effective recombination coefficient,  $\alpha(h)$ , were tried, and the final choice (which is entirely consistent with published estimates of  $\alpha$ ) was influenced by reference to rocket data on D-region electron densities during auroral absorption events. The procedure eventually arrived at gives electron density profiles that agree reasonably well with the analyses of accumulations of rocket data by Friedrich and Turkar (1983) and by Miyazaki et al. (1981).

This study is being published in full in the Journal of Atmospheric and Terrestrial Physics.

## REFERENCES

- Friedrich, M. and K. M. Torkar (1983), J. Atmos. Terr. Phys., 4, 77.
- Kennel, C. K. and H. E. Petscheck (1966), J. Geophys. Res., 71, 1.
- Miyazaki, S., T. Ogawa and H. Mori (1981), Memoirs Nat. Inst. Polar Res. Japan, Special Issue No. 18, p. 304.
- Penman, J. M., J. K. Hargreaves and C. E. McIlwain (1979a), Planet. Space Sci., 27, 445.
- Penman, J. M., J. K. Hargreaves and C. E. McIlwain (1979b), Space Research, 19, 363.
- Rees, M. H. (1963), Planet. Space Sci., 11, 1209.

N85

20485

UNCLAS

N85-20485

HIGH-ENERGY PARTICLE EFFECTS IN THE D-REGION DURING  
AND AFTER GEOMAGNETIC STORMS

E. A. Lauter and C. -U. Wagner

Academy of Sciences of the G.D.R.  
Central Institute of Solar-Terrestrial Physics  
(Heinrich-Hertz-Institute)  
DDR-1199 Berlin-Adlershof, G.D.R.

## ABSTRACT

The precipitation of energetic particles from the magnetosphere produces a remarkable modification of the mid-latitude D-region structure during daytime and at dawn and dusk conditions. Beside the heavily fluctuating precipitation during the main storm phase there exists a more continuous input of high energy electrons into the mesosphere in the belt between  $\phi = 50^\circ$  and the auroral zone up to ten days after the disturbance. The excessive D-region ionisation, the after-effect of geomagnetic storms, is caused at least partly by additional nitric oxide production. Especially the winter anomaly effects are amplified and prolonged by this effect. The source of this mid-latitude particle precipitation is thought to be situated in magnetospheric slot region processes.

N85

20486

UNCLAS

N 85 - 2048 6

193

SOLAR FLARE AND IMF SECTOR STRUCTURE EFFECTS IN THE LOWER IONOSPHERE

J. Lastovicka

Geophysical Institute, Czechoslovak Academy of Sciences  
141 31 Prague 4, Czechoslovakia

ABSTRACT

About 1% of all SIDs observed at the Panska Ves Observatory (Czechoslovakia), has been found to be not of solar-XUV origin. Among them, the very rare SWF events (observed at  $L = 2.4$ ) of corpuscular origin are the most interesting.

The IMF sector structure effects in the midlatitude lower ionosphere are minor in comparison with effects of solar flares, geomagnetic storms, etc. There are two basic types of effects. The first type is a disturbance, best developed in geomagnetic activity, and observed in the night-time ionosphere. It can be interpreted as a response to sector structure related changes of geomagnetic (= magnetospheric) activity. The other type is best developed in the tropospheric vorticity area index and is also observed in the day-time ionosphere in winter. This effect is quietening in the ionosphere as well as troposphere. While the occurrence of the former type is persistent in time, the latter is severely diminished in some periods (e.g. 1974-77). All the effects are stronger for so-called "proton" sector boundaries. As regards the stratosphere, the 10-mb level temperature and height above Berlin-Teepelhof do not display any observable IMF sector structure effect.

SOLAR FLARE EFFECTS

Are all sudden ionospheric disturbances (SID), recorded at high midlatitudes, of solar flare origin (or more precisely of solar-XUV origin)? About 1% of all SIDs, observed at the Panska Ves Observatory (Czechoslovakia) during the period 1960-1973, has been found to be not of solar XUV-origin. The SID monitoring system at Panska Ves consists of SWF, SFA, SEA and SDA. Almost all peculiar SIDs, however, have been recorded by one SID monitoring method only. Among them, the very rare SWF events of corpuscular origin, observed at  $L = 2.4$ , are most interesting. They are shown in Table 1. The first event was observed under quite calm solar conditions. The second event was associated with a very weak radio burst at the beginning of the event, and with a very weak radio burst and subflare near the end of the event. The third event was accompanied by an unconfirmed flare with its maximum before the beginning of the event. None of these three events was associated with X-ray bursts. On the other hand, these events were observed under considerably enhanced geomagnetic activity, which is favourable for precipitation of high-energy electrons ( $E > 20-40$  keV).

A similar event was observed on 17 June 1970 near noon (1048-1055-110 UT) as a SWF of a medium importance and a very weak SFA accompanied by a weak flare with quite insufficient X-ray flux to explain the observed SWF. The event was observed near the maximum of a moderate geomagnetic storm. Fortunately, the COSMOS-348 satellite, which measured high-energy electrons (both trapped and penetrating fluxes, crossed  $L = 2.4$  at 1052 UT (i.e. during the event). Figure 1 shows energetic spectra of trapped electrons observed at the same local time and place at  $L = 2.4$  during the event and during a strong geomagnetic storm a few days later. These spectra demonstrate well the extremely strong and unexpected enhancement of high-energy electrons during the event. Fluxes of precipitating electrons were sufficiently large to explain the observed SWF.

Table 1: Peculiar SWF events of corpuscular origin, recorded at 2775 kHz (reflection point 52°27' N, 12°27' E, L = 2.4) and 2614 kHz (reflection point 52°08' N, 11°00' E, L = 2.4). x - unconfirmed flare.

Date	start	max SWF	end	imp	X-rays (1.8Å)	Optical flare		Radio burst			K <sub>p</sub>	
						start	end	imp	start	end		imp
1971 09/25	0602	0610	0627	1	no burst	no flare		no burst			5-29*	
1972 08/26	0637		0737	2	no burst	0718	0736 -N	0633	0638 weak	0706	0712 weak	5-25-
1973 10/18	1249		1330	1	no burst	1236	1254 IF <sup>x</sup> max 1238	no burst			5-28*	

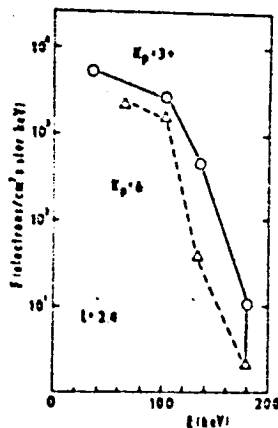


Figure 1. Energetic spectra of trapped electrons between 20-200 keV at L = 2.4 for the SID event in question (top curve) and for a severe geomagnetic storm (bottom curve) as measured onboard COSMOS-348 (after LASTOVICKA and FEDOROVA, 1976).

(LASTOVICKA and FEDOROVA, 1976). Unfortunately, this result is not full proof, because the satellite measurements were performed over the Southern Hemisphere, but it strongly supports the corpuscular origin of such peculiar SWFs.

#### IMF SECTOR STRUCTURE EFFECTS

There are several effects of the interplanetary magnetic field (IMF) - those of the north-south component  $B_z$ , those of changes of polarity of the azimuthal,  $B_y$ , and radial,  $B_x$ , components, and those of crossing of the IMF sector boundary. The effects of changes of polarity and magnitude of all three IMF components in the lower ionosphere are essentially a response to the IMF generated changes in geomagnetic (i.e., magnetospheric substorm) activity. This not the case, however, when the IMF sector boundary crossing effects are concerned.

The IMF sector boundary is a well developed physical structure, a warped current sheet (WILCOX, 1979) dividing the interplanetary space into two parts with opposite prevailing  $B_z$  polarity. A crossing of such a well-developed space structure, accompanied by an increase of the IMF magnitude  $B$  (LASTOVICKA, 1979) and of its geosactive southward component  $B_z$  (SCHREIBER, 1977), affects the Earth's magnetosphere, ionosphere and even troposphere.

There are two basic types of responses to the IMF sector boundary crossing (Fig. 2), both being observed, among others, in the ionosphere. The geomagnetic type is manifested best in geomagnetic activity. This effect is a disturbance and consists in a change across the sector boundary and in a significant difference between the level before and after boundary crossing. In equinoctial periods, the effect of IMF polarity changes ( $B_z$ ) becomes comparable to that of the sector boundary crossing itself. The effect has been observed in  $B_z$  southward  $B_z$  and cosmic rays (LASTOVICKA, 1979). The tropospheric type is manifested best in the tropospheric vorticity area index (VAI) and consists in a narrow deep depression centered at the day of boundary crossing. This effect is quietening, not a disturbance.

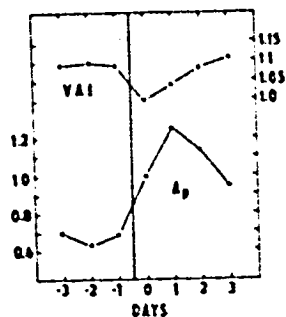


Figure 2. The IMF sector boundary crossing effect of the geomagnetic type in  $A_p$  (logarithmic mean) and of the tropospheric type  $P$  in VAI (tropospheric vorticity area index at the 500 mb level). The data are expressed in ratio to the zero-day values. Vertical line - boundary crossing (reported to 00 UT).

Figure 3 shows the geomagnetic type effect in the nighttime radio wave absorption in the lower ionosphere over Central Europe in winter. The absorption is higher after the crossing than before at both frequencies. The effect in absorption is much weaker than that in  $A_p$ , minor in comparison with geomagnetic storm or solar activity effects in the lower ionosphere.

In order to estimate the statistical significance of data points in Figs. 3-5, the significance of the difference between extreme mean data points,  $P$ , and the probability of this difference being positive in individual crossings,  $B$ , are given in Table 2.  $P$  represents mainly the reliability of the effects, while  $B$  mainly their importance. The effect at 245 kHz is statistically significant and important but the effect at 272 kHz appears to be unimportant. This is caused by different L-shells of reflection points - 2.7 and 2.1. Fluxes of precipitating electrons controlled by geomagnetic activity are considerably weaker at  $L = 2.1$ .

The geomagnetic-type effect is observed in the lower ionosphere in winter only at night. In equinoctial periods, we can again observe the geomagnetic-type effect in absorption only at night. No significant effect is observed near noon. The boundary crossing effect itself is a little weaker than that in winter, but the effect of changes in IMF polarity is comparable to (or even stronger than) that of boundary crossing (LASTOVICKA, 1982).

Figure 4 shows the tropospheric type effect in the noon radio wave absorp-

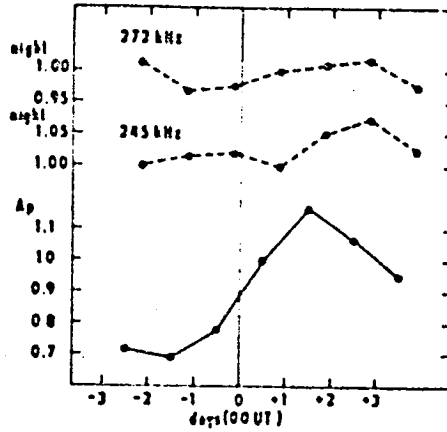


Figure 3. The geomagnetic-type effect in  $A_p$  and nighttime radio wave absorption in the lower ionosphere over Central Europe in winter (1966-73 - after LASTOVICKA, 1979). The data are expressed in ratio to the crossing-day values.

Table 2: Statistical significance of the difference between extreme mean data points, P, the probability of this difference being positive in individual crossings, B, and the number of boundary crossings used, n.

	night			day	
	272 kHz	245 kHz	2775 kHz	245 kHz	5kHz
P	86%	99.5%	98.5%	99.5%	99%
B	57%	64%	62%	64%	62%
n	41	69	56	70	61

tion in the lower ionosphere over Central Europe in winter. The behaviour of the absorption is similar to that of VAI - a narrow decrease of absorption (even if considerably smaller than that in VAI), i.e. quietening in the lower ionosphere, just after boundary crossing. Table 2 shows that the effect is statistically significant and important at both frequencies. The effect of such type is observed in the lower ionosphere in winter during day-time only.

Figure 5 shows the IHF sector boundary crossing effect at the 5 kHz and 27 kHz integrated level of atmospheric absorption observed in Central Europe in winter. In view of differences in the patterns from different observatories, of the shape of curves and of the low statistical significance of the results, hardly any effect can be observed at 27 kHz. However, the 5 kHz atmospheric absorption display

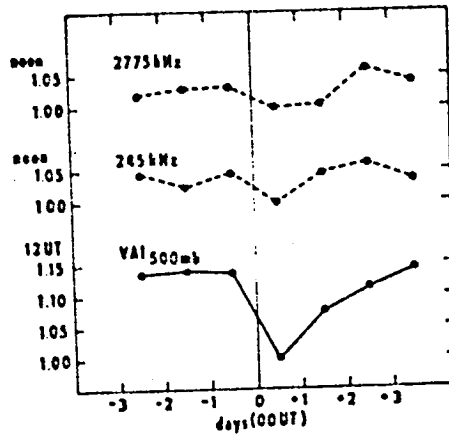


Figure 4. The tropospheric-type effect in  $VAI_{500mb}$  and noon radio wave absorption in the lower ionosphere over Central Europe in winter (1966-73 - after LASTOVICKA, 1979).

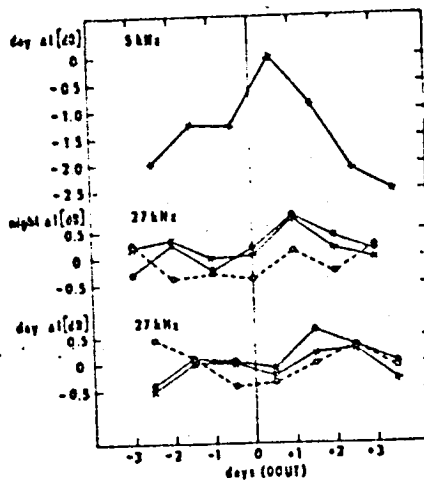


Figure 5. Sector boundary crossing effects in 5 kHz and 27 kHz atmospherics in winter (1966-73 - LASTOVICKA and SATORI, 1982). Full circles - Uppsala (59.8°N, 17.6°E); open circles - Kuhlungsborn (54.1°N, 11.8°E); crosses - Panska Ves (50.5°N, 14.6°E).

a sharp maximum just after crossing. The shape of the 5 kHz curve resembles an inverse form of the VAI curve from Fig. 4. Unfortunately, comparing the SID, geomagnetic storm and Forbush decrease effects in the 5 kHz atmospheric, it is difficult to say definitely, whether the observed effect is quietening or not.

As regards the stratosphere, the IMF sector structure effects were studied in the 10-mb level temperature and the 10-mb level height above Berlin-Tempelhof during day-time (LASTOVICKA, 1979). No significant effect was observed in either quantity in spite of the fact that statistically significant effects were observed in the lower ionosphere in the same geographic region.

General solar activity ( $F_{10.7}$ ) increased quasimonotonically from the -3 to the +2 day by about 1.5%. Thus the solar XUV radiation did not affect the obtained results significantly.

The  $f_{F2}$  response to the IMF sector structure is quite similar to that of the lower ionosphere. We observe simultaneously the geomagnetic-type effect in the lower ionosphere and the F2 region, and the same is valid also for the tropospheric-type effect (LASTOVICKA, 1982, 1983; LASTOVICKA and SATORI, 1982; TRISKOVA, 1982). There is only very weak (if any) effect of the IMF sector structure in the E-region over Central Europe (LASTOVICKA, 1982; LASTOVICKA and SATORI, 1982). Thus the vertical pattern of the IMF sector structure effect in the F2 region, small effect (if any) in the E-region, a significant effect in the lower ionosphere, no effect rather than any in the stratosphere and significant effect in the troposphere (only of the tropospheric type).

The geomagnetic type effect is ionospheric response to the IMF sector structure related changes in geomagnetic activity. It consists of two components - IMF polarity changes and the boundary crossing itself. According to my opinion, the latter effect is caused by crossing-related changes of E or geoactive southward  $B_z$ .

The tropospheric type effect is quite a new phenomenon. It cannot be explained in terms of geomagnetic, cosmic ray or general solar activity. The effect seems to be caused by an action of the sector boundary (= warped current sheet) itself. The main problem with finding the mechanism is that the effect is quietening. The effect looks like switching off, not switching on, an energy source. However, this is not acceptable to solar, solar wind and magnetospheric physics.

There are two factors, which make studies of the IMF sector structure effects more difficult. The tropospheric (but not the geomagnetic) type effect practically disappears in some periods. LASTOVICKA (1981) showed that, in the period 1974-1977, the tropospheric-type effect practically disappeared not only in the troposphere (VAI), but simultaneously also in the lower ionosphere. However, the situation in the years 1974-77 (solar minimum) was quiet enough. Perhaps no other important quietening was possible.

The geoactivity of different sector boundaries varies. SVESTKA et al. (1976) found some sector boundaries (called proton boundaries) to be followed by streams of low-energy protons. WILCOX (1979) found the effect of such proton boundaries in VAI, as well as in geomagnetic activity, to be considerably stronger than that of non-proton boundaries. Figure 6 shows the effect of proton as well as non-proton boundaries on radio wave absorption in the lower ionosphere in winter. The effects of proton boundary crossing are considerably stronger and evidently more important than the effects of crossings of non-proton boundaries. However, as far as I know, information on proton boundaries is available only for the period 1963-1969.

In conclusion it can be said that the IMF sector structure effects in the

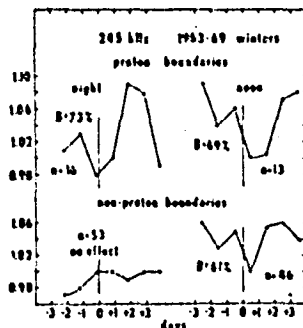


Figure 6. Sector boundary crossing effects in absorption at 245 kHz separated for night and noon, proton and non-proton sector boundaries. Winters 1963-1969. The data are expressed in ratio to the crossing-day values.

midlatitude ionosphere are minor in comparison with the effects of solar flares, geomagnetic storms etc., and are of two different types. The geomagnetic-type effect is a disturbance, representing an ionospheric response to changes in geomagnetic (= magnetospheric) activity, and its mechanism is at least qualitatively understood. The tropospheric-type effect is developed best in the tropospheric vorticity area index with possible relations to weather. It is a quietening, not a disturbance, in the troposphere as well as in the ionosphere. Its mechanism is not understood. The IMF sector structure effects are partly different for different seasons and they are considerably stronger for proton than for non-proton sector boundaries. I think the main task of this field of research is to discover the mechanism of the tropospheric-type effect and to determine the role of the IMF effects among various solar-terrestrial relations.

#### REFERENCES

- Lastovicka, J. (1979), *J. Atmos. Terr. Phys.*, **41**, 995.  
 Lastovicka, J. (1981), *Studia Geoph. et Geod.*, **25**, 208.  
 Lastovicka, J. (1982), *Studia Geoph. et Geod.*, **26**, 74-80.  
 Lastovicka, J. (1983), *Indian J. Radio Space Phys.*, (in print).  
 Lastovicka, J. and N. I. Fedorova (1976), *Geomag. and Aeronomy*, **16**, 1018.  
 Lastovicka, J. and G. Satori (1982), *Phys. Solariterrestris*, Potsdam, No. 18, 39-46.  
 Schreiber, H. (1977), *J. Geophys.*, **42**, 271.  
 Svestka Z., L. Fritzoza-Svestkova, J. T. Nolte, H. W. Dodson-Prince and E. R. Hedeman (1976), *Solar Phys.*, **50**, 490.  
 Triskova, L. (1982), *J. Atmos. Terr. Phys.*, **44**, 37.  
 Wilcox, J. M. (1979), *J. Atmos. Terr. Phys.*, **41**, 753.  
 Wilcox, J. M. (1979), *Nature*, **278**, 840.

N85

20487

UNCLAS

DEPENDENCE OF THE HIGH LATITUDE MIDDLE ATMOSPHERE IONIZATION  
ON STRUCTURES IN INTERPLANETARY SPACE

J. Bremer and E. A. Lauter

Academy of Sciences of the GDR,  
Central Institute of Solar-Terrestrial Physics,  
Observatory of Ionosphere Research, DDR-2565 Kuhlungsborn, GDR

As known from LAUTER et al. (1978) the precipitation of high-energetic electrons during and after strong geomagnetic storms into heights below 100 km in middle and subauroral latitudes is markedly modulated by the structure of the interplanetary magnetic field (IMF). In the present paper we want to show that also under relative quiet conditions the D-region ionization caused by high energetic particle precipitation (energies greater 20 - 50 keV) depends on changes of the interplanetary magnetic field and also on the velocity of the solar wind.

Following investigations by DUNGEY (1961) and by RUSSEL and McPHERRON (1973) the negative  $B_z$  component of the interplanetary magnetic field in the solar magnetospheric coordinate system should play an important role for the interaction of the solar wind with the magnetosphere and the accompanying acceleration processes. Such negative  $B_z$  components are induced in the solar magnetospheric coordinate system by the normal IMF sector structures only in dependence on regular daily and seasonal changes of the position of the dipole axis of the Earth's magnetic field in respect to the solar axis. If we assume a mean IMF field strength of 5 nT we obtain a seasonal variation of the vertical magnetic field strength in the solar magnetospheric coordinate system as shown in Fig. 1. Here we have calculated only daily mean values, neglecting the daily variation of  $B_z$ . Whereas T-sectors induce in spring maximum negative and in autumn maximum positive values, A-sectors cause opposite results. As we believe that negative  $B_z$ -values should favor particle precipitation into the lower ionosphere but positive  $B_z$ -values should reduce precipitation we define A-sectors in autumn and T-sectors in spring as so called 'pro-sectors', and T-sectors in autumn and A-sectors in spring as 'anti-sectors'.

To test this assumption, we have investigated the influence of IMF-sector boundary crossings on ionospheric absorption data of high and middle latitudes by the superposed-epoch method, with the first day of a new sector as "zero" key day. The dates of the sector crossings were taken from the catalog of SVALGAARD (1975), or from Solar Geophysical Data. In Fig. 2, the result of this analysis can be seen for noontime absorption measurements at vertical incidence on 1.75 MHz and 3.0 MHz as well as CNA observations on 22.4 MHz, obtained by the GDR participation groups during the 21st - 23rd Soviet Antarctic Expeditions at Novolazarevskaya (11.83°E, 70.77°S). A total of 67 sector crossings between June 1976 and November 1978 have been used. In the upper part of Fig. 2 the influence of all sector boundary crossings on the absorption data is presented (dashed-dotted lines) whereas in the lower part these data are subdivided into transitions from pro- to anti-sector (dotted lines) and from anti- to pro-sector conditions (full lines). In contrast to the small variations of absorption if all sector crossings are superimposed, a very pronounced influence of the IMF sector structure can be observed during the transition from anti- to pro- or pro- to anti-sector conditions. Absorption differences of about 8 -

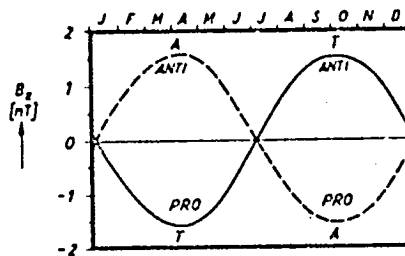


Figure 1. Mean seasonal variation of the  $B_z$ -component in solar-magnetospheric coordinate system for an undisturbed interplanetary magnetic field (magnitude  $B = 5$  nT) with A- and T-polarization.

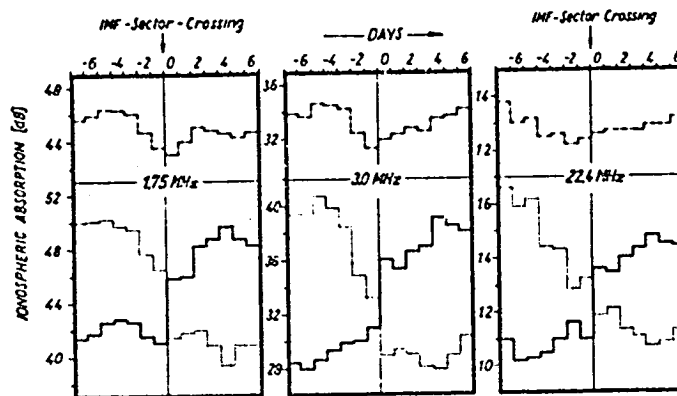


Figure 2. Variation of ionospheric absorption at high latitudes (Novolazarevskaya:  $70.8^{\circ}\text{S}$ ;  $11.8^{\circ}\text{E}$ ) during IMF-sector boundary crossings  
 -.-.-.-: all sector crossings  
 ———: only crossings from anti- to pro-sector  
 . . . .: only crossings from pro- to anti-sector

10 dB at 1.75 or 3 MHz, and about 0.4 dB at 22.4 MHz, demonstrate the importance of negative  $B_z$ -values of the IMF for the precipitation of high-energetic particles in high latitudes.

For the same sector boundary passages we have also investigated the behavior of  $f_{\text{min}}$ -data from ionosonde measurements in different latitudes. Fig. 3 shows the results. Whereas in high latitudes a strong dependence of the  $f_{\text{min}}$ -data on pro- and anti-sector condition could be detected, this influence is smaller in middle latitudes. A somewhat larger effect can be seen again at Port Stanley where particle precipitation is more effective because of the South Atlantic anomaly of the Earth's magnetic field. In lower latitudes there seems to be also a retardation of about 3 or 4 days of the ionospheric effect in respect to the sector crossing, most clearly seen for the anti- to pro-sector transition at Juliusruh and Port Stanley. This effect may be caused by the

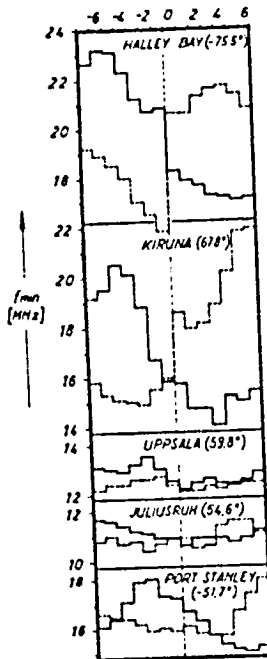


Figure 3. Variation of  $f_{\min}$ -data during IMF-sector boundary crossings in dependence on latitude (geogr. lat. in brackets)  
 . . . . : crossings from anti- to pro-sector  
 - - - - : crossings from pro- to anti-sector

diffusion of high-energetic electrons from high to middle latitudes, an effect which we know also from investigations of post storm events (LAUTER et al., 1979).

Besides the IMF sector structure, the velocity of the solar wind could be important for particle precipitation, especially in high latitudes. Therefore, we have also tested the influence of solar "high speed plasma streams" after a catalogue of LINDBLAD and LUNDSTEDT (1981). High speed plasma streams were mainly defined as solar plasma streams which increase their velocities by more than 100 km/s within 24 hours with simultaneous enhancements of their ion density and/or changes of the interplanetary magnetic field. From the period between 1964 and 75 we used 171 such streams with a duration of more than 4 days and investigated their influence on  $f_{\min}$ -data of Halley Bay, and on the geomagnetic AE index.

In Fig. 4 the results of a corresponding superposed-epoch analysis with the  $f_{\min}$ -data are represented. The "zero" key day is the beginning of the high speed plasma stream. The data analysis was made for two data sets: high speed plasma streams with small velocity changes  $\Delta v \leq 230 \text{ km s}^{-1}$  (a) and large velocity changes  $\Delta v \geq 300 \text{ km s}^{-1}$  (b). With the beginning of the plasma stream also the ionospheric absorption increases, rather slightly at low velocity streams (a) but very pronouncedly with high velocity streams (b). In the lower part of Fig. 4 the two collectives of data were again divided into streams with IMF of pro- and anti-sector conditions. For low velocity streams (c) the influence of the sector structure dominates markedly, e.g. plasma streams during anti-sector conditions cause far less particle precipitation than before the occurrence of the streams. At high velocity streams (d) the precipitation during the stream is always higher than before, but again markedly modulated by the IMF sector structure.

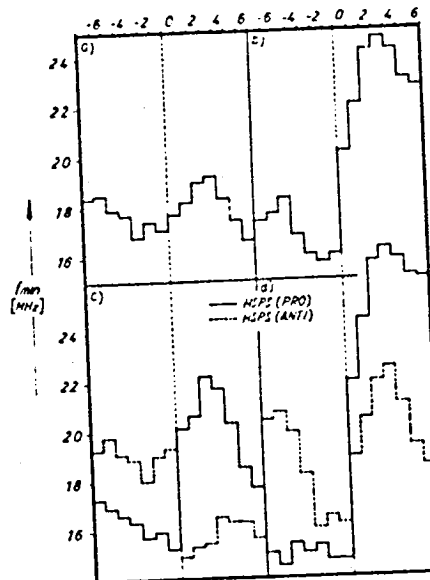


Figure 4. Variation of  $f_{\min}$ -data (Halley Bay) during high speed plasma streams (HSPS) with  $\Delta v < 230$  km/s (a and c) or  $\Delta v > 300$  km/s (b and d). In (c) and (d) the data of (a) and (b) are subdivided corresponding to their IMF polarity during pro- and anti-sector conditions.

For investigating a comparable dependence of the lower energetic particle precipitation we have chosen as indicators the geomagnetic  $A_p$  index and the auroral electrojet index, AE, which are mainly produced by ionospheric currents in polar latitudes between about 100 and 120 km corresponding to 1 - 10 keV electron precipitation, in contrast to the absorption measurements which may be influenced below 100 km corresponding to energies of more than 20 keV. Fig. 5 shows the result of a superposed-epoch analysis of AE-values for the same high speed plasma streams as in Fig. 4. The lower-energetic particle precipitation is positively correlated with the velocity changes of the plasma streams, too, but in contrast to the  $f_{\min}$ -values the influence of sector structure changes is obviously not so dominant. For instance, with low velocity plasma streams the AE Index is enhanced also with IMF anti-sector conditions, contrarily to the  $f_{\min}$ -variations in Fig. 4. These differences in particle precipitation at different energies indicate that the higher-energetic electron precipitation is stronger controlled by sector structure changes than the lower one. This can be a hint that the IMF structures do differentiate the magnetospheric acceleration processes of energetic particles. Finally the following conclusions should be mentioned: The presented results on the dependence of particle precipitation on the negative  $B_z$ -component of the interplanetary magnetic field and on the velocity of the solar wind support the concept of AKASOFU's energy transfer function (PERREAULT and AKASOFU, 1978) as a first approximation for the description of the energy transfer from the solar wind into the atmosphere. The observed differences in the precipitation of particles in dependence on their energy, however, cannot be explained by this energy transfer function.

For investigations of the influence of IMF sector boundary crossings upon the plasma of the middle atmosphere the different physical behaviour of the

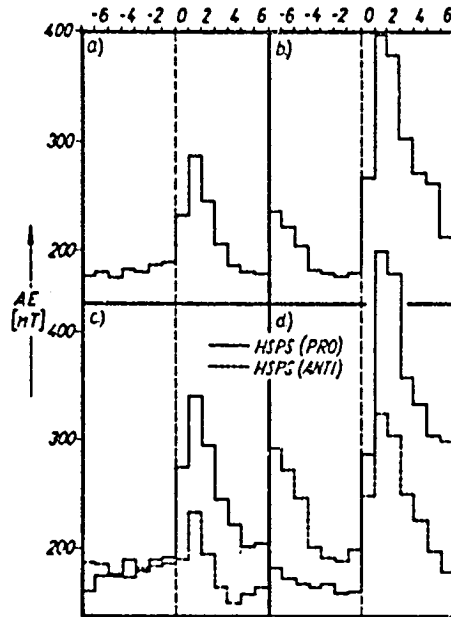


Figure 5. Same as in Fig. 4 but for AE-data.

IMF-sectors during the spring and autumn halfyear should be taken into consideration. Our classification of IMF-sectors after their B-components in the solar magnetospheric coordinate system (pro-, anti-sectors) seems to be more appropriate than the usual classification after the direction of the IMF in relation to the sun (A- and T-sectors).

As the excessive D-region ionization due to precipitation of high energetic particles markedly influences the radio wave propagation especially in high latitudes, the derived dependence of particle precipitation on structures of the interplanetary magnetic field can improve the prediction of radio propagation conditions in polar regions.

#### REFERENCES

- Dungey, J. W. (1961), *Phys. Rev. Lett.*, **6**, 47.  
 Lauter, E. A., J. Lstovicka and T. ZS. Rapoport (1978), *Phys. Solariterr.*, Potsdam, No. 7, 73.  
 Lauter, E. A., A. Grafe, B. Nikutowski, J. Taubenheim and C. U. Wagner (1979), *Gerlands Beitr. Geophys.*, Leipzig, **88**, 73.  
 Lindblad, B. A. and H. Lundstedt (1981), *Solar Physics*, **74**, 197.  
 Perreault, P. and S. I. Akasofu (1978), *Geophys. J. R. Astr. Soc.*, **54**, 547.  
 Russel, C. T. and R. L. McPherron (1973), *J. Geophys. Res.*, **78**, 92.  
 Solar Geophysical Data. NOAA, National Geophysical Data Center, Boulder, Colorado.  
 Svalgaard, L. (1975), SUIPR Report No. 629.  
 UAG-Reports No. 22, 29, 31, 33, 37, 39, 45, 47, 59, 73, 76, WDC A for Solar-Terr. Phys. NOAA Boulder, Colorado.

N85

20488

UNCLAS

N 85 - 20488 <sup>D33</sup>  
205

SOLAR-TERRESTRIAL INFLUENCES ON THE D-REGION AS SHOWN  
BY THE LEVEL OF ATMOSPHERIC RADIO NOISE

G. Satori\* and B. Schaning\*\*

\*Geodetical and Geophysical Research Institute of the Hungarian Academy of  
Sciences, H-9401 Sopron, Hungary

\*\*Central Institute of Solar-Terrestrial Physics, Observatory of Ionosphere  
Research, DDR-2565 Kuhlungsborn, GDR

Measurements of the integrated atmospheric radio noise field strength at 27 kHz, used here, were made in the period 1965 - 75 at three unified European stations: Uppsala (60°N), Kuhlungsborn (54°N) and Prague-Panska Ves (50.5°N). For some cases, also measurements at 5 kHz from Prague-Panska Ves were available.

In earlier papers it has been shown by the superposed epoch method that during Forbush-decreases the level of atmospheric radio noise also decreases at middle latitudes. In case of occurrence of both Forbush-decrease and geomagnetic storm, the level of atmospheric radio noise generally increases (SATORI, 1976). In course of the theoretical interpretation, using the VLF waveguide mode theory, the attenuation of VLF electromagnetic waves has been computed considering electron density changes due to the Forbush-decrease, variations of the cut-off rigidity and particle precipitation (SATORI, 1978).

We consider the large-scale meteorological situation by comparing solar disturbed and undisturbed periods under similar weather situations. In order to show the effects of the precipitating high-energy particle (HEP) flux and of the Forbush-decrease on the noise level of all three stations simultaneously, the correlation of the noise level between pairs of stations were computed as deviations from the monthly median,  $\Delta E$  (dB), day by day for all six periods studied here. We computed the correlation coefficients for noon as well as for night values. These correlation coefficients were compared with those for solar undisturbed periods.

- As expected, the correlation of the noise level is highest when the HEP and the FORBUSH-decrease during disturbed periods predominantly control the propagation conditions. The influences on the noise level are more distinct at Uppsala than at Panska Ves.

- The average correlation coefficient between Uppsala and Kuhlungsborn for the disturbed periods is  $r = 0.72$  ( $n = 22$ ) for the day-time (1200-1600 LMT) and  $r = 0.71$  ( $n = 21$ ) for the night-time noise level (2200-0200 LMT). It decreases to  $r = 0.4$  ( $n = 26$ ) and  $r = 0.43$  ( $n = 26$ ), respectively, for undisturbed periods.

- For the correlation between Kuhlungsborn and Panska Ves there were no significant differences between the analogous correlation pairs  $r = 0.69$  ( $n = 22$ ),  $r = 0.75$  ( $n = 22$ ) and  $r = 0.68$  ( $n = 27$ ). But the noise level variation for a disturbed period is very similar at all three stations.

By some case-studies of the level of atmospheric radio noise it has been demonstrated that after proactive flares the nearly simultaneous effects of Forbush-decrease and that of the post-storm-event (PSE) result in different noise level changes, depending on the strength of the Forbush-decrease and that of the geomagnetic storm (the energy spectra of precipitating electrons), as well as on the onset and the duration of events as compared to each other.

Fig. 1 shows the extremely strong event of August, 1972 from the point of view of both Forbush-decrease and geomagnetic storm. The geomagnetic activity is characterized by  $A_p$ -indices, the Forbush-decrease is given in percent of the basis of Moscow neutron monitor data. We studied both the day-time (1200-1600 LMT) and the night-time (2200-0200 LMT) noise level changes as deviations from the monthly medians  $M$  (dB). The seasonal variation is also removed from the medians of noise level.

Using the terminology of different phases of post-storm event, namely PSE I, PSE II, PSE III (after LAUTER et al., 1979), it may be seen that during PSE I the noise level at the different observatories decreases on 27 kHz and also on 5 kHz, simultaneously with the main depression of Forbush-decrease both day and night. During PSE II, the noise level increases at day, depending on latitude and frequency, but its enhancement is much more moderate as compared to the PSE II in absorption (LAUTER et al., 1979). This circumstance may be connected both with the differential energy spectra of precipitating electrons and with the modification of noise level by the still lasting Forbush-decrease. During PSE III, the noise level increases again and it is more developed than PSE III in the LF absorption. This increase may be connected with the hardening of energy spectra of precipitating electrons and with the fact that the Forbush-decrease already ended. At night the picture is similar, but the PSE II is longer, than at day; its first part is destroyed, but the second part of PSE II is well developed, when the Forbush-decrease ended. There is a moderate noise level rise corresponding to PSE III.

Fig. 2 shows the extraordinary event of December 1971, when a strong geomagnetic storm (max.  $K_p = 7+$ ) occurred with a very weak absorption response mainly at higher latitudes, when the precipitation of particles has also been observed by satellite 1971-089A (LARSEN et al., 1976; LASTOVICKA and RAPOPORT, 1979). It has to be noted that over Ottawa the quasi-trapped fluxes may be 3 - 4 orders of magnitude larger than those over other mid-latitude stations in central Europe (10°E). The Forbush-decrease was also strong and it ended only after the period studied here. The noise level changes show the daylight responses to the Forbush-decrease, which have been moderated at higher latitudes by the opposite effect of the geomagnetic storm. Therefore a virtual opposite latitude dependence of the effect of Forbush-decreases may be seen. The night noise level changes are ambiguous.

Fig. 3 shows an event with a moderate Forbush-decrease and geomagnetic storm. The Forbush-decrease begins three days earlier than the geomagnetic storm. In this case the changes of the atmospheric radio noise level show a picture quite similar to the LF absorption post-storm effect both day and night. In the noise level at daylight hours the PSE I is less, the PSE III is more intensive as compared to the LF absorption in Kullingsborn.

Fig. 4 shows a collection of different events referring to the effect of the geomagnetic storm and the Forbush-decrease for Kullingsborn in daylight hours. The days of occurrence of the geomagnetic storms are indicated by the vertical line. In case of the event of March, 1970, the opposite effects of the Forbush-decrease and the geomagnetic storm practically cancel each other.

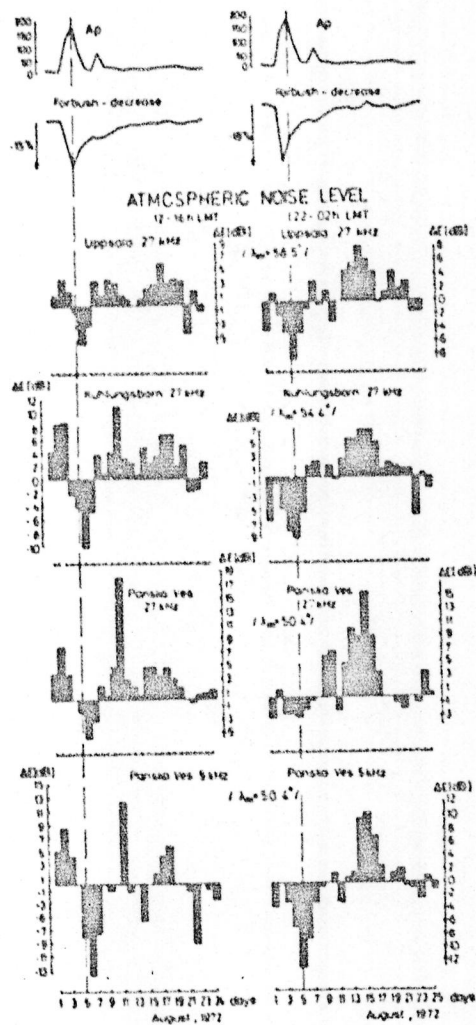


Figure 1.

Summarizing we can see that the VLF noise level changes due to the joint effect of Forbush-decreases and geomagnetic storms show a much more varied picture as compared to the LF absorption post storm effects in case of different events. But by means of the VLF noise level the direct influence of the galactic cosmic rays in the lower D-region may be studied.

## REFERENCES

- Larsen, T. R., J. B. Reagan, W. L. Imhof, L. E. Montbriand and J. S. Belrose (1976), *J. Geophys. Res.*, **81**, 2200.

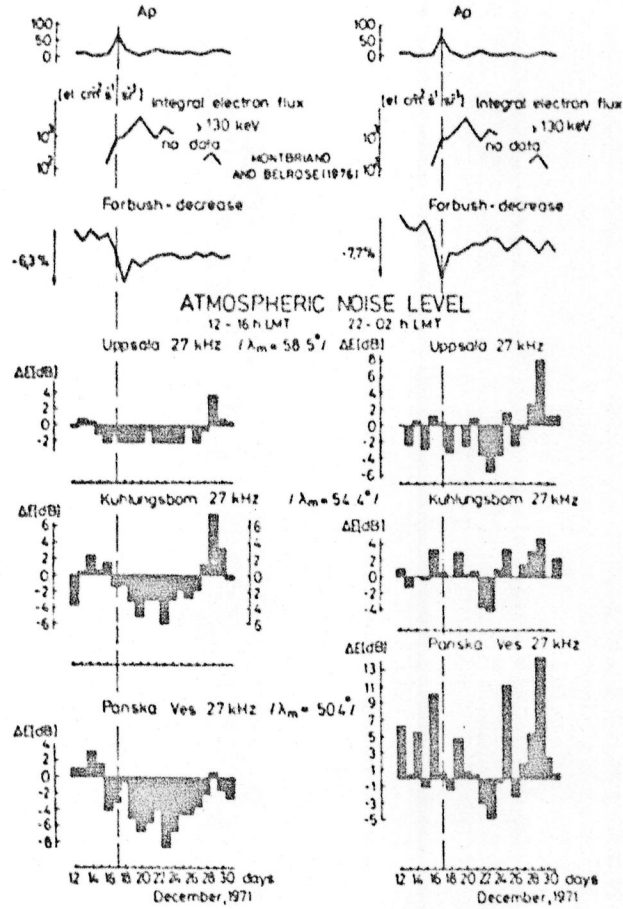


Figure 2.

- Lastovicka, J. and Z. Ts. Rapoport (1979), *Studia Geoph. et Geod.*, **23**, 263.  
 Lauter, E. A., A. Grafe, B. Nikutowski, J. Taubenheim and C. U. Wagner (1979),  
*Gerlands Beitr. Geophysik*, Leipzig, **88**, 73.  
 Satori, G. (1976), *Acta Geod. Geoph. Mont. Hung.*, **11**, 229.  
 Satori, G. (1978), *Acta Geod. Geoph. Mont. Hung.*, **13**, 475.

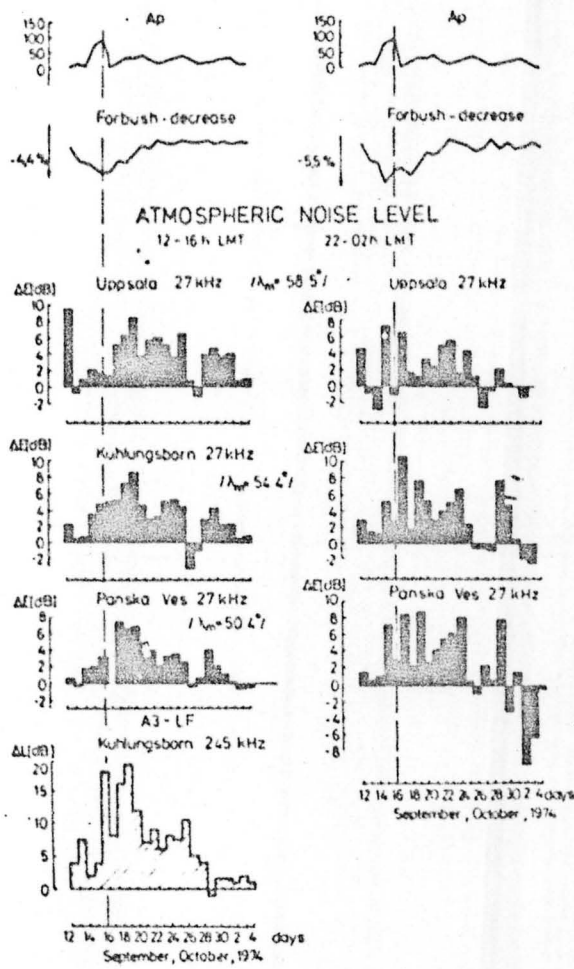


Figure 3.

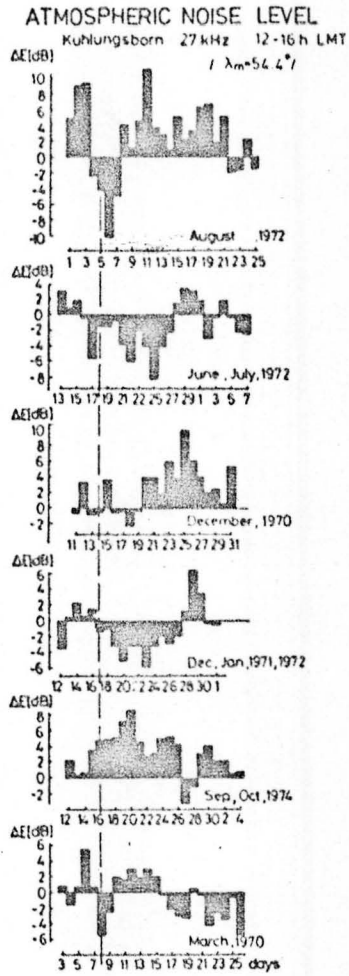


Figure 4.

N85

20489

UNCLAS

N 85 - 2048 9

211

LATITUDINAL DEPENDENCE OF THE ENERGY INPUT INTO  
THE MESOSPHERE BY HIGH-ENERGY ELECTRONS

C. U. Wagner\*, B. Nikutowski\* and H. Ranta\*\*

\*Central Institute of Solar-Terrestrial Physics, DDR-1199 Berlin-Adlershof, GDR

\*\*Geophysical Observatory Sodankyla, SF-99600 Sodankyla, Finland

Night-time ionospheric absorption measurements (A2, A3) give the possibility to study the precipitation of high-energy electrons into the mesosphere during and after magnetospheric storms. The uniform Finnish riometer network together with A3-measurements from Kuhlungsborn and Collm (GDR) have been used to investigate the night-time absorption as a function of latitude ( $L = 6.5 - 2.5$ ) and storm-time for seven storms (WAGNER et al., 1982 a). The common trends visible in all these events can be summarized in a schematic average picture (see Figure), showing the distribution of increased ionospheric absorption as a function of latitude (L-value) and storm-time. During the main phase of a storm enhanced precipitation of high-energy electrons has been found for all L-shells ( $2.5 < L < 6.0$ ). During the recovery phase the precipitation in auroral latitudes can be relatively low, but in medium latitudes an electron precipitation belt starts to develop. The position of the poleward boundary of this precipitation belt is found to be a function of storm-time. It reaches  $L \approx 4.5$  at the end of the recovery phase. The ionospheric absorption increase is only a rough indicator for the flux of precipitating electrons, because it is only a height-integrated and energy-integrated information. Either in-situ measurements onboard of low-altitude satellites or pitch-angle distribution measurements made in the equatorial plane may be used to gain more detailed information about the energy input into the region below 100 km by precipitating electrons. Measurements of the pitch-angle distribution of electrons for four energy channels (35 - 70, 75-120, 120-240, 240-560 keV) made onboard of Explorer-45 for  $2 < L < 5.2$  in the equatorial plane have been used to study the variations of the electron population for two storms in August 1972 (WAGNER et al., 1982 b). During the main phase of the storm the slot region is filled up totally and the electron fluxes increase by one order of magnitude for the 35-70 keV electrons and by three orders of magnitude for the 240-560 keV electrons. Some energy is at once released to the ionosphere by precipitation, but a great amount of this energy is stored in the electron radiation belt. During the recovery phase the input of new high-energy electrons into the radiation belt decreases and the stored energy is transferred to the ionosphere by precipitation. The number of high-energy electrons inside a magnetic tube of  $1 \text{ cm}^2$  area at 100 km altitude, the so-called flux tube content, has been determined in dependence on L, energy channel, and stormtime. During the recovery phase the flux tube content decreases exponentially in a rather steady way. The time constant of this decrease is determined by the lifetime of the electrons against pitch-angle diffusion processes and by the time constant of the electron input due to radial diffusion. The lifetime against pitch-angle diffusion and the flux tube content just after the main phase control the precipitation into the ionosphere.

The energy input rates for the recovery phase of the magnetospheric storm August 9 (15.15 UT) through August 14 (10.00 UT), 1972 have been estimated for  $L = 3$  and  $L = 4$  in dependence on energy. The total energy input by high-energy electrons ( $35 < E_e < 560 \text{ keV}$ ) for that part of the recovery phase has been found

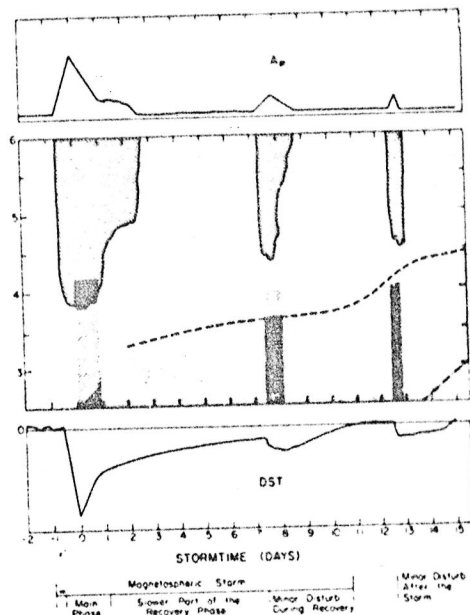


Figure 1.

to be more than  $100 \text{ erg/cm}^2$  at  $L = 3$ . Electrons with high energies (but lower fluxes) transfer more energy into the ionosphere than electrons with  $35 < E_e < 120 \text{ keV}$ . At the beginning of the recovery phase the energy input from electrons with  $120 < E_e < 560 \text{ keV}$  is higher by a factor 2-3. During the recovery phase the energy input by electrons with  $35 < E_e < 70 \text{ keV}$  decreases from  $2 \times 10^{-4}$  to  $7 \times 10^{-6} \text{ erg/cm}^2 \text{ s}$ , and that by electrons from the highest energy channel decreases from  $7 \times 10^{-4}$  to  $6 \times 10^{-5} \text{ erg/cm}^2 \text{ s}$ . The higher the energy of the precipitating electrons, the lower the stopping height (see, e.g., REES 1963). For the energies mentioned above the energy input maximum occurs between 95 km ( $\sim 40 \text{ keV}$ ) and about 75 km ( $\sim 500 \text{ keV}$ ). As has been shown above the energy is transferred only to a narrow belt ( $2 < L < 4$  to  $4.5$ ) in midlatitudes. For the part of the recovery phase (August 9-14, 1972), which has been used to estimate energy rates, the total energy released in this belt has been estimated to be  $3 \cdot 10^{19} \text{ erg}$ . During the whole recovery phase of that storm about  $5 \cdot 10^{19}$  have been transferred to this belt by high-energy electrons.

In comparison with other storm processes such as ring current injections (some  $10^{23} \text{ erg}$ ), auroral particle precipitation or Joule heating (some  $10^{22} \text{ erg}$ ) the energy input by high-energy electrons which had been stored in the radiation belt is small. But the special properties of this energy input are interesting: (a) The energy is directly deposited below 90 km altitude. (b) Energy is transferred into the lower ionosphere for many days up to some weeks after storms. (c) The energy input occurs only in a midlatitudinal belt ( $2 < L < 4$  to  $4.5$ ).

## REFERENCES

- Rees, M. H. (1963), *Planet. Space Sci.*, **11**, 1209.  
 Wagner, C. U., H. Ranta and A. Ranta (1982a), *J. Atmosph. Terr. Phys.*, **44**, 747.  
 Wagner, C. U., A. Grafe and B. Nikutowski (1982b), *Gerlands Beitr. Geophysik*, Leipzig **91**, 457.

N85

20490

UNCLAS

N 85 - 2049 0

D40  
213

OZONE MEASUREMENTS IN THE MESOSPHERE DURING A SOLAR PROTON EVENT

W. Lippert and D. Felske

Institute of Space Research, DDR-2080 Neustrelitz, GDR.  
Academy of Sciences of the German Democratic Republic

INTRODUCTION

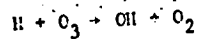
Charged particle precipitation in the Earth's atmosphere produces odd nitrogen and odd hydrogen. These species take part in catalytic reactions which destroy atmospheric ozone in the stratosphere and mesosphere. Modeling efforts regarding the impact of these ionization events on the neutral atmosphere (e.g. SOLOMON and CRUTZEN, 1981; THORNE, 1980) describe ozone depletions in good agreement with observations in the stratosphere and mesosphere.

CRUTZEN and SOLOMON (1980), discussing the photochemical effects of the solar proton event (SPE) of August 1972, presented calculations for higher altitudes (70-90 km) indicating that after a brief reduction during and immediately following intense particle precipitation, ozone will later reach higher concentrations than those present before the event.

MESOSPHERIC PHOTOCHEMISTRY

In order to study mesospheric photochemistry with regard to ozone we follow the discussions of CRUTZEN and SOLOMON (1980). Water vapour photolysis is the major source of odd hydrogen (H, OH, HO<sub>2</sub>) under normal conditions. The odd hydrogen may then be converted to H<sub>2</sub> by the reaction  $H + HO_2 \rightarrow H_2 + O_2$ . This process is responsible for the decrease in the H<sub>2</sub>O mixing ratio.

Charged particle precipitation events are calculated to cause the same effect of producing odd hydrogen. The odd hydrogen has a lifetime on the order of hours for altitudes of 70 - 80 km. For the first few hours following a particle precipitation event, odd hydrogen concentrations will remain high. Odd hydrogen is by far the most important factor in the destruction of ozone or more generally of odd oxygen via reactions such as



The increased odd hydrogen concentrations are therefore expected to yield a reduction in ozone during and within a few hours after the event.

The normal supply of water vapour by eddy diffusion from lower altitudes is too slow to make up for the rapid depletion of water vapour taking place during the SPE. A decrease of odd hydrogen concentration and eventually an increase of ozone a few hours after the event will be the result.

EXPERIMENTAL RESULTS

It is the aim of this paper to examine our experimental ozone densities as to a possible influence by solar proton events according to the mechanism proposed by CRUTZEN and SOLOMON (1980). We derived vertical density profiles of ozone between 55 and 82 km from INTERKOSMOS - 11 occultation measurements during local sunset.

The period between early September and early October 1974 has been chosen. Three solar proton events occur during this time as given by Solar Geophysical Data. Our data base comprises 37 ozone density profiles between 10 September and 3 October 1974 (see Fig. 1). The geomagnetic position of the profiles varies from lower northern latitudes to medium and high southern latitudes.

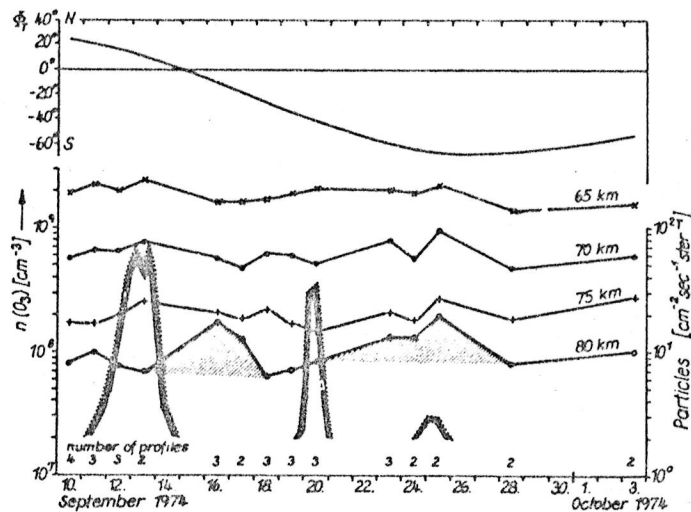


Figure 1.

Our ozone densities seem in general to reflect at least some of the predicted features. The proton event with its peak on 13 September as well as the one on 20 September seem to be followed by pronounced enhancements of densities at 80 km height a few days after the event. Even the third event around 25 September seems to contribute to the ozone enhancement. The densities at lower altitudes possibly indicate that during the first event the response to the particle influx penetrates down to altitudes of only 70 km and with increasing time delay while during the second and third events altitudes as low as 65 km have obviously been reached. This could be explained by different energy spectra of the precipitating protons (KARSZENBAUM and GAGLIARDINI 1981).

Figure 2 illustrates the difference in ozone density for normal conditions and those influenced by the particle precipitation event. The 10 September comprising 4 profiles has been chosen as a reference. The curve for 16 September comprising 3 individual profiles represents the maximum of enhanced ozone density of the first event. The ratio  $\rho(O_3)$  between both profiles is shown in Fig. 3. No enhancement has been found below 70 km. A maximum seems to occur around 80 km with enhanced ozone densities of up to a factor of 2.4, considerably higher than value of 1.4 predicted by CRUTZEN and SOLOMON (1980). The particulars of the measurements do not provide sufficient temporal resolution in order to study the relatively short phase of the predicted ozone decrease during and a few hours after the event. The behavior of ozone density during the first event seems nevertheless to indicate that such a process is indeed taking place.

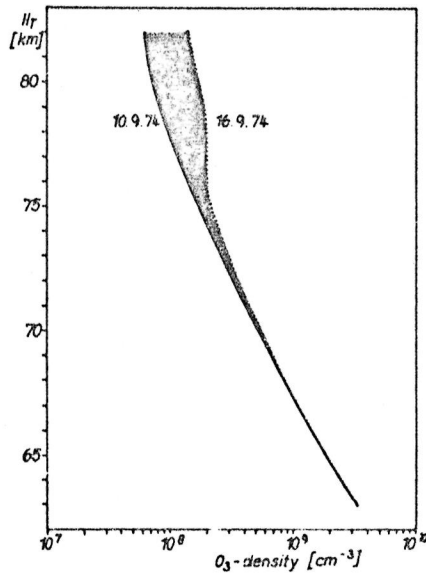


Figure 2.

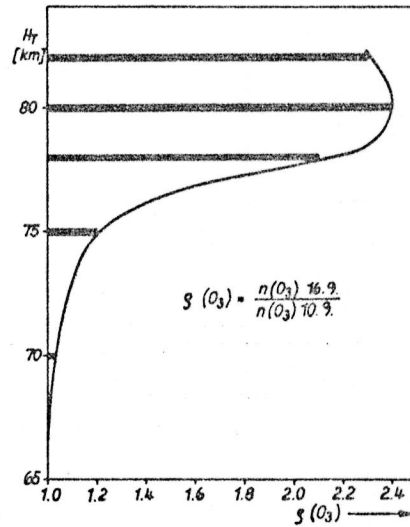


Figure 3.

## CONCLUSIONS

Ozone densities at altitudes of 55 - 82 km have been examined as to their reaction to solar proton events. It seems that at least some of the features predicted by CRUTZEN and SOLOMON (1980) are reflected in the data. While the shorttime decrease is not amenable to the experimental method used the ozone density increase, lasting for several days, seems to be well pronounced around 80 km. More data are however necessary in order to provide information on dynamic processes and on the role of odd hydrogen in controlling the ozone balance in the mesospheric region.

## REFERENCES

- Crutzen, P. J. and S. Solomon (1980), *Planet. Space Sci.*, **28**, 1147.  
 Karszenbaum, H. and D. A. Gagliardini (1981), *Adv. Space Res.*, **1**,  
 Cospar, pp. 35-38.  
 Solomon, S. and P. J. Crutzen (1981), *Journ. Geophys. Res.*, **86**, 1140.  
 Thorne, R. M. (1980), *Pageoph.*, **118**, 128.

N85  
20491

UNCLAS

## GEOMAGNETIC DISTURBANCES CAUSED BY INTERNAL ATMOSPHERIC DYNAMICS

G. Sonnemann

Academy of Sciences of the GDR  
Institute of Space Research, DDR-2080 Neustrelitz, GDR

## INTRODUCTION

It is commonly believed that geomagnetic disturbances are caused by external influences connected with the solar wind. The 27-day recurrence of perturbations seems to be a strong hint for this interaction. But frequently geomagnetic disturbances occur without any relation to sunspot numbers or radiowave fluxes. This was one of the reasons for introducing hypothetical M-regions on the sun and their relation to solar wind activities.

McPHERRON et al. (1982) have reported that only one half of the variance of the geomagnetic AL-index could be related to the solar wind. Therefore they concluded that internal processes of the magnetosphere were responsible for additional geomagnetic activity. This paper discusses arguments, which might lead to the suggestion of geomagnetic disturbances as being caused by internal atmospheric dynamics and tries to establish a rather preliminary scenario of those processes.

## STATISTICAL STUDIES

Fig. 1 shows median and arithmetic mean values of the local geomagnetic activity index  $\Sigma K_1$  of the station Niemegk (GDR) for the October-November period of 41 years. This period obviously exhibits recurring meso-scale variations of remarkable amplitudes. The  $A_k$ -index data presented for 26 years show a similar behaviour. Particularly the end of Oct. with a peak about October 28 possesses a distinct activity maximum followed by a pronounced minimum about November 6. The statistical certainty of the  $\Sigma K_1$ -data amounts to 98.5 to 99.9%. Such a distribution of rather strong perturbations is evident also during other periods of the year particularly about and after the equinoxes.

Regarding individual years this statistical finding is not immediately evident, so that it proves only the existence of periods with enhanced probability of disturbed or quiet days, but not an annual recurrence of such events. Solar parameters such as the sunspot number or the 10.7-cm flux gave no hint to explain this phenomenon. Although a period of 2 years very well fits a number of 27 solar rotations, no 2-years' recurrence has been found. This may be seen also on Fig. 2 showing similar variations of the  $A_k$  medians during the April/May period, but being out of phase of the 27-day rotation period. Rather strong negative ionospheric disturbances frequently occur approximately between October 25 and November 2. We have called this period the MID-period - period of major ionospheric disturbances (SONNEMANN, 1983). Fig. 3 shows the 11-years mean day-time level of the critical frequency foF2 compared with corresponding values of geomagnetic activity. Clearly visible is the breakdown of the critical frequency after its seasonal peak. A proper ionospheric activity index processed in a special way, shown in the upper part of this figure, exhibits a distinct maximum at the same date.

If we consider other parameters such as radio wave absorption no significant hints for a relation to the D-region parameters can be found. The air pressure mean values show maximum values even before and during the MID-period with a small decrease simultaneously with the decrease of the critical frequency. Also the semiannual exospheric density variation has its maximum about

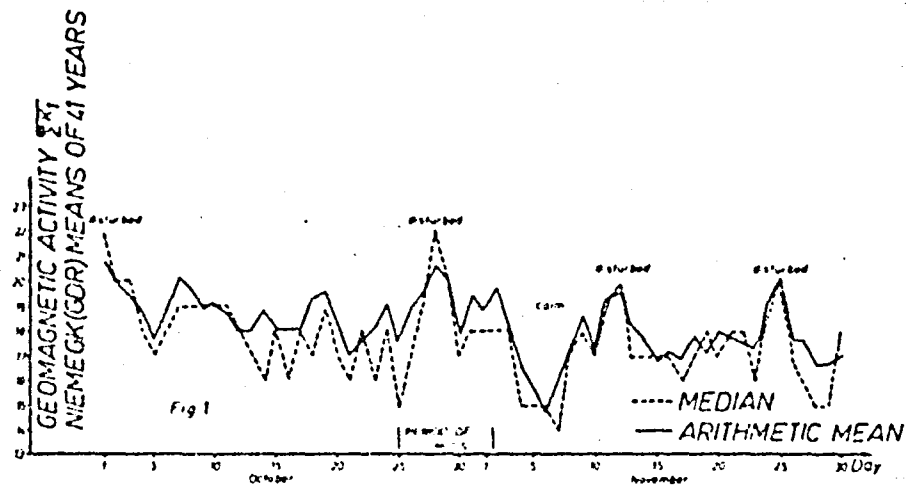


Figure 1.

COMPARISON OF  $A_k$ -MEDIAN VALUES OF THE PERIODS  
AFTER EQUINOXES SHOWS SIMILARITIES IN THE STRUCTURES  
SAE-SEMI-ANNUAL-EFFECT OF EXOSPHERIC DENSITY VARIATION

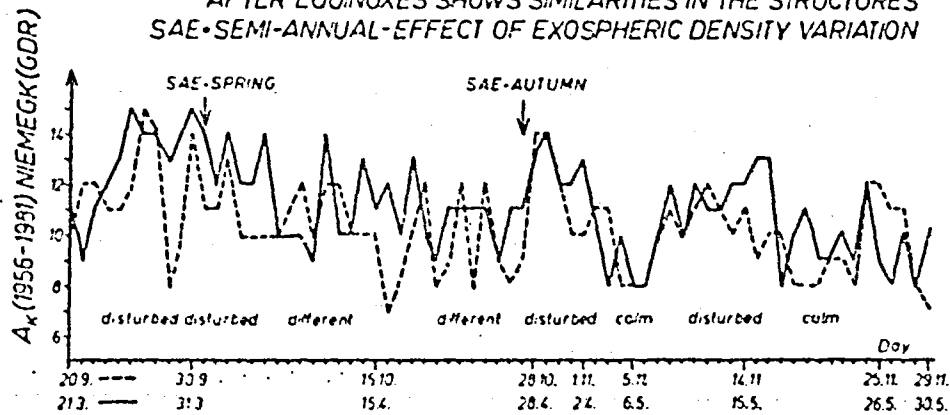


Figure 2.

October 27, indicating an imminent dependence.

#### SATELLITE OBSERVATIONS

We were able to derive neutral gas profiles of the European sector from occultation measurements of the Solrad-10 satellite for certain ionospheric disturbances related to geomagnetic perturbations. During a major disturbance about October 29, 1971, we derived some results on structural variations of the neutral gas (composition and density) between about 90 and 300 km using Solrad-10 measurements, as shown in Fig. 4. During the positive storm phase the

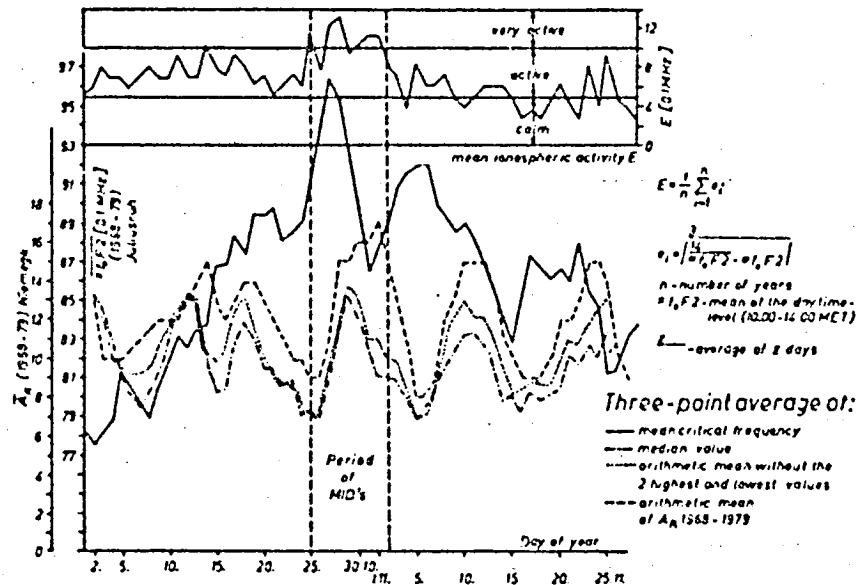


Figure 3.

molecular components decrease and atomic oxygen increases, the profiles are strongly disturbed. The day of negative storm is distinguished by a resonance-like upwelling of the molecular components, while thermospheric atomic oxygen decreases below about 250 km and further increases above 250 km. The mean thermospheric temperature deduced from the density gradient reaches maximum values. The recovery phase starts with a sudden thermospheric cooling, the molecular components decrease but the atomic oxygen density above 250 km attains maximum values.

#### DISCUSSION

In order to solve the puzzle we shall try to establish a scenario of possible relations. The observed structural variations of the neutral gas are related to perturbations, which are evident even in medium latitudes in the mesosphere, below those altitudes which are sufficiently influenced by precipitating particles caused by external geomagnetic disturbances. This, together with the above statistical results, leads to the suggestion that internal atmospheric dynamics is responsible for perturbations of this type. Geomagnetic variations and perturbations could be connected with wind shears within the dynamo region, particularly at high latitudes. It can be excluded, however, that they are directly and completely caused by the dynamo region currents. More likely, E-fields generated by the dynamo region currents, e.g. the auroral electrojet could be responsible, affecting plasma drifts within the magnetosphere. According to WILLIAMS (1982), only a certain part of the plasma of the ring current originates from the solar wind, while the other part has an ionospheric source. The magnitude of the ring current depends on the balance between injection from the solar wind and decay by charge exchange of ring current plasma with neutrals of the geocorona (DESSLER et al. 1961, TINSLEY 1977). That means that the ring current grows with increasing solar-wind flux (external influence) or with a decrease of the density of neutrals which could be understood by a respiration

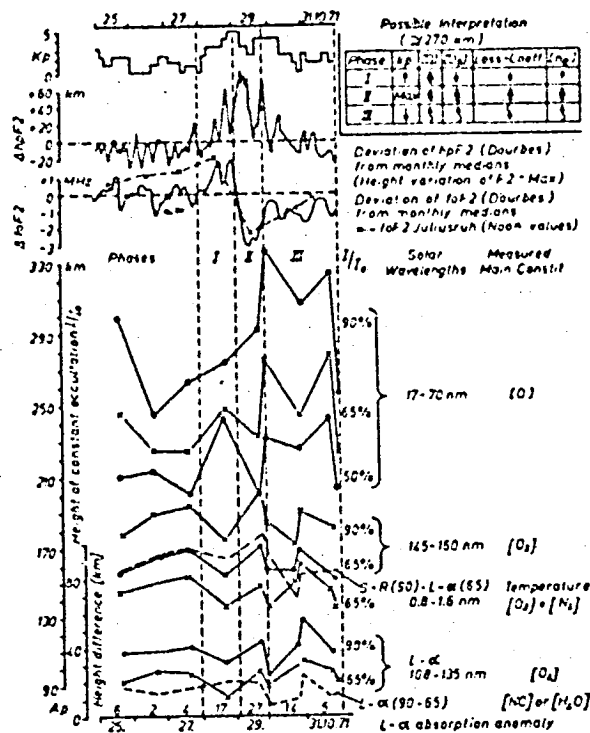


Figure 4.

of the geocorona caused by dynamical processes of the lower atmospheric layers. Due to their short lifetime of about 2 hours, hydrogen ions decay first, followed by a decay of heavier ions such as helium and oxygen with lifetimes 6 times larger. Therefore composition changes of geocoronal neutrals have to be regarded, too. As TINSLEY et al. (1982) pointed out, fast neutrals of several keV energy created by charge exchange cross through the magnetosphere on straight trajectories and precipitate within denser layers, particularly influencing mean and equatorial geomagnetic latitudes. The neutral hydrogen penetrates to an altitude of 200 - 110 km while atomic oxygen precipitating in the second phase reaches only heights of 250 - 300 km. The estimated energy input by fast neutrals amounts to 10% or more related to the EUV-input and may lead to an important enhancement of the nighttime ionisation. This might be deduced from the TEC-data during the night before the negative storm. But the possibility of downward plasma transports caused by equator-to-pole winds and a considerable reduction of the dissociative recombination due to composition change has to be considered. Not regarding other details of the complex process, the neutral influx causes on one hand by its upper thermospheric energy input a positive feedback taking into consideration the upwelling of atomic oxygen and the negative reaction of hydrogen on an enhancement of exospheric temperature. On the other hand, the creation of  $N_2^-$ -ions and of vibrationally excited  $N_2$  could be a source of sufficiently large quantities of NO particularly within equatorial and mean geomagnetic latitudes.

The neutral density of the thermosphere, particularly at medium and higher latitudes of the winter hemisphere, shows variations with planetary time and space scales (SONNEMANN et al. (1982)). These variations are connected with plasma variations of the lower E-region (SONNEMANN et al. 1979). As analysed by SATO (1981) SSC-events are followed by excessive absorption simultaneously within a large longitudinal sector explained by sectorwise precipitation of high energetic electrons. From our measurements, however, it follows that the  $O_2$  density changes simultaneously within a large longitudinal sector, linked with  $O_2$ -gradient enhancements in the lower thermosphere in phases of low  $O_2$ -density and low radio wave absorption and vice versa. This varying gradient may explain the varying absorption of ionising radiation, but a certain influence of precipitating particles cannot be excluded.

The density variations, however, indicate also relations to processes of the lower atmosphere. Particularly, the change from summer to winter circulation patterns could give rise to neutral impact to the thermosphere and geocorona.

External and internal influences do not occur separate from each other but rather combined, including the actual particle and EUV fluxes of the Sun. The internal disturbances can only be understood by considering the whole atmospheric dynamics including meteorological processes and wave phenomena, taking into account various feedbacks.

#### REFERENCES

- Dessler, A. J., W. B. Hanson and E. N. Parker, (1961), Journal Geophys. Res., 66, 3631.
- McPherron, R. L., M. G. Kivelson, L. F. Barger, D. Baker, C. R. Clauer and C. Searls, (1982), Paper No. STP. III. 1.1. presented to COSPAR-Meeting, Ottawa.
- Sato, I., (1981), Journal Geophys. Res., 86, 9137.
- Sonnemann, G., (1983), Gerlands Beitr. Geophysik, Leipzig, 92, in press.
- Sonnemann, G., R. Knuth, K. H. Ohle and R. Reimer, (1979), Space Res., Vol. XIX, 301.
- Sonnemann, G., D. Felske and R. Knuth, (1983), Adv. Space Res., 3, No. 1, 103-106.
- Tinsley, B. A., (1977), Journal Atmos. Terr. Phys., 39, 1203.
- Tinsley, B. A., R. P. Rohrbaugh, Y. Sahai and E. R. Teixeira, (1982), Geophys. Res. Lett., 9, 543.
- Tinsley, B. A. and R. P. Rohrbaugh, (1982), Paper No. STP IV. 1.7., presented to COSPAR-meeting, Ottawa.
- Williams, D. J., (1982), Paper No STP. L.2. presented to COSPAR-meeting, Ottawa. Preprint APL/INU 82-17.

END

DATE

FILMED

MAY 16 1985

LANGLEY RESEARCH CENTER



3 1176 00184 9984

